Universidad Zaragoza
1542

Tesis Doctoral

RESPUESTA RADICULAR A LA DEFICIENCIA DE Fe Y LA TOXICIDAD POR Cd

Autor

Rodríguez Celma, Jorge

Director/es

López Millán, Ana Flor

FACULTAD DE CIENCIAS
Departamento de Bioquímica y Biología Molecular y Celular

2011

TESIS DOCTORAL

Respuesta radicular a la deficiencia de Fe y toxicidad de Cd

Memoria presentada por:
Jorge Rodríguez Celma

Esta Tesis Doctoral es un compendio de trabajos previamente publicados y consta de las siguientes publicaciones:

Andaluz S, **Rodríguez-Celma J**, Abadia A, Abadía J, López-Millán AF. (2009). Time course induction of several key enzymes in Medicago truncatula roots in response to Fe deficiency. *Plant physiology and biochemistry*, **47**: 1082-1088.

Rodríguez-Celma J, Rellán-Alvarez R, Abadía A, Abadía J, López-Millán AF. (2010). Changes induced by two levels of cadmium toxicity in the 2-DE protein profile of tomato roots. *Journal of proteomics*, *73*: 1694-1706.

Rodríguez-Celma J, Lattanzio G, Grusak MA, Abadía A, Abadía J, López-Millán AF. (2011). Root responses of *Medicago truncatula* plants grown in two different iron deficiency conditions: changes in root protein profile and riboflavin biosynthesis. *Journal of proteome research*, **10**: 2590-2601

Rodríguez-Celma J, Vázquez-Reina S, Orduna J, Abadía A, Abadía J, Álvarez-Fernández A, López-Millán AF. (2011). Characterization of flavins in roots of Fe-deficient Strategy I plants, with *Medicago truncatula* on the focus. *Plant & cell physiology*, in press.

AUTORIZACIÓN DE PRESENTACIÓN DE TESIS DOCTORAL EN MODALIDAD DE COMPENDIO DE PUBLICACIONES

ANA FLOR LÓPEZ MILLÁN, Científico Titular del CSIC

AUTORIZA

La presentación en la modalidad de compendio de publicaciones de la Tesis doctoral titulada "Respuesta radicular a la deficiencia de Fe y toxicidad de Cd", presentada por el Licenciado en Bioquímica D. JORGE RODRÍGUEZ CELMA, para optar al Grado de Doctor por la Universidad de Zaragoza, y certifica que ha sido realizada bajo su dirección en la Estación Experimental de Aula Dei del Consejo Superior de Investigaciones Científicas.

Zaragoza, Octubre de 2011

Fdo. Ana Flor López Millán

INTRODUCCIÓN

Las plantas, además de dióxido de carbono, oxígeno y agua, necesitan elementos minerales para un correcto desarrollo. Estos elementos minerales se pueden clasificar en macronutrientes y micronutrientes en función de la cantidad de elemento necesitada por la planta. Muchos de los micronutrientes, denominados de este modo por requerirse en bajas cantidades, pertenecen al grupo de los metales pesados. Dentro de este grupo se incluyen Fe, Mn, Cu, Zn, Ni y Mo. Estos metales son esenciales para los organismos del reino vegetal, ya que son imprescindibles para funciones vitales como la fotosíntesis y la respiración, entre otras (Marschner, 1995). La homeostasis de estos micronutrientes está finamente regulada debido a que, a pesar de ser necesarios, cuando se encuentran en exceso causan alteraciones en algunos procesos como la transpiración (Richardson et al., 1993), la fotosíntesis (Yruela et al., 1996), la biosíntesis de clorofila (Mocquot et al., 1996) y el mantenimiento de la integridad de la membrana plasmática (De Vos et al., 1993).

Por otro lado, existen metales pesados con propiedades físico-químicas muy similares a las de los micronutrientes que, sin embargo, no son esenciales para el correcto desarrollo de las plantas. Debido a este parecido son adquiridos por medio de los mecanismos de asimilación existentes para los micronutrientes. Los metales pesados no esenciales, como Cd, Pb y Hg, no cumplen ninguna función biológica y pueden resultar fitotóxicos incluso a bajas concentraciones (Vázquez et al., 1992). Por tanto, las plantas han desarrollado mecanismos de desintoxicación basados tanto en la regulación de su adquisición como en su compartimentación en lugares de baja actividad metabólica tales como el apoplasto, la pared celular o la vacuola (Hall, 2002).

Los procesos de homeostasis de metales pesados esenciales y los de desintoxicación de metales pesados no esenciales presentan muchos puntos en común. Ello se debe a la mencionada similitud de sus características físico-químicas, que hacen que compartan los mecanismos de adquisición y transporte. En muchas ocasiones, la presencia de un metal no esencial supone una disminución de la entrada en la planta, tejido o compartimento subcelular de aquel micronutriente con el que comparte vías de adquisición y/o transporte (López-Millán et al., 2009). Por ejemplo, se ha descrito que la presencia de Cd puede producir una deficiencia de Fe en la planta debido a que es capaz de entrar en la raíz utilizando el transportador habitual del Fe, el IRT (Iron Regulated Transporter; (Guerinot, 2000). Por otro lado, la presencia de elevadas concentraciones de metales esenciales puede jugar un papel protector frente a metales pesados tóxicos al impedir la entrada de los mismos, como se ha descrito para el Zn y el Cd (He et al., 2005; Perfus-Barbeoch et al., 2002).

En general, los cambios metabólicos inducidos tanto por la deficiencia de Fe como por la toxicidad de Cd se han caracterizado basándose en las actividades enzimáticas y las concentraciones de determinados grupos de metabolitos. El conjunto de las proteínas de una planta constituye la parte activa de la cadena genoma-transcriptoma-proteoma y se denomina, por analogía con estos términos, proteoma. La proteómica, junto con la genómica y transcriptómica permiten tener un conocimiento de cómo puede ser el

comportamiento general de la planta en un determinado contexto medioambiental (estrés biótico y abiótico, estado nutritivo, etc.) (Dixon et al., 2006; Fiehn, 2002). Tanto la complejidad intrínseca como la similitud de los mecanismos de homeostasis y desintoxicación, hacen que una aproximación holística desde el punto de vista proteómico sea un enfoque apropiado para abordar el estudio de las alteraciones nutricionales producidas por metales pesados en plantas. Además, la aproximación proteómica nos permite elucidar aquellas rutas metabólicas compartidas en los procesos de homeostasis y desintoxicación. Este enfoque también puede poner de manifiesto respuestas específicas a estas alteraciones nutricionales que con un enfoque clásico podrían pasar desapercibidas. Recientemente, varios estudios proteómicos han descrito la influencia de estos estreses sobre las membranas tilacoidales, los cultivos celulares y algunos tejidos como raíz y hoja (Andaluz et al., 2006; Brumbarova et al., 2008; Clemens et al., 2009; Donnini et al., 2010).

Un mejor conocimiento de los procesos derivados del estrés por metales pesados en la planta nos ayudaría no solamente a evitar problemas agrícolas como la deficiencia y toxicidad de metales en cultivos, sino también a mejorar el contenido en nutrientes de los alimentos vegetales y a favorecer la fitorremediación de suelos contaminados por metales pesados.

El cadmio en las plantas

El Cd es un metal pesado que no tiene ninguna función biológica conocida. Es uno de los metales pesados más contaminantes debido a su alta movilidad en el suelo, al potencial de bioacumulación y a la alta toxicidad para los seres vivos (Alloway et al., 1990; Barceló y Poschenrieder, 1990). La mayor fuente de ingesta de Cd en el ser humano proviene de alimentos de origen vegetal (Pinot et al., 2000), y por consiguiente el principal riesgo de exposición a Cd es la contaminación de la cadena alimenticia. El Cd causa daños en los seres vivos incluso a muy bajas concentraciones y se ha descrito que plantas aparentemente saludables pueden contener concentraciones de Cd tóxicas para mamíferos (Chen et al., 2007). Se ha observado que animales alimentados con plantas contaminadas desarrollan daños renales y pulmonares (Ryan et al., 1982), e incluso ciertos tipos de cáncer (Huff et al., 2007).

El Cd se acumula en las plantas debido a que presenta analogías químicas con otros elementos esenciales. Su presencia en el suelo no sólo supone un riesgo para la seguridad alimentaria sino también una disminución de la productividad. Su comportamiento químico es similar al del Zn, si bien es más afín por el S y algo más móvil en ambientes ácidos. En general, el Cd interfiere en la entrada, transporte y utilización de elementos esenciales y del agua, provocando desequilibrios nutricionales e hídricos en la planta (Poschenrieder et al., 1989; Sandalio et al., 2001). El Cd es capaz, por ejemplo, de desplazar al Zn de algunos de sus sitios activos y de competir con el Fe en el transporte a través de la membrana plasmática de raíz (Guerinot, 2000).

Presencia de Cd en el suelo

La concentración natural de Cd en el suelo es generalmente inferior a 1 mg kg^{-1}. Sin embargo, en algunos suelos, como aquellos próximos a depósitos de Cd o en zonas ricas en minerales de Zn puede existir en concentraciones superiores de forma natural. La contaminación por Cd de los suelos puede tener causas naturales o antropogénicas. Entre las primeras destacan la actividad volcánica, la lixiviación de rocas y los incendios forestales. Las fuentes antropogénicas, por otro lado, son muy variadas. Aunque es un metal relativamente raro, está presente en pequeñas cantidades como impureza en minerales de Zn y por ello aparece como subproducto industrial de la producción de este metal (Adriano y Weber, 2001). También existe como residuo en procesos en los que se utilizan Cu y Pb. El Cd también puede sustituir al Ca en la apatita y la calcita, de tal forma que puede estar presente en fertilizantes fosfatados. Otras causas como la incineración de materiales que contienen Cd, los combustibles fósiles, las aguas residuales municipales y las descargas de lodos (Kirkham, 2006) también influyen en la contaminación ambiental por Cd.

En los suelos contaminados, el Cd se encuentra predominantemente en forma de catión libre, y su movilidad depende del pH del suelo y de la presencia de agentes quelantes u otros metales (Hardiman y Jacoby, 1984).

Adquisición de Cd por la planta

Por ser un metal no esencial se asume que no existen mecanismos de entrada específicos para el Cd. Estudios en *Arabidopsis thaliana* y *Oryza sativa* indican que existen miembros pertenecientes a distintas familias de transportadores de metales esenciales que son capaces de transportar varios cationes divalentes, entre ellos el Cd. Esta falta de especificidad permite el paso de Cd a las raíces, especialmente en situaciones en las que el Cd se encuentra en concentraciones elevadas. Ejemplos específicos son el transportador de Fe a la raíz AtIRT1, el SpLCT1 (Low-affinity Cation Transporter), el TcZNT (transportador de Zn), que son capaces de transportar Cd además de sus cationes diana (Clemens et al., 1998; Guerinot, 2000; Korshunova et al., 1999; Nakanishi et al., 2006; Pence et al., 2000). También se ha descrito que el Cd puede entrar en la raíz utilizando canales de Ca, alterando de este modo también el equilibrio hídrico de la planta (Perfus-Barbeoch et al., 2002).

Una vez en el citosol, al no tener función biológica puede producir efectos tóxicos para la planta. Estos efectos se atenúan cuando el Cd se coordina con ligandos de S, tales como glutatión (GSH) o fitoquelatinas (PCs), o con ácidos orgánicos (OA) como por ejemplo el citrato (Domínguez-Solís et al., 2004; Clemens, 2006). Otras moléculas que pueden acomplejar Cd son las metalotioneínas (MTs), pequeñas proteínas ricas en cisteína, si bien no son las principales responsables de la desintoxicación, al contrario de lo que ocurre en células animales (Hamer, 1986). Los complejos Cd-ligando se pueden movilizar en el interior de la planta hacia lugares donde no ejerzan efectos tóxicos. Su destino principal es el almacenamiento en vacuolas (Cobbett y Goldsbrough, 2002).

Existen distintas familias de transportadores de cationes implicadas en el tráfico de Cd hacia y desde la vacuola. Para la entrada a la vacuola, se han descrito transportadores de las familias CAX (CAtion eXchangers), ABC (ATP-Binding Cassette transporters) y HMA (type 1B Heavy Metal–transporting ATPases). Los transportadores de cationes AtCAX2 y AtCAX4 de la familia CAX (Edmond et al., 2009; Korenkov et al., 2007; Park et al., 2005; Schneider et al., 2009) son capaces de transportar Cd además de Ca y Mn al interior de la vacuola. En el tonoplasto de *A. thaliana* se han descrito transportadores que proporcionan tolerancia frente a concentraciones elevadas de Cd, como el transportador de la subfamilia de las ATPasas tipo P, HMA3 (Morel et al., 2009) y el transportador ABC AtMRP3 (Bovet et al., 2003; Hanikenne et al., 2005), que ha sido aislado también en la hiperacumuladora *T. caerulescens* (Maestri et al., 2010). Un reciente estudio proteómico en tonoplasto de cebada confirmó el aumento en la expresión del transportador MRP3 en presencia tanto de altas como de bajas concentraciones de Cd en el medio de cultivo (Schneider et al., 2009). EL Cd puede salir de la vacuola aprovechando canales para otros metales, como los AtNRAMP3 implicado en el transporte de Fe (Maestri et al., 2010).

El paso de Cd al xilema está mediado por los transportadores HMA2 y HMA4 en *A. thaliana* (Verret et al., 2004) y los correspondientes homólogos en las especies hiperacumuladoras *Thlaspi caerulescens* y *A. halleri* (Hanikenne et al., 2008; Papoyan y Kochian, 2004). No existen estudios definitivos sobre la forma química en que se encuentra el Cd en el xilema. Se ha propuesto desde su existencia como ion libre (Ueno et al., 2008) hasta la existencia de diversos complejos con fitoquelatinas, citrato, histidina, cisteína, glutatión y nicotianamina (Gong et al., 2003; Salt et al., 1995; Senden et al., 1994). Una vez traslocado a la parte aérea se almacena en las vacuolas de las células del mesófilo (Kupper et al., 2000; Ueno et al., 2008).

En la Figura 1 se muestra un esquema de los transportadores de Cd descritos en el texto, incluyendo los de adquisición radicular, movilización a vacuola y descarga a xilema.

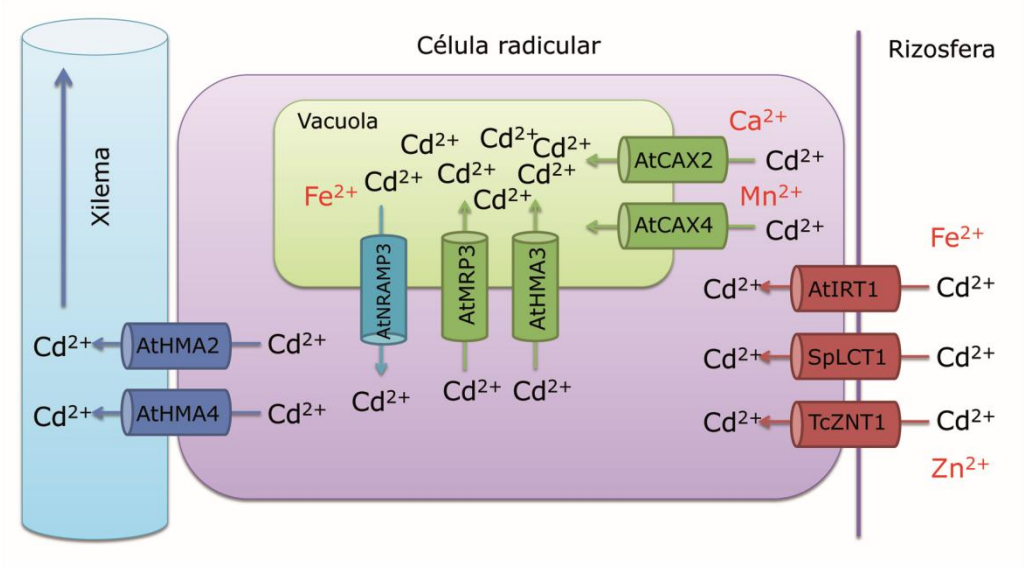

Fig. 1 Transportadores de Cd a nivel radicular.

Efectos tóxicos del Cd en la planta

Los efectos tóxicos del Cd sobre las plantas han sido ampliamente estudiados (Benavides et al., 2005; Sanitá di Toppi y Gabbrielli, 1999). Los síntomas más comunes de la toxicidad de Cd en plantas son una marcada reducción del crecimiento (Larbi et al., 2002) y la aparición de síntomas de clorosis en hojas, con zonas necróticas en los casos más graves (Larbi et al., 2002; López-Millán et al., 2009). Se ha comprobado que, en general, el Cd interfiere en la entrada, transporte y utilización de elementos esenciales y del agua, provocando desequilibrios nutricionales e hídricos en la planta (Poschenrieder et al., 1989; Sandalio et al., 2001; Singh y Tewari, 2003). Las plantas expuestas a suelos contaminados con Cd presentan modificaciones en la apertura estomática, fotosíntesis y transpiración (Sandalio et al., 2001). La presencia de Cd produce alteraciones en la funcionalidad de la membrana plasmática (Fodor et al., 1995; Sandalio et al., 2001),

reducción de la actividad ATPasa de la membrana plasmática (Astolfi et al., 2005), y desequilibrios en el metabolismo del cloroplasto, inhibiendo la síntesis de clorofila y reduciendo la actividad de enzimas implicadas en la fijación de CO_2 (Ali et al., 2000; Maksymiec et al., 2007). Las células del mesófilo muestran concentraciones de Mg más altas de lo normal, lo que se ha interpretado como un mecanismo de defensa frente a la sustitución del Mg por Cd en las moléculas de clorofila (Küpper et al., 2002). Los posibles mecanismos por los que el Cd produce estos efectos son la inducción de estrés oxidativo y la competición con otros metales, como Zn, Fe o Mn, que son cofactores de numerosas enzimas (Dong et al., 2006; Lin et al., 2007).

El Cd no experimenta cambios redox y por lo tanto no actúa directamente en la generación de especies reactivas de oxigeno (ROS). Sin embargo, existen evidencias de que la presencia de Cd produce efectos relacionados con el estrés oxidativo, como la peroxidación de lípidos de membrana (Balestrasse et al., 2004; Lozano-Rodríguez et al., 1997; Sandalio et al., 2001; Wua et al., 2003) y daños oxidativos en proteínas (Romero-Puertas et al., 2002). Esto se puede explicar porque el Cd afecta tanto a los agentes protectores ante el estrés oxidativo (enzimas antioxidantes, ascorbato, glutatión…) como a los procesos naturales productores de ROS, alterando de este modo el equilibrio oxidativo. Por un lado, el Cd es capaz de alterar la actividad de enzimas antioxidantes como superóxido dismutasa (SOD), glutatión reductasa (GR), ascorbato peroxidasa (APX), peroxidasas (POD) y la catalasa (CAT), encargadas de la defensa celular frente a ROS, reduciendo o incrementando de su actividad en función de la concentración de Cd incluida en el medio de crecimiento, la duración del tratamiento, el tipo de tejido y la especie vegetal de que se trate (Benavides et al., 2005; Sandalio et al., 2001). Por otro lado, al sustituir a otros metales esenciales en enzimas implicadas en procesos redox naturales (como la respiración) altera su correcto funcionamiento, aumentando la producción de ROS (Garnier et al., 2006; Olmos et al., 2003; Romero-Puertas et al., 2004). Estos dos efectos combinados del Cd se traducen en un aumento del daño oxidativo.

Mecanismos de desintoxicación y tolerancia

Existen distintos mecanismos de tolerancia a la presencia de metales pesados, que pueden actuar ya sea por separado o en combinación. Por un lado, las plantas tolerantes tienen mayor capacidad para restringir la entrada del metal en la planta bien sea disminuyendo la entrada o aumentando su exportación por la raíz. Por otro lado, una vez que el elemento ha entrado en la raíz, otra estrategia consiste en secuestrarlo en compartimentos donde sus efectos tóxicos sean menores como la vacuola o pared celular, generalmente acomplejado con fitoquelatinas. Por ejemplo, las plantas que sobreexpresan la enzima fitoquelatina sintasa muestran una mayor tolerancia frente al Cd (Pomponi et al., 2006). La mayoría de especies vegetales restringen el transporte de Cd a la parte aérea de la planta acumulándolo en raíz. En esta línea se ha descrito la inmovilización del Cd en el apoplasto por unión a los componentes de las paredes celulares, por ejemplo pectinas y carbohidratos extracelulares (Benavides et al., 2005).

El hierro en las plantas

El hierro es un micronutriente esencial para las plantas, animales y otros organismos, ya que es un constituyente indispensable de un gran número de enzimas y agentes redox que intervienen en algunas de las principales funciones del metabolismo de los seres vivos. La gran versatilidad del Fe en sus funciones biológicas es debida al potencial del par redox Fe(III)/Fe(II), que varía dependiendo del ligando al que se encuentre unido, permitiendo así su uso en forma de grupos hemo o cluster Fe-S.

En plantas, el Fe interviene en las síntesis de clorofila y es esencial para la fotosíntesis y el mantenimiento de la estructura del cloroplasto (Abadía y Abadía, 1993). Además, interviene en procesos como la respiración, la fijación de nitrógeno (Clark, 1983) y en la síntesis de DNA y hormonas (Briat y Lobréaux, 1997). Aproximadamente un 63% del hierro de la hoja está asociado a proteínas, y un 80% del total está localizado en los cloroplastos (Young y Terry, 1982).

Sin embargo, a pesar de ser un elemento esencial, el Fe libre en la célula puede reaccionar con el oxígeno (Guerinot y Yi, 1994) y generar especies reactivas de oxígeno (ROS) que conducen a una situación de estrés oxidativo. Por este motivo, la homeostasis del Fe en la planta está finamente regulada a nivel de órgano, tejido y célula, con el fin de mantener un aporte suficiente de metal para el metabolismo, evitando al mismo tiempo niveles excesivos que pueden ser tóxicos para la planta. Para prevenir el daño oxidativo, el Fe se encuentra habitualmente acomplejado con compuestos de bajo peso molecular o unido a proteínas.

Presencia de Fe en el suelo

El Fe es el cuarto elemento más abundante de la corteza terrestre. Sin embargo, en suelos alcalinos y calcáreos el Fe se encuentra en forma de óxidos e hidróxidos de muy baja solubilidad, por lo que su disponibilidad para la planta es baja. En la figura 2 se muestra la solubilidad de los distintos minerales de Fe en función del pH. Diversos factores, incluyendo un pH elevado, altas cantidades de arcillas y carbonatos (Kashirad y Marschner, 1974), alta humedad, alta salinidad y altas cantidades de fosfatos (Lindsay y Schwab, 1982) generan una baja solubilidad y/o movilidad del Fe en la solución del suelo, y por lo tanto pueden causar deficiencia de Fe en plantas.

La deficiencia de Fe afecta a un alto porcentaje de las plantaciones de frutales en toda el área mediterránea (Sanz et al., 1992; Tagliavini et al., 2000). Esta deficiencia es el problema de explotación más importante desde el punto de vista técnico y económico en muchos frutales cultivados en esta zona, ya que, si la deficiencia no se corrige, el crecimiento de los árboles se ve afectado, la floración es más escasa y los frutos son menos numerosos y más pequeños, pudiéndose llegar en casos extremos a la muerte prematura del árbol. Sólo en la cuenca del Ebro se ha estimado en más de 13 millones de euros por año el gasto que suponen los tratamientos correctores de la clorosis férrica (Sanz et al., 1992).

Las plantas deficientes en Fe muestran diversos síntomas, entre los que el más clásico es el amarilleamiento de las hojas jóvenes denominado clorosis férrica (Terry y Abadía, 1986) que se debe a un cambio en la composición pigmentaria de los cloroplastos de las hojas (Morales et al., 1990, 1994; (Abadía y Abadía, 1993). En casos extremos, la hoja puede adquirir prácticamente color blanco, presentar necrosis y puede incluso provocar la muerte de la planta.

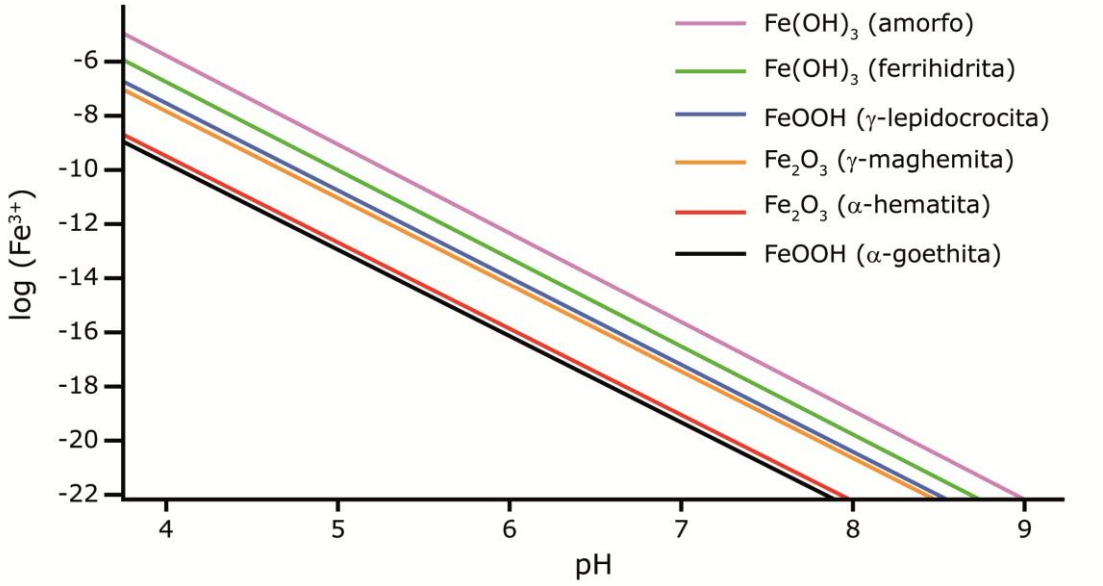

Fig. 2 Solubilidad de los principales minerales de Fe en el suelo en función del pH

Causas de la deficiencia de Fe

La deficiencia de Fe en la planta puede estar producida tanto por factores que afecten a su disponibilidad y absorción radicular como a su movilidad dentro de la planta, ya que el 80% del Fe absorbido se moviliza a las hojas.

La absorción a nivel radicular depende de las características del suelo. Factores como un elevado pH (Fig. 2), una estructura muy cristalina de los minerales de Fe, suelos aireados, una baja cantidad de agentes quelantes (Loeppert, 1986), alta salinidad (Award et al., 1988) y altas cantidades de fosfatos (Lindsay y Schwab, 1982) influyen negativamente en la solubilidad del Fe en el suelo y, por tanto, producen una disminución en su biodisponibilidad. Otros factores como la compactación del suelo y el encharcamiento (Chen y Bark, 1982; Chaney, 1984), las bajas temperaturas y los herbicidas (Chaney, 1984) pueden dificultar el desarrollo radicular, e influir de forma indirecta en la adquisición de Fe.

Otras causas que propician la aparición de deficiencia de Fe son aquellas que afectan a la movilidad del Fe en la planta una vez absorbido por la raíz. Se ha descrito que en frutales crecidos en el campo, el contenido en Fe de hojas de plantas deficientes en Fe puede ser similar o incluso algo superior al de las hojas verdes (Morales et al, 1998;

Römheld, 2000), y sin embargo, las hojas presentan un amarilleamiento en la zona internerval, síntoma de deficiencia de Fe. La alta concentración de Fe en hojas deficientes parece indicar que el Fe podría estar acumulado en una forma no utilizable por la planta. Se ha propuesto que los fosfatos y un elevado pH del apoplasto podrían provocar la precipitación del Fe en el exterior de las células impidiendo su utilización (Mengel y Geurtzen, 1986). Sin embargo, la explicación de éste fenómeno, conocido como la "paradoja de la clorosis férrica", está todavía por elucidar (Tomasi et al., 2009; Jimenez et al., 2009).

El bicarbonato es un factor que merece una mención especial, ya que afecta tanto a la absorción del Fe como a su actividad dentro de la planta. Los factores que favorecen la formación de bicarbonato, como la humedad alta del suelo, la compactación y el aporte de materia orgánica fresca, también son inductores de clorosis (Chaney, 1984). Todavía no se conocen con certeza las bases fisiológicas de la deficiencia de Fe en plantas inducida por una concentración alta de bicarbonato (Loeppert y Hallmark, 1985; Mengel, 1994), pero no parecen deberse ni al alto pH *per se* (Alhendawi et al., 1997) ni a la disminución en la disponibilidad fisiológica del Fe por precipitación en las hojas debido a la alcalinización del apoplasto y citoplasma (Romera et al., 1992; Mengel, 1994).

Adquisición de Fe por la raíz

Las plantas se pueden clasificar en dos grandes grupos en función de su mecanismo de adquisición de Fe por la raíz. La Estrategia I, o reductora, incorpora el Fe en forma de Fe(II), mientras que la Estrategia II, o quelante, adquiere el Fe en forma de quelato de Fe(III) (Fig. 3; (Abadía et al., 2011).

Las plantas pertenecientes a la Estrategia I, dicotiledóneas y monocotiledóneas no gramíneas, necesitan reducir el Fe antes de su adquisición. El mecanismo de adquisición consta de al menos tres componentes principales: una reductasa férrica de membrana perteneciente a la familia FRO (Ferric Reductase Oxidase) (Robinson et al., 1999), un transportador específico de Fe perteneciente a la familia ZIP (ZNT-IRT like protein) de transportadores de metales (AtIRT1, (Eide et al., 1996; Fox y Guerinot, 1998) y una H^+-ATPasa que disminuye el pH de la rizosfera (Santi y Schmidt, 2009).

Las plantas pertenecientes a la Estrategia II son las gramíneas. Las raíces de estas plantas sintetizan y excretan compuestos de bajo peso molecular, llamados fitosideróforos (PS), que son péptidos de aminoácidos no proteogénicos derivados del ácido mugineico. Estos fitosideróforos son excretados por transportadores específicos (HvTOM1, Transporter Of Mugineic acid family phytosiderophores 1, Noyoze et al., 2010) y debido a su alta afinidad por el Fe lo solubilizan de forma muy eficaz por quelación, produciendo complejos Fe(III)-fitosideróforo que son introducidos al interior de la raíz a través de un transportador específico situado en la membrana plasmática (ZmYS1; Yellow Stripe), sin que exista reducción previa (Curie et al., 2001; Von Wiren et al., 1994). Una vez dentro de la planta, se produce la liberación del Fe y el fitosideróforo se degrada o se excreta al exterior.

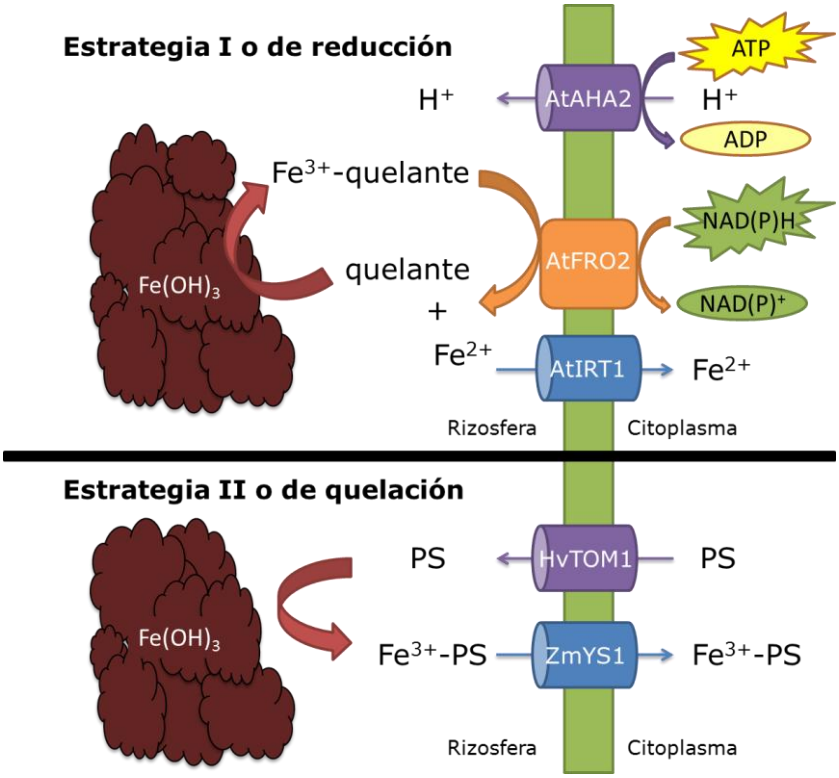

Fig. 3 Mecanismos de adquisición de Fe por la planta

Respuesta a la deficiencia de Fe

El mecanismo más conocido para mantener la homeostasis del Fe en caso de deficiencia consiste en la adaptación de los mecanismos de adquisición de Fe a las condiciones externas. En general, ante la deficiencia de Fe las plantas eficientes aumentan su capacidad de toma de Fe del suelo.

Mecanismos de adaptación en plantas de Estrategia I

En condiciones de deficiencia de Fe, las plantas de Estrategia I desarrollan una serie de respuestas que afectan a la fisiología y morfología de las raíces.

Cambios morfológicos

Los cambios morfológicos más destacados son un aumento del número de raíces laterales, un engrosamiento de las puntas apicales y en algunas especies un amarilleamiento de las raíces. Estos cambios morfológicos van encaminados al aumento de la superficie de contacto entre la raíz y el suelo, incrementando de esta forma la posibilidad de adquisición de Fe por la planta. Se produce una disminución en el crecimiento de la raíz primaria (Hutchinson, 1967; Brown y Ambler, 1978; Römheld y Marschner, 1981) acompañada por un aumento en el número de raíces laterales (Moog et al., 1995; Pinton et al., 1998). Estos cambios son evidentes después de un largo tiempo en

deficiencia de Fe, mientras que otros cambios macroscópicos como la formación de pelos radiculares (Schmidt, 1999) y el engrosamiento de las zonas subapicales de la raíz (Landsberg, 1982; López-Millán et al., 2000; Welkie y Miller, 1993) ocurren antes de que se observe una disminución en el crecimiento de la raíz. El engrosamiento de las puntas de raíz, que no se observa en todas las especies (Wei et al., 1997), es debido por una parte al aumento del tamaño de las células corticales y por otra a un incremento del número de células en la rizodermis e hipodermis. El engrosamiento de las raíces coincide espacialmente con aquellas zonas donde se produce la inducción en la reducción de Fe (Bell et al., 1988) y la extrusión de protones (Alcántara et al., 1991). Los cambios microscópicos consisten en la formación de células de transferencia, tanto en la rizodermis como en la hipodermis, aumentando así la superficie de contacto entre la pared celular y el citoplasma (Welkie y Miller, 1993).

Cambios fisiológicos

Además de los cambios morfológicos, se producen cambios en la fisiología de las raíces a nivel bioquímico para aumentar la eficiencia de la adquisición de Fe. Estos cambios incluyen una inducción de todos los mecanismos de adquisición de Fe de la Estrategia I: un aumento de la actividad reductasa férrica de la raíz, un aumento de la extrusión de protones (lo que conlleva una acidificación de la rizosfera) y un aumento en la expresión del transportador de Fe(II) de la familia ZIP (IRT). Junto a estos cambios en los componentes principales de la Estrategia I, muchas especies son capaces de exportar a la rizosfera pequeños compuestos de bajo peso molecular, incluyendo fenoles, ácidos orgánicos y flavinas, además de sufrir una reorganización de su metabolismo (Fig. 4).

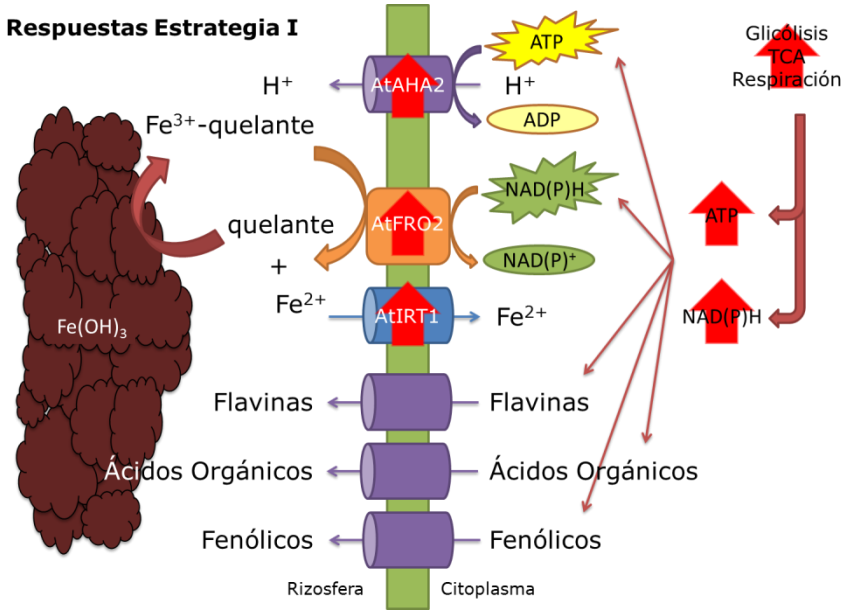

Fig. 4 Respuestas a la deficiencia de Fe en plantas de Estrategia I

Inducción de la actividad reductasa

En las plantas de Estrategia I, la reducción del Fe(III) en la membrana plasmática es un paso obligatorio antes de la adquisición y transporte de este microelemento al interior de la planta (Chaney et al., 1972). En deficiencia de Fe, la capacidad de reducción aumenta hasta alcanzar un máximo de actividad que varía, dependiendo de la especie, siendo en muchos casos entre 2 y 20 veces (López-Millán et al., 2000; Moog y Brüggemann, 1994; Susín et al., 1996). La reducción de Fe en raíces se ajusta a una cinética de tipo Michaelis-Menten con un pH óptimo para la reducción de Fe(III)-EDTA de 5,5 (Rosenfield et al., 1991; Schmidt y Janiesch, 1991), y una K_m que oscila entre 28 y 230 µM (Cornett y Johnson, 1991; Brüggemann et al., 1990). La actividad reductasa se localiza generalmente en la superficie de las partes subapicales de las raíces que muestran engrosamiento, así como en los pelos radiculares (Moog y Brüggemann, 1994).

En la mayor parte de las especies para las cuales se conoce el gen de la reductasa (*A. thaliana*, *Medicago truncatula*, *Solanum lycopersicum* o *Pisum sativum*) se ha descrito un aumento inducido por la deficiencia de Fe, tanto en la expresión del gen correspondiente en raíces como en la actividad de la enzima (Robinson et al., 1999; López-Millán et al., 2005; Li et al., 2004; Waters et al., 2002).

Transportador de Fe

Una vez que el Fe se ha reducido, éste debe ser transportado al interior de la raíz. Datos bioquímicos indican que este transporte muestra una cinética de tipo Michaelis-Menten y está inducido en condiciones de deficiencia de Fe (Cohen et al., 1998). Estudios moleculares en estos últimos años han caracterizado la familia de transportadores de metales ZIP, que actúa no sólo en el transporte de este elemento en la membrana plasmática de raíz sino también en su distribución dentro de la planta. El primer miembro identificado de esta familia como transportador de Fe, el gen AtIRT1, se caracterizó en *A. thaliana* (Eide et al., 1996, Vert et al., 2002). El AtIRT1 es un transportador de Fe(II) pero también puede transportar Mn(II), Zn(II), Cd(II) y Co(II) (Korshunova et al., 1999; Rogers et al., 2000). El gen se expresa en la epidermis de la raíz y su expresión se induce después de 1 ó 2 días de crecimiento en condiciones de deficiencia de Fe, pero cuando las plantas deficientes son sometidas a experimentos de adición de Fe la sobreexpresión desaparece en 12 - 24 horas, evitando la acumulación perjudicial del metal y manteniendo así su homeostasis en la planta (Connolly et al., 2002). Además de esta regulación, la expresión del gen también está sujeta a una regulación post-traduccional por ubiquitinación (Kerkeb et al., 2008).

Genes homólogos han sido caracterizados en guisante (PsIRT1: Cohen et al., 1998) y tomate (LeIRT1 y LeIRT2: Eckhardt et al, 2001). Todos ellos se expresan en raíz, pero sólo PsIRT1 y LeIRT1 se inducen por deficiencia de Fe.

Acidificación de la rizosfera

La solubilidad del Fe en el suelo depende principalmente del pH, disminuyendo más de 1000 veces por cada aumento de unidad de pH (Fig. 1). Por lo tanto, debilitar el enlace Fe-O por acidificación de la rizosfera es un método eficiente para incrementar la disponibilidad de Fe. La excreción neta de protones en deficiencia de Fe ha sido descrita en muchas especies (girasol, remolacha, pepino, tomate) y ha sido atribuida a un aumento de la actividad ATPasa de la membrana plasmática (Römheld et al., 1984; Susín et al., 1994; Dell'Orto et al., 2000; Schmidt et al., 2003). En raíces de tomate, la cantidad de la proteína H^+-ATPasa aumenta principalmente en las células de transferencia formadas en la rizodermis bajo condiciones de deficiencia de Fe (Schmidt et al., 2003). Recientemente se ha descrito que en *Arabidopsis* el gen responsable de esta acidificación es el AtAHA2 (Santi y Schmidt, 2009).

El aumento de la excreción de protones podría tener otras funciones, además de aumentar la solubilidad del Fe en la rizosfera. La afinidad del quelato de Fe por la reductasa aumenta en condiciones de pH bajo, probablemente debido a una neutralización de las cargas negativas superficiales del sitio de reducción, que podría evitar la repulsión de los quelatos de Fe cargados negativamente (Schmidt y Janiesch, 1991; Cohen et al., 1997).

Excreción de compuestos de bajo peso molecular

Muchas plantas de Estrategia I son capaces, cuando se encuentran en condiciones de deficiencia de Fe, de acumular y/o excretar, ya sea de forma activa o pasiva, gran variedad de compuestos orgánicos, incluyendo ácidos orgánicos, flavinas, compuestos fenólicos, azúcares reductores y aminoácidos (Abadía et al. 2002; Cesco et al. 2010; Jin et al. 2007; Ohwaki & Sugahara 1997; Rodríguez-Celma et al. 2011). Las cantidades excretadas pueden suponer hasta un 20% del carbono asimilado. Algunos de estos compuestos tienen características redox o capacidades acomplejantes de metales que pueden mejorar la disponibilidad del Fe tanto en la rizosfera como en el apoplasto (Cesco et al. 2010; Ishimaru et al. 2011; Jin et al. 2007).

Entre los compuestos fenólicos identificados en exudados se encuentran los ácidos caféico, p-cumárico (Olsen et al., 1981), y clorogénico (Hether et al., 1984). Recientemente se ha descrito en un estudio proteómico una fuerte inducción de la ruta de biosíntesis de los fenilpropanoides en deficiencia de Fe (Lan et al., 2011). Inicialmente se atribuyó a estos compuestos fenólicos una función reductora de Fe(III). Sin embargo, diversos estudios mostraron que las cantidades excretadas no son suficientes para explicar la tasa de reducción encontrada en las plantas deficientes (Chaney et al., 1972; Barret-Lennard et al., 1983; Bienfait et al., 1983), y que la adición de estos compuestos no afecta sino que incluso disminuye la actividad reductasa de Fe(III)-EDTA de las raíces (Römheld y Marschner, 1983). Probablemente el papel principal de los compuestos

fenólicos consista en la inhibición de la degradación de los ácidos orgánicos, cuyo papel en la nutrición férrica como quelantes de Fe es muy importante (Schmidt, 1999). Una función alternativa de estos compuestos podría estar relacionada con la pérdida de suberina, recubrimiento protector de las células corticales de la raíz, que presentan las raíces deficientes en Fe (Sijmons et al., 1984a). También se ha mostrado su papel en la remobilización del Fe apoplástico (Jin et al. 2007), hecho que ha sido apoyado por la reciente identificación del transportador OsPEZ1 (Ishimaru et al., 2011).

En condiciones de deficiencia de Fe, las plantas dicotiledóneas acumulan en las raíces y exportan ácidos orgánicos, principalmente citrato y malato (Brown, 1966; de Vos et al., 1986; Brancadoro et al., 1995). Debido a que poseen grupos carboxílicos, los ácidos orgánicos pueden acomplejar metales de la solución del suelo. Gracias a estas propiedades están implicados en un gran número de procesos relacionados con la movilización y toma de nutrientes (p. ej. Fe y P) por las plantas y microorganismos, la desintoxicación de metales por las plantas (p. ej. Zn y Al), la proliferación de microorganismos en la rizosfera y la disolución de minerales del suelo (Jones, 1998). En condiciones de deficiencia de Fe, la función más probable de estos ácidos consiste en la solubilización de Fe(III). Cuando el pH del suelo es bajo, tanto citrato como malato forman complejos estables con el Fe(III) favoreciendo su disolución en la solución del suelo (Jones et al., 1996). En suelos calcáreos, con pH alto, la movilización del Fe por malato y citrato es lenta, puesto que los complejos que se forman son inestables y se degradan rápidamente (Jones et al., 1996; Gerke, 1997). Sin embargo, en estas condiciones, la combinación del poder de acidificación de la ATPasa de la raíz con el poder acomplejante del citrato (que aumenta conforme disminuye el pH) podrían constituir un mecanismo viable para movilizar el Fe de la rizosfera (Jones, 1998). La excreción de estos ácidos orgánicos puede ocurrir por difusión pasiva, gracias al gradiente de potencial electroquímico de la membrana plasmática (Jones y Darrah, 1995). Sin embargo, también se ha sugerido la posible existencia de canales o transportadores acoplados con la ATPasa de la membrana plasmática (Dinkelaker et al., 1995; Fox et al., 1996), y recientemente se han identificado miembros de la familia MATE (Multidrug And Toxic compound Extrusion) que podrían estar también involucrados en este trasporte (Furukawa et al., 2007; Piñeros et al., 2007; HUeng et al., 2009).

Antes incluso de que se describieran los mecanismos de la Estrategia I, se observó el amarilleamiento tanto de raíces como de soluciones nutritivas de plantas deficientes en Fe (Frolich & Wallace 1966; Nagarajah & Ulrich 1966; Pound & Welkie 1958; Wallace 1971; Weinstein, Robbins & Perkins 1954). La flavina mayoritaria encontrada fue la riboflavina (Kannan y Seshyri, 1988; Shinmachi et al., 1994, 1995; Welkie, 1996) y posteriormente, en algunas plantas como remolacha y espinaca, se describió la presencia de sulfatos de riboflavina (Susín, 1994; Susín et al., 1993, 1994). A pH alto, las flavinas se acumulan en la zona subapical de la raíz (Susín et al., 1993), mientras que a pH bajo se exportan al medio de crecimiento (Susín et al., 1994a,b). Las plantas que producen flavinas, como por ejemplo remolacha (Welkie y Miller, 1988; Susín et al., 1993, 1994; Susín, 1994), tabaco (Welkie y Miller, 1988), lechuga (Welkie y Miller, 1992), melón y

alfalfa (Rodríguez-Cema et al., 2011a,b), pimiento (Shinmachi et al., 1995), y pepino (Shinmachi et al., 1992) son generalmente muy eficientes en la adquisición de Fe (Welkie y Miller, 1993), aunque no parecen estar distribuidas en una ordenación taxonómica evidente (Welkie, 2000).

El papel de las flavinas en la deficiencia de Fe es todavía desconocido. Sin embargo, el hecho de que la acumulación de flavinas sea concomitante con el aumento de la actividad reductasa sugiere que estos compuestos podrían ser parte integral de los sistemas de reductasa férrica de las raíces (Cakmak et al., 1987; Susín et al., 1993). Además, el gen de la reductasa férrica pertenece a la familia de los flavocitocromos y contiene un sitio de unión a FAD (Robinson et al., 1999). Otra posible función de los compuestos flavínicos, una vez excretados a la rizosfera, podría ser una acción antimicrobiana en la rizosfera, disminuyendo la posibilidad de que los microorganismos del entorno compitan con la planta por la adquisición de Fe. Los compuestos flavínicos también podrían inducir una mejora de la adquisición de Fe, mejorando su biodisponibilidad (Jordan, Wakeman & DeVay 1992; Susín et al. 1993; Yang et al. 2002).

Reorganización del metabolismo

La respuesta a la deficiencia de Fe es más compleja que la simple activación del mecanismo de adquisición de Fe por la raíz, ya que también se producen cambios metabólicos a nivel de planta entera, dirigidos a potenciar las actividades enzimáticas implicadas en la adquisición, transporte y utilización de Fe.

Para mantener la activación de los procesos de reducción y excreción de protones bajo condiciones de deficiencia de Fe, es necesario incrementar las tasas de regeneración de NAD(P)H y ATP. Tanto la proporción NADPH:$NADP^+$ (Sijmons et al., 1984; Schmidt y Schuck, 1996) como la concentración de ATP (López-Millán et al., 2000a; Espen et al., 2000) son más altas en condiciones de deficiencia de Fe en especies como judía, *Plantago lanceolata*, remolacha y pepino. Se ha demostrado también, que después de la adición de compuestos férricos aumenta el estado oxidado de los pares NADH/NAD^+ y NADPH/$NADP^+$ en plantas de judía (Sijmons et al., 1984b) y *P. lanceolata* (Schmidt y Schuck, 1996) crecidas en deficiencia de Fe. En condiciones aeróbicas, la recarga de estos substratos requiere la aceleración del metabolismo unido a la ruta respiratoria. De este modo, se ha demostrado que la tasa de oxígeno incorporado por las raíces aumenta en deficiencia de Fe (López-Millán et al., 2000a; Espen et al., 2000), aunque es difícil asociar esta mayor utilización de oxígeno únicamente a la cadena oxidativa de transporte electrónico, ya que también están presentes rutas oxidativas alternativas (López-Millán et al., 2000a). Asimismo, parte del oxígeno podría estar siendo utilizado directamente por la reductasa férrica cuando las plantas crecen en completa ausencia de Fe. Observaciones por microscopía electrónica de segmentos apicales de raíz mostraron que el número de mitocondrias aumenta en secciones de puntas deficientes (Landsberg, 1994; Dell'Orto et al., 2002; Schmidt et al., 2003). El aumento en el consumo de oxígeno podría estar por tanto asociado al aumento en el número de

mitocondrias y no al incremento de su actividad. Además, la deficiencia de Fe provoca una disminución de la cantidad de enzimas que contienen Fe, entre ellas varias pertenecientes a la cadena transportadora de electrones mitocondrial. Por ello, se ha propuesto la existencia de un sistema oxidativo alternativo en la membrana mitocondrial que compensaría el par NAD(P)H/NAD(P) (Vigani et al., 2010).

Por otro lado, en condiciones de Fe limitado, algunas enzimas asociadas con el metabolismo anaeróbico como la lactato deshidrogenasa y la piruvato descarboxilasa presentan un incremento en su actividad (López-Millán et al., 2000a). Este comportamiento ha sido apoyado por análisis de microarrays (Thimm et al., 2001), que muestran una inducción de las enzimas de metabolismo anaeróbico lactato deshidrogenasa, piruvato descarboxilasa y alcohol deshidrogenasa. Estos resultados podrían interpretarse como un sistema de by-pass para mantener el flujo de carbono y la producción de energía por reacciones glicolíticas cuyo factor limitante parece ser el oxígeno.

La glucosa es la principal fuente para la síntesis de substratos energéticos y para el aporte de esqueletos carbonados a las raíces. En un tejido metabólicamente activo, el aporte de glucosa viene bien de la traslocación de fotosintatos desde la parte aérea o bien de la degradación del almidón almacenado en raíces. Esto ocurre, por ejemplo, en judía (de Vos et al., 1986) donde la concentración de azúcares en el floema de plantas deficientes es doble con respecto al control. También en raíces de pepino deficientes en Fe se ha descrito una disminución en la concentración de almidón, que ocurre al mismo tiempo que un aumento en la concentración de carbohidratos sencillos, principalmente glucosa-6-fostato y, en menor extensión, fructosa-6-fosfato (Espen et al., 2000). Además, la actividad de enzimas participantes en la glicólisis, como la gliceraldehido-3-fosfato deshidrogenasa (Sijmons y Bienfait, 1983; Rabotti et al., 1995; Espen et al., 2000), la piruvato quinasa y la fructosa-6-fosfato quinasa (Espen et al., 2000), también aumentan en deficiencia de Fe. Estos resultados parecen indicar que la adaptación a la deficiencia de Fe implica, por parte de las raíces, una activación de las reacciones glicolíticas y una disminución de la síntesis de carbohidratos. La activación de la glicólisis proporciona una serie de elementos necesarios para la activación de las respuestas características de la Estrategia I (ATP para mantener el aumento de actividad de la ATPasa, equivalentes de reducción para la reductasa férrica y fosfoenolpiruvato) y, finalmente, contribuye a la regulación del pH citosólico.

Además, otras rutas metabólicas y actividades enzimáticas citosólicas, encaminadas a aumentar la producción de equivalentes reductores necesarios para mantener el aumento de actividad de la reductasa férrica, también están activadas durante la deficiencia de Fe. Así, se han encontrado aumentos de actividad en deficiencia de Fe en la enzima glucosa-6-fosfato deshidrogenasa (G6PDH), perteneciente a la ruta de las pentosas fosfato (Sijmons y Bienfait, 1983; Rabotti et al., 1995; López-Millán et al., 2000a), la malato deshidrogenasa (Sijmons y Bienfait, 1983; Rabotti et al., 1995, López-Millán et al., 2000a), y la isocitrato deshidrogenasa (ICH) (López-Millán et al., 2000a).

Entre las actividades metabólicas que están aumentadas en deficiencia de Fe, la fosfo*enol*piruvato carboxilasa (PEPC) merece una mención especial, ya que, en muchos casos, su activación no sólo es comparable sino aún mayor que la de otras respuestas características de la Estrategia I, como por ejemplo la actividad reductasa férrica. La PEPC es una enzima muy abundante en plantas y cataliza la fijación de bicarbonato a fosfo*enol*piruvato para producir oxalacetato y fósforo inorgánico. En plantas C3 y tejidos no fotosintéticos, la PEPC actúa como fuente anaplerótica de intermediarios para el ciclo de Krebs y de esqueletos carbonados para la síntesis de aminoácidos, así como en la regulación del pH citosólico. En condiciones de deficiencia de Fe, la actividad de la enzima PEPC aumenta 4 veces en raíces de pepino (De Nisi y Zocchi, 2000) y 60 veces en puntas amarillas de raíz de remolacha (López-Millán et al., 2000a). Este aumento en la actividad puede ser debido a tres factores: a una alta regulación alostérica de la enzima similar a la descrita en otros casos (Chollet et al., 1996), a un aumento de la cantidad de la proteína (De Nisi y Zocchi, 2000, Andaluz et al., 2002), y a una posible inducción de la transcripción no estudiada hasta el momento.

El aumento de la actividad PEPC en raíz de pepino deficiente en Fe ocurre principalmente en las capas externas de las células corticales que, a su vez, son muy activas en la extrusión de protones (De Nisi et al., 2002). Así mismo, el aumento en la actividad PEPC coincide con una acumulación de ácidos orgánicos en las raíces deficientes (López-Millán et al., 2000a; Abadía et al., 2002). La activación de la PEPC produce un aumento en la concentración de oxalacetato y/o malato, y estos compuestos son utilizados como fuente de carbono en el ciclo de Krebs. Esta función anaplerótica de reposición de intermediarios del ciclo de Krebs es importante para producir tanto ATP como ácidos orgánicos (LMWOA) que son exportados desde la mitocondria al citosol. Los LMWOAs pueden realizar distintas funciones: pueden ser liberados a la rizosfera y utilizados posteriormente para facilitar la adquisición de Fe del suelo mediante la formación de complejos LMWOA-metal, y/o pueden ser trasportados hacia el xilema, donde también podrían acomplejar Fe, facilitando así su transporte a la parte aérea (Tiffin, 1966; López-Millan et al., 2000b; Rellán-Álvarez et al., 2010). En las hojas cloróticas, los ácidos orgánicos podrían ser utilizados también como fuente anaplerótica de carbono para mantener procesos básicos como la respiración y el crecimiento (Abadía et al., 2002), ya que se ha descrito que la fotosíntesis en estas hojas deficientes en Fe está muy afectada (Terry, 1980).

Estrategia II

En especies de Estrategia II cultivadas en condiciones de deficiencia de Fe, la producción y excreción de fitosideróforos aumenta y la tolerancia a la deficiencia de este elemento se relaciona con la cantidad y clase de fitosideróforo secretado.

Los fitosideróforos son derivados del ácido muginéico (Takagi, 1976). El paso inicial de su síntesis, catalizado por la nicotianamina sintasa (NAS), consiste en la condensación de tres moléculas de S-adenosil metionina para producir una molécula de nicotianamina (NA). Aunque la síntesis de NA se produce tanto en plantas de Estrategia I como II, los pasos siguientes hasta la obtención de los distintos ácidos muginéicos son específicos para las plantas de Estrategia II (Curie y Briat, 2003). La actividad de las enzimas nicotianamina sintasa (NAS) y nicotianamina aminotransferasa (NAAT), primer y segundo enzima de la ruta biosintética, aumenta en raíces de cebada deficientes en Fe (Mori, 1999), al igual que lo hace la expresión de los genes de cebada que codifican tanto los enzimas de la ruta biosintética de los ácidos muginéicos como algunos factores de transcripción asociados: Hvnas1-7, naatA, naatB, ids2 e ids3 (Higuchi et al., 1999; Nakanishi et al., 1993; Okumura et al., 1994; Takahashi et al., 1999).

Se ha demostrado que los fitosideróforos se exportan como aniones monovalentes (Sakaguchi et al.,1999), probablemente a través de canales aniónicos o mediante exocitosis. Muy recientemente se ha descrito un primer transportador de membrana plasmática de fitosideróforos, TOM1, que se sobreexpresa en deficiencia de Fe y cuya sobre-expresión produce un aumento constitutivo en la excreción de fitosideróforos, independientemente del estatus de Fe de las plantas (Nozoye et al., 2011).

La expresión del gen YS1 está incrementada en condiciones de deficiencia de hierro, tanto en la raíz como en la parte aérea. La acumulación de mRNA del gen YS1 en la parte aérea de la planta en deficiencia de Fe sugiere otra posible función del transportador YS1 en el transporte de Fe a lo largo de la planta (Curie y Briat, 2003). YS1 funciona como un transportador de complejos PS-metal, incluídos Fe(III), Zn(II), Cu(II), y Ni(II) (Schaaf et al., 2004).

Búsquedas de secuencias homólogas a YS1 en *A. thaliana* han demostrado la existencia de 8 secuencias con alta homología a YS1 (alrededor del 80%). Se les ha llamado YSL (Yellow-Stripe-Like) y se han clasificado dentro de la misma subclase de la familia OPT (Curie et al., 2001; Yen et al., 2001). Este descubrimiento es sorprendente, ya que *A. thaliana* pertenece a las plantas de Estrategia I y entre las plantas superiores sólo las gramíneas sintetizan y excretan fitosideróforos, el substrato del transportador YS1. Dado que todas las plantas producen nicotianamina (NA), y esta molécula es muy similar tanto en estructura como en su capacidad para unir Fe a los fitosideróforos, se podría especular con una posible función transportadora de complejos Fe-NA de las proteínas YSL en plantas no gramíneas. Además, la NA se ha encontrado en el floema, dónde es probable que forme complejos con varios metales, incluyendo Fe, Zn, Ni y Cu,

participando en la homeostasis de estos metales a distintos niveles: transporte a larga distancia, compartimentalización o señalización del contenido de metales (Stephan et al., 1994; Pich et al., 1994).

Las estrategias de reducción o quelación para la adquisición de Fe por parte de la planta no son mutuamente excluyentes. Se ha visto que en condiciones de deficiencia tanto arroz como cebada aumentan la adquisición de Fe en forma de Fe(III)-PS, pero también aumentan la expresión del transportador de Fe(II), el IRT1 (Ishimaru et al., 2007; Pedas et al., 2008). A pesar de ello, el arroz no puede llevar a cabo la reducción del Fe(III), lo que sugiere que la expresión de IRT1 se debe más a una adaptación a las condiciones del suelo, inundados y pobres en oxígeno, donde los niveles de Fe(II) libre pueden ser altos (Walker y Connolly, 2008). El hecho de que el transportador AtYSL3 se sobreexprese en raíces de *A. thaliana* en deficiencia de Fe (Dinneny et al., 2008), podría sugerir la adquisición directa de complejos de Fe por parte de plantas de Estrategia I.

Proteómica

Proteómica

La proteómica se encarga del estudio del proteoma, que es el conjunto de proteínas expresadas por un organismo, o parte de él, en un momento dado (Wilkins et al., 1996). El proteoma, al contrario que el genoma, tiene un carácter dinámico, ya que la expresión de proteínas cambia en diferentes etapas del ciclo celular y también en respuesta al entorno (Fijéis, 2003). En lugar de la caracterización de proteínas individuales, como ocurre con las técnicas bioquímicas clásicas, las técnicas proteómicas se dirigen al estudio del sistema dinámico, interactivo y complejo del conjunto de proteínas. El enfoque consiste en el análisis de una mezcla muy compleja de proteínas y va dirigido al análisis masivo de datos. El grado de complejidad del proteoma puede ser mucho mayor que el del genoma o transcriptoma, ya que en él influyen también la localización subcelular, fenómenos de "splicing" alternativo, así como diversas interacciones (proteína-proteína, proteína-RNA, proteína-DNA…) y modificaciones post-traduccionales (fosforilación, alquilación, glicosilación…) (Peng y Gygi, 2001).

El rápido desarrollo de la proteómica se ha hecho posible gracias al progreso en la instrumentación analítica, especialmente en espectrometría de masas (MS, de "mass spectrometry"), con la introducción de espectrómetros de masas cada vez más potentes, y las mejoras en las técnicas de ionización suave. No menos importantes son los avances tecnológicos y metodológicos en la separación de proteínas y péptidos, así como en la reducción de la complejidad de las muestras, que se lleva a cabo, principalmente, por técnicas de cromatografía líquida y electroforesis. La bioinformática es la otra gran herramienta responsable del avance de la proteómica, gracias a su cada vez mayor capacidad para recolectar, almacenar, procesar y visualizar la gran cantidad de datos que se generan en los estudios proteómicos.

Se pueden diferenciar, según su objetivo, dos grandes tipos de estudios proteómicos. Por un lado, los estudios denominados de mapeo son aquellos en los que el objetivo final es la caracterización e identificación del mayor número posible de las proteínas presentes en nuestro objeto de estudio. Por otro lado, en los estudios denominados de proteómica diferencial el objetivo no es caracterizar la totalidad de la población proteica, sino la fracción de esa población que responde de modo diferencial en nuestro sujeto de estudio a dos o más situaciones diferentes. Así, podemos caracterizar tanto respuestas a factores externos (estrés abiótico o biótico, enfermedad…) como internos (genotipos, variedades…). Esta comparación provee la información necesaria sobre las interacciones de proteínas específicas, sus funciones, y las fluctuaciones que pueden jugar un papel importante en el sistema celular. La coordinación de esta información proteómica con la obtenida mediante técnicas de genómica y metabolómica puede proporcionar una comprensión holística del sistema biológico en estudio (McCormack, 2005).

Para llevar a cabo un estudio de proteómica diferencial debemos cumplir una serie de requisitos. En primer lugar, es necesario obtener perfiles proteicos reproducibles y

cuantificables, ya sea de modo relativo (lo más común) o absoluto. Se necesitan un elevado número de réplicas, para que, a pesar de la alta variabilidad inherente a los sistemas biológicos, se puedan observar diferencias estadísticamente relevantes. Una vez conseguido esto, es necesario identificar las proteínas de interés e inferir su relevancia biológica.

Para cumplir todos estos objetivos es necesario un buen fraccionamiento de la muestra, dado que el número de especies proteicas es muy elevado, por lo que se necesitan técnicas de alta resolución.

Técnicas proteómicas de alta resolución

En los experimentos de proteómica diferencial hay dos aproximaciones bien diferenciadas. La más clásica es la que utiliza la electroforesis en gel como método de separación de las proteínas de una muestra, y la segunda es la que se basa en la cromatografía líquida multidimensional para conseguir la separación. El objetivo final de ambas técnicas es conseguir separar los componentes proteicos de la muestra de tal modo que puedan ser cuantificados e identificados por las técnicas de espectroscopía de masas, e inferir de estas identificaciones la respuesta biológica estudiada (Fig. 5). Ambas aproximaciones tienen sus ventajas e inconvenientes.

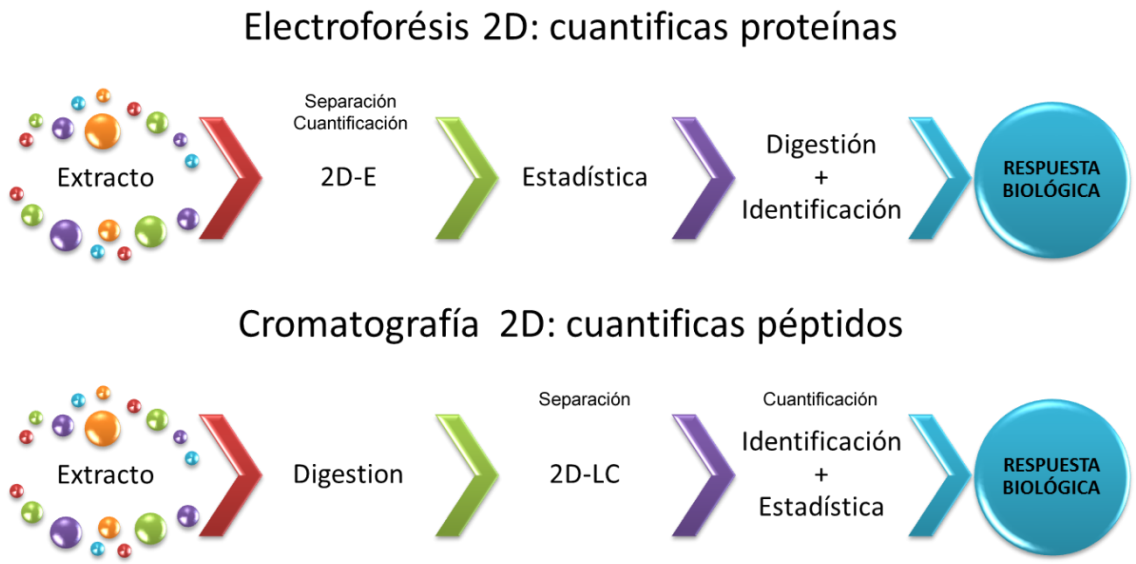

Fig. 5 Flujo de trabajo de las técnicas proteómicas según su método de separación

Técnicas electroforéticas: Electroforesis Bidimensional

La electroforesis bidimensional es una metodología con gran poder resolutivo, que se utiliza con frecuencia para la identificación de proteínas en mezclas complejas. Existen gran variedad de protocolos de electroforesis bidimensional, aunque el más ampliamente

utilizado es el llamado 2-DE, que se basa en separar las proteínas por su punto isoeléctrico y su peso molecular. En la primera dimensión se separan las proteínas de acuerdo a su punto isoeléctrico (pI), por medio de un proceso de isoelectroenfoque (IEF). En una segunda dimensión se separan las proteínas por su masa molecular, mediante una electroforesis en geles de poliacrilamida en presencia de un potente detergente aniónico, SDS (SDS-PAGE).

Las proteínas se cuantifican en el mismo gel mediante tinciones o métodos de marcaje que permiten llevar a cabo un análisis cuantitativo basado en la intensidad de su señal. Cada mancha ("spot") resultante corresponde, al menos, a una proteína en la muestra (Fig. 6). Aquellas que presentan interés por sus cambios relativos en los distintos tratamientos pueden ser detectadas en el gel, extraídas del mismo e identificadas mediante análisis de MS.

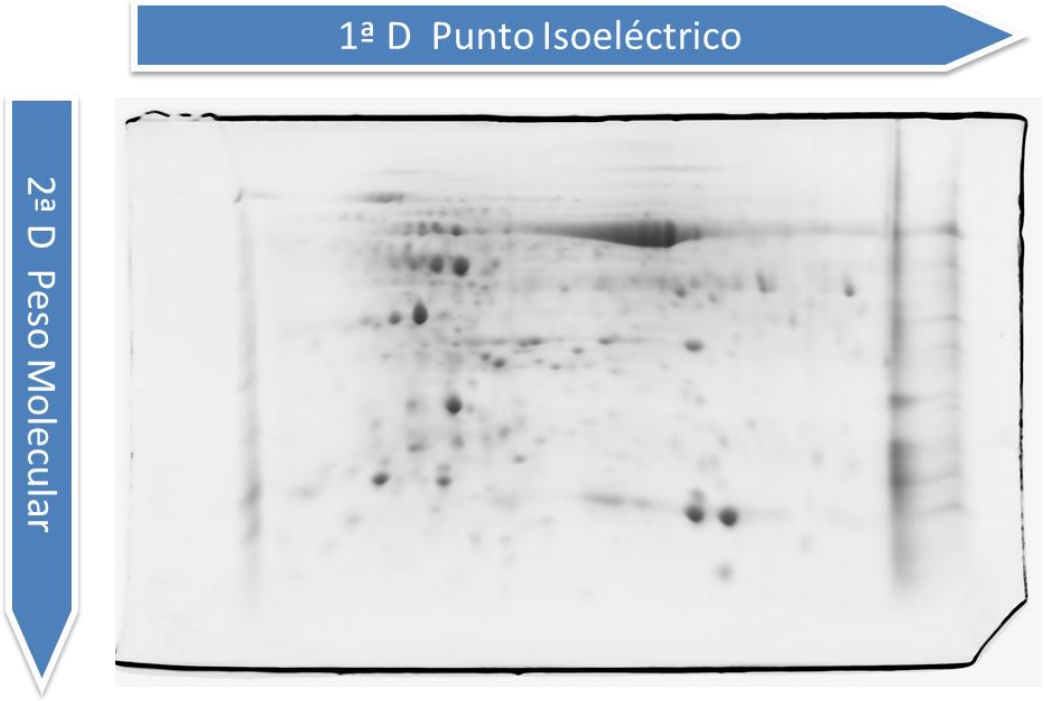

Fig. 6 Separación de proteínas por 2DE

Las proteínas presentes en las bases de datos abarcan aproximadamente un rango de pI entre 3 y 13, y de peso molecular entre 1 y 500 kDa. Sin embargo, cerca de un 80% de las proteínas se sitúan en un margen más estrecho, entre 3,5 y 10 de pI y entre 10 y 100 kDa de masa, que es el margen habitualmente presente en los geles bidimensionales. Se sabe que la resolución de las proteínas por 2-DE aumenta a medida que la cantidad de proteínas aplicada disminuye (Fey y Larsen, 2001). Esto puede ser un problema para la visualización de proteínas minoritarias en el extracto, que quedarían apantalladas por las más abundantes.

La 2-DE presenta diversas ventajas que explican su popularidad en los estudios proteómicos. Entre otras destaca el hecho de que permite una visualización directa del proteoma estudiado, a diferencia de los métodos de fraccionamiento cromatográfico. Ello permite la identificación de isoformas proteicas y sus modificaciones post-traduccionales, así como la comparación con otros mapas proteicos existentes en las bases de datos. La resolución de los geles 2-DE es suficiente para detectar unas 2.000 proteínas de manera individual, dependiendo del tamaño de los geles y de otros factores. El uso de geles de electroforesis de gran tamaño, así como la múltiple superposición de distintos gradientes inmovilizados de pH (IPG, Immobilized pH gradients), permiten la identificación de entre 5.000 y 10.000 proteínas en algunos casos (Gorg et al., 2004; Wittmann-Liebold et al., 2006). El desarrollo de los IPG eliminó gran parte de las limitaciones que presentaban los geles 2-DE basados en anfolitos portadores, tales como la baja reproducibilidad o la dificultad de detección de proteínas muy ácidas, básicas o de baja abundancia (Bjellqvist et al., 1982; Gorg et al., 2004).

La principal desventaja de la técnica 2-DE radica en la dificultad de solubilización en la primera dimensión IEF de proteínas altamente hidrofóbicas, tales como las intrínsecas de membrana (Gorg et al., 2000; Paulsen et al., 1998). Se estima que el 30% de las proteínas totales de una célula son de membrana, y solamente alrededor de un 1% de ellas han sido identificadas en geles 2-DE (Garrels et al., 1997). La solubilización de este tipo de proteínas ha mejorado enormemente con el uso de mejores detergentes (Molloy, 2000; Komatsu 2008), aunque su solubilización parece depender del número de hélices transmembrana que posean (Nouri y Komatsu, 2010). Se han desarrollado otras técnicas de separación bidimensional en gel para proteínas de membrana y/o complejos proteicos, como la Blue Native PAGE (BN-PAGE). Esta técnica aprovecha la capacidad del azul de Coomasie para conferir cargas negativas a los complejos de membrana, manteniéndolos solubles e intactos en una primera separación electroforética nativa, que luego se completa con una desnaturalizante clásica. Esta técnica se ha usado con éxito para la caracterización proteómica de cloroplastos (Herranen et al., 2004; Rexroth et al., 2003; Kügler et al., 1997; Suorsa et al., 2004; Thidholm et al., 2002; Ciambella et al., 2005; Heinemeyer et al., 2004), tilacoides (Andaluz et al., 2006) y mitocondrias (Klodmann et al., 2011). Por ello, generalmente las poblaciones estudiadas por 2-DE están sesgadas hacia las moléculas más hidrofílicas, mientras que las proteínas hidrofóbicas se analizan preferentemente mediante combinaciones de técnicas cromatográficas y de SDS-PAGE o mediante su previa digestión tríptica.

No obstante las limitaciones descritas, la electroforesis bidimensional tiene una gran capacidad resolutiva (Klose and Kobalz, 1995), y es de coste moderado, por lo que aún es la técnica más usada para el análisis de proteomas, tanto en la identificación de proteínas como en estudios de proteómica comparativa.

Tinción de los geles

Convencionalmente, las proteínas pueden ser teñidas con Coomassie Blue G-250 y R-250 (Neuhoff et al., 1988; Candiano et al., 2004), plata (Rabilloud et al., 1994; Chevallet et al., 2008), o mediante fluorescencia (como por ejemplo usando la tinción de SYPRO Ruby o los fluorocromos CyDye). Varios autores han comparado en detalle distintos métodos de tinción de proteínas disponibles (Miller et al., 2006; Patton, 2002).

Los métodos de tinción a base de Coomassie (Fakezas et al., 1963) y plata (Switzer et al., 1979) fueron desarrollados mucho antes de la actual era post-genómica, y aún hoy permanecen como técnicas rutinarias con las que detectar proteínas en los geles 2-DE. El reactivo Coomassie es un colorante textil de triarilmetano que se une a los grupos amino de las proteínas en solución ácida. Los beneficios de esta tinción son su fácil uso, bajo coste y la alta compatibilidad que presenta con el análisis de MS. La tinción de Coomassie se ha optimizado en gran medida, tanto para reducir el ruido de fondo producido por su unión a señales inespecíficas, como para mejorar su sensibilidad y rango lineal de detección (Candiano et al., 2004; Rabilloud et al., 1994; Diezel et al., 1972; Neuhoff et al., 2005). Sin embargo, tanto su sensibilidad como su rango lineal siguen siendo sus principales limitaciones, además de la dificultad para controlar la reproducibilidad de la tinción entre distintos geles (Patton, 2002).

La tinción de plata normalmente se lleva a cabo mediante uso de nitrato de plata y formaldehído revelado en una solución de carbonato alcalino, aunque existen muchos protocolos alternativos (Rabilloud, 1990). La tinción de plata es un método relativamente sensible que permite la detección de cantidades de proteínas del orden de 1 ng, si bien con este método de tinción se han detectado hasta niveles de 0,1 ng (Heukeshoven and Dernick, 1988). El estrecho rango lineal es la mayor desventaja de la tinción de plata, por lo que en caso de necesitar resultados cuantitativos no la hacen una técnica muy fiable (Patton, 2002) y generalmente se limita a estudios cualitativos o de mapeo. Además, la reacción de tinción tiene que ser parada en un tiempo arbitrario de exposición con el fin de prevenir una sobresaturación de la señal, lo que produce problemas en la reproducibilidad de los geles teñidos (James et al., 1993). La tinción de plata también interfiere con el análisis de MS posterior.

El desarrollo de marcadores fluorescentes ha mejorado de manera dramática la cuantificación de proteínas en geles 2-DE (Patton, 2002; Patton and Beechem, 2002), incrementándose tanto el rango dinámico de la cuantificación, como la reproducibilidad de las tinciones. Las proteínas se marcan con la señal fluorescente antes o después de la electroforesis y se detectan tras ser excitadas mediante el uso de luz ultravioleta o láser. Existen gran variedad de tinciones fluorescentes (SYPRO, Flamingo red, Deep Purple, etc.), que son tan sensibles como lo es la tinción de plata, pero ofrecen un rango dinámico lineal más amplio y son compatibles con MS (López et al., 2000). El problema es que no son visibles al ojo humano y requieren de equipamiento específico y muy costoso.

Las características principales de cada tinción están recogidas en la tabla 1, donde se especifica la sensibilidad, rango lineal y compatibilidad con las técnicas de espectroscopía de masas de cada una de ellas.

Método de Tinción	Sensibilidad	Rango lineal	Compatibilidad con MS
Coomassie	50 ng	50-500 ng	++++
Coomassie coloidal	10 ng	10-500 ng	++++
Tinción de Plata	0,1-1 ng	1-10 ng	+
Tinción Fluorescente	0,1-1 ng	1-1000 ng	++++

Tabla 1 Características de los métodos de tinción más habituales

Otra opción para detectar proteínas en geles de electroforesis es el uso de los fluorocromos derivados de la cianina CyDye, utilizados en el método conocido como gel de electroforesis diferencial (DIGE, Difference gel electrophoresis) (Tonge et al., 2001; Unlu et al., 1997). Las proteínas son marcadas antes de la 2-DE y se pueden analizar hasta tres muestras distintas a la vez, mediante exposición de cada una de ellas a un marcador distinto. Una de estas muestras suele ser un estándar interno constituido por cantidades equimolares de todas las muestras que participan en el experimento, marcada con uno de los fluorocromos, la cual proporciona un patrón interno con el que se compara la intensidad de marcaje de las proteínas presentes en las distintas muestras. Esta técnica permite la detección de diferencias cuantitativas en la expresión proteica de distintas muestras en un solo gel, lo que, a la vez que mejora la reproducibilidad de los resultados, reduce el consumo de tiempo y reactivos. La principal desventaja de este método es la necesidad de llevar a cabo un marcaje mínimo de las proteínas (entre el 1% y el 3% de las mismas), requerido con el fin de mantenerlas solubles durante su separación electroforética. Esta imposición provoca una ligera desviación en la masa molecular de las proteínas marcadas respecto a las no marcadas, resultando en una diferencia en la migración electroforética de ambas (Tonge et al., 2001). Otro inconveniente lo supone el alto coste de los marcadores, del equipo necesario para la detección y del paquete informático asociado con el que se realiza el análisis de imagen.

Técnicas cromatográficas: cromatografía 2D

Las técnicas cromatográficas son otra potente estrategia con la que se pueden fraccionar mezclas de proteínas. En estos métodos las proteínas se digieren antes de ser separadas mediante cromatografía multidimensional, para luego analizarlas de manera automatizada mediante espectrometría de masas en tándem (también denominadas MS/MS).

Se llevan a cabo sucesivos fraccionamientos empleando como fases estacionarias columnas de fase reversa (RP, Reverse Phase), de exclusión molecular (SEC, Size Exclusion Cromatography), de intercambio catiónico (SCX, Strong Cation Exchange) o aniónico (SAX, Strong Anion Exchange), de afinidad o de hidroxiapatito (Righetti et al., 2005). En las primeras aplicaciones de la cromatografía multidimensional para estudios proteómicos se usó tanto la cromatografía de exclusión por tamaño molecular como el intercambio catiónico, combinados en línea con una cromatografía en fase reversa (Link et al., 1999; Opiteck et al., 1997). A partir de estos experimentos iniciales han sido muchas las combinaciones introducidas en la separación cromatográfica mediante el uso de instrumentos de cromatografía líquida de alta resolución (HPLC, High Performance Liquid Cromatography), conectados en línea con equipos de MS/MS.

La creciente popularidad del fraccionamiento basado en la cromatografía es consecuencia de su capacidad para superar algunas de las limitaciones de los métodos basados en la 2-DE, siendo capaz de detectar proteínas de membrana o con baja abundancia (Peng and Gygi, 2001; Blonder et al., 2004; Han et al., 2001; Stockwin et al., 2006; Washburn et al., 2001; Wu et al., 2003). En la electroforesis 2-DE las proteínas se separan para ser digeridas posteriormente, mientras que en la cromatografía multidimensional son primero digeridas a péptidos y después son estos péptidos los fraccionados. De este modo se superan los problemas inherentes a la solubilización de proteínas de membrana (los péptidos digeridos sí que son solubles) y debido a la alta sensibilidad se detectan proteínas poco representadas en la muestra. Además, la cromatografía multidimensional permite el análisis automatizado y simultáneo de un mayor número de muestras que la 2-DE. La resolución de la cromatografía multidimensional es tan buena como la de la electroforesis 2-DE, permitiendo la identificación de más de 1.000 proteínas en una muestra dada. Sin embargo, la detección de isoformas y modificaciones post-traduccionales resulta más complicada que con las técnicas 2-DE.

El problema inicial de esta técnica era la baja reproducibilidad de las intensidades detectadas, inherente al detector, lo que las hacía de difícil aplicación a estudios de proteómica diferencial. Aun así, el uso del fraccionamiento cromatográfico en los estudios de proteómica cuantitativa se ha visto incrementado por la reciente aparición de marcajes mediante isótopos estables, así como por la mejora en la reproducibilidad de los sistemas de detección. En la proteómica basada en cromatografía acoplada a espectrometría de masas la cuantificación se lleva a cabo normalmente marcando las proteínas o péptidos mediante isótopos estables, de manera que una de las muestras se marca con un isótopo ligero (o natural), mientras que la otra se marca con el isótopo pesado correspondiente. Los isótopos estables pueden ser incorporados metabólica-, química- o enzimáticamente a las proteínas o péptidos presentes en la muestra (Corthals and Rose, 2007; Goshe and Smith, 2003; Ong and Mann, 2005). Los péptidos así marcados producen, en el análisis de MS, parejas de picos con una diferencia de *m/z* característica, dependiendo de los isótopos usados. La abundancia relativa de los péptidos puede medirse por comparación de las áreas de pico en los espectros de MS. Estas

técnicas permiten el análisis simultáneo de un número limitado de muestras debido al precio de los materiales necesarios para el marcaje.

Alternativamente, los péptidos pueden marcarse mediante marcadores isobáricos. En este caso, los péptidos presentarán la misma masa tras su marcaje, pero en el análisis de MS/MS estos marcadores producen fragmentos iónicos distinguibles que pueden ser usados para la cuantificación. Las técnicas de marcaje isobárico, basadas en los espectros de MS/MS, ofrecen un número mayor de posibles canales de cuantificación que las técnicas isotópicas.

A continuación se describen las características de las técnicas de marcaje isotópico e isobárico más utilizadas:

Marcaje isotópico: ICAT

El desarrollo del marcaje isotópico ICAT (Gygi et al., 1999), produjo un salto cualitativo en los análisis de proteómica cuantitativa basada en la espectrometría de masas, al permitir la identificación y cuantificación a gran escala de mezclas complejas de proteínas. Los reactivos de ICAT están constituidos por tres partes funcionales, un grupo reactivo, un grupo de unión y un marcador de biotina. El grupo reactivo es la iodoacetamida, que se une covalentemente con los grupos sulfhidrilos de las cisteínas. El marcador de biotina permite la purificación de los péptidos marcados mediante una cromatografía de afinidad por la avidina. La cadena de unión entre la iodoacetamida y la biotina del reactivo pesado está constituida por ocho átomos de deuterio, mientras que en el caso del reactivo ligero está constituida por ocho átomos de hidrógeno. También existe una versión de los reactivos ICAT en la que se usan isótopos de carbono (C12/C13) en vez de los de hidrógeno (Yi et al., 2005).

Con el protocolo de marcaje ICAT, las proteínas de dos muestras son marcadas con el reactivo ligero o pesado, para luego mezclarlas y digerirlas con tripsina. Los péptidos resultantes son primero fraccionados por cromatografía de intercambio catiónico y estas fracciones son luego purificadas por cromatografía de afinidad por avidina. Los péptidos marcados y purificados por afinidad se separan por cromatografía en fase reversa usando una cromatografía líquida en escala nano antes de someterlos al análisis por espectrometría de MS/MS. En primer lugar, en el análisis de MS los péptidos se cuantifican por comparación de las áreas de los picos de cada péptido en su versión ligera o pesada, y a continuación se identifican por MS/MS.

Marcaje isobárico: iTRAQ

Siguiendo al éxito del marcaje de ICAT, se ha desarrollado una nueva generación de marcadores llamada iTRAQ (Isotope Tagged Relative and Absolute Quantification) (Ross et al., 2004). Inicialmente se disponía de cuatro marcadores distintos, aunque en la actualidad se disponen de ocho (Pierce et al., 2008; Ross et al., 2004). Estos marcadores

se componen de tres regiones bien diferenciadas, un grupo reactivo, un grupo compensador y un grupo reportero.

El grupo reactivo es derivado de la N-hidroxisuccimida y reacciona con el grupo ε-amino de los residuos de lisina y el extremo N-terminal de todos los péptidos. El grupo compensador se utiliza para igualar la masa total. De esta manera, y dado que la suma de los pesos moleculares de las tres partes de cada reactivo es constante, cada péptido (marcado) se detecta como un pico único en el espectro MS. Durante la fragmentación en MS/MS de los péptidos marcados, los grupos reporteros se liberan de los mismos, pudiendo ser detectados en el espectro de MS/MS como picos con una relación *m/z* de 113,1; 114,1; 115,1; 116,1; 117,1; 118,1; 119,1 y 121,1. La concentración relativa de los péptidos se obtiene por comparación de las intensidades de las señales MS/MS de los grupos reporteros.

En el protocolo estandarizado para el marcaje de iTRAQ, las proteínas de una muestra dada se digieren en primer lugar con tripsina, y los péptidos resultantes se marcan con un reactivo iTRAQ diferente para cada muestra. Todas las muestras marcadas se combinan, se fraccionan por cromatografía de intercambio catiónico y las fracciones resultantes se analizan por LC-MS/MS. El espectro de MS/MS se usa tanto para la identificación como para la cuantificación. Los reactivos de iTRAQ se incorporan a todos los péptidos presentes en la muestra, lo que incrementa la confianza de las identificaciones proteicas realizadas, al alcanzarse un mayor porcentaje de cobertura de las secuencias polipeptídicas de las proteínas identificadas. Sin embargo, como el iTRAQ no reduce la complejidad de la muestra, como sí ocurre en el ICAT (en el que sólo se marcan los péptidos que contengan cisteína), el fraccionamiento de la misma adquiere una gran importancia.

Identificación de proteínas

La identificación de proteínas en los estudios proteómicos se realiza ya sea a partir de la huella peptídica (PMF, "Peptide Mass Fingerprintig") obtenida por MS, o bien a partir de los espectros de fragmentación y secuenciación de péptidos mediante MS/MS.

Identificación por MS: PMF

Se han desarrollado distintas herramientas informáticas que asisten en la identificación de proteínas mediante ambos métodos. Para PMF se compara el valor *m/z* de cada péptido del espectro de masas experimental con los valores teóricos de bases de datos como NCBI (http://www.ncbi.nlm.nih.gov) o UniProt (http://www.uniprot.org/). En caso de concordancia entre los valores experimentales y teóricos para una proteína dada, ésta se asigna al espectro de masas experimental, siempre con una cierta probabilidad de acuerdo al algoritmo utilizado. Los valores *m/z* teóricos para una proteína dada se obtienen mediante su traducción y digestión *in silico*, utilizando las secuencias de DNA

de los genes presentes en las bases de datos. Si no hay posibilidad de disponer de datos genómicos del sujeto de estudio, las proteínas también pueden ser identificadas directamente por secuenciación *de novo* (Standing, 2003; Hernández et al., 2006).

Existen multitud de algoritmos, tales como Mascot (Perkins et al., 1999), MS-Fit (Clauser et al., 1999), Profound (Zhang et al., 2002), PeptideSearch (Mann and Wilm, 1997), PeptIdent (Wilkins and Williams, 1997), Aldente (Tuloup et al., 2003) y PepFrag (Fenyo et al., 1998), que permiten evaluar la similitud entre los valores *m/z* de los espectros experimentales obtenidos y los teóricos. Todos estos programas asignan una puntuación, valor probabilístico o "score" estadístico que indica lo bien correlacionados que se encuentran entre sí los valores experimentales y los teóricos. A la hora de asignar un score a la identificación realizada estos algoritmos tienen en cuenta varios parámetros, entre los que se incluyen la precisión e intensidad de las señales, los péptidos que no aparecen en el espectro experimental, la presencia de aminoácidos modificados, los fragmentos no digeridos, los errores presentes en las secuencias peptídicas descritas en las bases de datos, la calibración del instrumento y la presencia de señales no específicas de la proteína identificada, entre otros (Palagi et al., 2006). En algunos algoritmos, la asignación del "score" está basada únicamente en el número de péptidos de ambos espectros que coinciden, mientras que otros usan algoritmos más sofisticados como MOWSE o variantes del mismo, sobre el que se sustenta el motor de búsqueda Mascot y que está basado en la distribución de las masas peptídicas presentes en las bases de datos (Pappin et al., 1993). Debido a las diferencias que presentan los algoritmos de búsqueda, los resultados obtenidos pueden diferir en cierto grado. Así, al comparar Profound, Mascot y MS-Fit, se observó como el último era capaz de identificar menos proteínas que los otros dos algoritmos (Chamrad et al., 2004). Ante la evidencia de este fenómeno, se hace aconsejable validar los resultados obtenidos mediante distintos algoritmos y/o usar métodos estadísticos que estimen la validez o significado de las identificaciones realizadas.

Identificación por MS/MS: PFF y secuenciación "de novo"

La identificación por MS/MS puede llevarse a cabo tanto por comparación con la información presente en las bases de datos (PFF, "Peptide Fragment Fingerprinting") como por secuenciación *de novo*. La primera opción se usa normalmente para la identificación de las proteínas presentes en mezclas complejas y cuando hay disponibilidad de acceso a la información genómica del organismo estudiado. En los análisis de MS/MS automatizados, el espectrómetro de masas selecciona los picos del primer espectro MS obtenido (iones precursores o parentales), para su fragmentación y posterior análisis de los espectros de fragmentación resultantes (espectros de MS/MS). La intensidad inicial del péptido en el espectro de MS es por tanto un parámetro crítico para obtener buenas fragmentaciones, y por tanto identificaciones adecuadas. Estos análisis generan cientos de espectros por hora, lo que requiere del uso de programas informáticos con los que realizar el análisis de los datos. Los análisis proteómicos a gran escala se han

visto beneficiados por el desarrollo de múltiples paquetes informáticos que permiten el análisis de los datos presentes en los espectros de MS/MS. Algunos de estos son Mascot (Perkins et al., 1999), Sequest (Eng et al., 1994), ProbID (Zhang et al., 2002), Phenyx (Colinge et al., 2003), X-Tandem (Craig and Beavis, 2004), GutenTag (Tabb et al., 2003), y Sonar MS/MS (Field et al., 2002). Todas estas herramientas, al igual que las descritas antes para PMF, comparan los espectros experimentales con los espectros teóricos y asignan un valor estadístico o "score" para cada espectro comparado. Cada una de estas herramientas informáticas aplica distintos algoritmos especializados y funciones de "score" que tienen en cuenta los diferentes factores que influyen en la identificación de proteínas descritos para el caso anterior y añaden algunos criterios específicos de esta técnica, tales como mutaciones no anotadas y variantes post-traduccionales de las proteínas, precisión en la masa del péptido precursor, así como en la de los fragmentos y sus intensidades y de nuevo, los errores presentes en las bases de datos (López-Ferrer et al., 2004; Hernández et al., 2006; Palagi et al., 2006).

Las capacidades de algunos de estos paquetes informáticos, así como de los algoritmos implementados se han comparado en algunos estudios, observándose como los distintos programas producen identificaciones proteicas solapadas, especialmente para las proteínas de alta abundancia, pero también identificaciones únicas de proteínas para cada uno de los paquetes informáticos de manera independiente, lo que pone de manifiesto la complementariedad en sus métodos de análisis (Chamrad et al., 2004; Moulder et al., 2005; Kapp et al., 2005).

Estudios proteómicos en vegetales

El campo de la proteómica en vegetales va un paso por detrás del desarrollado en cultivos celulares y microorganismos. Esto se debe principalmente al retraso en la secuenciación de genomas vegetales, lo que compromete la calidad de las identificaciones obtenidas por espectrometría de masas (van Wijk, 2001).

En los últimos años se han desarrollado nuevas metodologías proteómicas, ganando en complejidad y precisión, y poco a poco estás nuevas metodologías se van aplicando a sistemas vegetales (Jorrín-Novo et al., 2009). La gran cantidad de datos generados ha posibilitado el desarrollo de bases de datos disponibles para la comunidad científica, como la PPDB http://ppdb.tc.cornell.edu (Sun et al., 2009); la PODB, http://proteome.dc.affrc.go.jp/Soybean/ y la base de datos Organellome, http://podb.nibb.ac.jp/Organellome (Mano et al., 2008). Uno de los mayores logros ha sido el establecimiento de una base de datos de MS/MS obtenida a partir de los datos recabados con *Arabidopsis*, *Chlamydomonas reinhardtii*, *Medicago truncatula*, *Solanum tuberosum* (patata), *Solanum lycopersicum* (tomate) y otras plantas (ProMEX; http://promex.mpimp-golm.mpg.de/home.shtml) (Hummel et al., 2007). Esta base de datos permite identificaciones más fiables. El grado de desarrollo de la proteómica vegetal en los últimos años se demuestra en el número de revisiones específicas dedicadas

a proteómica publicadas (van Wijk, 2001; Jorrín-Novo et al., 2007, 2009; Weckwerth et al., 2008; Komatsu et al., 2008; Agrawal et al., 2009; Thelen and Peck, 2007).

Las técnicas proteómicas también han sido aplicadas al estudio de los estreses producidos por metales pesados en plantas. Se han estudiado los efectos de la toxicidad por Cd tanto en cultivos celulares en *Arabidopsis* y cebada (Sobkowiak, 2006; Sarry, 2006), como en hojas de espinaca, cebada, *Thlaspi caerulescens* y álamo (Schneider, 2009; Kieffer, 2008; Kieffer, 2009; Tuomainen, 2006; Fagioni, 2009). La mayoría de los estudios publicados hasta ahora se han centrado en especies modelo como *A. thaliana* (Roth, 2006) y en especies tolerantes o hiperacumuladoras de metales, como el álamo, *T. caerulescens* y *Brassica juncea* (Kieffer, 2009; Toumainen, 2006; Álvarez, 2009). También se han publicado dos estudios proteómicos en los que se discuten los efectos protectores que la simbiosis con micorrizas puede tener sobre la exposición a Cd en guisante y alfalfa (Ombretta, 2003; Aloui, 2009).

Las técnicas de proteómica diferencial también se han utilizado para el estudio de las respuestas a la deficiencia de Fe por parte de las plantas en varias condiciones. Se han descrito los cambios a nivel proteico en tilacoide de diversas especies (Andaluz, 2006; Laganowsky, 2009; Timperio, 2007), así como los cambios producidos en raíz de tomate (*Solanum lycopersicum*) (Brumbarova, 2008; Li, 2008) y remolacha (*Beta vulgaris*) (Rellán-Álvarez, 2010).

La gran información que se puede obtener mediante estudios de proteómica diferencial hacen de esta técnica una buena herramienta para el estudio de estreses medioambientales como los abordados en el presente trabajo: la deficiencia de Fe y la toxicidad de Cd. La complejidad y al mismo tiempo la similitud de los mecanismos de homeostasis y desintoxicación, hacen que una aproximación holística, desde el punto de vista proteómico, sea un enfoque apropiado para abordar el estudio de las alteraciones nutricionales producidas por metales pesados en plantas. Este enfoque puede poner de manifiesto respuestas específicas a estas alteraciones nutricionales que con un enfoque clásico podrían pasar desapercibidas. Además, la aproximación proteómica nos permitirá elucidar aquellas rutas metabólicas compartidas en los procesos de homeostasis y desintoxicación. Por último, un mejor conocimiento de los procesos derivados del estrés por metales pesados en la planta nos ayudaría no solamente a evitar problemas agrícolas como la deficiencia y toxicidad de metales en cultivos, sino también a mejorar el contenido en nutrientes de los alimentos vegetales y a favorecer la fitorremediación de suelos contaminados por metales pesados.

OBJETIVOS

El objetivo general de la tesis doctoral consiste en estudiar los efectos de la deficiencia de Fe y de la toxicidad por Cd en las raíces de dos plantas modelo, *Solanum lycopersicum* y *Medicago truncatula*, desde el punto de vista de la proteómica. Con este enfoque se pretende en primer lugar dibujar un mapa general de las alteraciones metabólicas producidas por ambos estreses nutricionales, y en segundo lugar utilizar esta plataforma para identificar posibles alteraciones desconocidas hasta la fecha que requieran un estudio en mayor profundidad. El estudio de estos estreses nutricionales tiene importancia desde el punto de vista agronómico, para evitar pérdidas de productividad, mejorar la calidad del cultivo y también para elaborar posibles estrategias de fitoremediación en suelos contaminados. Este proyecto también es interesante desde el punto de vista de seguridad alimentaria, con el fin último de establecer bases científicas para mejorar el contenido de Fe en cultivos comestibles o forrajeros y evitar el paso de Cd a la cadena trófica.

Se plantean los siguientes objetivos específicos:

1- Caracterización de los cambios producidos por la toxicidad leve y severa por Cd en el perfil proteico de la raíz de tomate.

2- Caracterización de las respuestas fisiológicas de la raíz de *Medicago truncatula* a la deficiencia de Fe.

3- Caracterización de los cambios producidos por deficiencia de Fe directa e inducida por la presencia de carbonato cálcico en el medio de cultivo en el perfil proteico de la raíz de *Medicago truncatula*.

4- Identificación de los compuestos de naturaleza flavínica producidos en las raíces de *Medicago truncatula* deficientes en Fe y caracterización del patrón de acumulación y excreción de los mismos.

5- Estudio de la posible relación entre la inducción de la producción y excreción de compuestos de naturaleza flavínica y las respuestas principales de la Estrategia I en especies de interés hortícola.

PUBLICACIONES

JOURNAL OF PROTEOMICS 73 (2010) 1694–1706

available at www.sciencedirect.com

ScienceDirect

www.elsevier.com/locate/jprot

Changes induced by two levels of cadmium toxicity in the 2-DE protein profile of tomato roots

Jorge Rodríguez-Celma, Rubén Rellán-Álvarez, Anunciación Abadía, Javier Abadía, Ana-Flor López-Millán*

Plant Nutrition Department, Aula Dei Experimental Station (CSIC), P.O. Box 13034, E-50080, Zaragoza, Spain

ARTICLE INFO

Article history:
Received 17 February 2010
Accepted 5 May 2010

Keywords:
Cadmium
Metabolism
Root
Tomato
Two-dimensional gel electrophoresis

ABSTRACT

Tomato is an important crop from nutritional and economical points of view, and it is grown in greenhouses, where special substrates and the use of recycled water imply an increased risk of Cd accumulation. We investigated tomato root responses to low (10 μM) and high (100 μM) Cd concentrations at the root proteome level. Root extract proteome maps were obtained by 2-DE, and an average of 121, 145 and 93 spots were detected in the 0, 10 and 100 μM Cd treatments, respectively. The low Cd treatment (10 μM) resulted in significant and higher than 2-fold changes in the relative amounts of 36 polypeptides, with 27 of them identified by mass spectrometry, whereas the 100 μM Cd treatment resulted in changes in the relative amounts of 41 polypeptides, with 33 of them being identified. The 2-DE based proteomic approach allowed assessing the main metabolic pathways affected by Cd toxicity. Our results suggests that the 10 μM Cd treatment elicits proteomic responses similar to those observed in Fe deficiency, including activation of the glycolytic pathway, TCA cycle and respiration, whereas the 100 μM Cd treatment responses are more likely due to true Cd toxicity, with a general shutdown of carbon metabolism and increases in stress related and detoxification proteins.

1. Introduction

Cadmium is highly toxic to plants and animals [1]. In particular, Cd toxicity in crops has become a serious problem, especially in developed countries. Cadmium is released into the environment by human activities such as mining, agricultural use of commercial fertilizers, sewage sludge, manure and lime and industrial activities that release air pollutants and effluents with high Cd concentrations [2,3]. Food chain contamination is the main Cd exposure risk for humans, and Cd taken up by plants is accepted to be the main source of Cd accumulation in foods [4]. Cadmium is suggested to cause damage even at very low concentrations, and healthy plants may contain Cd levels that are toxic for mammals [5].

In polluted soils, Cd is generally present as a free ion or in other soluble forms, and its mobility depends on pH and on the presence of chelating substances and other cations [6]. It is accepted that Cd is taken up by roots via Fe/Zn transporters because of the low metal specificity of these proteins. There is evidence that metal transporters from different families such as ZIP and Nramp are able to transport several divalent cations, including Cd [7,8]. Also, it has been described that a Ca

Abbreviations: ACN, Acetonitrile; GADPH, Glyceraldehyde 3-phosphate dehydrogenase; GDH, Glutamate dehydrogenase; GST, Glutathione S-transferase; HSP, Heat shock protein; KOBAS, KEGG orthology-based annotation system; MDAR, Monodehydroascorbate reductase; MDH, Malate dehydrogenase; PCs, Phytochelatins; PDH, Pyruvate dehydrogenase; PTMs, Post translational modifications; TCA, Tricarboxylic acid cycle.

* *Corresponding author*. Tel.: +34 976716056; fax: +34 976716145.
E-mail address: jabadia@eead.csic.es (J. Abadía).

1874-3919/$ – see front matter © 2010 Elsevier B.V. All rights reserved.
doi:10.1016/j.jprot.2010.05.001

transport mechanism could be involved in Cd uptake [9]. Little is known about the chemical form(s) in which this heavy metal is present in the xylem, although it has been suggested that it may be associated with organic acids [10].

Common symptoms of Cd toxicity in plants are a marked growth inhibition [11], leaf chlorosis and appearance of leaf necrotic spots [11,12]. Physiological effects of Cd toxicity in plants include changes in photosynthetic efficiency, respiration and transpiration [11–13] and alterations in nutrient homeostasis, including changes in Mn, K, Mg and Ca uptake rates [11,14] and a Cd-induced Fe deficiency [11,12]. At the cellular level, Cd toxicity is known to cause alterations such as membrane damage, disruption of electron transport, inhibition/activation of enzymes and interaction with nucleic acids [15,16]. Possible mechanisms by which these disorders are generated are an induction of oxidative stress and competition with other metals such as Zn, Fe, and Mn, which are cofactors of many enzymes [14,17]. One of the main Cd detoxification mechanisms in plant cells is the synthesis of phytochelatins (PCs) [18]. Phytochelatins have high affinity for heavy metals and the metal–PC complexes are transported and sequestered in vacuoles to avoid metal toxicity [19]. Information about other detoxification/tolerance mechanisms comes mainly from the study of Cd-hyperaccumulators [20] and Cd-tolerant plants [21], whereas less information is available in commercial crops such as tomato. These processes include metal complexation with organic acids, PCs, cysteine, metallothioneins and other low molecular weight thiols [18,22–25] and both cellular and subcellular compartmentation [22,26].

In recent years, proteomic profiling has been used to study the effects of Cd toxicity in plants in different scenarios. Changes in proteomic profiles induced by Cd toxicity have been described in *Arabidopsis thaliana* and barley cell cultures [27,28] and in spinach, barley, *Thlaspi caerulescens* and poplar leaves [29–33]. Most of the root proteomic studies published so far have focused in model species such as *A. thaliana* [34] and Cd-tolerant or hyperaccumulator species such as poplar, *T caerulescens* and *Brasica juncea* [31,32,35]. Also, two proteomic studies have described the protective effects conferred by mycorrhizal symbiosis to roots of Cd-exposed *Pisum sativum* and *Medicago truncatula* plants [36,37]. To our knowledge, just one study on Cd toxicity including a species of agronomical interest, rice, has been published so far [38].

Tomato is a very important crop from nutritional and economical points of view (FAOSTAT Database, http://faostat.fao.org/). A large part of this crop is grown in greenhouses, using special substrates and fertilization techniques involving reutilization of water, therefore implying a significant risk of heavy metal concentration increases [39]. We have recently studied changes in growth, metal accumulation and physiology in tomato plants grown with low (10 μM) and high (100 μM) Cd concentrations [12]. In the present study we further investigate tomato responses to 10 and 100 μM Cd concentrations at the root proteomic level, using 2-DE techniques. Roots were selected as the first tissue to explore since they are the first step in plant Cd assimilation, thus being the main site of toxic metal exposure, and also because previous results suggested that one of the Cd detoxification strategies in tomato plants relies on Cd allocation in roots [12]. Proteomic approaches have been taken elsewhere to study other stress related responses in tomato such as Fe deficiency in roots [40] and waterlogging in leaves [41], among others, and in general could provide a good overview of major metabolic changes occurring in response to stress.

2. Materials and methods

2.1. Plant culture

Tomato (*Lycopersicon esculentum* Mill cv. Tres Cantos) plants were grown in a controlled environment chamber, as indicated in [12]. Seeds were grown for two weeks in vermiculite, for two additional weeks in half-strength Hoagland nutrient solution and then transplanted to 10 L plastic buckets (18 plants per bucket) containing half-strength Hoagland nutrient solution with 45 μM Fe(III)-EDTA and 0, 10 or 100 μM $CdCl_2$, and grown in these conditions for ten more days. Whole roots were harvested, frozen in liquid N_2 and stored at −80 °C until further analysis. Five different batches of plants (5 biological replicates) were grown and analysed for proteomic profiling (Fig. S1).

2.2. Protein extraction

For protein extraction, roots of two plants from the same treatment in a given batch were pooled; approximately 1 g of root material was ground in liquid N_2 using a Retsch M301 mill (Retsch GmbH, Haan, Germany), and then homogenized in 5 mL of phenol, saturated with Tris-HCl 0.1 M (pH 8.0) containing 5 mM β-mercaptoethanol, by stirring for 30 min at 4 °C. After incubation, the homogenate was filtered (PVDF, 0.45 μm) and centrifuged at 5000×*g* for 15 min. The phenol phase was re-extracted for 30 min with one volume of phenol-saturated Tris-HCl 0.1 M (pH 8.0) containing 5 mM β-mercaptoethanol, and centrifuged as described above. The phenol phase was collected, and proteins precipitated by adding four volumes of 0.1 M ammonium acetate in cold methanol, using an incubation of at least 4 h at −20 °C. Samples were then centrifuged at 5000×*g* for 15 min and the pellet was washed three times with cold methanol, dried with N_2 gas and resuspended in sample rehydration buffer containing 8 M urea, 2% (w/v) CHAPS, 50 mM DTT, 2 mM PMSF and 0.2% (v/v) 3–10 ampholytes (Amersham, Uppsala, Sweden). After rehydration, samples were incubated at 38 °C for 2.5 h and then centrifuged at 15,000×*g* for 10 min at 20 °C. Protein concentration was measured with RC DC Protein Assay BioRad (BioRad, Hercules, CA, USA) based on the Lowry method. Samples were analysed by 2-DE immediately.

2.3. Protein 2-DE separation

Preliminary 2-DE experiments were carried out using a first dimension IEF separation with a linear pH gradient 3–10; in these conditions most of the spots were concentrated in the central region of the 2-DE gel (results not shown); therefore, to prevent protein co-migration and improve resolution a narrower pH gradient was chosen. A first dimension IEF separation [42] was carried out on 7 cm ReadyStrip IPG Strips

(BioRad) with a linear pH gradient pH 5–8 in a Protean IEF Cell (BioRad). Strips were rehydrated for 16 h at 20 °C in 125 μL of rehydration buffer containing 100 μg of root extract proteins and a trace of bromophenol blue, and then transferred onto a strip tray. IEF was run at 20 °C, for a total of 14,000 V h (20 min with a 0–250 V linear gradient, 2 h with a 250–4000 V linear gradient and 4000 V until 10,000 V h). After IEF, strips were equilibrated for 10 min in equilibration solution I (6 M urea, 0.375 M Tris-HCl, pH 8.8, 2% (w/v) SDS, 20% (v/v) glycerol, 2% (w/v) DTT) and for another 10 min in equilibration solution II (6 M urea, 0.375 M Tris-HCl pH 8.8, 2% (w/v) SDS, 20% (v/v) glycerol, 2.5% (w/v) iodoacetamide).

For the second dimension SDS PAGE, equilibrated IPG strips were placed on top of vertical 12% SDS-polyacrylamide gels (8×10×0.1 cm) and sealed with melted 0.5% agarose in 50 mM Tris-HCl, pH 6.8, containing 0.1% SDS. SDS PAGE was carried out at 20 mA per gel for approximately 1.5 h, until the bromophenol blue reached the plate bottom, in a buffer containing 25 mM Tris, 1.92 M glycine, and 0.1% SDS, at room temperature. Gels were subsequently stained with Coomassie-blue R-250 (Sigma, Barcelona, Spain). Gels were made from independent root preparations from five different batches of plants for each treatment.

2.4. Gel image and statistical analysis

Stained gels were scanned with a Bluescan48 Scanner (LaCie, Portland, OR, USA). Spot detection, gel matching and interclass analysis were performed with PDQuest 8.0 software (BioRad). The spots were also manually checked, and a high level of reproducibility between normalized spot volumes was found in the different replicates (Table S1).

Univariate and multivariate statistical analyses were carried out, using only spots present at least in 80% of gels in the same treatment. Differentially expressed spots were defined using a Student *t*-test ($p<0.10$). Partial Least Square (PLS) analysis was carried out using Statistica software (v. 9, Statsoft Inc. Tulsa, OK), either using all the spots or only those identified successfully by MS (see below).

2.5. In gel digestion and sample preparation for mass spectrometric analysis

Spots showing changes statistically significant (at $p<0.10$) and above a 2-fold threshold were excised automatically using a spot cutter (ProPic station from Genomic Solutions, Holliston, MA, USA, or EXQuest from BioRad) and then digested automatically using a ProGest protein digestion station (Genomic Solutions). The digestion protocol started with two de-staining steps, 30 min each, with 40% v/v acetonitrile (ACN) containing 200 mM NH_4HCO_3, followed by two washing steps, first with 25 mM NH_4HCO_3 for 5 min and then with 50% v/v ACN containing 25 mM NH_4HCO_3, for 15 min. After washing, gel spots were dehydrated with 100% ACN for 5 min, and then dried. Gel spots were rehydrated with 10 μL of a trypsin solution (12.5 ng μL^{-1} in 25 mM $(NH_4)_2CO_3$) for 10 min and then digested for 12 h at 37 °C. Digestion was stopped by adding 10 μL of TFA 0.5%. Peptides were purified automatically using a ProMS station (Genomic Solutions) with a C_{18} microcolumn (ZipTip, Millipore, MA, USA), and eluted directly onto a MALDI plate with 1 μL of matrix solution (5 mg mL^{-1} CHCA in 70% ACN/ 0.1% TFA v/v).

2.6. MALDI–TOF–MS, LIFT TOF–TOF analysis and identification of proteins

Peptide mass fingerprint spectra were determined on a 4700 Proteomics Analyzer (Applied Biosystems, Foster City, US) in positive ion reflector mode. Each spectrum was internally calibrated with *m/z* signals of porcine trypsin autolysis ions, and the typical mass measurement accuracy was ±20 ppm. Whenever possible, fragmentation spectra of the five most intense peaks were obtained for each sample. The measured tryptic peptide masses were searched in the NCBInr database 20070131, taxonomy Viridiplantae (283,672 sequences), using MASCOT software (Matrix Science, London, UK). When available, MS–MS data from LIFT TOF–TOF spectra were combined with MS peptide mass fingerprint data for database search. The following parameters were used for the database search: green plants taxonomic group, complete carbamidomethylation of cysteine residues, partial oxidation of methionine residues, mass tolerance of 100 ppm and one miscleavage allowed. MASCOT protein scores >76 were considered as significant ($p<0.05$). Protein scores are derived from ion scores as a non-probabilistic basis for ranking protein hits. Sequence coverage was always above 16% and at least 9 peptides were matched to the identified protein when peptide sequencing was not possible.

2.7. Metabolic pathway identification for proteins

We used the KOBAS software (http://kobas.cbi.pku.edu.cn) to assign the biochemical pathway for each protein identified by MS [40]. This software assigns a given set of proteins to known pathways in the KEGG database (http://www.genome.jp/kegg/pathway.html). All proteins in a common pathway were grouped manually. When no information was available in the KEGG database we searched for GO (http://www.geneontology.org/) annotation of the individual proteins.

3. Results and discussion

In a previous study we found that plant growth was reduced in both Cd treatments (10 and 100 μM Cd), and that leaves showed chlorosis symptoms when grown at 10 μM Cd and necrotic spots when grown at 100 μM Cd [12]. Root browning was observed in both treatments. Changes in plant mineral concentrations, including Cd, and in several metabolic activities related to C metabolism and in photosynthetic parameters were also found [12]. These previous results suggested that Cd detoxification strategies in tomato plants grown in the presence of Cd rely on root Cd accumulation, although at high Cd concentrations roots are overloaded with Cd and a significant mobilization to the shoots occurs.

3.1. Protein expression profiles and pathway analysis

Changes induced by Cd toxicity in the polypeptide pattern of root extracts from tomato plants grown at different Cd

concentrations (0, 10 and 100 μM Cd) were studied by 2-DE (IEF–SDS PAGE). Typical real scans of 2-DE gels obtained from root extracts from 0, 10 and 100 μM Cd supplied plants are shown in Fig. 1A, B and C, respectively. A total of 140 spots were consistently detected in gels of root extracts (spots present at least in 80% gels of one class or 50% of total gels). The average number of detected spots was (in mean ± SD) 121 ± 33, 145 ± 35 and 93 ± 38 in 0, 10 and 100 μM Cd 2-DE gels, respectively; approximately 87, 86 and 78% of spots were consistent in each class, respectively. To better describe changes in polypeptide composition we built a composite averaged virtual map containing all spots present in all 15 gels (5 per treatment; Fig. 1D, E and F).

The intensity of 43 and 45 spots changed significantly in the 10 and 100 μM Cd treatments, respectively, when compared to the control (Student *t*-test, $p < 0.10$). From these, 36 and 41 spots showed a relative intensity change above 2-fold in the 10 and 100 μM Cd treatments, respectively, when compared to the control. The PLS analysis showed a good separation between treatments when using all spots (Fig. 2A), and similar results were obtained when the analysis was carried out using only identified spots (Fig. 2B). The importance of the different spots in the PLS analysis is shown in Table S2; 19 out of the 25 most important spots were among those identified (Table 1).

The statistical analysis of averaged maps indicated that 10 μM Cd caused increases in signal intensity of 22 spots (orange symbols in Fig. 1E), whereas 6 spots were present in the 10 μM Cd treatment but absent in the control (red symbols in Fig. 1E). Among them, 21 spots matched reliably to known proteins in the NCBInr database (spots labeled 1–21 in Fig. 3A and Table 1), and their metabolic functions were assessed using KOBAS. Up-accumulated proteins belonged to different metabolic pathways including carbohydrate metabolism (spots 5, 12, 18, 19 and 21), cell wall organization (spots 2, 4, 8, 13 and 20), TCA cycle (spots 9 and 10), energy metabolism (spots 16 and 17), and protein metabolism, including protein folding (spots 1, 7, 11, 14 and 15) and peptidases (spots 3 and 6). A smaller group of spots showed decreases in relative intensity in plants grown at 10 μM Cd when compared to the controls. These included 7 spots with lower signal intensity (green symbols in Fig. 1E) and 1 spot not detected in Cd treated plants (blue symbol in Fig. 1E). Out of them, six were identified (spots labeled 22–27 in Fig. 3A and Table 1), and according to KOBAS assigned to glycolysis (spots 22, 24, 25 and 26), cell wall organization (spot 23) and TCA cycle (spot 27).

When comparing the averaged map of the 100 μM Cd treatment with that of control plants, 9 spots showed relative increases in signal intensity (orange symbols in Fig. 1F) and 2 more were detected *de novo* (red symbols in Fig. 1F). All of them were identified (spots labeled 28–36, and spots 8 and 18 in Fig. 3B and Table 1). Up-accumulated proteins in the 100 μM Cd treatment belonged to metabolic pathways including cell wall organization (spots 8, 28 and 36), glycolysis (spots 18 and 31)

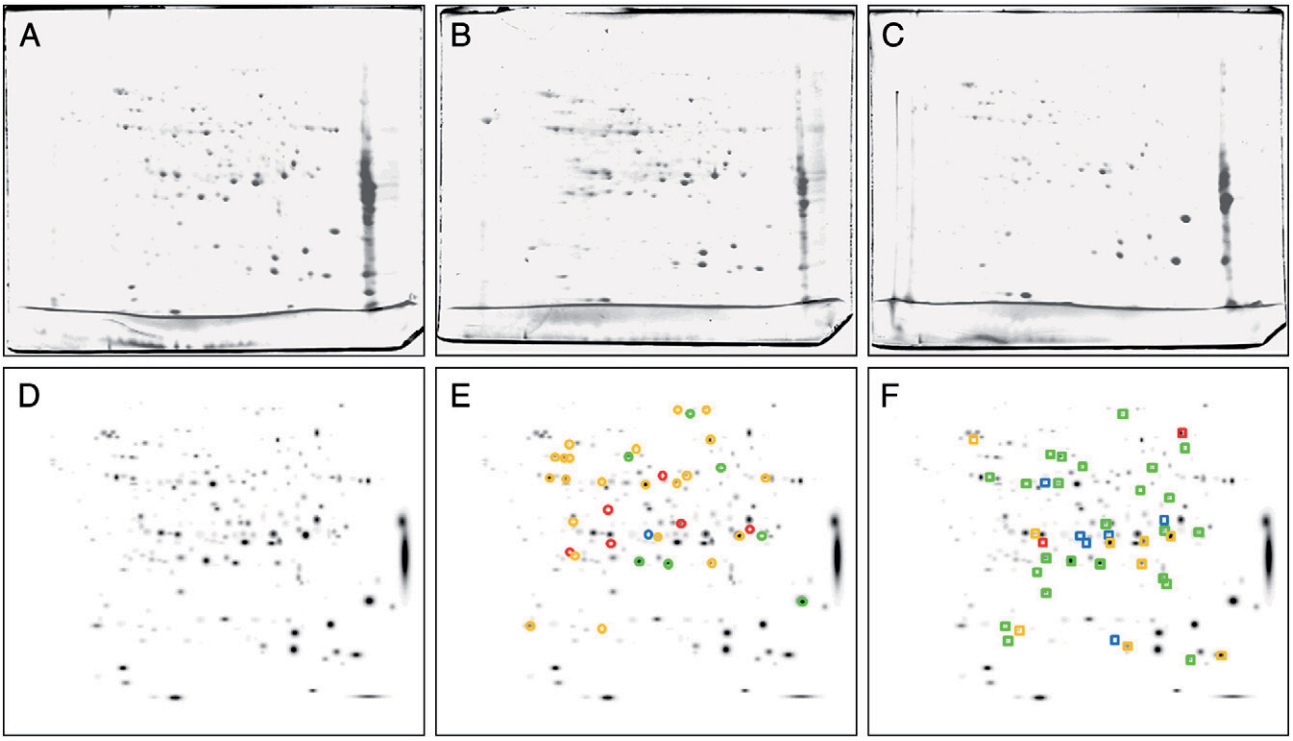

Fig. 1 – 2-DE IEF–SDS PAGE proteome maps of root extracts from 0, 10 and 100 μM $CdCl_2$ treated tomato plants. Proteins were separated in the first dimension in linear (pH 5–8) IPG gel strips and in the second dimension in 12% acrylamide vertical gels. Scans of typical gels of roots from 0, 10 and 100 μM Cd treated plants are shown in A, B and C, respectively. To facilitate visualization of the studied spots, a virtual composite image (D, E, and F) was created containing all spots present in the real gels A, B and C. In E (10 μM Cd) and F (100 μM Cd) spots whose intensities decreased or were no longer detected when compared to control maps were marked with green and blue symbols, respectively, and those with increased intensities or newly detected ones were marked with yellow and red symbols, respectively.

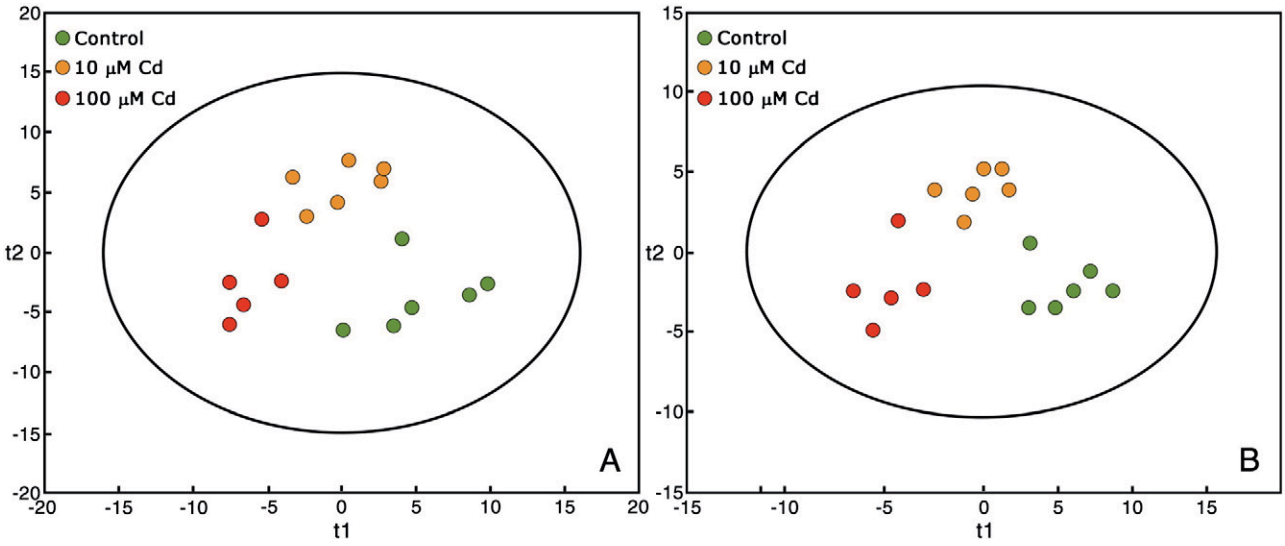

Fig. 2 – Multivariate statistical analysis (Partial Least Square, PLS) of 2-DE gels. Score scatter PLS plot of component 1 *vs.* component 2 after analysis of all (A) and identified spots (B) from roots of tomato plants grown in control 0 (green circles), 10 (orange circles) and 100 μM Cd (red circles). Only spots present in at least 80% of the gels in a given treatment were considered.

and TCA cycle (spots 32 and 33). Proteins involved in different stress related processes such as pathogenesis (spots 29 and 35), protein folding (spot 30), and glutathione metabolism (spot 34) showed also relative intensity increases. A large number of spots showed decreases in relative intensity in root extracts from plants grown at 100 μM Cd when compared to control plants. These included 24 spots with decreased intensity (green symbols in Fig. 1F) and 6 more not detected in 100 μM Cd treated plants (blue symbols in Fig. 1F). Among them, 22 spots were identified (Fig. 3B and Table 1) and according to KOBAS assigned to carbohydrate metabolism (spots 22, 24, 25, 26, 37, 38, 39, 41, 50, and 52), TCA cycle (spots 27 and 51), energy metabolism (spot 47 and 48), gene regulation (spots 40, 45 and 46), cell wall organization (spots 42 and 44), oxidative stress protection (spot 49), N metabolism (spot 53), and ascorbate metabolism (spot 43).

To summarize, between 93 and 145 spots were detected in gels from root extracts and approximately 25% and 44% of these spots showed significant changes in relative intensities as a result of exposure to 10 and 100 μM Cd, respectively (Table S3). The total number of spots detected was relatively low when compared to other proteomic studies in tomato roots [40,43]. Several causes may account for this discrepancy, including i) protein extraction method and amount of protein loaded in the gels, ii) gel size, iii) pI range and iv) sensitivity of the staining method. Proteomic results described to date have shown changes in relative intensity in 5–20% of spots in response to Cd toxicity in different plant species and tissues [30–34].

3.2. *Effect of Cd toxicity on metabolic pathways*

3.2.1. *Primary carbon metabolism*

3.2.1.1. Carbohydrate metabolism and glycolysis. Five spots corresponding to three proteins of the glycolytic pathway, pyruvate dehydrogenase (PDH), glyceraldehyde 3-phosphate dehydrogenase (GADPH) and enolase (3 spots) increased in relative amount in roots grown with 10 μM Cd when compared to the controls (Table 1). GADPH (spot 18) and two spots identified as enolase (spots 5 and 12) increased 2-, 3- and 4-fold, respectively, while PDH (spot 21) and one spot identified as enolase (spot 19) were newly detected in the 10 μM Cd treatment when compared to the controls. In the 100 μM Cd treatment, PDH (spot 31) and GADPH (spot 18) also increased, although only 2-fold. On the other hand, Cd exposure caused decreases in intensity in 3 and 7 proteins involved in carbohydrate metabolism in the low and high Cd treatments, respectively. In the 10 μM Cd treatment, decreases (expressed as % of control values) of 60, 50, 60 and 70% were measured for fructokinase (spots 22 and 26), dihydrolipoamide dehydrogenase (spot 25) and phosphoglycerate mutase (PGM) (spot 24), respectively. In the 100 μM Cd treatment, large decreases in intensity were measured for enolase (60% for spot 37; spot 50 was lost), GADPH (spot 39, 70%; spot 52 was lost), phosphoglycerate kinase (spot 38, 70%), triosephosphate isomerase (spot 41, 60%), PGM (spot 24, 60%), dihydrolipoamide dehydrogenase (spot 25, 80%) and fructokinase (spots 22 and 26, 70% each).

Overall, our results show that an up-regulation of the glycolytic pathway occurs at 10 μM Cd, whereas at 100 μM Cd a general down-regulation of the carbohydrate metabolism takes place. Reports in the literature regarding Cd-induced changes in carbohydrate metabolism proteins have been contradictory. Decreases in several proteins (enolase, GADPH, fructokinase and PGM) have been described in roots of two Cd-tolerant plants, poplar and *B. juncea*, after exposure to 20 and 250 μM Cd, respectively, whereas in the model plant *A. thaliana* grown with 10 μM Cd and in *A. thaliana* cell cultures increases in GADPH and other glycolytic enzymes were measured [28,34,35,44]. These reports, together with those in the present study, indicate that changes in carbohydrate metabolism upon Cd exposure are dose and species dependent.

Several changes were common to both levels of Cd toxicity including the increase in PDH and the decreases in fructokinase,

Table 1 – Proteins identified in 2-DE IEF–SDS PAGE gels. MS[1] Protein score is –10*Log (P), where P is the probability that the observed match is a random event. Protein scores > 76 were considered significant ($p < 0.05$). – indicates no changes in relative abundance.

No.	Teor. MW/pI	Exp. MW/pI	*vs.* 10 Cd/ *vs.* 100 Cd	Cov.	Score/pep/ion	ID	Homology	Species	Matched pathway in KEGG
1	62/5.2	67/5.8	+3.0/–	44	240/20/3	gi|300265	HSP68 heat stress DNAK homolog	*Solanum perivarum*	Chaperones and folding catalysts; pores ion channels; MAPK signaling pathway
2	38/5.3	43/5.9	+5.6/–	31	139/11/2	gi|3219772	Actin-51	*Solanum lycopersicum*	Cytoskeleton proteins
3	27/5.6	28/6.1	+2.2/–	75	328/15/3	gi|77999303	Proteasome-like protein alpha subunit	*Solanum tuberosum*	Peptidases; proteasome
4	42/5.8	40/6.6	+4.5/–	56	459/23/4	gi|48478827	UDP-glucose:protein transglucosylase-like protein Sl-UPTG1	*Lycopersicon esculentum*	
5	48/5.7	50/6.4	+3.0/–	63	890/22/5	gi|119354	Enolase 2-phosphoglycerate-dehydratase	*Solanum lycopersicum*	Glycolysis/gluconeogenesis
6	61/7.9	52/6.8	+2.5/–	41	276/21/3	gi|27463709	Neutral leucine aminopeptidase preprotein	*Solanum lycopersicum*	Peptidases
7	65/5.8	70/7.0	+2.4/–	17	83/7/2	gi|28973653	Putative TPR-repeat protein	*Arabidopsis thaliana*	Chaperones and folding catalysts
8	38/6.6	35/7.0	+2.7/+28.9	56	481/19/4	gi|461978	Glucan endo 1–3 beta glucosidase A	*Solanum lycopersicum*	Starch and sucrose metabolism
9	98/5.8	96/7.0	+3.0/–	46	535/32/4	gi|30407706	Aconitase	*Solanum pennellii*	Citrate cycle (TCA cycle); reductive carboxylate cycle (CO2 fixation); glyoxylate and dicarboxylate metabolism
10	70/5.9	64/6.4	+5.0/–	31	210/16/2	gi|15240075	SDH1-1	*Arabidopsis thaliana*	Citrate cycle (TCA cycle); oxidative phosphorylation
11	63/5.7	59/5.8	+11.6/–	37	332/18/5	gi|1762130	Chaperonin 60 beta subunit	*Solanum tuberosum*	Chaperones and folding catalysts
12	48/5.7	51/6.1	+4.5/–	64	735/24/5	gi|119354	Enolase 2-phosphoglycerate-dehydratase	*Solanum lycopersicum*	Glycolysis/gluconeogenesis
13	52/5.7	51/6.7	+4.4/–	50	576/35/4	gi|136739	UTP-glucose-1-phosphate uridylyltransferase (UDP-glucose pyrophosphorylase)	*Solanum tuberosum*	Pentose and glucuronate interconversions; nucleotide sugars metabolism; galactose metabolism
14	63/5.7	59/5.7	+2.3/–	37	310/19/4	gi|1762130	Chaperonin-60 beta subunit	*Solanum tuberosum*	Chaperones and folding catalysts
15	58/5.3	59/5.8	+2.3/–	36	226/16/2	gi|24637539	Heat shock protein 60	*Prunus dulcis*	Chaperones and folding catalysts
16	60/5.9	51/5.7	+2.4/–	53	758/22/5	gi|114421	ATP synthase subunit beta, mitochondrial precursor	*Nicotiana plumbaginifolia*	Oxidative phosphorylation
17	60/5.9	51/5.8	+2.4/–	53	758/22/5	gi|114421	ATP synthase subunit beta, mitochondrial precursor	*Nicotiana plumbaginifolia*	Oxidative phosphorylation
18	37/6.3	40/7.2	+2.4/+2.7	61	526/19/4	gi|22094849	Glyceraldehyde 3-phosphate dehydrogenase	*Solanum tuberosum*	Glycolysis/gluconeogenesis
19	48/5.7	52/6.6	New/–	68	751/24/5	gi|119354	Enolase 2-phosphoglycerate-dehydratase	*Solanum lycopersicum*	Glycolysis/gluconeogenesis
20	39/5.9	43/6.8	New/–	43	523/15/4	gi|7430935	Probable cinnamyl–alcohol dehydrogenase (EC1.1.1.195)	*Solanum lycopersicum*	Other enzymes
21	44/8.1	41/7.3	New/–	54	423/22/4	gi|12003246	Pyruvate dehydrogenase	*Solanum lycopersicum*	Glycolysis/gluconeogenesis; butanoate metabolism; valine, leucine and isoleucine biosynthesis; alanine and aspartate metabolism; pyruvate metabolism
22	35/5.8	35/6.4	–2.6/–3.4	81	853/29/5	gi|75221385	Fructokinase-2	*Solanum lycopersicum*	Fructose and mannose metabolism; starch and sucrose metabolism

(continued on next page)

Table 1 *(continued)*

No.	Teor. MW/pI	Exp. MW/pI	*vs.* 10 Cd/ *vs.* 100 Cd	Cov.	Score/pep/ion	ID	Homology	Species	Matched pathway in KEGG
23	35/6.2	31/7.7	−2.9/–	53	521/11/5	gi|544011	Basic 30 kDa endochitinase precursor	*Solanum lycopersicum*	Aminosugars metabolism
24	61/5.4	59/6.3	−2.1/−2.8	41	426/16/2	gi|4582924	Phosphoglycerate mutase	*Solanum tuberosum*	Glycolysis/gluconeogenesis
25	53/6.9	53/7.1	−2.3/−6.0	38	146/13/1	gi|23321340	Dihydrolipoamide dehydrogenase precursor	*Solanum lycopersicum*	Citrate cycle (TCA cycle); pyruvate metabolism; glycolysis/gluconeogenesis; valine, leucine and isoleucine degradation; alanine and aspartate metabolism; glycine, serine and threonine metabolism
26	35/5.8	35/6.6	−2.0/−2.7	47	101/13/0	gi|75221385	Fructokinase-2	*Solanum lycopersicum*	Fructose and mannose metabolism; starch and sucrose metabolism
27	36/5.7	40/6.5	Lost/Lost	58	187/15/2	gi|83283965	Malate dehydrogenase-like protein	*Solanum tuberosum*	Citrate cycle (TCA cycle); pyruvate metabolism; reductive carboxylate cycle (CO2 fixation); glyoxylate and dicarboxylate metabolism; carbon fixation
28	28/5.9	28/6.0	–/+4.0	69	323/12/4	gi|544007	Acidic 26 kDa endochitinase precursor	*Solanum lycopersicum*	Aminosugars metabolism
29	28/5.8	23/7.6	–/+2.8	45	402/6/4	gi|31095603	PR5-like protein	*Solanum lycopersicum*	
30	73/5.1	73/5.6	–/+2.1	43	611/29/4	gi|1346172	Luminal-binding protein precursor (BiP) (78 kDa glucose-regulated protein homolog)	*Solanum lycopersicum*	MAPK signaling pathway; pores ion channels; chaperones and folding catalysts
31	40/5.5	40/6.1	–/+2.4	17	148/6/2	gi|3851003	Pyruvate dehydrogenase E1 beta subunit isoform 3	*Zea mays*	Pyruvate metabolism; glycolysis/ gluconeogenesis; butanoate metabolism; valine, leucine and isoleucine biosynthesis; alanine and aspartate metabolism
32	36/6.1	39/6.7	–/+2.1	70	451/17/3	gi|77999077	Malate dehydrogenase	*Lycopersicon chilense*	Pyruvate metabolism; reductive carboxylate cycle (CO2 fixation); glyoxylate and dicarboxylate metabolism; citrate cycle (TCA cycle); carbon fixation
33	36/8.8	39/7.0	–/+2.2	46	106/9/1	gi|52139816	Mitochondrial malate dehydrogenase	*Lycopersicon esculentum*	Pyruvate metabolism; reductive carboxylate cycle (CO2 fixation); glyoxylate and dicarboxylate metabolism; citrate cycle (TCA cycle); carbon fixation
34	24/5.8	24/6.9	–/+2.4	39	195/7/4	gi|2290782	Glutathione S-transferase, class phi	*Solanum commersonii*	MAPK signaling pathway; metabolism of xenobiotics by cytochrome P450; glutathione metabolism
35	38/6.7	75/7.3	–/New	13	118/7/1	gi|2230959	Pathogenesis related protein P69G	*Lycopersicon esculentum*	

36	42/5.8	38/6.2	–/New	45	135/14/1	gi|48478827	UDP-glucose:protein transglucosylase-like protein SlUPTG1	*Lycopersicon esculentum*	
37	48/5.7	51/6.3	–/–2.5	63	417/20/4	gi|119354	Enolase (2-phosphoglycerate-dehydratase)	*Solanum lycopersicum*	Glycolysis/gluconeogenesis
38	42/6.0	43/6.7	–/–3.5	38	285/12/3	gi|82621108	Phosphoglycerate kinase-like	*Solanum tuberosum*	Glycolysis/gluconeogenesis Carbon fixation
39	32/5.9	41/7.2	–/–3.6	19	111/4/1	gi|2078298	Glyceraldehyde 3-phosphate dehydrogenase	*Lycopersicon esculentum*	Glycolysis/gluconeogenesis
40	99/8.1	34/6.1	–/–3.0	21	82/16/0	gi|108710078	Transposon protein, putative, CACTA, En/Spm sub-class	*Oryza sativa*	
41	28/5.5	28/5.9	–/–2.5	17	279/4/3	gi|1351282	Triosephosphate isomerase, cytosolic	*Stellaria longipes*	Glycolysis/gluconeogenesis; carbon fixation; fructose and mannose metabolism; inositol metabolism
42	70/8.0	65/7.4	–/–13.6	39	507/23/4	gi|37359708	LEXYL2	*Solanum lycopersicum*	Starch and sucrose metabolism; cyanoamino acid metabolism; phenylpropanoid biosynthesis
43	43/8.9	49/7.0	–/–29.9	49	269/18/3	gi|72011375	Monodehydroascorbate reductase	*Lycopersicon esculentum*	Ascorbate and aldarate metabolism
44	39/6.7	41/7.5	–/–2.3	21	311/9/3	gi|13591616	UDP-D-glucuronate carboxy-lyase	*Pisum sativum*	Polyketide sugar unit biosynthesis; biosynthesis of vancomycin group antibiotics; streptomycin biosynthesis; nucleotide sugars metabolism
45	29/7.0	32/6.2	–/–2.2	25	76/5/1	gi|82621186	Transcription factor APFI-like	*Solanum tuberosum*	
46	22/9.6	33/7.2	–/–12.7	45	77/9/0	gi|110681480	Putative transcription factor	*Platanus x acerifolia*	
47	60/6.3	53/6.5	–/–2.1	50	447/22/4	gi|410633	Cytochrome c reductase-processing peptidase subunit I, MPP subunit I,	*Solanum tuberosum*	Peptidases
48	60/5.9	52/5.7	–/–2.9	56	706/23/5	gi|114421	ATP synthase subunit beta, mitochondrial precursor	*Nicotiana plumbaginifolia*	Oxidative phosphorylation
49	22/6.0	22/7.4	–/–2.3	26	221/5/2	gi|15239652	FQR1 (flavodoxin-like quinone reductase 1)	*Arabidopsis thaliana*	General function prediction only
50	48/5.7	51/6.2	–/Lost	63	624/21/5	gi|119354	Enolase (2-phosphoglycerate-dehydratase)	*Solanum lycopersicum*	Glycolysis/gluconeogenesis
51	36/8.9	38/6.5	–/Lost	55	193/11/2	gi|52139816	Mitochondrial malate dehydrogenase	*Solanum chilense*	Carbon fixation; citrate cycle (TCA cycle); pyruvate metabolism; reductive carboxylate cycle (CO2 fixation); glyoxylate and dicarboxylate metabolism
52	32/5.9	40/6.7	–/Lost	45	342/11/4	gi|2078298	Glyceraldehyde 3-phosphate dehydrogenase	*Lycopersicon esculentum*	Glycolysis/gluconeogenesis
53	45/6.3	44/7.2	–/Lost	52	420/20/4	gi|71834851	NADH-glutamate dehydrogenase	*Lycopersicon esculentum*	D-glutamine and D-glutamate metabolism; arginine and proline metabolism; nitrogen metabolism; glutamate metabolism

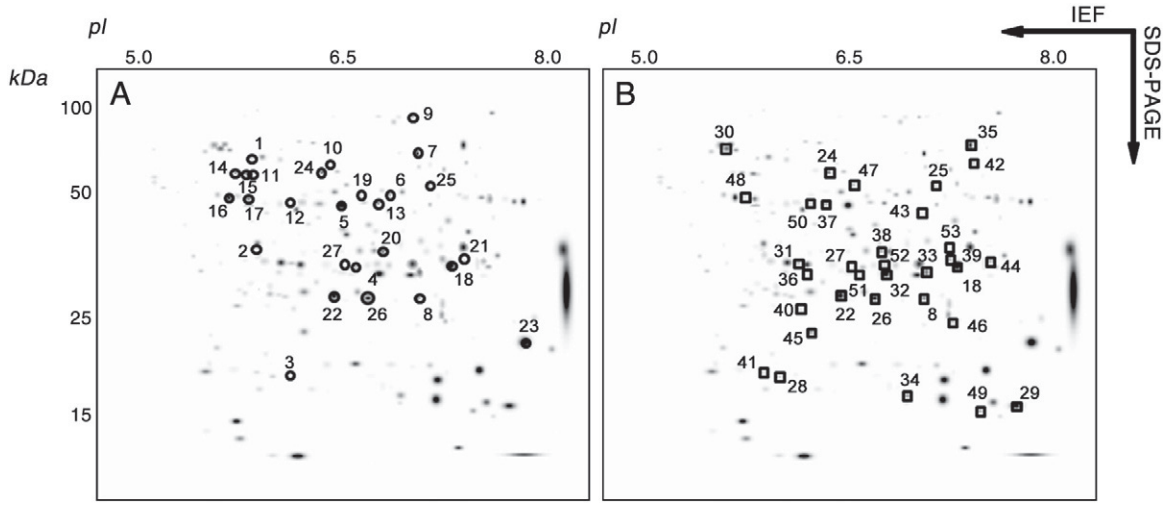

Fig. 3 – Polypeptides identified in root extracts of plants grown with 10 (circles in A) and 100 μM Cd (squares in B). Polypeptides with significant homologies to proteins present in databases (using MALDI MS–MS and MASCOT, described in detail in Table 1) were annotated on a virtual composite gel image (see Fig. 1).

PGM and dihydrolipoamide dehydrogenase, which may constitute a general response to Cd toxicity in tomato. The decrease in the relative amount of fructokinase in Cd toxicity indicates that glucose is preferred over fructose as initial substrate in the glycolytic pathway, and this could be related to the use of starch as an energy source instead of sucrose. This hypothesis would be in consonance with the low photosynthetic rates measured in these plants [12] that would cause a shortage of available sucrose.

Interestingly, changes in the glycolytic pathway observed in the 10 μM Cd treatment have been described at the proteomic level in roots of Fe-starved tomato plants [40]. Moreover, a Cd-induced Fe deficiency has been described before at the physiological level [11,12,45]; also, the Fe concentration in leaves of tomato plants grown at low Cd concentrations were 50% lower than that measured in control plants while in plants grown at 100 μM Cd leaf Fe concentrations did not change [12]. Therefore, we propose that the toxicity changes observed at low Cd are likely due to a Cd-induced Fe deficiency; conversely, changes found when plants are exposed to high Cd would reflect a shutdown of carbohydrate metabolism as result of true Cd toxicity.

3.2.1.2. *TCA cycle*. Aconitase (spot 9) and succinate dehydrogenase (spot 10) increased 3- and 5-fold in the 10 μM Cd treatment when compared to control plants, suggesting an up-regulation of the TCA cycle; however, at 100 μM Cd no changes in these proteins were found. Concerning malate dehydrogenase (MDH), four different spots were identified. One of them was no longer detected at 10 μM Cd (spot 27), whereas at 100 μM Cd the two more abundant spots were up-regulated (spots 32 and 33, approximately 2-fold) and the two less abundant spots disappeared (spots 27 and 51) (Table S1). Increases in root activities of several TCA cycle enzymes, including MDH, have been described in tomato plants grown with 10 and 100 μM Cd [12]. Also, in *Arabidopsis* roots and *Arabidopsis* cell cultures increases in proteins involved in the TCA cycle have been measured after Cd exposure [28,34]. In contrast, the relative amount of a large number of TCA-related proteins decreased in poplar roots exposed to a Cd excess [44]. These facts are in line with changes observed in glycolysis, and may point to differences between Cd-tolerant and Cd-sensitive species. Also, increases in TCA-related proteins and activities have been described in roots of Fe-deficient plants [40,46], which again supports that low Cd exposure may elicit a response similar to that of Fe deficiency. Differences in the MDH polypeptidic pattern in Cd exposed tomato roots may be due to the existence of different isoforms, possibly with different intracellular localization (cytosolic and mitochondrial) and functions (TCA and non-TCA-related), and/or the presence of PTMs.

3.2.2. *Energy metabolism*

Low Cd treatment (10 μM) caused an increase in the relative amount of the ATP synthase subunit beta, represented by 2 spots (spots 16 and 17; 2-fold increases over control values). However, at high Cd supply, energy production seemed to be down-regulated, since the ATP synthase subunit beta (spot 48), and cytochrome c reductase-processing peptidase subunit I (spot 47) decreased markedly (by 70 and 50%, respectively) when compared to the controls. Again, results suggest that low Cd concentrations elicit responses similar to those observed in Fe-deficient roots, where respiratory activities increase [40,46]. Interestingly, no changes in ATP synthase were measured in Cd treated poplar [44]. The decrease in energy production at 100 μM Cd might be related not only to the decreased glycolysis and TCA activities, but to other effects of Cd toxicity, as suggested by the decrease in the relative amount of a proccessing peptidase responsible for cytochrome c reductase synthesis.

3.2.3. *Cell wall and cytoskeleton*

Root Cd exposure caused a reorganization of cell wall composition at both Cd concentrations, as revealed by several protein changes. Ten micromolar induced relative increases in three proteins related to cell wall organization, Sl-UPTG1,

glucan endo 1–3 betaglucosidase A and UTP-glucose-1-phosphate uridyltransferase (spots 4, 8 and 13; 5-, 3- and 4-fold, respectively). Also, cinnamyl–alcohol dehydrogenase (spot 20) was detected *de novo*, and a 6-fold increase in a cytoskeleton protein, actin-51 (spot 2), was observed at 10 μM Cd. In the 100 μM Cd treatment, three of such proteins, Sl-UPTG1 (spot 36), glucan endo 1–3 betaglucosidase (spot 8) and acidic 26 kDa endochitinase precursor (spot 28) increased markedly (newly appearing, 29- and 4-fold, respectively). On the other hand, several proteins related to cell wall organization were down-regulated with Cd toxicity; this included a 70% decrease in a basic 30 kDa endochitinase precursor (spot 23) at 10 μM Cd and 93 and 50% decreases of LEXYL2 (spot 42) and UDP-D-glucuronate carboxy-lyase (spot 44) at 100 μM Cd.

Cell walls participate in metal binding and can play an important role in metal tolerance and accumulation. Cell wall reorganization has been described previously in heavy metal toxicities, including Cd [47]. In particular, an increase in cynnamyl alcohol deshydrogenase has been described previously in roots grown at Cu and Cd toxic concentrations [48]. Cell wall related changes observed in both Cd treatments were different to those observed in Fe-deficient tomato roots; for instance, decreases in glucan endo 1–3 betaglucosidase occur with Fe deficiency [40]. This suggests that changes found are not related specifically to Fe deficiency but instead may reflect generic heavy metal or stress responses, as also suggested by changes in several chitinases.

3.2.4. *Protein metabolism: protein folding and proteolysis*

Seven proteins related to protein metabolism were up-regulated in the 10 μM Cd treatment, whereas just one increased with 100 μM Cd. In the 10 μM Cd treatment there were relative increases in five chaperones: heat shock protein (HSP) 68 (spot 1; 3-fold), putative TPR-repeat protein (spot 7; 2-fold), chaperonin 60 beta subunit (spots 11 and 14; 12- and 2-fold) and HSP 60 (spot 15; 2-fold) and two peptidases: proteasome-like protein alpha subunit (spot 3; 2-fold) and neutral leucine aminopeptidase preprotein (spot 6; 3-fold). The 100 μM Cd treatment caused a 2-fold increase in a luminal-binding protein precursor (spot 30). Increases in chaperonin as well as in peptidase relative amounts have been described previously as a result of heavy metal toxicity and are a common marker of plant stress [44]. Chaperonins could prevent protein denaturation even in the presence of Cd in the cytoplasm, while proteases could recycle proteins unfolded by Cd. Interestingly, a larger number of these proteins was increased in the 10 μM when compared to the 100 μM Cd treatment, suggesting that in the high Cd treatment the plant has ceased to try to overcome Cd toxicity.

3.2.5. *Others*

The 100 μM Cd treatment caused increases in two plant stress related proteins, the PR5-like protein (spot 29; 3-fold) and the pathogenesis related protein P69G (spot 35; newly appearing), and also in gluthatione S-transferase class phi (GST; spot 34; 2-fold), a protein involved in gluthatione metabolism. Increases in GST, an enzyme that conjugates GSH to cytotoxic products, have been found in all root and cell culture proteomic studies on Cd toxicity to date, suggesting that this is a general plant response to Cd toxicity. On the other hand, PC synthesis has been widely described as a mechanism of Cd detoxification [19]. However, no components of S assimilation, cysteine or GSH biosynthesis were detected to change in response to Cd exposure in the present work, and just a couple of proteins related to S assimilation have been described to increase in other proteomic studies [34,35,44]. The absence of PCs in our gels may be due to the low MWs of these peptides, but also to experimental limitations as commented above (Section 3.1).

A 97% and a 60% decrease in monodehydroascorbate reductase (spot 43; MDAR) and flavin mononucleotide-binding flavodoxin-like quinone reductase (spot 49; FQR1), oxidative stress protecting enzymes [49], were measured at 100 μM Cd, and this might be associated with the increase in GST [44]. A decrease in MDAR has been also found with Cd treatment in poplar roots [44], although the opposite occurs in *B. juncea* roots [35]. Interestingly, MDAR changes were not observed in tomato roots grown at 10 μM Cd. High Cd treatment caused the disappeareance of glutamate dehydrogenase (GDH, spot 53), an enzyme involved in N metabolism. A similar decrease was measured in poplar roots [44] whereas in *A. thaliana* cell cultures an increase in this enzyme was found [28]. A general decrease in N assimilation in roots of Cd exposed plants has been described [44,50]. In a previous study with Cd treated tomato roots [50], protein concentration and transcript abundance of GDH did not change with Cd toxicity whereas GDH activity increased, suggesting the existence of allosteric regulation. Since GDH was the only enzyme related to N metabolism that changed with Cd toxicity, no conclusions can be drawn from our results regarding N metabolism.

Three proteins involved in gene regulation, the transposon protein CACTA (spot 40), the transcription factor APFI-like (spot 45) and the putative transcription factor (spot 46), decreased in the 100 μM Cd treatment (by 70, 50, and 92%, respectively).

4. Conclusion

An overview of the results is presented in Fig. 4. Our data suggest that different responses of the primary C metabolism occur in low *vs.* high Cd exposures. Low Cd toxicity (10 μM Cd) causes an up-regulation of the glycolytic pathway, TCA cycle and respiration, likely to produce energy to cope with the low photosynthetic rates of these plants [12]. These root responses, along with the leaf chlorophyll and Fe decreases [12], are similar to those observed in Fe-deficient plants, suggesting that at least some of the low Cd tomato responses are due to Fe deficiency, as also suggested by physiological studies [11,12,40,45]. At high Cd concentrations (100 μM) major decreases in growth [12], a shutdown of the carbohydrate metabolism and decreases in respiration occur, with no consistent changes in TCA cycle-related proteins (Fig. 4). Also, evidence for an increase in detoxifying activities (GST) was found. This suggests that effects are mainly linked to true Cd toxicity, perhaps associated to protein degradation by oxidative stress.

Also, these results, along with those of other proteomic and physiological studies, indicate that different responses of the primary C metabolism at low Cd concentrations are observed in tolerant *vs.* non tolerant plants. In non tolerant plants, such

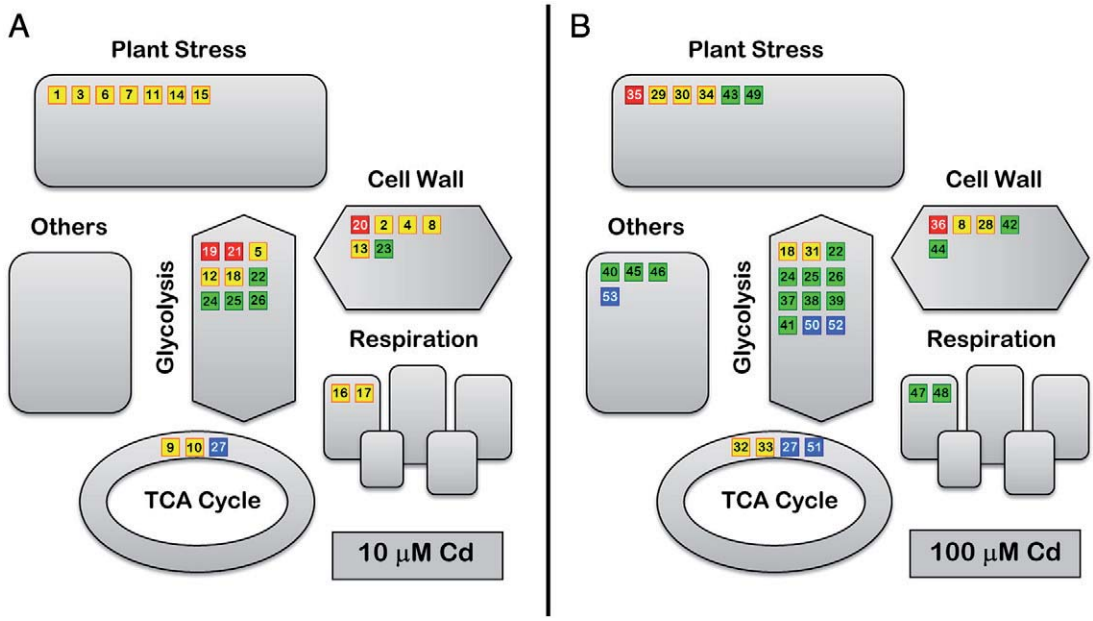

Fig. 4 – Changes in metabolic pathways as affected by Cd. Panels A and B are for 10 and 100 μM Cd treated plants, respectively. Pathways related to the identified proteins were integrated according to the KEGG database. A statistical Student t-test was performed to show relevant changes between samples. Red symbols mean newly detected proteins in Cd treated roots and yellow symbols proteins showing increases in intensity compared to control (using a 2-fold threshold change). The same threshold (decreases larger than 50%) was selected for proteins showing decreases in intensity (green symbols). Blue symbols indicate proteins not detected in Cd treated roots. Numbers correspond to those in Table 1.

as tomato, C and energy metabolism increase, whereas in tolerant plants, such as poplar, C metabolism decreased and energy metabolism did not change [30].

Acknowledgements

JRC and RRA were supported by I3P and FPI predoctoral fellowships from the CSIC and MCINN (Spanish Ministry of Science and Innovation), respectively. This work was supported by the MICINN (project AGL2007-61948, cofinanced with FEDER) and the Aragón Government (group A03). The authors thank Adelina Calviño for her help in growing and harvesting the plants.

Appendix A. Supplementary data

Supplementary data associated with this article can be found, in the online version, at doi:10.1016/j.jprot.2010.05.001.

REFERENCES

[1] Alloway BJ, Jackson AP, Morgan H. The accumulation of cadmium by vegetables grown on soils contaminated from a variety of sources. Sci Total Environ 1990;91:223–36.
[2] Adams ML, Zhao FJ, McGrath SP, Nicholson FA, Chambers BJ. Predicting cadmium concentrations in wheat and barley grain using soil properties. J Environ Qual 2004;33:532–41.
[3] Iribar V, Izco F, Tames P, Antigüedad I, da Silva A. Water contamination and remedial measures at the Troya abandoned Pb–Zn mine (The Basque Country, Northern Spain). Environ Geol 2000;39:800–6.
[4] Pinot F, Kreps SE, Bachelet M, Hainaut P, Bakonyi M, Polla BS. Cadmium in the environment: sources, mechanisms of biotoxicity, and biomarkers. Rev Environ Health 2000;15:299–323.
[5] Chen W, Chang AC, Wu L. Assessing long-term environmental risks of trace elements in phosphate fertilizers. Ecotoxicol Environ Saf 2007;67:48–58.
[6] Hardiman RT, Jacoby B. Absorption and translocation of Cd in bush beans *Phaseolus vulgaris*. Physiol Plant 1984;61:670–4.
[7] Korshunova YO, Eide D, Clark WG, Guerinot ML, Pakrasi HB. The IRT1 protein from *Arabidopsis thaliana* is a metal transporter with a broad substrate range. Plant Mol Biol 1999;40:37–44.
[8] Thomine S, Wang R, Ward JM, Crawford NM, Schroeder JI. Cadmium and iron transport by members of a plant metal transporter family in *Arabidopsis* with homology to Nramp genes. Proc Natl Acad Sci U S A 2000;97:4991–6.
[9] Perfus-Barbeoch L, Leonhardt N, Vavasseur A, Forestier C. Heavy metal toxicity: cadmium permeates through calcium channels and disturbs the plant water status. Plant J 2002;32:539–48.
[10] Senden MHMN, Wolterbeek HT. Effect of citric acid on the transport of cadmium through xylem vessels of excised tomato stem-leaf systems. Acta Bot Neerl 1990;39:297–303.
[11] Larbi A, Morales F, Abadía A, Gogorcena Y, Lucena JJ, Abadía J. Effects of Cd and Pb in sugar beet plants grown in nutrient solution: induced Fe deficiency and growth inhibition. Funct Plant Biol 2002;29:1453–64.
[12] López-Millán A-F, Sagardoy R, Solanas M, Abadía A, Abadía J. Cadmium toxicity in tomato (*Lycopersicon esculentum*) plants grown in hydroponics. Environ Exp Bot 2009;65:376–85.

[13] Ciscato M, Vangronsveld J, Valcke R. Effects of heavy metals on the fast chlorophyll fluorescence induction kinetics of photosystem II: a comparative study. J Biosci 1999;54:735–9.
[14] Dong J, Wu F, Zhang G. Influence of cadmium on antioxidant capacity and four microelement concentrations in tomato seedlings (*Lycopersicon esculentum*). Chemosphere 2006;64: 1659–66.
[15] Cuypers A, Vangronsveld J, Clijsters H. The chemical behaviour of heavy metals plays a prominent role in the induction of oxidative stress. Free Radic Res 1999;31:S39–43 Suppl.
[16] Chen YX, He YF, Luo YM, Yu YL, Lin Q, Wong MH. Physiological mechanism of plant roots exposed to cadmium. Chemosphere 2003;50:789–93.
[17] Lin R, Wang X, Luo Y, Du W, Guo H, Yin D. Effects of soil cadmium on growth, oxidative stress and antioxidant system in wheat seedlings (*Triticum aestivum* L.). Chemosphere 2007;69:89–98.
[18] Cobbett C, Goldsbrough P. Phytochelatins and metallothioneins: roles in heavy metal detoxification and homeostasis. Annu Rev Plant Biol 2002;53:159–82.
[19] Cobbett CS. Phytochelatins and their roles in heavy metal detoxification. Plant Physiol 2000;123:825–32.
[20] Lombi E, Tearall KL, Howarth JR, Zhao FJ, Hawkesford MJ, McGrath SP. Influence of iron status on cadmium and zinc uptake by different ecotypes of the hyperaccumulator *Thlaspi caerulescens*. Plant Physiol 2002;128:1359–67.
[21] Zhao FJ, Jiang RF, Dunham SJ, McGrath SP. Cadmium uptake, translocation and tolerance in the hyperaccumulator *Arabidopsis halleri*. New Phytol 2006;172:646–54.
[22] Kupper H, Mijovilovich A, Meyer-Klaucke W, Kroneck PM. Tissue- and age-dependent differences in the complexation of cadmium and zinc in the cadmium/zinc hyperaccumulator *Thlaspi caerulescens* (Ganges ecotype) revealed by X-ray absorption spectroscopy. Plant Physiol 2004;134:748–57.
[23] Weber M, Harada E, Vess C, Roepenack-Lahaye E, Clemens S. Comparative microarray analysis of *Arabidopsis thaliana* and *Arabidopsis halleri* roots identifies nicotianamine synthase, a ZIP transporter and other genes as potential metal hyperaccumulation factors. Plant J 2004;37:269–81.
[24] Ueno D, Ma JF, Iwashita T, Zhao FJ, McGrath SP. Identification of the form of Cd in the leaves of a superior Cd-accumulating ecotype of *Thlaspi caerulescens* using 113Cd-NMR. Planta 2005;221:928–36.
[25] Hernández-Allica J, Garbisu C, Becerril JM, Barrutia O, García-Plaizaola JI, Zhao FJ, et al. Synthesis of low molecular weight thiols in response to Cd exposure in *Thlaspi caerulescens*. Plant Cell Environ 2006;29:1422–9.
[26] Ma JF, Ueno D, Zhao FJ, McGrath SP. Subcellular localisation of Cd and Zn in the leaves of a Cd-hyperaccumulating ecotype of *Thlaspi caerulescens*. Planta 2005;220:731–6.
[27] Sobkowiak R, Deckert J. Proteins induced by cadmium in soybean cells. J Plant Physiol 2006;163:1203–6.
[28] Sarry JE, Kuhn L, Ducruix C, Lafaye A, Junot C, Hugouvieux V, et al. The early responses of *Arabidopsis thaliana* cells to cadmium exposure explored by protein and metabolite profiling analyses. Proteomics 2006;6:2180–98.
[29] Schneider T, Schellenberg M, Meyer S, Keller F, Gehrig P, Riedel K, et al. Quantitative detection of changes in the leaf-mesophyll tonoplast proteome in dependency of a cadmium exposure of barley (*Hordeum vulgare* L.) plants. Proteomics 2009;9:2668–77.
[30] Kieffer P, Dommes J, Hoffmann L, Hausman JF, Renaut J. Quantitative changes in protein expression of cadmium-exposed poplar plants. Proteomics 2008;8:2514–30.
[31] Kieffer P, Planchon S, Oufir M, Ziebel J, Dommes J, Hoffmann L, et al. Combining proteomics and metabolite analyses to unravel cadmium stress-response in poplar leaves. J Proteome Res 2009;8:400–17.
[32] Tuomainen MH, Nunan N, Lehesranta SJ, Tervahauta AI, Hassinen VH, Schat H, et al. Multivariate analysis of protein profiles of metal hyperaccumulator *Thlaspi caerulescens* accessions. Proteomics 2006;6:3696–706.
[33] Fagioni M, Zolla L. Does the different proteomic profile found in apical and basal leaves of spinach reveal a strategy of this plant toward cadmium pollution response? J Proteome Res 2009;8:2519–29.
[34] Roth U, von Roepenack-Lahaye E, Clemens S. Proteome changes in *Arabidopsis thaliana* roots upon exposure to Cd^{2+}. J Exp Bot 2006;57:4003–13.
[35] Alvarez S, Berla BM, Sheffield J, Cahoon RE, Jez JM, Hicks LM. Comprehensive analysis of the *Brassica juncea* root proteome in response to cadmium exposure by complementary proteomic approaches. Proteomics 2009;9:2419–31.
[36] Aloui A, Recorbet G, Gollotte A, Robert F, Valot B, Gianinazzi-Pearson V, et al. On the mechanisms of cadmium stress alleviation in *Medicago truncatula* by arbuscular mycorrhizal symbiosis: a root proteomic study. Proteomics 2009;9:420–33.
[37] Ombretta R, Gwénaelle B-C, Eliane D-G, Graziella B, Vivienne G-P, Silvio G. Targeted proteomics to identify cadmium-induced protein modifications in *Glomus mosseae*-inoculated pea roots. New Phytol 2003;157:555–67.
[38] Aina R, Labra M, Fumagalli P, Vannini C, Marsoni M, Cucchi U, et al. Thiol-peptide level and proteomic changes in response to cadmium toxicity in *Oryza sativa* L. roots. Environ Exp Bot 2007;59:381–92.
[39] Gil C, Boluda R, Ramos J. Determination and evaluation of cadmium, lead and nickel in greenhouse soils of Almeria (Spain). Chemosphere 2004;55:1027–34.
[40] Li J, Wu XD, Hao ST, Wang XJ, Ling HQ. Proteomic response to iron deficiency in tomato root. Proteomics 2008;8:2299–311.
[41] Ahsan N, Lee DG, Lee SH, Kang KY, Bahk JD, Choi MS, et al. A comparative proteomic analysis of tomato leaves in response to waterlogging stress. Physiol Plant 2007;131:555–70.
[42] Andaluz S, López-Millán AF, De las Rivas J, Aro EM, Abadía J, Abadía A. Proteomic profiles of thylakoid membranes and changes in response to iron deficiency. Photosynth Res 2006;89:141–55.
[43] Brumbarova T, Matros A, Mock HP, Bauer P. A proteomic study showing differential regulation of stress, redox regulation and peroxidase proteins by iron supply and the transcription factor FER. Plant J 2008;54:321–34.
[44] Kieffer P, Schroder P, Dommes J, Hoffmann L, Renaut J, Hausman JF. Proteomic and enzymatic response of poplar to cadmium stress. J Proteomics 2009;72:379–96.
[45] Fodor F, Gaspar L, Morales F, Gogorcena Y, Lucena JJ, Cseh E, et al. Effects of two iron sources on iron and cadmium allocation in poplar (*Populus alba*) plants exposed to cadmium. Tree Physiol 2005;25:1173–80.
[46] López-Millán AF, Morales F, Andaluz S, Gogorcena Y, Abadía A, De Las Rivas J, et al. Responses of sugar beet roots to iron deficiency. Changes in carbon assimilation and oxygen use. Plant Physiol 2000;124:885–98.
[47] Kováčik J, Klejdus B. Dynamics of phenolic acids and lignin accumulation in metal-treated *Matricaria chamomilla* roots. Plant Cell Rep 2008;27:605–15.
[48] Kováčik J, Klejdus B, Hedbavny J, Štork F, Bačkor M. Comparison of cadmium and copper effect on phenolic metabolism, mineral nutrients and stress-related parameters in *Matricaria chamomilla* plants. Plant Soil 2009;320:231–42.

[49] Laskowski MJ, Dreher KA, Gehring MA, Abel S, Gensler AL, Sussex IM. FQR1, a novel primary auxin-response gene, encodes a flavin mononucleotide-binding quinone reductase. Plant Physiol 2002;128:578–90.

[50] Chaffei C, Pageau K, Suzuki A, Gouia H, Ghorbel MH, Masclaux-Daubresse C. Cadmium toxicity induced changes in nitrogen management in *Lycopersicon esculentum* leading to a metabolic safeguard through an amino acid storage strategy. Plant Cell Physiol 2004;45:1681–93.

Plant Physiology and Biochemistry 47 (2009) 1082–1088

Contents lists available at ScienceDirect

Plant Physiology and Biochemistry

journal homepage: www.elsevier.com/locate/plaphy

Research article

Time course induction of several key enzymes in Medicago truncatula roots in response to Fe deficiency

Sofía Andaluz, Jorge Rodríguez-Celma, Anunciación Abadía, Javier Abadía*, Ana-Flor López-Millán

Department of Plant Nutrition, Estación Experimental de Aula Dei, Consejo Superior de Investigaciones Científicas (CSIC), P.O. BOX 13034, E-50080 Zaragoza, Spain

ARTICLE INFO

Article history:
Received 9 January 2009
Accepted 24 July 2009
Available online 15 August 2009

Keywords:
Acidification
Iron
Iron reductase
Medicago truncatula
Phospho*enol*pyruvate carboxylase
Riboflavin
6,7-Dimethyl-8-ribityllumazine synthase

ABSTRACT

Medicago truncatula constitutes a good model for Strategy I plants, since when this plant is challenged with Fe shortage the most important root physiological responses induced by Fe deficiency are developed, including the yellowing of root tips. A better understanding of the mechanisms involved in root adaptation to Fe deficiency in *M. truncatula* may strengthen our ability to enhance Fe efficiency responses in other plant species, especially in different agronomically relevant legumes. Riboflavin concentration, phospho*enol*pyruvate carboxylase (EC 4.1.1.31) and Fe reductase activities, and acidification capacity have been determined in *M. truncatula* roots at different time points after imposing Fe deficiency. Root riboflavin concentrations increased with Fe deficiency and concomitantly *MtDMRL* was upregulated at the transcriptional level, supporting a role for flavins in the Fe deficiency response. Root Fe reductase and phospho*enol*pyruvate carboxylase activities as well as acidification capacity were higher in roots of Fe-deficient than in control plants, and the corresponding genes, *MtFRO1*, *MtPEPC1* and *MtHA1* were also upregulated by Fe deficiency. Expression of these genes and their corresponding physiological activities followed different patterns over time, suggesting the existence of both transcriptional and post-transcriptional regulation.

1. Introduction

Iron is an essential micronutrient for all living organisms, including plants, since it takes part in fundamental biological redox processes, such as respiration and photosynthesis [21]. Although Fe is the fourth most abundant element in the earth's crust, plant Fe deficiency is a worldwide problem, especially in high pH, calcareous soils. In these soils, Fe is present in oxidized forms with low solubility that are not readily available to plants [19]. Plants can be broadly classified into two groups based on the root mechanism for Fe uptake: Strategy I plants, which include dicotyledonous and non-grass monocotyledonous species, and Strategy II plants, which include Poaceae species (see [15] for a review).

When grown under Fe deficiency, Strategy I plant species develop a series of morphological and biochemical changes that increase their capacity for Fe uptake. Morphological changes include the swelling of root tips and formation of lateral roots, root hairs and transfer cells [16,28]. These changes lead to an increase of the root surface that allows plants to maximize Fe uptake. Biochemical changes usually include i) an enhanced excretion of protons to the rhizosphere (mediated by a plasma membrane-bound H^+-ATPase), which lowers soil pH, in turn increasing Fe(III) solubility [9,26,29]; ii) the induction of a plasma membrane ferric reductase enzyme that reduces Fe(III) to Fe(II) in root epidermal cells [22,28]; iii) the activation of a plasma membrane transport system for Fe(II) uptake [6,11]; and iv) the excretion to the growth medium of compounds such as phenolics, organic acids, and flavins, which may facilitate reduction and solubility of external Fe [32,38].

On the other hand, in Strategy I plants several changes occur at the metabolic level, in order to sustain the increased Fe uptake capacity when Fe is scarce (see [40] for a review). These changes include accumulation of organic acids (reviewed in [1]), shifts in the redox state of the cytoplasm [40] and increases in the activity of phospho*enol*pyruvate carboxylase (PEPC) and different enzymes of the Krebs cycle and the glycolitic pathway [1,40]. All hypotheses proposed so far to explain such metabolic changes grant a key role to PEPC [1,40].

Also, some Strategy I plants, when challenged with Fe deficiency, are able to accumulate and excrete to the growth medium

Abbreviations: BPDS, bathophenanthroline disulphonate; DMRL, 6,7-dimethyl-8-ribityllumazine synthase; PAR, photosynthetic active radiation; PEPC, Phospho*enol*pyruvate carboxylase; PPFD, photosynthetic photon flux density.

* Corresponding author at: Department of Plant Nutrition, Aula Dei Experimental Station, CSIC, P.O. BOX 13034, E-50080 Zaragoza, Spain. Tel.: +34976716056; fax: +34976716145.
E-mail address: jabadia@eead.csic.es (J. Abadía).

0981-9428/$ – see front matter © 2009 Elsevier Masson SAS. All rights reserved.
doi:10.1016/j.plaphy.2009.07.009

flavin compounds such as riboflavin and other flavin derivatives [32,33,38]. Iron has been shown to down-regulate riboflavin synthesis in flavinogenic yeast strains and some bacteria [31,39]. The role these flavin compounds play in the Fe efficiency response in plants is still not known, although it has been suggested that flavins accumulated in Fe-deficient sugar beet roots could act as a redox bridge for electron transport to the Fe(III) reductase [20]. Moreover, FRO2 belongs to a superfamily of flavocytochrome oxidoreductases [25] and a recent study of the topology of the *FRO2* gene confirmed that the protein contains FAD sequence motifs on the inside of the membrane [27].

Some of the key components of Strategy I mechanisms have been identified at the molecular level. The acidification is related to the activation of one or more members of the H^+-ATPase family in plants [4,24] such as *AtHA1* in *Arabidopsis* [13] and *CsHA1* in cucumber [26]. The plasma membrane bound Fe reductase in roots is encoded by genes of the *FRO* family (Fe reductase family), which includes At*FRO2* in *Arabidopsis* [25], *PsFRO1* in *Pisum sativum* [37], and *LeFRO1* in *Lycopersicon esculentum* [18]. Iron transporter genes involved in root uptake have been cloned from several plant species, including *IRT1* and *IRT2* in *Arabidopsis*, *RIT1* in *P. sativum*, *LeIRT1* and *LeIRT2* in *L. esculentum* and *MtZIP6* in *Medicago truncatula* (see [12] for a review). A relatively large number of PEPC cDNA sequences have been reported in a wide range of plant species, including *M. truncatula*. Also, a gene encoding for 6,7-dimethyl-8-ribityllumazine synthase (DMRL synthase, EC:2.5.1.9), the enzyme that catalyzes the previous to last step in riboflavin synthesis, has been characterized in *Spinacia oleracea* [14], and homologues have been identified in *A. thaliana* (At2g20690) and *Nicotiana tabacum* (AAD44809). However, the effect of Fe deficiency in the expression of the DMRL gene has not been studied so far.

M. truncatula is an emerging model legume with a number of genetic and molecular tools available. A better understanding of the mechanisms involved in root Fe acquisition and homeostasis in this species may strengthen our ability to enhance Fe-efficiency responses in other plant species, especially legumes of agronomical interest. The aim of this work was to study the time-course elicitation of some of the major Strategy I responses to Fe deficiency in roots of *M. truncatula*, including Fe reductase activity and root acidification capacity using intact roots, PEPC activity in root extracts and flavin concentrations in whole roots. The expression patterns of the corresponding genes, *MtFRO1*, *MtHA1*, *MtPEPC* and *MtDMRL*, were also studied.

2. Results

2.1. Morphological responses

M. truncatula plants grown in hydroponics with 0.5 μM Fe(III)-EDTA developed visible symptoms of leaf chlorosis gradually, whereas plants grown with 20 μM Fe(III)-EDTA were green throughout the experiment. Roots of plants grown in Fe-deficient nutrient solution developed more secondary roots than Fe-sufficient plants, and had yellowish patches as early as 3 days after treatment onset.

2.2. Riboflavin concentration

Riboflavin concentration (expressed in nmol g FW^{-1}) in roots of Fe-sufficient plants did not change markedly over time, decreasing from 2.7 at day 1 to 0.3 at day 11 after treatment onset (Fig. 1A). The more abundant flavin in Fe-deficient roots was riboflavin, with other derivatives present in smaller amounts (not shown). Riboflavin concentration increased from approximately 4 at day 1 to 28 at day 7, and decreased thereafter to approximately 11 at day 11 after treatment onset (Fig. 1A). Therefore, riboflavin concentration was from 2- to 58-fold higher in Fe-deficient roots than in the corresponding Fe-sufficient roots, and the highest increase occurred at day 7.

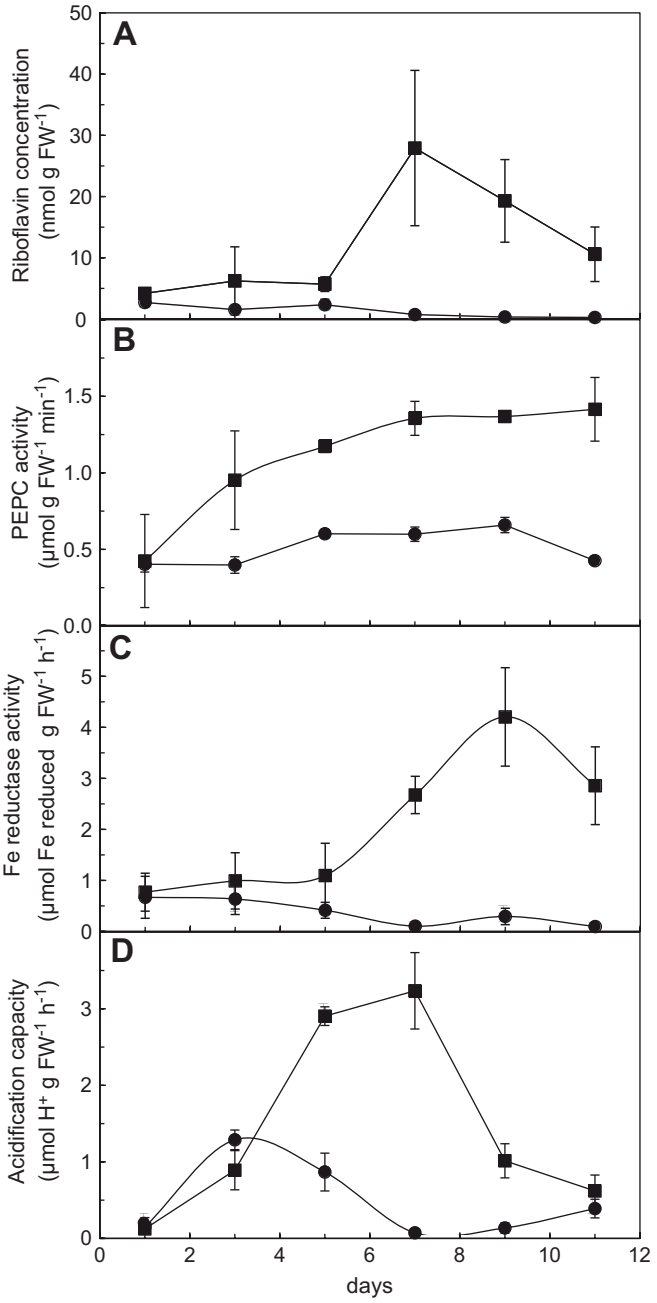

Fig. 1. Parameters measured in *M. truncatula* plants grown with 20 μM Fe (circles) or 0.5 μM Fe (squares) in the nutrient solution, 1, 3, 5, 7, 9, and 11 days after treatment onset. A) Root riboflavin concentration (nmol g FW^{-1}); B) PEPC activity in root extracts (μmol g FW^{-1} min^{-1}); C) Root iron reductase activity (μmol Fe reduced g FW^{-1} h^{-1}); and D) Root acidification capacity (μmol H^+ g FW^{-1} h^{-1}). Data are means ± SD of 3 batches of plants with 3 plants per batch.

2.3. PEPC activity

Root phospho*enol*pyruvate carboxylase activity in Fe-sufficient plants did not change markedly over time, ranging from approximately 0.4–0.7 μmol g FW^{-1} min^{-1} (Fig. 1B). In Fe-deficient plants,

PEPC activity in root extracts increased over time from 0.4 μmol g FW^{-1} min^{-1} at day 1 to 1.4 μmol g FW^{-1} min^{-1} at day 11 after treatment onset (Fig. 1B). Therefore, from day 3, root PEPC activity in Fe-deficient roots was 2- to 3-fold higher than in the corresponding Fe-sufficient roots, and the highest relative increase occurred at day 11.

2.4. Root iron reductase

Iron reductase activity in roots of Fe-sufficient plants decreased gradually over time from 0.7 μmol Fe reduced g FW^{-1} h^{-1} at day 1 to 0.1 μmol Fe reduced g FW^{-1} h^{-1} at day 11 after treatment onset (Fig. 1C). In Fe-deficient plants, root Fe reductase activities (in μmol Fe reduced g^{-1} FW h^{-1}) increased from 0.8 at day 1 to 4.2 at day 9, and then decreased to 2.9 at day 11, although this latter change was not statistically significant (Fig. 1C). Therefore, root Fe reductase activity was 27-, 14- and 29-fold higher in Fe-deficient than in Fe-sufficient roots at days 7, 9 and 11, respectively.

2.5. External acidification of the medium

In Fe-sufficient plants, root proton extrusion (expressed in μmol H^+ g FW^{-1} h^{-1}) ranged from 0.1 to 1.3 and had a maximum at day 3 after treatment onset (Fig. 1D). In Fe-deficient plants, proton extrusion increased over time from 0.1 at day 1 to 3.2 at day 7 after treatment onset, and decreased thereafter to 0.6 at day 11 (Fig. 1D). Therefore, the acidification activity of Fe-deficient roots at days 5, 7 and 9 after treatment onset was 3-, 44-, and 7-fold higher, respectively, than that of the corresponding Fe-sufficient roots.

2.6. Gene expression analysis

To identify putative PEPC and DMRL synthase open reading frames in *M. truncatula*, we performed database searches looking for ESTs and TCs with sequence similarity to previously reported genes from different species, including *A. thaliana*, *L. esculentum*, *Glycine max*, *P. sativum*, *Medicago sativa, N. tabacum* and *S. oleracea*. We identified two TCs in the TIGR *M. truncatula* gene index: *MtGI TC129218* for PEPC and *MtGI TC115110* for DMRL synthase, which contained full-length open reading frames representing putative *PEPC* and *DMRL* synthase homologues. PCR products of 2.3 kb for *PEPC* and 687 bp for *DMRL* synthase were amplified and sequenced. The translated amino acid sequence for the DMRL synthase open reading frame (228 aminoacids) displayed 61, 58 and 57% identity at the amino acid level to the DMRL synthase sequences of *A. thaliana*, *N. tabacum* and *S. oleracea*, respectively. The translated amino acid sequence for the PEPC open reading frame (744 aminoacids) displayed 94% identity at the amino acid level to the *G. max* PEPC sequence, and 80–83% to the *A. thaliana*, *L. esculentum, P. sativum,* and *M. sativa* sequences. Also, both open reading frames are tentatively annotated as *DMRL* and *PEPC* in the *M. truncatula* gene index database. Therefore, for the present work we have assigned the name *MtPEPC1* and *MtDMRL* to the amplified transcripts.

Transcript levels of Fe reductase (*MtFRO1*-AY439088), ATPase (*Mtha1*-AJ132892), PEPC (*MtPEPC1*-TC129218) and DMRL (*MtDMRL*-TC115110) were assessed by semi-quantitative RT-PCR in Fe-sufficient and Fe-deficient roots, at days 1, 3, 5, 7, 9 and 11 after treatment onset. Transcript abundance for all studied genes in roots from Fe-sufficient plants did not change significantly over time as judged by the RT-PCR images (Fig. 2) and calculated band intensities (Fig. 3). In roots from Fe-deficient plants, band intensities for all the studied genes were higher than in Fe-sufficient roots throughout the treatment (Figs. 2 and 3). In Fe-deficient roots *MtPEPC1* transcripts increased slightly over time from day 1 to day 9 and decreased at day 11 (Figs. 2 and 3), whereas *MtDMRL* and *MtFRO1* transcript abundances increased over time with a maximum at days 3–7, and 5–7, respectively, to decrease thereafter (Figs. 2 and 3). The *MtHA1* band intensities in Fe-deficient roots did not change significantly over time (Figs. 2 and 3).

3. Discussion

M. truncatula constitutes a good model for the study of Strategy I, since the most important physiological responses described so far to be induced by Fe deficiency in roots are developed in this species, including flavin accumulation, PEPC and Fe reductase activity elicitation and acidification capacity. The sequence of events upon Fe deficiency establishment was as follows: the first event was an up-regulation of *MtHA1*, which occurred already at day 1 after the

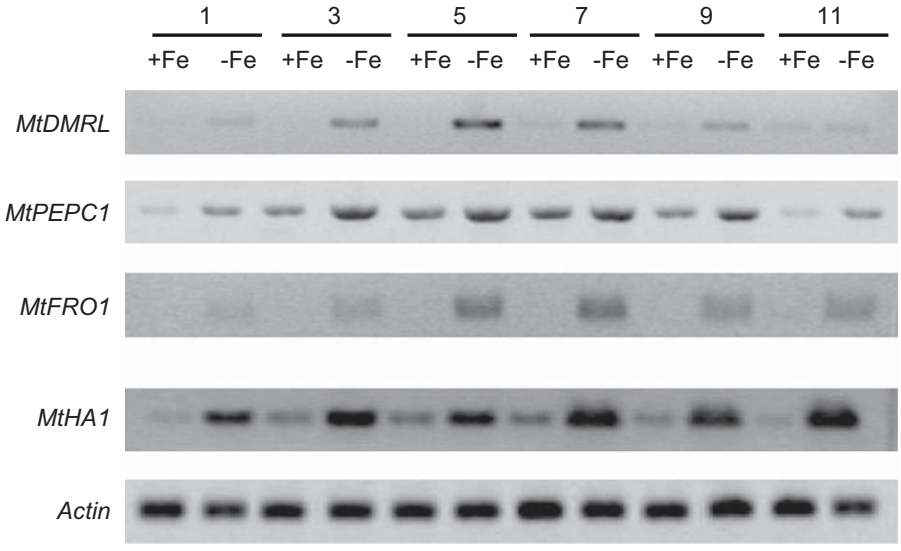

Fig. 2. Semi-quantitative RT-PCR analysis of *MtDMRL*, *MtPEPC1*, *MtFRO1*, and *MtHA1* in roots from *M. truncatula* plants grown with 20 μM Fe (+Fe) or 0.5 μM Fe (−Fe) in the nutrient solution. RNA was isolated from roots pooled from two plants per day and treatment. Three batches of plants were analyzed and PCR reactions were repeated 2 times with conditions indicated in Table 1. Images shown are representative for these PCR reactions. Actin was used as a control of RNA template.

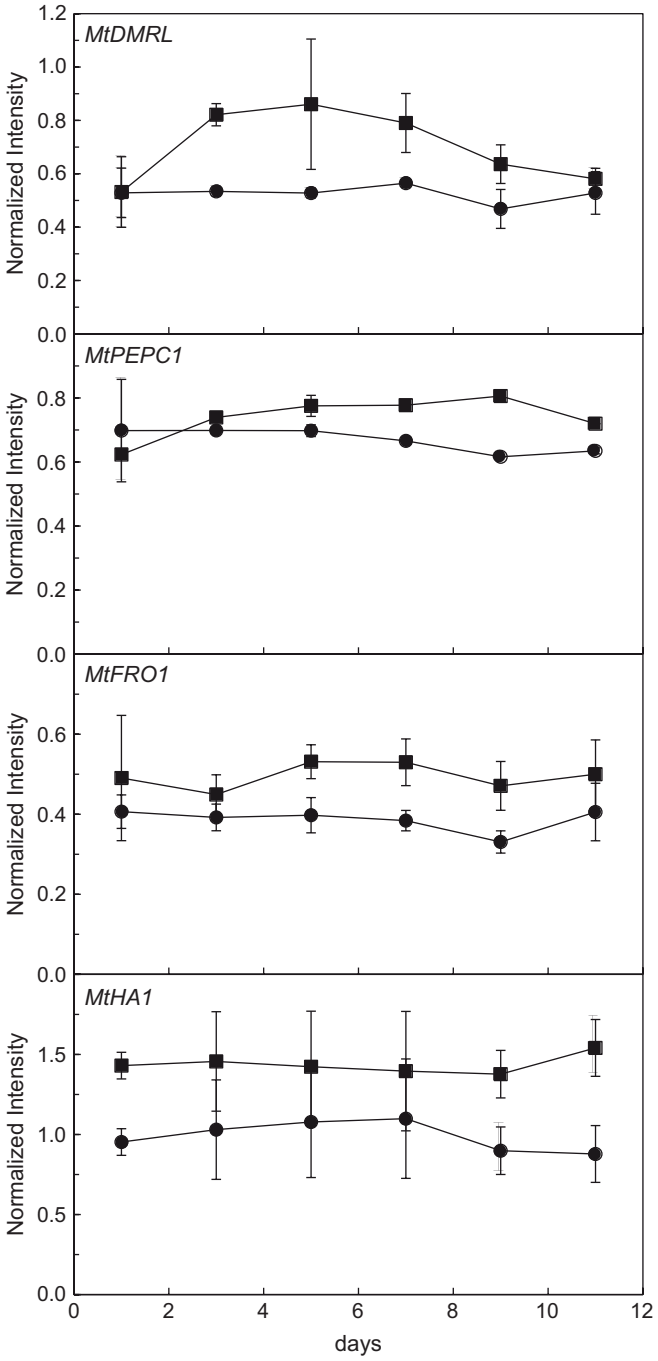

Fig. 3. Normalized band intensities from semi-quantitative RT-PCR analysis of *MtDMRL*, *MtPEPC1*, *MtFRO1*, and *MtHA1* transcripts in roots from *M. truncatula* plants grown with 20 μM Fe (circles) or 0.5 μM Fe (squares) in the nutrient solution. Intensities were normalized by dividing band area by the corresponding actin band area. Data are means ± SD of 6 replications (3 plant batches, 2 PCR reactions each).

onset of Fe deficiency, and was maintained until the end of the experiment. At day 1, this was not accompanied by an increase in acidification capacity. Then, at day 3 an increase in PEPC activity was found, although without a significant increase in *MtPEPC1* expression. This increase in PEPC activity with Fe deficiency was maintained until the end of the experiment. Also at day 3, an up-regulation of *MtDMRL* occurred, before a significant increase in root flavin concentration could be detected. At day 5, significant up-regulation of the *MtFRO1* and *MtPEPC1* genes was measured for the first time, joining the pre-existing up-regulation of *MtHA1* and *MtDMRL*. Also at day 5, a major increase in acidification capacity occurred. At day 7, acidification capacity was maintained at high levels, whereas the Fe reductase activity and riboflavin concentration increased considerably. Then, at day 9, the maximum for Fe reductase occurred, whereas acidification capacity decreased considerably and riboflavin concentration and PEPC activity were maintained at high levels. Finally, at day 11, acidification capacity and flavin concentrations decreased, whereas PEPC activity and Fe reductase remained high.

Therefore, in Fe-deficient *M. truncatula* plants, four key root responses to Fe deficiency increase while the corresponding genes, *MtDMRL*, *MtFRO1*, *MtPEPC1* and *MtHA1* were up-regulated, indicating that adaptation to Fe deficiency in *M. truncatula* roots is mediated, in part, by a transcriptional regulation of these genes by Fe status. Results provide new data for two responses whose time course development was not known, namely riboflavin root concentration and PEPC activity.

Accumulation of flavin compounds, including riboflavin and riboflavin 3′- and 5′ sulphate has been described in Fe-deficient roots of several plant species [30,32,33,38]. However, this is the first time, to our knowledge, that an up-regulation of MtDMRL, which codifies for the previous to the last enzyme in the riboflavin biosynthesis pathway, has been reported to occur with Fe-deficiency. The increase in *MtDMRL* expression occurred only 3 days after treatment onset (only after *MtHA1* upregulation), and the transcript intensity increases were the highest of all transcripts measured. A connection between Fe deficiency perception and riboflavin excretion has been described to occur through two different basic helix-loop-helix (bHLH) transcription factors in *A. thaliana* [36]. However, the exact role of these flavin compounds in Fe deficiency is still unknown. It has been hypothesised, based on the similar location of flavin accumulation and Fe reduction and on the fact that the Fe reductase is a flavin-containing protein that flavins may play an important role in the mechanism for Fe reduction in roots [5,20]. Our results support this hypothesis, since riboflavin accumulation and Fe reductase activity as well as transcript intensity of the corresponding genes in *M. truncatula* Fe-deficient roots showed similar trends over time.

PEPC activity increased only 3 days after Fe-deficiency onset in *M. truncatula* roots and remained high for the whole experiment, indicating a key role of this enzyme in the root response to Fe efficiency, whereas *MtPEPC1* was up-regulated at day 5. Increases in PEPC activity with Fe deficiency have been described in root extracts from several plant species (see reviews [1,40]). Iron deficiency induces an increase in the amount of PEPC protein in roots of cucumber [23], sugar beet [3] and tomato [17]. Also, up-regulation of the PEPC transcript by Fe status has been reported to occur in roots of Fe-deficient *A. thaliana* [34].

The increase in PEPC activity is mainly localized to the external layers of the cortical cells of Fe-deprived root apical sections, which are very active in proton extrusion [9]. Therefore, it has been proposed that cytoplasm alkalinisation caused by proton extrusion would activate PEPC activity (pH-stat theory [8]). However, our data indicate that induction of PEPC activity and acidification capacity in Fe-deficient roots did not follow a similar time course, since PEPC activity not only preceded but also survived acidification capacity increases. This also suggests that proton extrusion is not the major cause for PEPC induction in Fe-deficient *M. truncatula* roots. Proton extrusion in Strategy I plants has been attributed to an increased activity of H^+-ATPase [9,29]. Both gene transcript and protein amount have been shown to increase in Fe-deficient conditions [9,10,26]. In agreement with these previous findings, *MtHA1* transcript abundance was increased within 1 day in Fe-deficient *M. truncatula* roots, although root *MtHA1* transcript

abundances and acidification capacities did not follow the same trend over time. Our results suggest that some type of post-transcriptional regulation is taking place, in addition to the transcriptional one. Alternatively, different H^+-ATPase gene(s) not measured in this work could be involved in proton extrusion in *M. truncatula*.

An increase in gene up-regulation and activity of plasma membrane Fe reductase has been found in a number of species [18,25,28,37]. Furthermore, *A. thaliana* lines with an inactivated *AtFRO2* gene have reduced Fe reductase activity, are chlorotic, and grow slowly without elevated Fe supply [25]. Our results also show that Fe reductase activity, as well as *MtFRO1* transcript abundance, were increased with Fe deficiency, although they did not follow the same exact trend over time, suggesting the existence of a post-transcriptional regulation for this enzyme. This kind of regulation has already been proven in *A. thaliana* by using *35S-FRO2* transgenic plants, where the increase in activity was only detectable when Fe-starved [7].

In summary, we have studied the time course development of four responses to Fe deficiency in roots of *M. truncatula*, two of them not previously studied in this context in any plant species. Our results show that all four components were up-regulated with Fe deficiency, although the time course development was different in each case, suggesting the existence of both transcriptional and post-transcriptional regulation. With respect to the two responses not previously studied, both were up-regulated with Fe deficiency. PEPC had an early elicitation, was stable over time and was not closely related to changes in acidification capacity, whereas riboflavin root accumulation seems to be quite closely associated with Fe reductase activity.

4. Materials and methods

4.1. Plant material

M. truncatula (ecotype A17) plants were grown in a controlled environment chamber with a photosynthetic photon flux density (PPFD) at leaf height of 350 μmol m^{-2} s^{-1} PAR and a 16 h-22 °C/8 h-20 °C, day/night regime. Seeds were scarified by nicking the seed coat, then soaked overnight in distilled water and germinated on filter paper for 4 days in darkness. The standard solution for hydroponically grown plants contained: (in mM) 0.6 K_2SO_4, 0.5 $Ca(NO_3)_2$, 1.0 NH_4NO_3, 0.3 KH_2PO_4, 0.2 $MgSO_4$, and (in μM) 25 $CaCl_2$, 25 H_3BO_3, 2 $MnSO_4$, 2 $ZnSO_4$, 0.5 $CuSO_4$, 0.5 H_2MoO_4, 0.1 $NiSO_4$, and 20 μM as Fe(III)-EDTA. All hydroponic solutions were buffered by the addition of 1 mM MES/KOH, pH 5.5. Plants were grown for 10 days (35 plants in a 10 L container), then Fe treatments were applied by using fresh nutrient solutions with either 0.5 or 20 μM Fe, and plants were grown for 11 days. Nutrient solutions were renewed weekly. Samples for the different physiological and molecular analysis were taken 4 h after the light period onset on days 1, 3, 5, 7, 9, and 11 after treatment initiation. The experiment was replicated 3 times with different batches of plants, and three replicates were used for each measurement in each batch.

4.2. Riboflavin concentration

Root material (*ca.* 100 mg FW) was frozen in liquid N_2 and ground in a mortar with 0.1 M ammonium acetate, pH 6.1. Extracts were centrifuged for 5 min at 14,000 × g and the supernatant stored at −80 °C until analysis. Flavin compounds were analyzed by HPLC using a 100 × 8 mm Waters Radial-Pak C18 radial compression column (Waters Corp., Milford, MA, USA) [33]. Samples were injected with a Rheodyne injector (50 μL loop). Mobile phase (water: methanol 70:30, v/v) was pumped at a flow rate of 1 mL min^{-1}. Flavins were detected at 445 nm with a 996 photodiode array detector. The peak corresponding to riboflavin was identified by comparison of the retention time and UV–VIS spectra with those of a known standard from SIGMA (Saint Louis, Missouri, USA). Quantification was made with known amounts of riboflavin standards using peak areas.

4.3. PEPC activity

Phospho*enol*pyruvate carboxylase (PEPC; EC 4.1.1.31) activity was measured in root extracts obtained by grinding 100 mg FW of root material in a mortar with 1 mL of extraction buffer containing 30 mM sorbitol, 1% BSA and 1% PVP in 100 mM HEPES-KOH, pH 8.0. The slurry was centrifuged for 15 min at 10,000 × g and 4 °C, the supernatant was collected and the enzyme activity measured immediately. PEPC activity was determined in a coupled enzymatic assay with malate dehydrogenase (L-malate:NAD- oxidoreductase; EC 1.1.1.37) as described in [20] with 75 μL of extract in 2 mM PEP, 10 mM $NaHCO_3$, 5 mM $MgCl_2$, 0.16 mM NADH, and 100 mM Bicine [N, N′-bis(2-hydroxyethylglycine)]-HCl, pH 8.5.

4.4. Root iron reductase assay

Root Fe reductase was measured in intact plants. At different times, plants were placed in aluminium foil wrapped beakers containing the assay solution (100 μM Fe(III)-EDTA, 100 μM bathophenanthroline disulphonate (BPDS) and 1 mM MES pH 5.5), and Fe reductase activity was determined in vivo by following at 535 nm the formation of the Fe(II)-BPDS complex from Fe(III)-EDTA. Reactions were run for 1 h in the dark and blanks without plants were used to correct for any non-specific photoreduction.

4.5. External acidification of the medium

For a quantitative determination of H^+ extrusion, each plant was placed for 24 h in the normal growth chamber regime, in a beaker containing 100 mL of nutrient solution (pH 5.5) without MES buffer. After this time, the pH of the solution was measured using a Metrohm 719 S Titrino pH-meter (Herisau, Switzerland).

4.6. Gene expression analysis

Expression analysis of the *M. truncatula* genes codifying for root Fe reductase, PEPC, H^+-ATPase and 6,7-dimethyl-8-ribityllumazine synthase (DMRL) was studied by semi-quantitative RT-PCR.

For PEPC and DMRL, database searches were performed with TBLASTX [2] using previously identified PEPC and DMRL synthase sequences from *A. thaliana* (AtPPC1: AT1G53310, AtDMRL: AT2G44050, respectively), *L. esculentum* (LePPC1: AJ243416), *P. sativum* (PsPEPC1: D64037), *M. sativa* (MsPEPC: Q02735), *G. max* (GmPEPC: AAS67006), *N. tabacum* (NtDMRL: AF422802) and *S. oleracea* (SoDMRL: AF147203). Two TC sequences from *M. truncatula* encoding possible orthologs for PEPC and DMRL synthase genes were identified. Alignment of the predicted protein sequences was performed using ClustalW software [35]. Based on these alignments, specific primers were designed to amplify the complete cDNA sequences of *PEPC* and *DMRL synthase* genes. Primers used were, for PEPC, f-ATGGCTACTCGTAACATTGAA and r-CTAACTCCGGTGTTGCACATCGGA; and for DMRL synthase, f-ATGGCTTTATCTGTTTCCACC and r-CTAATTCAGATGATGCTCGAA). After PCR amplification, products were sequenced to ensure sequence accuracy and RT-PCR specific primers for PEPC and DMRL cDNAs were designed based on the sequences obtained (Table 1). For root Fe reductase and H^+-ATPase genes, known *M. truncatula* cDNA sequences (*MtFRO1*: AY439088, *MtHA1*: AJ132892) were used as templates to design gene specific primers (Table 1).

Table 1
Forward and reverse specific primers utilized for the semi-quantitative PCR amplification of the different genes. Annealing temperature (T^m, °C), number of PCR cycles and volume of cDNA (μl) used for amplification and the size of the fragments amplified (bp) are also shown.

	Forward primer	Reverse primer	T^m (°C)	No of cycles	Volume cDNA (μl)	Fragment size (bp)
Actin	AAGAGYTAYGARYTNCCWGATGG	TTRATCTTCATGCTRCTRCTWGGAGC	55	25	1	290
MtFRO	GGTGACACGTGGATCATCTG	TTGCAATCCACAGGAACAAA	55	28	2	239
MtPEPC	ATGGCTACTCGTAACATTGAA	CATTATATGGGACACGTTCGT	65	35	3	825
MtHA1	GCACAAGTATGAGATTGTGAAGA	ATCACCAGTCATGCCACAAA	55	30	2	68
MtDMRL	ATGGCTTTATCTGTTTCCACC	CTAATTCAGATGATGCTCGAA	55	30	2	666

Total RNA from roots was isolated using the RNeasy Plant Mini kit (Quiagen GmbH, Hilden, Germany) according to the manufacturer's instructions. The concentrations of RNAs were assessed using a UV-2101PC spectrometer (Shimadzu, Kyoto, Japan). The structural integrity of the RNAs was checked with non-denaturing agarose gel and ethidium bromide staining. Two plants per treatment were pooled to extract RNA, and three batches of plants were analyzed. A sample aliquot containing 3 μg total RNA was subjected to reverse transcription with 25 μg mL^{-1} oligo (dT) primer, 0.05 mMdNTP mix, and 15 units Cloned AMV Reverse Transcriptase (InVitrogen, Carlsbad, USA) in a volume of 20 μL, according to the manufacturer's instructions. PCR reactions were carried out with the volumes of resulting cDNA solution indicated in Table 1 using gene specific primers (Table 1). Additional reaction components were 75 mM Tris HCL (pH 9.0), 50 mM KCl, 20 mM $(NH_4)_2SO_4$, 200 μM dNTPs, 2 mM Cl_2Mg, 1 μM gene specific primers and 0.5 units Taq polymerase (Biotools, Madrid, Spain). PCR cycling conditions and fragment size are listed in Table 1. Amplified products from 15 μl of PCR reaction were visualized on a 1% TBE agarose gel containing ethidium bromide. Bands were photographed and band area measured using the Quantity One 4.5.1 Chemidoc EQ software (Bio-Rad, CA, USA), using actin as housekeeper. To calculate normalized signal intensities, each band area was divided by the corresponding area of the actin band. The experiment was repeated 3 times and 2 PCR reactions were carried out for each batch of plants.

Acknowledgements

This study was supported by the Spanish Ministry of Science and Education (Project AGL2007-61948 to J.A., co-financed with FEDER) and the Aragón Government (group A03). S.A. was supported by an FPI pre-doctoral fellowship from the Spanish Ministry of Education and Culture and J.R.-C. by an I3P pre-doctoral fellowship from the CSIC. We thank I. Tacchini for technical assistance in HPLC and A. Calviño for assistance in growing plants.

References

[1] J. Abadía, A.F. López-Millán, A. Rombolà, A. Abadía, Organic acids and Fe deficiency: a review, Plant and Soil 241 (2002) 75–86.
[2] S.F. Altshul, D.J. Lipman, Protein database searches for multiple alignments, P. Natl. Acad. Sci. U.S.A. 87 (1990) 5509–5513.
[3] S. Andaluz, A.F. López-Millán, M.L. Peleato, J. Abadía, A. Abadía, Increases in phosphoenolpyruvate carboxylase activity in iron-deficient sugar beet roots: analysis of spatial localization and post-translational modification, Plant and Soil 241 (2002) 43–48.
[4] K.B. Axelsen, M.G. Palmgren, Inventory of the superfamily of P-type ion pumps in *Arabidopsis*, Plant Physiol. 126 (2001) 696–706.
[5] I. Cakmak, D.A.M. van de Wetering, H. Marschner, H.F. Bienfait, Involvement of superoxide radical in extracellular ferric reduction by iron-deficient bean roots, Plant Physiol. 85 (1987) 310–314.
[6] R.L. Chaney, J.C. Brown, L.O. Tiffin, Obligatory reduction of ferric chelates in iron uptake by soybeans, Plant Physiol. 50 (1972) 208–213.
[7] E.L. Connolly, N.H. Campbell, N. Grotz, C.L. Prichard, M.L. Guerinot, Overexpression of the *FRO2* ferric chelate reductase confers tolerance to growth on low iron and uncovers posttranscriptional control, Plant Physiol. 133 (2003) 1102–1110.
[8] D.D. Davies, The fine cont rol of cytosolic pH, Physiol. Plant 67 (1986) 702–706.
[9] M. Dell'Orto, L. Pirovano, J.M. Villalba, J.A. González-Reyes, G. Zocchi, Localization of the plasma membrane H^+-ATPase in Fe-deficient cucumber roots by immunodetection, Plant and Soil 241 (2002) 11–17.
[10] M. Dell'Orto, S. Santi, P. De Nisi, S. Cesco, Z. Varanini, G. Zocchi, R. Pinton, Development of Fe-deficiency responses in cucumber (*Cucumis sativus* L.) roots: involvement of plasma membrane H^+-ATPase activity, J. Exp. Bot. 51 (2000) 695–701.
[11] D. Eide, M. Broderius, J. Fett, M.L. Guerinot, A novel iron-regulated metal transporter from plants identified by functional expression in yeast, P. Natl. Acad. Sci. U.S.A. 93 (1996) 5624–5628.
[12] B.P. Hall, M.L. Guerinot, The role of ZIP family members in iron transport, in: L.L. Barton, J. Abadía (Eds.), Iron Nutrition in Plants and Rhizospheric Microorganisms, Springer, Dordrecht, 2006, pp. 311–326.
[13] J.F. Harper, L. Manney, N.D. DeWitt, M.H. Yoo, M.R. Sussman, The *Arabidopsis thaliana* plasma membrane H(+)-ATPase multigene family. Genomic sequence and expression of a third isoform, J. Biol. Chem. 265 (1990) 13601–13608.
[14] D.B. Jordan, K.O. Bacot, T.J. Carlson, M. Kessel, P.V. Viitanen, Plant riboflavin biosynthesis. Cloning, chloroplast localization, expression, purification, and partial characterization of spinach Lumazine synthase, J. Biol. Chem. 274 (1999) 22114–22121.
[15] T. Kobayashi, N.K. Nishizawa, S. Mori, Molecular analysis of iron-deficient graminaceou s plants, in: L.L. Barton, J. Abadía (Eds.), Iron Nutrition in Plants and Rhizospheric Microorganisms, Springer, Dordrecht, 2006, pp. 395–436.
[16] E. Landsberg, Transfer cell formation in the root epidermis: a prerequisite for Fe-efficiency? J. Plant Nutr. 3 (1982) 579–592.
[17] J. Li, X.D. Wu, S.T. Hao, X.J. Wang, H.Q. Ling, Proteomic response to iron deficiency in tomato root, Proteomics 8 (2008) 2299–2311.
[18] L.H. Li, X.D. Cheng, H.Q. Ling, Isolation and characterization of Fe(III)-chelate reductase gene *LeFRO1* in tomato, Plant Mol. Biol. 54 (2004) 125–136.
[19] W.L. Lindsay, A.P. Schwab, The chemistry of iron soils and its availability to plants, J. Plant Nutr. 5 (1982) 821–840.
[20] A.F. López-Millán, F. Morales, S. Andaluz, Y. Gogorcena, A. Abadía, J. De Las Rivas, J. Abadía, Responses of sugar beet roots to iron deficiency. Changes in carbon assimilation and oxygen use, Plant Physiol. 124 (2000) 885–897.
[21] H. Marschner, Mineral Nutrition of Higher Plants, Academic Press, London, 1995.
[22] P. Moog, W. Brüggemann, Iron reductase systems on the plant plasma membrane—a review, Plant and Soil 165 (1994) 241–260.
[23] P.D. Nisi, G. Zocchi, Phosphoenolpyruvate carboxylase in cucumber (*Cucumis sativus* L.) roots under iron deficiency: activity and kinetic characterization, J. Exp. Bot. 51 (2000) 1903–1909.
[24] M.G. Palmgren, Plant plasma membrane H^+-ATPases: powerhouses for nutrient uptake, Ann. Rev. Plant Physiol. Plant Mol. Biol. 52 (2001) 817–845.
[25] N.J. Robinson, C.M. Procter, E.L. Connolly, M.L. Guerinot, A ferric-chelate reductase for iron uptake from soils, Nature 397 (1999) 694–697.
[26] S. Santi, S. Cesco, Z. Varanini, R. Pinton, Two plasma membrane H^+-ATPase genes are differentially expressed in iron-deficient cucumber plants, Plant Physiol. Biochem. 43 (2005) 287–292.
[27] U. Schagerlof, G. Wilson, H. Hebert, S. Al-Karadaghi, C. Hagerhall, Transmembrane topology of *FRO2*, a ferric chelate reductase from *Arabidopsis thaliana*, Plant Mol. Biol. 62 (2006) 215–221.
[28] W. Schmidt, Mechanisms and regulation of reduction-based iron uptake in plants, New Phytol. 141 (1999) 1–26.
[29] W. Schmidt, Iron homeostasis in plants: sensing and signaling pathways, J. Plant Nutr. 26 (2003) 2211–2230.
[30] F. Shimanchi, Characterization of iron deficiency response system with riboflavin secretion in some dycotiledonous plants, in: T. Ando, K. Fujita, T. Mae, H. Matsumoto, S. Mori, J. Sckiya (Eds.), Plant Nutrition for Sustainable Food Production and Environment, Kluwer Academic, Dordrecht, 1997, p. 277.
[31] N.N. Stenchuk, V.I. Kutsiaba, B.V. Kshanovskaya, D.V. Fedorovich, Effect of the rib83 mutation on riboflavin synthesis and iron acquisition in the yeast *Pichia guilliermondii*, Microbiology 70 (2001) 647–651.
[32] S. Susin, J. Abián, M.L. Peleato, F. Sanchez-Baeza, A. Abadía, E. Gelpí, J. Abadía, Flavin excretion from roots of iron-deficient sugar-beet (*Beta vulgaris L*), Planta 193 (1994) 514–519.
[33] S. Susín, J. Abián, F. Sanchez-Baeza, M.L. Peleato, A. Abadía, E. Gelpí, J. Abadía, Riboflavin 3'- and 5'-sulfate, two novel flavins accumulating in the roots of iron-deficient sugar beet (*Beta vulgaris*), J. Biol. Chem. 268 (1993) 20958–20965.
[34] O. Thimm, B. Essigmann, S. Kloska, T. Altmann, T.J. Buckhout, Response of *Arabidopsis* to iron deficiency stress as revealed by microarray analysis, Plant Physiol. 127 (2001) 1030–1043.

[35] J.D. Thompson, D.G. Higgins, T.J. Gibson, CLUSTAL W: improving the sensitivity of progressive multiple sequence alignment through sequence weighting, position-specific gap penalties and weight matrix choice, Nucl. Acids Res. 22 (1994) 4673–4680.
[36] A. Vorwieger, C. Gryczka, A. Czihal, D. Douchkov, J. Tiedemann, H.P. Mock, M. Jakoby, B. Weisshaar, I. Saalbach, H. Bäumlein, Iron assimilation and transcription factor controlled synthesis of riboflavin in plants, Planta 226 (2007) 147–158.
[37] B.M. Waters, D.G. Blevins, D.J. Eide, Characterization of *FRO1*, a pea ferric-chelate reductase involved in root iron acquisition, Plant Physiol. 129 (2002) 85–94.
[38] G. Welkie, G. Miller, Riboflavin excretion from roots of iron-stressed and reciprocally gr afted tobacco and tomato plants, J. Plant Nutr. 11 (1988) 691–700.
[39] D.J. Worst, M.M. Gerrits, C.M.J.E. Vandenbroucke-Grauls, J.G. Kusters, *Helicobacter pylori* ribBA-mediated riboflavin production is involved in iron acquisition, J. Bacteriol. 180 (1998) 1473–1479.
[40] G. Zocchi, Metabolic changes in iron-stressed dicotyledoneus plants, in: L.L. Barton, J. Abadía (Eds.), Iron Nutrition in Plants and Rhizospheric Microorganisms, Springer, Dordrecht, 2006, pp. 359–370.

Journal of proteome research

ARTICLE

pubs.acs.org/jpr

Root Responses of *Medicago truncatula* Plants Grown in Two Different Iron Deficiency Conditions: Changes in Root Protein Profile and Riboflavin Biosynthesis

Jorge Rodríguez-Celma,[†] Giuseppe Lattanzio,[†] Michael A. Grusak,[‡] Anunciación Abadía,[†] Javier Abadía,[†] and Ana-Flor López-Millán*[,†]

[†]Plant Nutrition Department, Aula Dei Experimental Station (CSIC), P.O. Box 13034, E-50080, Zaragoza, Spain

[‡]USDA-ARS Children's Nutrition Research Center, Department of Pediatrics, Baylor College of Medicine, 1100 Bates Street, Houston, Texas 77030, United States

Supporting Information

ABSTRACT: Iron deficiency is a yield-limiting factor with major implications for field crop production in one-third of the world's agricultural areas, especially those with high soil $CaCO_3$. In the present work, a two-dimensional gel electrophoresis proteomic approach was combined with a study on the riboflavin synthesis pathway, including qPCR and riboflavin determination, to investigate Fe-deficiency responses in *Medicago truncatula* plants grown with and without $CaCO_3$. Iron deficiency caused a *de novo* accumulation of DMRLs and GTPcII, proteins involved in riboflavin biosynthesis, as well as marked increases in root riboflavin concentrations and in the expression of four genes from the riboflavin biosynthetic pathway. Two novel changes found were the increased accumulation of proteins related to N recycling and protein catabolism. Other identified changes were consistent with previously found increases in glycolysis, TCA cycle, and stress-related processes. All effects were more marked in the presence of $CaCO_3$. Our results show that the riboflavin biosynthesis pathway was up-regulated at the genomic, proteomic, and metabolomic levels under both Fe-deficiency treatments, especially in the presence of $CaCO_3$. Results also indicate that N recycling occurs in *M. truncatula* upon Fe deficiency, possibly constituting an additional anaplerotic N and C source for the synthesis of secondary metabolites, carboxylates, and others.

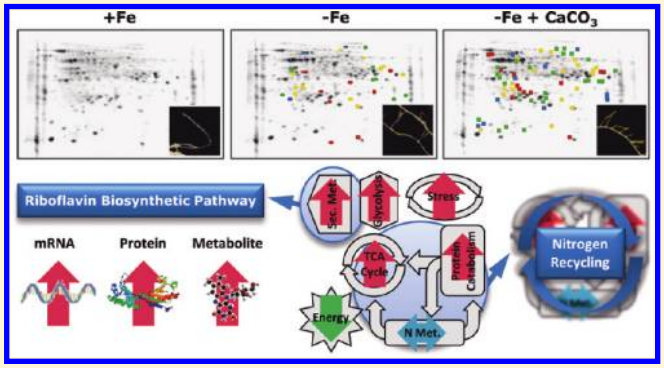

KEYWORDS: Calcium carbonate, DMRLs, iron, C/N metabolism, riboflavin, root, two-dimensional gel electrophoresis

INTRODUCTION

Iron is an essential micronutrient for all living organisms including plants, since it takes part in fundamental biological redox processes such as photosynthesis and respiration. Although Fe is the fourth most abundant element in the earth's crust, the bioavailability for plants is low, due to its poor solubility in the rhizosphere at neutral or basic pH. Therefore, Fe deficiency is a yield-limiting factor with major implications for field crop production in many agricultural areas of the world. For instance, it has been estimated that 20−50% of fruit trees in the Mediterranean basin suffer from Fe deficiency.[1] The most prevalent cause of Fe deficiency in this area, where calcareous soils are predominant, is the presence of high $CaCO_3$ contents. Plants can be broadly classified into two groups based on their mechanism of Fe acquisition: Strategy I plants use a Fe(III) reduction-based mechanism and include dicotyledonous and non-Graminaceae monocotyledonous species, whereas Strategy II plants use a Fe(III) chelation-based mechanism and include Graminaceae species.[2] The response of Strategy II plants to Fe shortage includes the biosynthesis and secretion of phytosiderophores, which specifically bind Fe(III) with high affinity, and the subsequent uptake of Fe(III)-PS complexes from the rhizosphere by specific cellular transport systems.[3]

When Fe is scarce, Strategy I plants develop morphological and biochemical changes leading to an increase in their Fe uptake capacity. Morphological changes include swelling of root tips and formation of lateral roots, root hairs, and transfer cells that increase the root surface in contact with the external medium, thereby increasing the Fe uptake capability.[4,5] Biochemical changes aimed to increase Fe uptake by roots and Fe solubility in the soil solution include the induction of a plasma-membrane Fe(III)-reductase[6,7] and an Fe(II) transporter,[8,9] and an enhanced proton extrusion capacity, the latter being supported by a plasma-membrane H^+-ATPase, whose activity lowers soil pH favoring the solubilization of inorganic Fe.[10,11] Other metabolic changes occur in order to sustain the elevated energy requirements for Fe uptake; these include accumulation of organic acids, mainly malate and citrate,[12] shifts in the redox

Received: January 19, 2011
Published: March 04, 2011

state of the cytoplasm[13,14] and increases in the activity of PEPC and several other enzymes of the Krebs cycle and the glycolytic pathway.[13,15,16]

Strategy I plants grown in Fe-deficient conditions also excrete a plethora of organic compounds, including carboxylates, phenolics and flavonoids, that can affect Fe availability and whose role is still not clear.[17] With regard to flavin compounds, there are reports as early as the 1960s describing a yellowing of Fe-deficient roots in certain plant species.[18,19] Later, riboflavin (Rbfl) sulphates were found to accumulate in specific parts of Fe-deficient roots,[20] and these compounds were also found in nutrient solution, implying an export from roots.[21] The function these flavin compounds play in plant Fe efficiency is still not known, but different roles have been hypothesized, including reduction or complexation of extracellular Fe,[17,22] bridging electron flow to the root Fe reductase,[13,23] and modification of the rhizosphere microbiome.[21,24,25] Riboflavin is the precursor of flavin mononucleotide (FMN) and flavin adenine dinucleotide (FAD), the latter being a cofactor for the root plasma membrane Fe(III)-reductase.[7,26] Also, a connection between Fe deficiency perception and Rbfl excretion has been described to occur in *Arabidopsis thaliana* through two basic helix−loop−helix (bHLH) transcription factors.[27]

Recently, 2-DE proteomic profiling has been used to study Fe-deficiency responses in plants in different scenarios. Changes in the protein profile of thylakoids from several species have been investigated,[28−30] as have root proteome changes in tomato (*Lycopersicon esculentum*)[31,32] and sugar beet (*Beta vulgaris*).[33] Regarding flavin synthesis, tomato does not accumulate or export flavin compounds when Fe-deficient, whereas sugar beet accumulates flavins in swollen yellow root tips and exports flavin compounds at low pH; however, this latter species has little molecular and genetic resources available for more detailed investigations. *Medicago truncatula* has emerged as a model legume with a number of genetic and molecular tools available.[34,35] A better understanding of the mechanisms involved in root Fe homeostasis in this model species may strengthen our ability to enhance Fe-efficiency responses in other plant species, especially legumes of agronomic interest. Also, it remains unclear whether the presence of $CaCO_3$, which is often found in field conditions in cases of Fe deficiency, causes effects in addition to to those of the direct Fe shortage used in most studies on the subject.[32,36] Therefore, the aim of this work was to investigate changes induced by direct Fe deficiency and carbonate-induced Fe deficiency in the root protein profile and underlying biochemical/molecular pathways of *M. truncatula*.

MATERIALS AND METHODS

Plant Culture

Medicago truncatula cv. "Jemalong" plants were grown in a controlled environment chamber with a photosynthetic photon flux density at leaf height of 350 μmol m^{-2} s^{-2} photosynthetically active radiation, 80% relative humidity and at a 16 h 23 °C/8 h 19 °C, day/night regime. Seeds were scarified by nicking the seed coat, then imbibed overnight in distilled water and germinated on filter paper for 3 days in darkness with full humidity. Seedlings were grown for an additional 2-week period in half-strength Hoagland nutrient solution (pH 5.5) with 45 μM Fe (III)-EDTA.[37] Plants were then transplanted to 10 L plastic buckets (six plants per bucket) containing half-strength Hoagland nutrient solution and treatments were imposed. Control plants were grown with 45 μM Fe(III)-EDTA (pH 5.5), and Fe-deficient plants were grown with no added Fe (0 μM Fe) with (pH 7.5) or without (pH 5.5) 1 g L^{-1} $CaCO_3$. After 6 days, roots were harvested, frozen in liquid N_2 and stored at −80 °C. Five independent batches of plants were grown and analyzed for protein profile and riboflavin content.

Protein Extraction

Roots of two plants from the same treatment in a given batch were pooled; approximately 1 g of the pooled material was ground to powder in liquid N_2 using a Retsch M301 mill (Retsch GmbH, Haan, Germany) and then homogenized in 5 mL of phenol saturated with Tris-HCl 0.1 M (pH 8.0) containing 5 mM β-mercaptoethanol, by stirring for 30 min at 4 °C. After incubation, the homogenate was filtered (PVDF, 0.45 μm) and centrifuged at 5000*g* for 15 min. The phenol phase was re-extracted for 30 min with one volume of Tris-HCl 0.1 M (pH 8.0) saturated with phenol containing 5 mM β-mercaptoethanol and centrifuged as described above. The phenol phase was collected, and proteins were precipitated by adding four volumes of 0.1 M ammonium acetate in cold methanol, using an incubation of at least 4 h at −20 °C. Samples were then centrifuged at 5000*g* for 15 min, and the pellet was washed three times with cold methanol, dried with N_2 gas and resuspended in sample rehydration buffer containing 8 M urea, 2% (w/v) CHAPS, 50 mM DTT, 2 mM PMSF and 0.2% (v/v) IPG buffer pH 3−10 (GE Healthcare, Uppsala, Sweden). After rehydration, samples were incubated at 38 °C for 2.5 h and then centrifuged at 15,000*g* for 10 min at 20 °C. Protein concentration was measured with the RC DC Protein Assay BioRad (BioRad, Hercules, CA, USA) based on the Lowry method. Protein in the extracts was analyzed immediately.

2-DE

Preliminary 2-DE experiments were carried out using a first dimension IEF separation with a linear pH gradient 3−10. With these conditions, most of the spots were located in the central region of the 2-DE gel (results not shown); therefore, to prevent protein comigration and to improve resolution, a narrower pH gradient was chosen. A first dimension IEF separation was carried out on 7 cm ReadyStrip IPG Strips (BioRad) with a linear pH gradient pH 5−8 in a Protean IEF Cell (BioRad). Strips were rehydrated for 16 h at 20 °C in 125 μL of rehydration buffer containing 150 μg of root extract proteins and a trace of bromophenol blue and then transferred onto a strip electrophoresis tray. IEF was run at 20 °C, for a total of 14,000 V h (20 min with 0−250 V linear gradient; 2 h with 250−4000 V linear gradient and 4000 V until 10,000 V h). After IEF, strips were equilibrated for 10 min in equilibration solution I [6 M urea, 0.375 M Tris-HCl, pH 8.8, 2% (w/v) SDS, 20% (v/v) glycerol, 2% (w/v) DTT] and for another 10 min in equilibration solution II [6 M urea, 0.375 M Tris-HCl pH 8.8, 2% (w/v) SDS, 20% (v/v) glycerol, 2.5% (w/v) iodoacetamide].

For the second dimension, polyacrylamide gel electrophoresis (SDS-PAGE), equilibrated IPG strips were placed on top of vertical 12% SDS-polyacrylamide gels (8 × 10 × 0.1 cm) and sealed with melted 0.5% agarose in 50 mM Tris-HCl (pH 6.8) containing 0.1% SDS. SDS-PAGE was carried out at 20 mA per gel for approximately 1.5 h, until the bromophenol blue reached the plate bottom, in a buffer containing 25 mM Tris Base, 1.92 M glycine, and 0.1% SDS, at room temperature. Gels were subsequently stained with Coomassie-blue R-250 (Sigma, Barcelona,

Spain). Gels were made from independent root preparations from five different batches of plants for each treatment.

Gel Image and Statistical Analysis

Stained gels were scanned with a Bluescan48 Scanner (LaCie, Portland, OR, USA). Experimental M_r values were calculated by mobility comparisons with Precision Plus protein standard markers (BioRad) run in a separate lane on the SDS-gel, and p*I* was determined by using a 5−8 linear scale over the total dimension of the IPG strips. Spot detection, gel matching and interclass analysis were performed with PDQuest 8.0 software (BioRad). First, normalized spot volumes based on total quantity were calculated for each 2-DE gel and used for statistical calculations of protein abundance; for all spots present in the gels, p*I*, M_r, and normalized volumes (mean values, SD, and CV) were determined. Only spots present in at least 4 of the 5 replicates from at least one treatment were considered as consistent and used in further analysis; missing spot volumes were estimated from the data set using a sequential K-Nearest Neighbor algorithm using an R 2.7.0 environment. After the input of missing values, a second normalization based on total spot intensity per gel was used to compensate for gel replicate variations. The spots were also manually checked, and a high level of reproducibility between normalized spot volumes was found in all five different replicates.

Univariate and multivariate statistical analyses were carried out. Differentially expressed spots were defined using a Student *t* test value $p < 0.10$ and a > 2-fold change. Principal Component Analysis (PCA) was applied to both the whole data set and the data set including only identified spots using SPSS v. Fifteen (SPSS Inc., Chicago, USA).

In-Gel Digestion and Sample Preparation for Mass Spectrometric Analysis

Spots showing statistically significant changes in intensity (at $p < 0.10$) and above a 2-fold threshold were excised automatically using a spot cutter EXQuest (BioRad) and then digested automatically using a ProGest protein digestion station (Genomic Solutions, Holliston, MA, USA). The digestion protocol started with two destaining steps, 30 min each, with 40% v/v acetonitrile (ACN) containing 200 mM NH_4HCO_3, followed by two washing steps, first with 25 mM NH_4HCO_3 for 5 min and then with 50% v/v ACN containing 25 mM NH_4HCO_3, for 15 min. After washing, gel spots were dehydrated with 100% ACN for 5 min, and then dried. Gel spots were rehydrated with 10 μL of a trypsin solution [12.5 ng μL^{-1} in 25 mM $(NH_4)_2CO_3$] for 10 min and then digested for 12 h at 37 °C. Digestion was stopped by adding 10 μL of 0.5% TFA. Peptides were purified automatically using a ProMS station (Genomic Solutions) with a C18 microcolumn (ZipTip, Millipore, MA, USA), and eluted directly onto a MALDI plate with 1 μL of matrix solution (5 mg mL^{-1} CHCA in 70% ACN/0.1% TFA v/v).

MALDI-TOF-MS, LIFT TOF/TOF Analysis and Identification of Proteins

Peptide mass fingerprint spectra were determined on a 4700 Proteomics Analyzer (Applied Biosystems, Foster City, US) in positive ion reflector mode. Each spectrum was internally calibrated with m/z signals of porcine trypsin autolysis ions, and the typical mass measurement accuracy was ±20 ppm. Whenever possible, fragmentation spectra of the five most intense peaks were obtained for each sample. The measured tryptic peptide masses were searched in the NCBInr (822947 sequences for 20100716 residues) and Plants EST (EST-104; 135437328 sequences for 23654962430 residues) databases, using MASCOT software (Matrix Science, London, U.K.). When available, MS/MS data from LIFT TOF/TOF spectra were combined with MS peptide mass fingerprint data for database search. The following parameters were used for the database search: green plants taxonomic group, complete carbamidomethylation of cysteine residues, partial oxidation of methionine residues, mass tolerance of 100 ppm for the precursor and 0.6 Da for the fragments, and one miscleavage allowed. Homology identification was retained with a probability set at 95%. Identifications were validated manually, with at least 13 peptides matched and sequence coverage above 25% for MS data, and at least one identified peptide with a score above homology and 10% sequence coverage for MS/MS data. We used the GO annotation (http://www.geneontology.org) of the individual identified proteins to assign the metabolic pathway(s) in which proteins are involved.

Quantitative RT-PCR

Expression of 6,7-dimethyl-8-ribityllumazine synthase (*DMRLs*), GTP cyclohydrolase II (*GTPcII*), riboflavin deaminase-reductase (*ribD*), and riboflavin synthase (*ribE*) was analyzed by qRT-PCR. Total RNA from lateral roots of three different batches of plants (15 plants per batch, 5 plants per treatment) was isolated using the RNeasy Plant mini kit from QIAGEN (QIAGEN Inc., Valencia, CA, USA) according to the manufacturer's instructions. RNA concentrations were assessed using a ND-1000 Nano Drop Full spectrum UV−vis spectrophotometer (Wilmington, DE, USA). The structural integrity of the RNAs was checked with nondenaturing agarose gel and ethidium bromide staining. To remove contaminating genomic DNA, RNAs were treated with the TURBO DNA-free kit from Ambion Inc. (Austin, TX, USA) according to the manufacturer's instructions. DNase-treated RNA samples (1.0 μg) were reverse transcribed with the High Capacity RNA to cDNA master mix (Applied Biosystems, Foster City, CA, USA) in a final volume of 20 μL according to the manufacturer's instructions. Quantitative real time polymerase chain reactions were performed in a 7900 HT Fast Real Time PCR system (Applied Biosystems) with 1.0 μL of the RT reaction using gene specific primers (0.5 μL of 10 mM stock solution) and SYBR green master mix (Applied Biosystems, Warrington, UK) in a final volume of 25 μL. Primer sequences and fragment sizes are listed in Table S1 in Supporting Information. The PCR program used was 50 °C for 2 min; 95 °C for 10 min, 40 cycles of 95 °C for 15 s, and 60 °C for 1 min; and a final dissociation stage of 95 °C for 15 s, 60 °C for 15 s, and 95 °C for 15 s. A previous experiment was performed to assess for primer efficiency with different sets of primers for each gene of interest. Actin was chosen as a control gene. Primer sets with a slope of the ΔCtgen-act vs log[cDNA] regression lower than 0.1 were chosen for the experiment. Primer efficiencies of the chosen sets are listed in the Supporting Information (Table S1).

Riboflavin Determination

Root material (ca. 100 mg) was ground using a Retsch M301 mill with 250 μL of 1 mM amonium acetate, pH 6.0, 5% methanol. Extracts were filtered through PVDF 0.45 μm ultrafree-MC centrifugal filter devices (Millipore, Billerica, MA, USA) and stored at −80 °C until analysis. For Rbfl export analysis, 500 mL of nutrient solution, collected six days after treatment onset, were concentrated to 2 mL using SepPack C18 cartridges

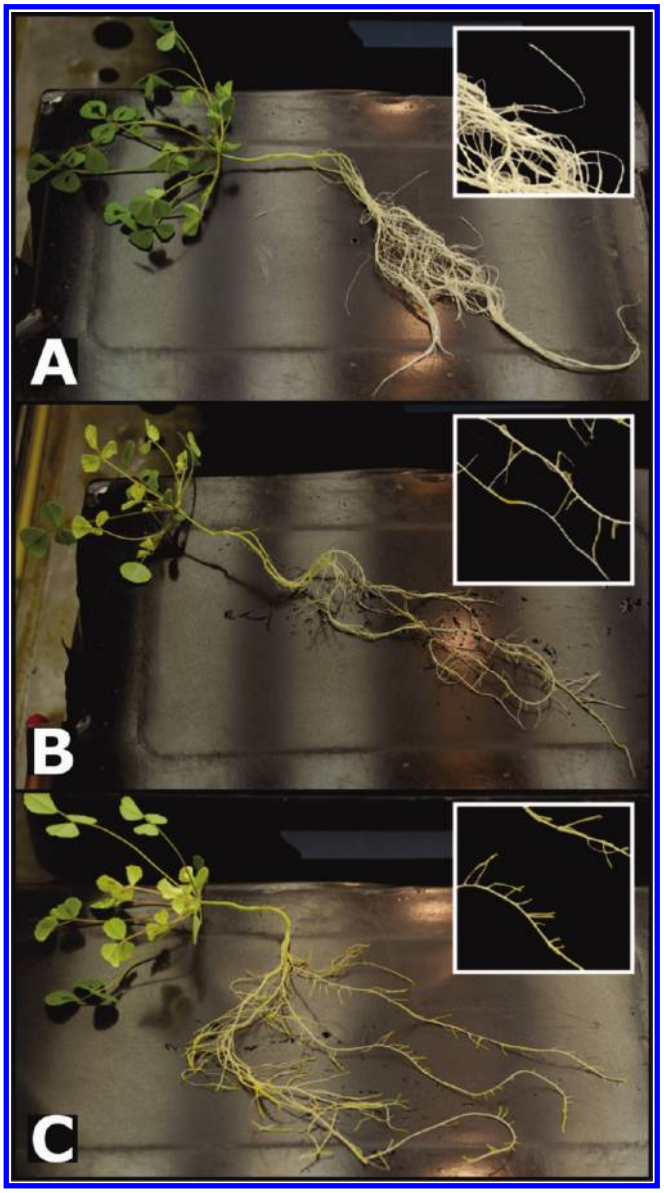

Figure 1. Picture of *Medicago truncatula* roots. General overview and detail (inset) of roots from Fe-sufficient (A), Fe-deficient (B), and Fe-deficient grown with $CaCO_3$ (C) plants.

(Waters Corp., Milford, MA, USA) according to manufacturer's instructions and stored at −80° until analysis. Riboflavin was analyzed by HPLC using a 100 × 8 mm Waters Radial-Pak C18 radial compression column.[21] Samples were injected with a Rheodyne injector (50 μL loop). Mobile phase (water/methanol 70:30, v/v) was pumped at a flow rate of 1 mL min^{-1}. Riboflavin was detected at 445 nm with a 996 photodiode array detector. The peak corresponding to Rbfl was identified by comparison of the retention time and UV−vis spectra with those of Rbfl standard from SIGMA (Saint Louis, Missouri, USA) and quantification was made with known amounts of Rbfl standard using peak areas. Data were expressed as nmol Rbfl g^{-1} root FW.

RESULTS

Root Morphological Changes

M. truncatula plants showed, in both Fe-deficiency treatments, a yellowing of the roots that is due to the accumulation of flavin compounds in the high micromolar range (see below). The presence of other possible compounds, such as flavonoids and others, in this concentration range can be fully excluded from the absorption spectra of the root extracts (not shown). Root yellowing occurred in a different manner depending on the treatment imposed. In the 0 μM Fe treatment, some yellow, swollen lateral roots and yellowish patches along the root length were observed as early as 3 days after treatment onset. In the 0 μM Fe plus $CaCO_3$ treatment, the yellow color was strictly localized to short swollen lateral roots (Figure 1).

Protein Expression Profiles

Changes in the protein profile of root extracts from Fe-deficient *M. truncatula* plants grown with or without $CaCO_3$ were studied by 2-D IEF−SDS-PAGE electrophoresis. Typical real scans of 2-DE gels obtained from root protein extracts of Fe-sufficient and Fe-deficient (without or with $CaCO_3$) plants are shown in Figure 2A−C, respectively. The average number of detected spots (mean ± SD) was 323 ± 25, 341 ± 27 and 345 ± 31 in gels from plants grown with 45 μM Fe, 0 μM Fe without $CaCO_3$ and 0 μM Fe with $CaCO_3$, respectively; approximately 90% of spots were consistently found in all five replicates within each treatment. The total number of spots consistently detected in the whole experiment (present in at least 80% of the gels of one treatment) was 335 (Supporting Information, Table S2). A composite averaged virtual map containing all spots present in all 15 gels (5 per treatment) is shown in Figure 2D−F.

Approximately 9% (31) and 20% (69) of the spots showed significant changes (Student t test, $p < 0.10$) and higher than 2-fold in relative intensities as a result of 0 μM Fe and 0 μM Fe plus $CaCO_3$ treatments, respectively, and from these, 72% were identified (Supporting Information, Table S3). The PCA analysis showed a good separation between treatments when using all consistent spots, and similar results were obtained when the analysis was carried out using only identified spots (Supporting Information, Figure S1).

The statistical analysis of averaged maps indicated that the direct Fe-deficiency treatment (0 μM Fe) caused increases in the relative signal intensity of 12 spots (yellow symbols in Figure 2E), whereas eight spots were present in the 0 μM Fe treatment but absent in the control (red symbols in Figure 2E). Among them, 15 spots matched reliably to known proteins (spots labeled 1, 2, 11−13, 20−23, 29, 30, 38, 39, 43, and 44 in Figure 3A and Table 1), and their metabolic functions were assessed manually by GO annotation. Proteins exhibiting increased relative intensities belonged to different metabolic pathways including protein metabolism (spots 1, 2), N metabolism (spots 11−13), glycolysis (spots 20−23), TCA cycle (spots 29, 30), secondary metabolism (spots 38, 39) and stress-related proteins (spots 43, 44). A smaller group of spots showed decreases in relative intensity in the 0 μM Fe treatment when compared to controls. These included eight spots with lower signal intensity (green symbols in Figure 2E) and three spots undetected in Fe-deficient plants (blue symbols in Figure 2E). Out of them, six spots were reliably identified (spots labeled 5, 10 and 34−37 in Figure 3A and Table 1) and were assigned to the protein metabolism (spots 5 and 10) and energy (spots 34−37) pathways.

When comparing the averaged map of the 0 μM Fe plus $CaCO_3$ treatment with that of controls, 19 spots showed relative increases in signal intensity (yellow symbols in Figure 2F) and 13 more were detected *de novo* (red symbols in Figure 2F). Among

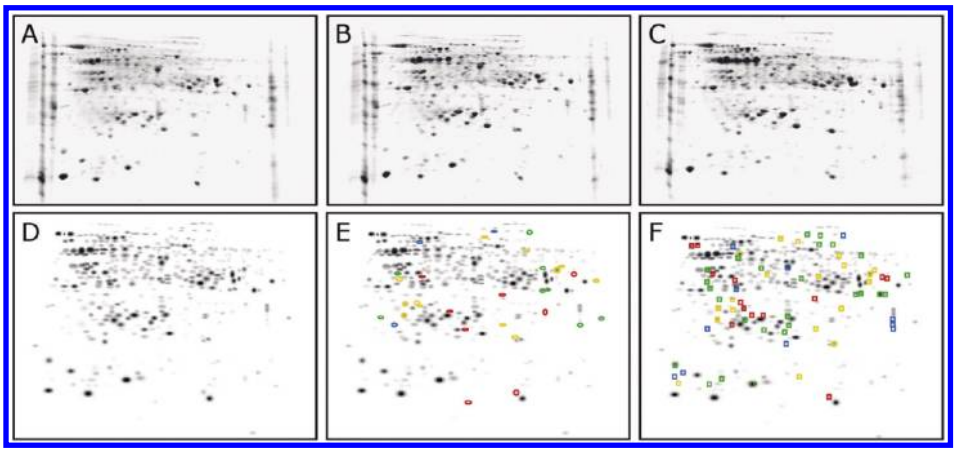

Figure 2. 2-DE IEF−SDS-PAGE protein profile maps of root extracts from *Medicago truncatula* plants. Proteins were separated in the first dimension in linear IPG pH 5−8 gel strips and in the second dimension in 12% acrylamide vertical gels. Scans of typical gels of roots from plants Fe-sufficient and Fe-deficient (0 μM Fe) without and with $CaCO_3$ are shown in A, B, and C, respectively. To facilitate visualization of the studied spots, a virtual composite image (D, E, and F) was created containing all spots present in the real gels A, B, and C. In E (0 μM Fe) and F (0 μM Fe plus $CaCO_3$), spots whose intensities decreased or were no longer detected when compared to control maps are marked with green and blue symbols, respectively, and those with increased intensities or newly detected ones are marked with yellow and red symbols, respectively.

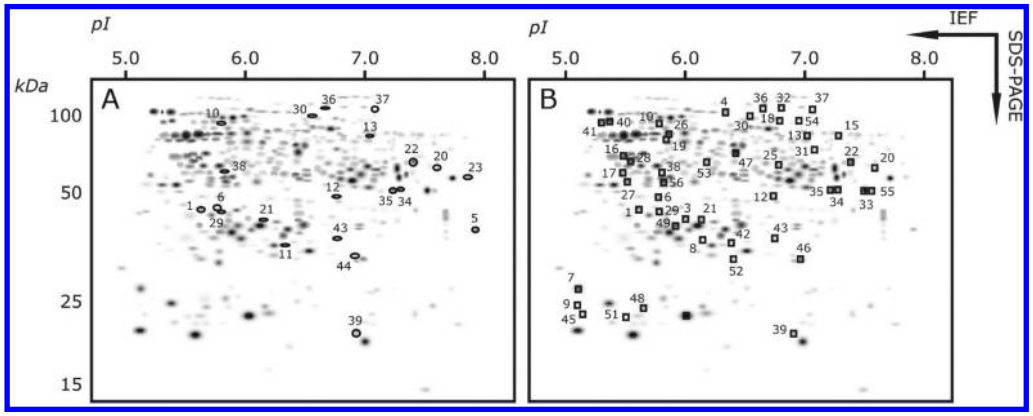

Figure 3. Polypeptides identified in root extracts of plants grown with 0 μM Fe (circles in A) and 0 μM Fe plus $CaCO_3$ (squares in B). Polypeptides with significant homologies to proteins present in databases (using MALDI MS/MS and MASCOT, described in detail in Table 1) were annotated on a virtual composite gel image (see Figure 1).

them, 24 were identified (spots 1, 3, 4, 12−14, 20−22, 24−26, 28−31, 38−41, 43, 45, 46, and 53 in Figure 3B and Table 1). Up-regulated metabolic pathways in the 0 μM Fe plus $CaCO_3$ treatment included protein metabolism (spots 1, 3, and 4), N metabolism (spots 12−14), glycolysis (spots 20−22 and 24−26), and TCA cycle (spots 28−31). Proteins belonging to secondary metabolism (spots 38−41), different stress-related processes (spots 43, 45 and *46*) and cell wall synthesis (spot 53) also showed increased relative intensities. Twenty-six spots showed decreases in relative intensity (green symbols in Figure 2F), whereas 11 more were no longer detected (blue symbols in Figure 2F). Among them, 27 spots were identified (spots 6−10, 15−19, 27, 32−37, 42, 47−52 and 54−56 in Figure 2B and Table 1) and assigned to protein metabolism (spots 6−10), N metabolism (spots 15−19), glycolysis (spot 27), energy (spots 32−37), secondary metabolism (spot 42), stress-related proteins (spots 47−52), and others (spots *54*−*56*).

Effect of Fe Deficiency and Fe Deficiency in the Presence of $CaCO_3$ on Metabolic Pathways

Protein Metabolism: Proteolysis and Protein Folding. In the 0 μM Fe treatment, two spots identified as cysteine proteases (spots 1 and 2) increased in relative signal intensity, whereas the proteasome α subunit type 7 (spot 5) decreased (Table 1, Figure 3A). The 0 μM Fe plus $CaCO_3$ treatment caused changes in more spots related to proteolysis, including increases in a cysteine protease (spot 1) and the proteasome subunit α type-6 (spot 3), and decreases in two protease inhibitors (spots 7 and 9), the proteasome β subunit type-1 (spot 8) and the peptidase A1 (spot 6) (Table 1, Figure 3B). With regard to chaperones, a spot identified as GroEL-like chaperone (spot 10) disappeared in both treatments, whereas the 0 μM Fe plus $CaCO_3$ treatment caused an increase in a TPR1 chaperone (spot 4) (Table 1, Figure 3A,B).

Nitrogen Metabolism. In the 0 μM Fe treatment, *S*-adenosylmethionine methyltranferase (spot 11) and UREG (spot 12) were detected *de novo*, and dihydrolipoamide dehydrogenase (LPD; spot 13) increased 2-fold (Table 1, Figure 3A). In the 0 μM Fe plus $CaCO_3$ treatment, UREG was also detected *de novo* and 2-fold increases were measured for LPD (spot 13) and aspartate aminotransferase (spot 14) (Table 1, Figure 3B). In the 0 μM Fe plus $CaCO_3$ treatment, decreases were measured

dx.doi.org/10.1021/pr2000623 |*J. Proteome Res.* 2011, 10, 2590–2601

Table 1. Proteins Identified in 2-D IEF−SDS-PAGE Gels[a]

no.	SSP	identification	species	ID	sco/pep/ion	CV	theor M_r/p*I*	expt M_r/p*I*	function	−Fe/−Fe + CO_3^{2-}
1	2206	cysteine protease	*Medicago sativa*	gi|5777611	170/6/2	33	23/5.37	30/5.81	protein metabolism	+11/+6
2	3201	cysteine protease	*Medicago sativa*	gi|5777611	201/7/2	33	23/5.37	30/5.94	protein metabolism	+3/(-)
3	4206	proteasome subunit α type-6	*Glycine max*	gi|12229897	209/9/3	14	27/5.83	28/6.17	protein metabolism	(-)/new
4	5903	TPR1-Heat shock chaperone	*Medicago sativa*	gi|31324052	771/13/6	39	40/6.33	74/6.48	protein metabolism	(-)/+2
5	9105	proteasome subunit α type 7	*Medicago truncatula*	gi|92886169	93/2/1	12	27/6.97	25/8.0	protein metabolism	−2/(-)
6	3203	peptidase A1, pepsin	*Medicago truncatula*	gi|87241358	210/8/2	24	44/5.50	33/5.96	protein metabolism	(-)/−5
7	0013	similar to hypothetical trypsin/ protease inhibitor	*Medicago truncatula*	GT137702	186/3/4	24	24/8.25	19/5.3	protein metabolism	(-)/−7
8	4108	proteasome subunit *β* type-1	*Petunia x hybrida*	gi|17380185	111/4/1	29	25/6.30	24/6.30	protein metabolism	(-)/−7
9	0015	similar to hypothetical trypsin/ protease inhibitor	*Medicago truncatula*	BQ155019	225/2/4	27	23/6.09	17/5.29	protein metabolism	(-)/lost
10	3709	GroEL-like chaperone, ATPase	*Medicago truncatula*	gi|92882356	171/8/2	15	61/6.27	62/5.97	protein metabolism	lost/lost
11	5109	putative *S*-adenosylmethionine-dependent methyltransferases	*Arabidopsis thaliana*	gi|12324243	76/14/0	41	44/8.51	25/6.48	N metabolism	new/(-)
12	6206	UREG (urease accessory protein G)	*Arabidopsis thaliana*	gi|15226754	103/4/1	14	30/6.03	34/6.85	N metabolism	new/new
13	7612	chain A, dihydrolipoamide dehydrogenase of glycine decarboxylase	*Pisum sativum*	gi|9955321	85/2/2	12	50/6.06	51/7.12	N metabolism	+2/+2
14	9401	aspartate aminotransferase	*Medicago sativa*	gi|777387	611/19/7	38	50/7.68	43/7.68	N metabolism	(-)/+2
15	8610	serine hydroxymethyltransferase	*Medicago truncatula*	gi|72256527	501/19/8	14	56/7.72	51/7.38	N metabolism	(-)/−2
16	2505	glutamine synthetase	*Medicago truncatula*	gi|28629470	525/15/6	16	47/6.29	44/5.70	N metabolism	(-)/−3
17	2307	OAS-TL4 cysteine synthase	*Glycine max*	gi|148562457	147/6/2	21	42/8.09	40/5.69	N metabolism	(-)/−4
18	7708	nitrite reductase	*Phaseolus vulgaris*	gi|500753	141/10/1	16	66/6.4	65/6.90	N metabolism	(-)/−5
19	3608	*S*-adenosyl-L-methionine synthetase	*Medicago sativa*	gi|139478060	144/7/2	21	44/5.77	49/6.02	N metabolism	(-)/lost
20	8416	putative fructose bisphosphate aldolase	*Medicago sativa*	gi|71534886	129/1/1	13	10/5.44	41/7.68	glycolysis	new/new
21	4109	glyceraldehyde-3-phosphate dehydrogenase	*Medicago sativa*	gi|145617261	546/13/6	75	22/9.13	27/6.29	glycolysis	new/new
22	8418	putative fructose bisphosphate aldolase	*Medicago sativa*	gi|71534886	156/2/2	30	10/5.44	43/7.49	glycolysis	+3/+4
23	9302	glyceraldehyde-3-phosphate dehydrogenase	*Medicago sativa*	gi|145617261	491/12/6	34	22/9.13	39/7.94	glycolysis	+3/(-)
24	3705	phosphoglycerate mutase	*Triticum aestivum*	gi|32400802	226/9/2	37	30/5.43	68/5.98	glycolysis	(-)/+2
25	7408	fructose-bisphosphate aldolase, cytoplasmic isozyme	*Cicer arietinum*	gi|3913008	403/12/5	70	39/6.21	42/6.89	glycolysis	(-)/+2
26	3607	enolase	*Glycine max*	gi|42521309	581/14/5	33	48/5.31	52/6.04	glycolysis	(-)/+2
27	2308	fructokinase-like protein	*Cicer arietinum*	gi|20975618	428/12/7	29	26/5.03	38/5.72	glycolysis	(-)/−2
28	2410	succinyl-CoA ligase beta subunit	*Caragana jubata*	gi|146215968	234/13/2	22	46/6.41	43/5.75	TCA cycle	(-)/new
29	3207	hydroxyacylglutathione hydrolase	*Medicago sativa*	gi|71534880	85/2/2	8	25/6.05	29/5.97	TCA cycle	+9/+7
30	6716	cytosolic NADP-malic enzyme	*Malus x domestica*	gi|83778968	166/8/3	12	71/6.21	70/6.66	TCA cycle	+7/+6
31	8507	2-oxoacid dehydrogenase family protein	*Arabidopsis thaliana*	gi|15240454	206/7/3	6	50/9.19	46/7.18	TCA cycle	(-)/+3
32	7907	EMB1467 (EMBRYO DEFECTIVE 1467); NADH dehydrogenase	*Arabidopsis thaliana*	gi|18421656	208/8/4	12	83/6.24	82/6.91	energy	(-)/−2
33	9201	ATRFNR2 (ROOT FNR 2)	*Arabidopsis thaliana*	gi|30691910	526/17/6	36	43/8.77	35/7.60	energy	(-)/−2

dx.doi.org/10.1021/pr2000623 |*J. Proteome Res.* 2011, 10, 2590–2601

Table 1. Continued

no.	SSP	identification	species	ID	sco/pep/ion	CV	theor M_r/pI	expt M_r/pI	function	−Fe/−Fe + CO_3^{2-}
34	8210	ATRFNR2 (ROOT FNR 2)	*Arabidopsis thaliana*	gi|30691910	397/16/5	32	43/8.77	36/7.38	energy	−3/−5
35	8211	ATRFNR2 (ROOT FNR 2)	*Arabidopsis thaliana*	gi|30691910	609/16/7	34	43/8.77	35/7.31	energy	−3/−5
36	6909	76 kDa mitochondrial complex I subunit	*Solanum tuberosum*	gi|3122572	76/20/0	28	81/5.87	82/6.76	energy	lost/−12
37	8906	quinonprotein alcohol dehydrogenase-like	*Medicago truncatula*	gi|124360970	237/11/3	21	59/5.96	80/7.17	energy	−6/lost
38	3405	NAD-dependent epimerase/ dehydratase	*Medicago truncatula*	gi|124360301	581/15/7	25	36/5.42	40/5.99	secondary metabolism	new/new
39	7002	DMRL synthase	*Medicago truncatula*	gi|217071658	240/2/2	22	22/7.72	15/7.01	secondary metabolism	new/new
40	1706	GTP cyclohydrolase II/3,4-dihydroxy-2-butanone 4-phosphate synthase	*Malus x domestica*	gi|33308405	366/10/6	7	58/5.71	64/5.56	secondary metabolism	(-)/new
41	1707	GTP cyclohydrolase II/3,4-dihydroxy-2-butanone 4-phosphate synthase	*Malus x domestica*	gi|33308405	303/8/4	7	58/5.71	63/5.49	secondary metabolism	(-)/new
42	5106	chalcone-flavanone isomerase	*Medicago truncatula*	gi|217073146	352/14/6	41	24/5.97	23/6.52	secondary metabolism	(-)/−4
43	6112	glutathione transferase	*Carica papaya*	gi|2853219	293/6/3	23	26/5.78	24/6.86	stress	+7/+6
44	7003	manganese superoxide dismutase-like protein	*Pistacia vera*	gi|149786150	214/6/2	31	26/7.14	22/7.00	stress	+3/(-)
45	0016	monodehydroascorbate reductase, seedling isozyme	*Cucumis sativus*	gi|50400859	78/13/0	26	48/5.29	16/5.34	stress	(-)/+4
46	7005	thaumatin-like protein PR-5b	*Cicer arietinum*	gi|3549691	182/3/2	10	27/5.26	22/7.06	stress	(-)/+2
47	5509	peroxidase	*Medicago sativa*	gi|537317	289/6/4	10	39/5.76	45/6.56	stress	(-)/−2
48	2009	superoxide dismutase [Cu−Zn], chloroplast precursor	*Medicago sativa*	gi|12230569	194/2/2	13	21/6.02	17/5.85	stress	(-)/−2
49	4102	L-ascorbate peroxidase	*Medicago sativa*	gi|71534930	667/10/7	58	13/9.44	26/6.09	stress	(-)/−2
50	4002	superoxide dismutase [Cu−Zn]	*Pisum sativum*	gi|401108	207/5/2	21	15/5.6	16/6.18	stress	(-)/−3
51	2001	similar to lipid-associated family protein	*Glycine max*	BF009814	84/2/2	10	18/5.44	16/5.72	stress	(-)/−12
52	5001	cold shock protein	*Medicago truncatula*	BF643519	192/3/4	36	12/5.32	22/6.54	stress	(-)/lost
53	4406	alpha-1,4-glucan-protein synthase [UDP-forming] 2	*Ricinus communis*	gi|34582499	79/16/1	39	42/5.71	43/6.33	cell wall synthesis	(-)/+3
54	7705	predicted protein	*Physcomitrella patens*	gi|168057049	101/4/1	33	71/8.1	65/7.05	others	(-)/−3
55	9206	guanine nucleotide-binding protein subunit beta-like protein	*Medicago sativa*	gi|3023847	216/9/4	34	36/7.07	35/7.66	others	(-)/−6
56	3307	annexin	*Medicago sativa*	gi|512400	439/19/5	49	35/5.41	38/6.01	others	(-)/lost

[a] MS1 protein score is −10(log P), where P is the probability that the observed match is a random event. Homology identification was retained with a probability set at 95%. Identifications were validated with at least 13 peptides matched and sequence coverage above 25% for MS data, and at least one identified peptide with a score above homology and 10% sequence coverage for MS/MS data. Function was inferred from GO annotation. The last column indicates relative spot intensity changes (in fold change, relative to the +Fe control) in the −Fe and −Fe + $CaCO_3$ treatments. (−) indicates no significant change, and "new" and "lost" indicate spots that have been newly detected or no longer detected in the −Fe treatments.

dx.doi.org/10.1021/pr2000623 |J. Proteome Res. 2011, 10, 2590–2601

in nitrite reductase (spot 18) and aminoacid metabolism related proteins, including serine hydroxymethyltransferase (SHMT, spot 15), glutamine synthetase (spot 16), OAS-TL4 cysteine synthase (spot 17) and *S*-adenosyl-L-methionine synthetase (spot 19) (Table 1, Figure 3B).

Primary Carbon Metabolism: Glycolysis and TCA. Four spots representing two proteins of the glycolytic pathway, fructose bisphosphate aldolase (spots 20 and 22) and glyceraldehyde-3-phosphate dehydrogenase (GADPH, spots 21 and 23), increased in the 0 μM Fe treatment (Table 1, Figure 3A). In the 0 μM Fe plus $CaCO_3$ treatment, increases were found in six spots representing four proteins: fructose bisphosphate aldolase (spots 20, 22 and 25), GADPH (spot 21), phosphoglycerate mutase (spot 24), and enolase (spots 26) (Table 1, Figure 3B). In this treatment, the relative intensity of a fructokinase-like protein (spot 27) decreased (Table 1, Figure 3B). With regard to TCA cycle related proteins, two spots identified as hydroxyacylglutathione hydrolase (spot 29) and a malic enzyme (spot 30) increased in relative intensity in the 0 μM Fe treatment (Table 1; Figure 3B). In the 0 μM Fe plus $CaCO_3$ treatment, these spots (spots 29 and 30) and two more identified as succinyl-CoA ligase (spot 28) and 2-oxoacid dehydrogenase (spot 31) also increased in relative intensity (Table 1, Figure 3B).

Energy Metabolism. Most of the spots identified as energy related proteins, all of them being Fe-containing proteins, decreased in relative intensity as a result of Fe deficiency. In the 0 μM Fe treatment, decreases were observed for root ferredoxin $NADP^+$ reductase (FNR, spots 34 and 35), 76 kDa mitochondrial complex I (spot 36), and a quinone-protein alcohol dehydrogenase (spot 37); in addition to these, a decrease in a NADH dehydrogenase (spot 32) was measured in the 0 μM Fe plus $CaCO_3$ (Table 1, Figure 3A,B).

Secondary Metabolism. Both treatments caused significant changes in proteins related to Rbfl metabolism. These changes included the *de novo* detection of DMRLs (spot 39) and a NAD-dependent epimerase (spot 38) in both treatments, and GTPcII (spots 40, 41) in the 0 μM Fe plus $CaCO_3$ treatment (Table 1, Figure 3A,B). A decrease in relative intensity of a chalcone-flavone isomerase (spot 42) was measured in this treatment, relative to the control (Table 1, Figure 3B).

Stress-Related. The 0 μM Fe treatment caused increases in two stress-related proteins, glutathione transferase (spot 43) and MnSOD (spot 44) (Table 1, Figure 3A). The 0 μM Fe plus $CaCO_3$ treatment caused increases in the relative intensity of glutathione transferase (spot 43), monodehydroascorbate reductase (MDAR, spot 45), and thaumatin PR-5b (spot *46*) and decreases in peroxidase (spot 47), CuZnSOD (spots 48 and 50), ascorbate peroxidase (APX, spot 49), a lipid associated protein (spot 51), and a cold shock protein (spot 52) (Table 1, Figure 3B).

Other Pathways. The 0 μM Fe plus $CaCO_3$ treatment caused an increase in the relative intensity of α-1,4-glucan-protein synthase (spot 53), a cell wall synthesis related protein, and decreases in a predicted protein (spot 54), a guanine nucleotide-binding protein (spot 55) and annexin (spot 56) (Table 1, Figure 3B); the first two are annotated as DNA interacting proteins, and the last one is a protein involved in vesicle trafficking.

qRT-PCR Analysis of Genes Involved in Riboflavin Synthesis

Expression of four genes involved in the plant Rbfl synthesis pathway, *DMRLs*, *GTPcII*, *ribD* and *ribE* (see annotation in Supporting Information), was assessed by quantitative RT-PCR in roots of *M. truncatula* plants grown with 45 μM Fe, 0 μM Fe without $CaCO_3$ and 0 μM Fe with $CaCO_3$. Expression of all genes assayed was significantly higher in Fe-deficient than in Fe-sufficient roots, irrespective of the presence of $CaCO_3$. Regarding the Fe-deficient treatments, gene expression increases over control values were higher in roots of plants grown in the presence of $CaCO_3$ (Figure 4). The highest induction was for *DMRLs* (30- and 99-fold without and with $CaCO_3$, respectively), followed by *GTPcII* (12- and 36-fold), *ribD* (4- and 24-fold) and *ribE* (2- and 6-fold).

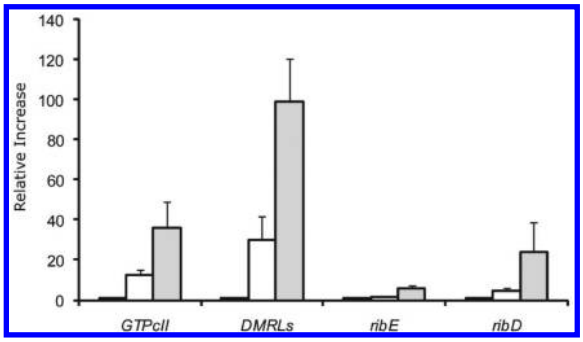

Figure 4. qRT-PCR analysis of genes from the riboflavin synthesis pathway. Root expression increases of *GTPcII*, *DMRLs*, *ribE* and *ribD* genes over Fe-sufficient values (black bars) of Fe-deficient plants grown without (white bars) and with $CaCO_3$ (light gray bars) in the nutrient solution.

Riboflavin Determination

The most abundant flavin in *M. truncatula* roots was Rbfl, with other Rbfl derivatives present in smaller amounts (data not shown). Riboflavin concentration in roots of Fe-sufficient plants was 2.5 ± 2.1 nmol g^{-1} FW, whereas in this treatment, Rbfl concentration in the nutrient solution was below the detection limit. Root Rbfl concentration was higher in Fe-deficient plants than in Fe-sufficient plants, with values being higher in roots of plants grown with than without $CaCO_3$ (862 ± 89 vs 194 ± 56 nmol g^{-1} FW, respectively). Riboflavin export to the nutrient solution after the 6-day treatment period was 16 ± 9 nmol g^{-1} FW for Fe-deficient plants grown with $CaCO_3$ and 39 ± 19 nmol g^{-1} FW for Fe-deficient plants grown without $CaCO_3$. Therefore, the percentages of Rbfl exported/Rbfl accumulated were 17/83 and 2/98 in the Fe-deficient treatments without and with $CaCO_3$, respectively (Figure 5).

DISCUSSION

In the present study we have documented the changes induced by Fe deficiency in the protein profile of root extracts from *M. truncatula* plants grown in hydroponics in two different Fe-deficiency conditions, with or without $CaCO_3$. Approximately 10−20% of the proteins changed in relative intensity as a consequence of the treatments imposed; these data are in consonance with previous studies describing changes in the relative intensity of 15% and 40% of the spots with Fe deficiency in sugar beet and tomato, respectively.[32,33] Morphological, proteomic, and transcriptomic changes induced by Fe deficiency were similar in both treatments but more intense in the presence of $CaCO_3$. Changes observed in the 0 μM Fe plus $CaCO_3$ treatment can be attributed to Fe deficiency itself but also to the presence of $CaCO_3$ and the high pH of the nutrient solution.

One of the major changes found in the protein profile of root extracts from *M. truncatula* plants grown in the two Fe-deficiency treatments was the *de novo* appearance of two proteins involved in the Rbfl biosynthesis pathway. DMRLs, which catalyzes the fourth step of the Rbfl biosynthesis pathway, appeared in both Fe-deficiency treatments, whereas GTPcII, a bifunctional enzyme that catalyzes the first two steps in Rbfl biosynthesis, appeared in the 0 μM Fe plus $CaCO_3$ treatment. Gene expression data further supported these results, with *MtDMRLs* showing the highest mRNA accumulation in both Fe-deficiency treatments, followed by *MtGTPcII*. Furthermore, *MtribE* and *MtribD*, coding for two other enzymes of the Rbfl biosynthetic pathway, were also up-regulated in both treatments. This indicates that the increase in the root synthesis of Rbfl is regulated by Fe, as it occurs in some flavinogenic yeast strains.[38] Our results suggest that DMRLs could be a key point for Fe-induced Rbfl synthesis regulation, although the involvement of other enzymes of the pathway, especially GTPcII, cannot be ruled out. It has been reported that the heterologous ectopic expression of *AtbHLH38* and *AtbHLH39*, two bHLH transcription factors strongly induced by Fe starvation, causes a constitutive, Fe-starvation independent export of Rbfl in species that show an Fe-induced flavin accumulation, such as sunflower and tobacco, but not in tomato, a species which does not accumulate flavins.[27] In *M. truncatula*, the amount of Rbfl exported to the growth media was minimal in the 0 μM Fe plus $CaCO_3$ treatment, where export only accounted for 2% of total Rbfl produced, whereas in the 0 μM Fe treatment 17% of the total Rbfl produced was exported to the medium. The presence of $CaCO_3$ maintains the pH of the nutrient solution at 7.5, whereas when $CaCO_3$ is absent the pH decreased from 5.5 to ca. 4.0 during the 6-days treatment period. This pH-regulation of root Rbfl export is consistent with previous studies using *Beta vulgaris*.[21] Therefore, we could hypothesize that riboflavin export may be taking place through a proton antiporter or driven by a proton gradient, since export is minimal in the presence of $CaCO_3$, which buffers nutrient solution pH at 7.5.

The exact role flavin compounds play in Fe deficiency in plants is still not known. However, it has been suggested that flavins accumulated in Fe-deficient roots could act as an electron donor either for the Fe(III) reductase or as a cofactor;[13,22,39] the fact that the Fe reductase enzyme contains FAD binding sequence motifs would support this hypothesis.[26] Also, a relationship between the enhanced root respiration induced by Fe deficiency and riboflavin accumulation/export has been proposed.[23] On the other hand, since flavin compounds are exported to the rhizosphere, it has been hypothesized that they could play a direct role in extracellular Fe reduction[22] and/or be involved in other indirect processes aimed at increasing soil Fe availability by, for instance, modifying the microbiology of the rhizosphere.[24,25] Flavins have been shown to mediate extracellular electron transfer in some bacteria.[40] Riboflavin is a metal chelator with avidity for Fe(II) over other metals,[41] and therefore the ability of Rbfl to chelate Fe has also been suggested by some authors.[42]

This study sheds new light on two novel aspects of the metabolic adaptation to Fe deficiency: an increase in N recycling processes and a boost of protein catabolism. We found consistent increases in two proteins related to N recycling in plants, UREG and LPD. This was found in both Fe-deficiency treatments and has not been reported, to the best of our knowledge, in any Fe-deficiency study so far. UREG is involved in the correct folding of urease, an enzyme that recycles N from urea yielding α-ketoacids and ammonia, whereas LPD is a component of the glycine decarboxylase complex, which catalyzes oxidative decarboxylation and deamination of glycine, leading to the formation of CO_2 and ammonia. In the 0 μM Fe plus $CaCO_3$ treated plants, the increase in N recycling could help to overcome the debilitated NO_3 assimilation caused by the major decrease in the Fe-containing enzyme nitrite reductase (5-fold decrease; spot 18). Ammonia produced by UREG and LPD can be metabolized by asparagine synthetase instead of glutamine synthetase, which was decreased in the 0 μM Fe plus $CaCO_3$ treatment. On the other hand, changes found in UREG, LPD and glutamine synthase suggest an increase in anaplerotic C supply, further supported by the increase in aspartate aminotransferase, an enzyme that interconverts major C and N compounds and is crucial to determine the C/N fate in legume species. In line with this hypothesis, the increases in LPD are accompanied by decreases in SHMT, resulting in a net positive balance of CO_2 that could in turn feed PEPC. There is molecular support to consider the glycine-serine interconversion caused by LPD and SHMT as a major C source in nonphotosynthetic tissues, especially when the needs of C for secondary metabolism are high.[43] Changes in protein catabolism were also observed in both Fe-deficiency treatments. In the 0 μM Fe treatment, increases in proteases and a decrease in the structural unit of the 20S proteasome were observed, whereas in the 0 μM Fe plus $CaCO_3$ treatment there was also a reorganization of the 20S proteasome subunits, an increase in peptidases and decreases in protease inhibitors. These data are in agreement with a recent proteomic study with Fe-deficient cucumber roots,[36] whereas other proteomic studies in sugar beet and tomato did not find increases in proteolysis.[31−33]

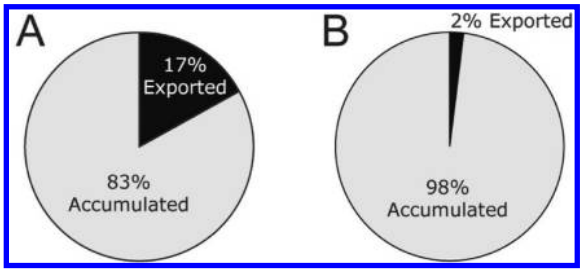

Figure 5. Percentage of riboflavin exported to the solution by Fe-deficient roots from plants grown without (A) and with $CaCO_3$ (B).

Other changes induced by Fe deficiency in *M. truncatula* deserve further attention, and two of them are described here for the first time. First, a decrease in two enzymes involved in the biosynthesis of the S-containing amino acids, Cys and Met, was found. In other species, an increase in Met synthesis has been observed with Fe deficiency, and authors hypothesized that this could account for an increased synthesis of nicotianamine.[32] However, in *M. truncatula* a decrease in the levels of enzymes involved in Met synthesis was found, perhaps related to the lower requirement of Fe−S cluster proteins due to Fe starvation; decreases in Fe-containing proteins related to energy metabolism, mostly Fe−S cluster proteins, were found in both treatments. Second, a GroEl-like chaperone (spot 10), demonstrated to facilitate folding of the mitochondrial malate dehydrogenase (MDH) isoform,[44] was no longer detected in either Fe-deficiency treatment. A decrease in the GroEl-like chaperone would cause an increased accumulation of the MDH precursor in the cytosol, which still retains catalytic activity, and this could contribute to the MDH activity increases measured in root extracts of Fe-deficient plants.[12,16]

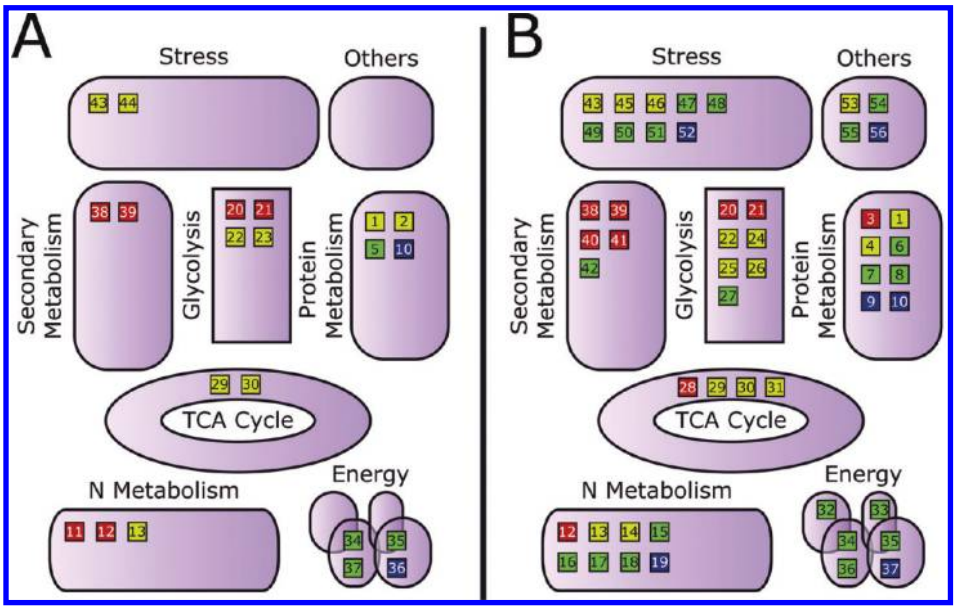

Figure 6. Changes in metabolic pathways as affected by Fe deficiency. Panels A and B are for 0 μM Fe and 0 μM Fe plus $CaCO_3$ treated plants, respectively. Pathways related to the identified proteins were integrated according to the KEGG database and GO annotation. A statistical Student *t* test was performed to show relevant changes between samples. Red symbols mark newly detected proteins in Fe-deficient roots, and yellow symbols proteins with increased intensity compared to controls (using a 2-fold threshold change). The same threshold (decreases larger than 50%) was selected for proteins with decreased intensity (green symbols). Blue symbols indicate proteins not detected in Fe-deficient roots. Numbers correspond to those in Table 1.

Other changes found support previous observations in Fe-deficient plants. For instance, the decrease in the mitochondrial complex I supports the reorganization of the electron transport chain with Fe deficiency, possibly involving increases in the activities of alternative dehydrogenases.[15] Also, stress-related proteins accounted for 10−17% of the changes in the protein profile in the 0 μM Fe and 0 μM Fe plus $CaCO_3$ treatments, respectively. A major change in both treatments was an increase in glutathione transferase, which conjugates glutathione to cytotoxic products. A reorganization of the SODs was also observed, most likely to compensate for FeSOD decreases. The increase in MDAR in the 0 μM Fe plus $CaCO_3$ treatment could compensate for the decrease in APX, an Fe-containing protein. An enhancement of the glycolytic pathway and TCA cycle agree with previous studies.[12,16] As also occurs in Fe-deficient tomato roots,[32] a decrease in fructokinase was found, suggesting that glucose is preferred over fructose as initial substrate in the glycolytic pathway, possibly related to the use of starch as an energy source instead of sucrose. This hypothesis is consistent with the low photosynthetic rates in Fe-deficient plants that would cause a shortage of available sucrose.

CONCLUSIONS

An overview of the results is shown in Figure 6. In general, more dramatic changes occur in plants exposed to $CaCO_3$, where the high external pH may account for some of the observed changes, but the same general response was observed. Fe deficiency caused a *de novo* accumulation of DMRLs and GTPcII, proteins involved in Rbfl biosynthesis, along with increases in the corresponding mRNA levels, suggesting that these enzymes may be control steps for the Fe-regulation of Rbfl synthesis. Overall, our results also suggest the occurrence of N recycling, possibly providing an additional anaplerotic N and C source for the synthesis of secondary metabolites, carboxylates and others. This was associated with increases in proteolysis, the already widely reported increases in glycolysis and TCA cycle, and changes in the electron transport chain in the mitochondria.

ASSOCIATED CONTENT

Supporting Information

Supporting material and methods: Identification of putative *DMRLs*, *GTPcII*, *ribD* and *ribE* genes in *Medicago truncatula*. Supporting results: Identification of putative *DMRLs*, *GTPcII*, *ribD* and *ribE* genes in *Medicago truncatula*; forward and reverse specific primers utilized for qRT-PCR; univariate statistical analysis of 2-DE gels; summary of protein profiling results; multivariate statistical analysis of 2-DE gels. This material is available free of charge via the Internet at http://pubs.acs.org.

AUTHOR INFORMATION

Corresponding Author

*Phone: +34976716052. FAX: +34976716145. E-mail: anaflor@eead.csic.es.

ACKNOWLEDGMENT

This work was supported by the Spanish Ministry of Science and Innovation (MICINN; grants AGL2009- 09018 and AGL2010-16515, co-financed with FEDER), the trilateral Project Hot Iron (ERA- NET Plant Genome Research KKBE; MICINN EUI2008-03618), the Aragón Government (group A03), and the U.S. Department of Agriculture, Agricultural Research Service (under Agreement number 58-6250-0-008 to MAG). J.R.-C. was supported by an I3P-CSIC predoctoral fellowship. The authors thank A. Calviño for assistance in growing and harvesting plants,

M. Klein for insights in the qPCR experiments and C. M. Li for assistance with molecular biology techniques. The contents of this publication do not necessarily reflect the views or policies of the U.S. Department of Agriculture, nor does mention of trade names, commercial products, or organizations imply endorsement by the U.S. Government.

REFERENCES

(1) Abadía, J.; Álvarez-Fernández, A.; Rombolà, A. D.; Sanz, M.; Tagliavini, M.; Abadía, A. Technologies for the diagnosis and remediation of Fe deficiency. *Soil Sci. Plant Nutr.* **2004**, *50*, 965–971.

(2) Abadía, J.; Vázquez, S.; Rellán-Álvarez, R.; El-Jendoubi, H.; Abadía, A.; Álvarez-Fernández, A.; López-Millán, A. F. Towards a knowledge-based correction of iron chlorosis. *Plant Physiol. Biochem.* **2011**, in press; DOI: 10.1016/j.plaphy.2011.01.026.

(3) Curie, C.; Panaviene, Z.; Loulergue, C.; Dellaporta, S. L.; Briat, J. F.; Walker, E. L. Maize yellow stripe1 encodes a membrane protein directly involved in Fe(III) uptake. *Nature* **2001**, *409* (6818), 346–349.

(4) Landsberg, E.-C. Transfer cell formation in the root epidermis: A prerequisite for Fe-efficiency? *J. Plant Nutr.* **1982**, *5* (4), 415–432.

(5) Muller, M.; Schmidt, W. Environmentally induced plasticity of root hair development in Arabidopsis. *Plant Physiol.* **2004**, *134* (1), 409–419.

(6) Moog, P.; Brüggemann, W. Iron reductase systems on the plant plasma membrane-A review. *Plant Soil* **1994**, *165* (2), 241–260.

(7) Robinson, N. J.; Procter, C. M.; Connolly, E. L.; Guerinot, M. L. A ferric-chelate reductase for iron uptake from soils. *Nature* **1999**, *397* (6721), 694–697.

(8) Eide, D.; Broderius, M.; Fett, J.; Guerinot, M. L. A novel iron-regulated metal transporter from plants identified by functional expression in yeast. *Proc Natl Acad Sci U.S.A.* **1996**, *93* (11), 5624–5628.

(9) Fox, T. C.; Guerinot, M. L. Molecular biology of cation transport in plants. *Annu. Rev. Plant Physiol. Plant Mol. Biol.* **1998**, *49*, 669–696.

(10) Santi, S.; Schmidt, W. Laser microdissection-assisted analysis of the functional fate of iron deficiency-induced root hairs in cucumber. *J Exp. Bot.* **2008**, *59* (3), 697–704.

(11) Santi, S.; Schmidt, W. Dissecting iron deficiency-induced proton extrusion in *Arabidopsis* roots. *New Phytol.* **2009**, *183* (4), 1072–1084.

(12) Abadía, J.; López-Millán, A.-F.; Rombolà, A.; Abadía, A. Organic acids and Fe deficiency: a review. *Plant Soil* **2002**, *241* (1), 75–86.

(13) López-Millán, A. F.; Morales, F.; Andaluz, S.; Gogorcena, Y.; Abadía, A.; De Las Rivas, J.; Abadía, J. Responses of sugar beet roots to iron deficiency. Changes in carbon assimilation and oxygen use. *Plant Physiol.* **2000**, *124* (2), 885–898.

(14) Schmidt, W. Mechanisms and regulation of reduction-based iron uptake in plants. *New Phytol.* **1999**, *141* (1), 1–26.

(15) Vigani, G.; Maffi, D.; Zocchi, G. Iron availability affects the function of mitochondria in cucumber roots. *New Phytol.* **2009**, *182* (1), 127–136.

(16) Zocchi, G., Metabolic changes in iron-stressed dicotyledonous plants. In *Iron Nutrition in Plants and Rhizospheric Microorganisms*; Barton, L. L., Abadía, J., Eds.; Springer: Dordrecht, 2006; pp 359−370.

(17) Cesco, S.; Neumann, G.; Tomasi, N.; Pinton, R.; Weisskopf, L. Release of plant-borne flavonoids into the rhizosphere and their role in plant nutrition. *Plant Soil* **2010**, *329* (1), 1–25.

(18) Nagarajah, S.; Ulrich, A. Iron nutrition of the Sugar beet plant in relation to growth, mineral balance, and riboflavin formation. *Soil Sci.* **1966**, *102* (6), 399–407.

(19) Welkie, G. W.; Miller, G. W. Iron nutrition of *Nicotiana tabacum L.* in relation to riboflavin, riboflavin-5-phosphate, and flavin adenine dinucleotide content. *Plant Physiol.* **1960**, *35* (4), 516–520.

(20) Susín, S.; Abián, J.; Sánchez-Baeza, F.; Peleato, M. L.; Abadía, A.; Gelpi, E.; Abadía, J. Riboflavin 3′- and 5′-sulfate, two novel flavins accumulating in the roots of iron-deficient sugar beet (*Beta vulgaris*). *J. Biol. Chem.* **1993**, *268* (28), 20958–20965.

(21) Susín, S.; Abián, J.; Peleato, M.; Sánchez-Baeza, F.; Abadía, A.; Gelpi, E.; Abadía, J. Flavin excretion from roots of iron-deficient sugar beet (*Beta vulgaris L.*). *Planta* **1994**, *193* (4), 514–519.

(22) González-Vallejo, E. B.; Susín, S.; Abadía, A.; Abadía, J. Changes in sugar beet leaf plasma membrane Fe(III)-chelate reductase activities mediated by Fe deficiency, assay buffer composition, anaerobiosis and the presence of flavins. *Protoplasma* **1998**, *205*, 163–168.

(23) Higa, A.; Mori, Y.; Kitamura, Y. Iron deficiency induces changes in riboflavin secretion and the mitochondrial electron transport chain in hairy roots of *Hyoscyamus albus*. *J. Plant Physiol.* **2010**, *167* (11), 870–878.

(24) Jordan, C. M.; Wakeman, R. J.; DeVay, J. E. Toxicity of free riboflavin and methionine-riboflavin solutions to *Phytophthora infestans* and the reduction of potato late blight disease. *Can. J. Microbiol.* **1992**, *38* (11), 1108–1111.

(25) Yang, G.; Bhuvaneswari, T. V.; Joseph, C. M.; King, M. D.; Phillips, D. A. Roles for riboflavin in the Sinorhizobium-alfalfa association. *Mol. Plant-Microbe Interact.* **2002**, *15* (5), 456–462.

(26) Schagerlof, U.; Wilson, G.; Hebert, H.; Al-Karadaghi, S.; Hagerhall, C. Transmembrane topology of FRO2, a ferric chelate reductase from *Arabidopsis thaliana*. *Plant Mol. Biol.* **2006**, *62* (1−2), 215–221.

(27) Vorwieger, A.; Gryczka, C.; Czihal, A.; Douchkov, D.; Tiedemann, J.; Mock, H. P.; Jakoby, M.; Weisshaar, B.; Saalbach, I.; Baumlein, H. Iron assimilation and transcription factor controlled synthesis of riboflavin in plants. *Planta* **2007**, *226* (1), 147–158.

(28) Andaluz, S.; López-Millán, A. F.; De las Rivas, J.; Aro, E. M.; Abadía, J.; Abadía, A. Proteomic profiles of thylakoid membranes and changes in response to iron deficiency. *Photosynth. Res.* **2006**, *89* (2−3), 141–155.

(29) Laganowsky, A.; Gómez, S. M.; Whitelegge, J. P.; Nishio, J. N. Hydroponics on a chip: analysis of the Fe deficient Arabidopsis thylakoid membrane proteome. *J. Proteomics* **2009**, *72* (3), 397–415.

(30) Timperio, A. M.; D'Amici, G. M.; Barta, C.; Loreto, F.; Zolla, L. Proteomics, pigment composition, and organization of thylakoid membranes in iron-deficient spinach leaves. *J. Exp. Bot.* **2007**, *58* (13), 3695–3710.

(31) Brumbarova, T.; Matros, A.; Mock, H. P.; Bauer, P. A proteomic study showing differential regulation of stress, redox regulation and peroxidase proteins by iron supply and the transcription factor FER. *Plant J.* **2008**, *54* (2), 321–334.

(32) Li, J.; Wu, X. D.; Hao, S. T.; Wang, X. J.; Ling, H. Q. Proteomic response to iron deficiency in tomato root. *Proteomics* **2008**, *8* (11), 2299–2311.

(33) Rellán-Álvarez, R.; Andaluz, S.; Rodríguez-Celma, J.; Wohlgemuth, G.; Zocchi, G.; Álvarez-Fernández, A.; Fiehn, O.; López-Millán, A. F.; Abadía, J. Changes in the proteomic and metabolic profiles of *Beta vulgaris* root tips in response to iron deficiency and resupply. *BMC Plant Biol.* **2010**, *10*, 120.

(34) Benedito, V. A.; Torres-Jerez, I.; Murray, J. D.; Andriankaja, A.; Allen, S.; Kakar, K.; Wandrey, M.; Verdier, J.; Zuber, H.; Ott, T.; Moreau, S.; Niebel, A.; Frickey, T.; Weiller, G.; He, J.; Dai, X.; Zhao, P. X.; Tang, Y.; Udvardi, M. K. A gene expression atlas of the model legume *Medicago truncatula*. *Plant J.* **2008**, *55* (3), 504–513.

(35) Colditz, F.; Braun, H. P. *Medicago truncatula* proteomics. *J. Proteomics* **2010**, *73*, 1974–1985.

(36) Donnini, S.; Prinsi, B.; Negri, A.; Vigani, G.; Espen, L.; Zocchi, G. Proteomic characterization of iron deficiency responses in *Cucumis sativus L.* roots. *BMC Plant Biol.* **2010**, *10* (1), 268.

(37) Terry, N. Limiting factors in photosynthesis: I. Use of iron stress to control photochemical capacity in vivo. *Plant Physiol.* **1980**, *65* (1), 114–120.

(38) Stenchuk, N. N.; Kutsiaba, V. I.; Kshanovskaia, B. V.; Fedorovich, D. V. Effect of *rib83* mutation on riboflavin biosynthesis and iron assimilation in *Pichia guilliermondii*. *Mikrobiologiia* **2001**, *70* (6), 753–758.

(39) Welkie, G. W.; Miller, G. W., Plant iron uptake physiology by nonsiderophore systems. In *Iron Chelation in Plants and Soil Microorganisms*; Barton, L. L., Hemming, B. C., Eds.; Academic Press: New York: 1993; pp 345−370.

(40) Marsili, E.; Baron, D. B.; Shikhare, I.; Coursolle, D.; Gralnick, J. A.; Bond, D. R. *Shewanella* secretes flavins that mediate extracellular electron transfer. *Proc. Natl. Acad. Sci. U.S.A.* **2008**, *105* (10), 3968–3973.

(41) Albert, A. Quantitative studies of the avidity of naturally occurring substances for trace metals. III. Pteridines, riboflavin and purines. *Biochem. J.* **1953**, *54* (4), 646–654.

(42) Wallace, A. Root excretions in tobacco plants and possible implications on the iron nutrition of higher plants. In *Regulation of the Micronutrients Status of Plants by Chelating Agents and Other Factors*; Wallace, A., Ed.; A. Wallace Publ.: Los Angeles, 1971; pp 136−139.

(43) Rajinikanth, M.; Harding, S. A.; Tsai, C. J. The glycine decarboxylase complex multienzyme family in *Populus*. *J. Exp. Bot.* **2007**, *58* (7), 1761–1770.

(44) Gietl, C.; Seidel, C.; Svendsen, I. Plant glyoxysomal but not mitochondrial malate dehydrogenase can fold without chaperone assistance. *Biochim. Biophys. Acta* **1996**, *1274* (1−2), 48–58.

Running title: Flavins in Fe-deficient Strategy I plants

Corresponding author:

Dr. Ana Flor López Millán

Department of Plant Nutrition, Aula Dei Experimental Station, CSIC, P.O. BOX 13034, E-50080 Zaragoza, Spain

Telephone: 34 976 715052

Fax: 34 976 71 6145

Email: anaflor@eead.csic.es

Subject Area

(2) environmental and stress responses

Figures

Black and White Figures: 3

Colour Figures: 4

Tables: 3

Characterization of Flavins In Roots of Fe-deficient Strategy I Plants, With *Medicago truncatula* On The Focus

Jorge Rodríguez-Celma[a], Saúl Vázquez-Reina[a], Jesús Orduna[b], Anunciación Abadía[a], Javier Abadía[a], Ana Álvarez-Fernández[a] and Ana-Flor López-Millán[a*]

[a]Plant Nutrition Department, Aula Dei Experimental Station (CSIC), P.O. Box 13034, E-50080, Zaragoza, Spain.

[b]New Organic Materials Unit, Institute of Materials Science of Aragón, CSIC-University of Zaragoza, c/ Pedro Cerbuna 12, E-50009 Zaragoza, Spain

***Corresponding author**

Abbreviations

Chl, Chlorophyll; FCR, ferric-chelate reductase; HOMO, highest occupied molecular orbital; LUMO, lowest unoccupied molecular orbital; PEPC, phospho*enol*pyruvate carboxylate; PM, plasma membrane; Rbfl, riboflavin

Abstract

The root accumulation and excretion of riboflavin (Rbfl) and Rbfl-derivatives has been studied in the model legume species *Medicago truncatula*, grown in hydroponics in two different Fe-deficiency conditions, with and without $CaCO_3$. Using high resolution mass spectrometry techniques coupled to liquid chromatography, three different flavin derivatives not previously reported in plants, putatively identified as 7-hydroxy-Rbfl, 7α-hydroxy-Rbfl and 7-carboxy-Rbfl, were found along with Rbfl in Fe-deficient *M. truncatula* roots. In the presence of $CaCO_3$ most of the flavins were accumulated in the roots, whereas in the absence of $CaCO_3$ there was partial export to the nutrient solution. The major flavins in roots and nutrient solution were Rbfl and 7-hydroxy-Rbfl, respectively. Flavins were located in the root cortex and epidermal cells, preferentially in a near-the-apex root region that also exhibited increased ferric chelate reductase activity. Six out of 15 different species of horticultural interest showed root increases in both Rbfl (four of them also having Rbfl derivatives) and ferric chelate reductase activity (FCR). No significant correlation was found between Rbfl and either PEPC or FCR activities, whereas the later two showed a good correlation between them. The possible roles of Rbfl and Rbfl-derivatives in roots and nutrient solutions are discussed. *Medicago truncatula* is proposed as a model system for flavin studies.

Key-words: *Medicago truncatula*, legume, riboflavin, riboflavin derivative identification, mass spectrometry, iron deficiency, root.

Introduction

Iron is an essential micronutrient for all living organisms and the fourth most abundant element in the earth's crust. However, Fe deficiency is a crop yield-limiting factor, especially in calcareous soils where Fe occurs in scarcely soluble oxidized forms that are not readily available to plants (Lindsay and Schwab 1982). When Fe-deficient, plants typically use two strategies aimed at increasing Fe uptake. Strategy I relies on an Fe reduction-based mechanism, whereas Strategy II (restricted to grasses) uses an Fe chelation-based mechanism (Abadía et al. 2011). Strategy I plant species develop a series of biochemical changes in roots, including the induction of an Fe(III) reductase (FCR) in the cell plasma membrane (PM), encoded by members of the FRO family (Mukherjee et al. 2006), an Fe(II) IRT transporter, which belongs to the ZIP family of metal transporters (Hall and Guerinot 2006), and a PM H^+-ATPase for proton excretion to the rhizosphere (Santi and Schmidt 2009). Other biochemical changes commonly found in Strategy I species are increases in the activity of phospho*enol*pyruvate carboxylase (PEPC) and other enzymes, constituting an anaplerotic pathway for CO_2 fixation that provides energy and reducing power to support Fe uptake (López-Millán et al. 2009). Morphological changes found in Strategy I species include an increase of the root area in contact with the rhizosphere, as well as root tip swelling and formation of lateral roots, root hairs and transfer cells (Schmidt 1999).

Many Strategy I plants, when challenged with Fe deficiency, accumulate and/or export to the growth medium a plethora of compounds such as phenolics, organic acids, flavonoids and flavins (Abadía et al. 2002; Cesco et al. 2010; Jin et al. 2007; Ohwaki and Sugahara 1997; Rodríguez-Celma et al. 2011). Some of these compounds have redox and/or metal-complexing capabilities that may facilitate Fe availability in the

rhizosphere as well as in the root apoplast (Cesco et al. 2010; Ishimaru et al. 2011; Jin et al. 2007). Although the release of these types of compounds by roots of Fe-deficient plants has been reported long time ago, detailed analyses of the specific compounds exported by different plant species and environments are still needed.

Long before the Strategy I mechanism was described, the yellowing of roots and nutrient solutions was observed with Fe deficient plants (Frolich and Wallace 1966; Nagarajah and Ulrich 1966; Pound and Welkie 1958; Wallace 1971; Weinstein et al. 1954), and the compound responsible of this colour was identified as riboflavin (Rbfl) based on its spectral properties. All flavins are yellow-coloured compounds sharing an isoalloxacine ring (7,8-dimethyl-10-alkylisoalloxacine). Iron-deficient plants accumulate in the roots and export to the growth media not only Rbfl (Higa et al. 2010; Rodríguez-Celma et al. 2011; Welkie 2000; Welkie and Miller 1960; Welkie and Miller 1993), but also other Rbfl derivatives such as the Rbfl 3' and 5'-sulphates found in in sugar beet and spinach (Susín et al. 1994; Susín et al. 1993). The capability to export flavins under Fe deficiency has been associated to the particularly high Fe-efficiency of some plant species, although it does not follow obvious taxonomical categories (Welkie 2000). Riboflavin and its main derivatives, FAD and FMN, are well-known enzymatic cofactors implied in many redox reactions, which play roles in one- and two-electron transfer processes. The redox potential of flavins change markedly depending on the local environment, making them exceptionally versatile molecules from the chemical and biochemical points of view (Massey 2000). The specific role(s) flavin compounds play in Fe-deficient plants is still unknown, although it has been suggested that the function could be related either to their accumulation in the root cell, as a cofactor or a component of redox reactions (González-Vallejo et al. 1998; Higa et al. 2010; López-

Millán et al. 2000; Welkie and Miller 1993), or to the export to the rizhosphere, improving Fe availability or modifying the rhizosphere microbiome (Jordan et al. 1992; Susín et al. 1993; Yang et al. 2002). A relationship between Fe and Rbfl biosynthesis and export has been described in some flavinogenic yeast strains and bacteria, where flavin biosynthesis is down-regulated by Fe and both Rbfl synthesis and excretion increase upon Fe deficiency (Stenchuk et al. 2001; Worst et al. 1998).

Medicago truncatula is an emerging model legume with a number of genetic and molecular tools available (Benedito et al. 2008; Colditz and Braun 2010) that displays most typical Fe deficiency Strategy I root responses, along with flavin root accumulation and export (Andaluz et al. 2009). In Fe-deficient *M. truncatula*, Rbfl accumulates in the roots when the external pH is high (Rodríguez-Celma et al. 2011), and is exported to the nutrient solution when external pH is low (Rodríguez-Celma et al. 2011). Two of the enzymes involved in Rbfl biosynthesis in *M. truncatula*, DMRLs and GTPcII, are up-regulated at the mRNA level and the amounts of the corresponding proteins increase in roots (Rodríguez-Celma et al. 2011). Although other minor flavins also accumulate in *M. truncatula*, their identification has not been achieved so far.

The main aim of this work was to characterize the whole set of flavin compounds accumulated and exported by Fe-deficient *M. truncatula* plants grown in hydroponics at two different nutrient solution pH values, with (pH 7.7) and without $CaCO_3$ (pH 5.5). Flavins occurring in roots and the growth medium were identified using high performance liquid chromatography (HPLC) coupled to two different high-resolution mass spectrometry methodologies [ESI-MS(TOF) and ESI-CID-MS^2(QTOF)]. Also, the localization of flavins in root tissues was carried out by optical and fluorescence microscopy. Furthermore, the possible association between flavin accumulation and

export and other Strategy I responses was studied in *M.truncatula* by comparing the localization of flavins as well as those of the Fe(III) reductase and acidification activities. Finally, other species of horticultural interest belonging to a wide spectrum of plant families were grown in nutrient solution under Fe deficiency in the presence of $CaCO_3$, and the flavins accumulated in the roots were characterized by the techniques indicated above. Also, the Fe reductase and PEPC activities were measured in the roots of these species, to gather information on the possible role of root flavin accumulation in the Fe deficiency response.

Results

Characteristics of *M. truncatula* plants grown under Fe deficiency

M. truncatula plants grown in hydroponics under Fe deficiency showed chlorosis symptoms, both in the absence (pH 5.5) and presence of $CaCO_3$ (pH 7.7) in the nutrient solution (Rodríguez-Celma et al. 2011). At 3 and 6 d after the onset of the treatment, root systems were larger in Fe-sufficient and Fe-deficient plants grown at pH 5.5 than those of plants grown at pH 7.7 (see Supplementary Fig. S1). Six d after the treatment onset, roots of Fe-deficient plants grown at pH 7.7 showed yellow and swollen root distal regions and short lateral roots (Rodríguez-Celma et al. 2011) (see Supplementary Fig. S1D). Two different yellow zones can be distinguished in the root distal region, a hair-free one (ca. 3-7 mm from the apex) and a sub-apical one that has root hairs (ca. 12-15 mm from the apex). Roots of Fe-deficient plants grown at pH 5.5 also developed yellow and swollen root distal regions, but lateral roots in these plants were longer than those of plants grown in the presence of $CaCO_3$. These roots often showed white zones between yellow areas, resulting in a characteristic yellow/white/yellow pattern along the roots (not shown). On the other hand, the yellow colour was completely absent in roots

from Fe-sufficient plants. The yellow colour of Fe-deficient *M. truncatula* roots was due not only to the presence of Rbfl, but also to other still unidentified flavins (Rodríguez-Celma et al. 2011). Therefore, we studied the whole set of flavin compounds accumulated and exported by Fe-deficient *M. truncatula* plants, using advanced HPLC-MS techniques.

Analysis of flavin-type compounds by HPLC/UV-VIS

Flavin compounds were separated in approximately 35 min using a C_{18} column, and detected at a wavelength of 445 nm (Fig. 1). Standards of Rbfl, FMN and FAD had retention times (RT) of 33.3, 28.4 and 27.4 min, respectively, and had similar UV-VIS spectra, with two broad maxima at approximately 370 and 445 nm (Fig. 1A). Riboflavin sulphates, known to be present in roots of Fe-deficient *B. vulgaris* (Susín et al. 1993) appeared at 29.9 and 30.7 min RT (not shown).

Chromatograms of root extracts from 6 d Fe-deficient *M. trucatula* plants showed four peaks (Fig. 1B), one corresponding to Rbfl (at 33 min RT) and three more minor unidentified peaks eluting at shorter RT (at 15.6, 24.2 and 26.0 min RT). These peaks were assigned to flavin-type compounds (FC) based on their UV-VIS spectra (Fig. 1B), and are thereafter called FC1, FC2 and FC3. The UV-VIS spectrum of FC1 showed, when compared to Rbfl, small hypsochromic shifts in the two main absorbance bands (Fig. 1B). In the case of FC2, the spectrum showed a hypsochromic shift in the low wavelength absorption band and a bathochromic shift in the high wavelength absorption band (Fig. 1B). The UV-VIS spectrum of FC3 showed a small hypsochromic shift in the low wavelength absorption band when compared to Rbfl (Fig. 1B).

Chromatograms of flavin compounds isolated from nutrient solutions where *M. truncatula* plants had been grown also showed four peaks, with identical RT and UV-VIS spectra to those found in the root extracts (Fig. 1C). However, the main flavin in nutrient solutions was FC2 (Fig. 1C).

Characterization of flavins in *M. truncatula* root extracts and nutrient solutions

The three unknown flavin-type compounds found in the *M. truncatula* root extracts and nutrient solutions were studied by HPLC coupled to two high-resolution MS techniques, HPLC/UV-VIS/ESI-MS(TOF) and HPLC/ESI-CID-MS^2(QTOF). The MS(TOF) spectra of Rbfl, FC1, FC2 and FC3 showed main ions (*m/z*, in positive/negative mode) at 377.15/375.13, 407.12/405.10, 379.12/377.11 and 393.14/391.13, respectively (Fig. 2). None of the three unknown ions were observed in the MS(TOF) spectra of Fe-sufficient roots and nutrient solutions where Fe-sufficient plants had been grown. Based on the exact mass measurements (with all *m/z* errors < 2 mDa; Table 1) and the isotopic signatures (with all SigmaFit^{TM} values < 0.04; Table 1), we assigned $C_{17}H_{18}N_4O_8$, $C_{16}H_{18}N_4O_7$ and $C_{17}H_{20}N_4O_7$ as the most likely elemental formulae for FC1, FC2 and FC3, respectively (Table 1). The *m/z* and elemental formulae differences found between the FC unknowns and Rbfl suggest the following: i) in FC1, the replacement of a methyl ($–CH_3$) for a carboxyl group (–COOH), resulting in a mass change of +29.97 Da; ii) in FC2, the replacement of a methyl for a hydroxyl group (–OH), leading to a change of +1.98 Da; and iii) in FC3, the addition of a hydroxyl group (–OH), resulting in a change of +16.00 Da. These modifications in chemical structure are in full agreement with the RT changes observed, which indicate relative polarities in the order FC1>FC2>FC3>Rbfl.

In order to gain structural information on FC1, FC2 and FC3, we used HPLC/ESI-CID-MS^2(QTOF), which allows obtaining fragmentation patterns of the parent ions containing exact mass measurements of each product ion. We used as fragmentation templates (in positive and negative mode) standards of Rbfl and other known Rbfl derivatives such as FAD, FMN and Rbfl-sulphates, which share the same isoalloxacine moieity and differ in the ribose chain moieities. In all of these standards we found a number of MS^2 product ions, in negative and positive mode, which can be assigned to the isoalloxacine moieity (shown for Rbfl in Supplementary Fig. S2). Therefore, Rbfl data were used as a fragmentation reference.

The MS^2 spectra of FC1, FC2 and FC3 showed product ions different from those found in the Rbfl template (Table 1, Fig. 2). However, some of these product ions corresponded, when compared to the non-fragmented parent ions, to losses identical to those found in Rbfl, confirming that all modifications in FC1, FC2 and FC3 were located in the isoalloxacine moieity (Table 1). A common feature of Rbfl, FC1, FC2 and FC3 was the neutral loss of $C_4H_8O_4$ in negative mode, which corresponds to a large part of the ribose chain (four out of the five C atoms; Table 1 and Supplementary Fig. S2): the differences in *m/z* found in the non-fragmented compounds (405.10, 377.11, 391.13 and 375.13 in FC1, FC2, FC3 and Rbfl, respectively) were identical to those found in the corresponding product ions (285.07, 257.07, 271.09 and 255.09 in FC1, FC2, FC3 and Rbfl, respectively). In the case of FC1 no other common losses with Rbfl were found, and we concluded that the carboxyl group replaces a methyl group in position 7α or 8α in the isoalloxazine moieity. In the case of FC2 and FC3, they shared with Rbfl four additional neutral losses in the positive mode fragmentation pattern ($C_7H_{11}NO_6$, $C_6H_{13}NO_5$, $C_6H_{11}NO_4$ and $C_5H_{10}O_4$; Table 1). These losses correspond to the full ribose

chain ($C_5H_{10}O_4$) and to different pieces of the heterocyclic part of the isoalloxacine moieity (see Supplementary Fig. S2). This indicates that the modifications in FC2 and FC3 do occur in the homocyclic ring of the isoalloxacine moieity. In the case of FC2, the replacement of CH_3 by OH could occur only at positions 7 or 8, whereas in the case of FC3, the OH addition could occur either in the 7α or 8α methyl groups or in positions 6 or 9 of the isoalloxazine moieity.

The changes in the UV-VIS spectra of FC1, FC2 and FC3 (Fig. 1) can provide, when compared to that of Rbfl, additional information for the structural elucidation of the flavin compounds. In the case of Rbfl, TDDFT calculations predict a one-electron HOMO to LUMO transition at 435 nm (2.85 eV), and this is in good agreement with the UV-VIS spectrum (Fig. 1). The molecular orbital topologies indicate that the electron densities in the HOMO and LUMO are preferentially located in C7 and C8, respectively (see Supplementary Fig. S3). Consequently, acceptor substituents in C7 cause a better stabilization in the HOMO compared to the LUMO, thus increasing the HOMO-LUMO gap and causing a hypsochromic shift; conversely, donor substituents in C7 cause a bathochromic shift. This situation is the opposite for substituents in C8, with acceptor and donor substituents leading to bathochromic and hypsochromic shifts, respectively. Therefore, the hypsochromic shift found in FC1 when compared to Rbfl indicates that the acceptor carboxyl group must be at C7; the calculated UV-VIS spectrum of FC1 predicts the lowest absorption band to occur at 412 nm, with a hypsochromic shift of 23 nm with respect to Rbfl, the same value found experimentally. Also, the bathochromic shift observed in FC2 indicates that the donor hydroxyl group must be at C7; calculations predict the lowest absorption band of FC2 to occur at 471 nm, with a 36 nm bathochromic shift that compares well to the 30 nm shift found experimentally. In the

case of FC3, the minor changes found experimentally in the UV-VIS spectrum suggest that the hydroxyl group is not directly linked to the aromatic ring, with its donor ability having little effect in the HOMO and LUMO energies. Among the possible positions that can explain the MS fragmentation (6, 9, 7α, 8α), only the 7α and 8α ones are consistent with the UV-VIS spectrum. Comparison to FC1 and FC2, which are modified at the 7 position, leads us to tentatively propose the 7α substitution for FC3 as well. Therefore, FC1, FC2 and FC3 were putatively identified as 7-carboxy-Rbfl, 7-hydroxy-Rbfl, and 7α-hydroxy-Rbfl (Fig. 2).

Root flavin accumulation and exudation

The quantification of flavins accumulated in the roots was carried out by HPLC/UV-VIS (Table 2). In extracts of control plants the only flavin present was Rbfl, in a concentration of approximately 2 nmol g^{-1} FW. In extracts of Fe-deficient roots Rbfl was the main flavin, with the other three Rbfl derivatives being present although in smaller amounts. In Fe deficient plants grown in the absence of $CaCO_3$, the root concentrations of Rbfl, 7-carboxy-Rbfl, 7-hydroxy-Rbfl, and 7α-hydroxy-Rbfl were approximately 194, 5, 48 and 51 nmol g^{-1} FW, respectively (Table 2). In Fe deficient plants grown with $CaCO_3$, the root concentrations of Rbfl, 7-carboxy-Rbfl, 7-hydroxy-Rbfl, and 7α-hydroxy-Rbfl were approximately 863, 4, 43 and 103 nmol g^{-1} FW, respectively (Table 2). In the case of Rbfl, root concentration values similar to those presented here were obtained in parallel experiments (Rodríguez-Celma et al. 2011).

In the nutrient solution of plants grown with Fe we only found traces of Rbfl (<1 nM), whereas in the nutrient solutions of plants grown in the two different Fe-deficiency treatments Rbfl, 7-carboxy-Rbfl, 7-hydroxy-Rbfl, and 7α-hydroxy-Rbfl were present (Table 2). In the absence of $CaCO_3$, Rbfl, 7-carboxy-Rbfl, 7-hydroxy-Rbfl, and

7α-hydroxy-Rbfl concentrations were approximately 23, 1, 62 and 5 nM, respectively [when expressed on a root fresh weight basis, this corresponds to a Rbfl, 7-carboxy-Rbfl, 7-hydroxy-Rbfl, and 7α-hydroxy-Rbfl effective export, in the 6 d treatment period, of approximately 40, 1, 109 and 9 nmol g^{-1} FW, respectively (Table 2)]. In the presence of $CaCO_3$, Rbfl, 7-carboxy-Rbfl, 7-hydroxy-Rbfl, and 7α-hydroxy-Rbfl and concentrations were approximately 7, <1, 20 and 1 nM, respectively [when expressed on a root fresh weight basis, this corresponds to a Rbfl, 7-carboxy-Rbfl, 7-hydroxy-Rbfl, and 7α-hydroxy-Rbfl effective export, in the 6 d treatment period, of approximately 16, <1, 46 and 3 nmol g^{-1} FW, respectively (Table 2)]. In the case of Rbfl, nutrient solution concentration values similar to those presented here were obtained in parallel experiments (Rodríguez-Celma et al., 2011).

Therefore, at pH 5.5 *M. truncatula* plants exported 35% of flavins to the nutrient solution, whereas 65% of the total remained in the roots. Conversely, at pH 7.7 export to the nutrient solution accounted for only 6% of the total, with most of the flavins (94%) accumulating in the roots. In both Fe-deficiency treatments, the major flavin exported to the nutrient solution (>65% of the total) was 7-hydroxy-Rbfl (FC2).

Localization and distribution of flavins in roots

The distribution of the flavin green fluorescence (emission at approximately 425 nm) along the root length was studied using root transversal slices 70 μm in thickness (Fig. 3). In roots of *M. truncatula* plants grown under Fe deficiency for 1 d no fluorescence was detected, whereas in those grown for 3 and 6 d flavin fluorescence occurred in the two yellow zones described above, with the highest fluorescence intensity being observed in the zone near the apex in both treatments (Fig. 3). A better separation, with sharper fluorescence peaks in the sub-apical and near the apex zones, was found in roots

of Fe-deficient plants grown at pH 7.7 when compared to those grown at pH 5.5, probably associated to the reduced growth in the presence of $CaCO_3$ (Fig. 3).

Transversal root sections indicate that flavin fluorescence was mainly located in root cortex cells (Fig. 4). In the zone near the apex flavins were observed in the whole cortex and also in epidermal cells (Fig. 4B, D, F, H), whereas in the sub-apical zone flavins were visible in the inner part of the root cortex (Fig. 4A, C, E, G). The 3-D flavin distribution along the root length can also be observed in Supplementary Fig. S4.

Regarding individual flavin compounds, the same composition pattern was found in sub-apical and near the apex root zones, in all Fe-deficiency treatments and sampling times: (from highest to lowest concentration) Rbfl > 7α-hydroxy-Rbfl > 7-hydroxy-Rbfl > 7-carboxy-Rbfl (Fig. 5). At 1 d, all flavins were already present in the zone near the apex at pH 5.5, whereas at pH 7.7 Rbfl occurred, although at a lower concentration, along with traces of 7α-hydroxy-Rbfl. At 3 d, both root zones had similar flavin concentrations, with Rbfl concentrations being similar in both treatments and concentrations of the three derivatives being higher at pH 5.5 than at pH 7.7. At 6 d, the flavin derivatives were present at similar concentrations in the sub-apical and near the apex yellow zones in both treatments, with Rbfl being more abundant at pH 7.7. Whereas data shown in Fig. 5 describe the relative flavin composition of the two major yellow root zones, the differences in Rbfl content were more prominent when looking at whole root sections, which include also the intermediate part of the root where flavins were almost absent (Table 2).

Localization of Fe reducing activity and acidification in excised roots

In situ localization in agar plates of root FCR and acidification activities in control and Fe-deficient plants grown with or without $CaCO_3$, 3 and 6 d after treatment onset, are shown in Supplementary Fig. S5. Red areas in the FCR activity assay indicate the formation of the complex Fe(II)-BPDS. Yellow areas in the acidification assay indicate agar pH values <5.2, whereas purple areas indicate agar pH values >6.8. FCR activity was visible at 3 d in root distal parts and lateral roots of plants from both Fe-deficiency treatments (see Supplementary Fig. S5E, I). At 6 d, a similar behaviour was observed for plants grown at pH 5.5 (see Supplementary Fig. S5F), whereas roots from plants grown at pH 7.7 showed red colour areas generally restricted to the near the apex zone of secondary roots (see Supplementary Fig. S5J). The acidification activity was visible from day one (data not shown), and was distributed along the whole root length in both treatments at 3 and 6 d (see Supplementary Fig. S5G, H, K, L). In the presence of $CaCO_3$, an increase in pH near the roots was observed, possibly associated to $CaCO_3$ adsorbed (or present in the apoplastic space) in roots.

Effects of Fe-deficiency on root morphology, Rbfl accumulation and FCR and PEPC activities in different plant species of horticultural interest

In all species studied, root FW decreased as a result of Fe deficiency, with decreases ranging from 6 to 89% (average decreases were approximately 40%; Table 3). The smallest decrease occurred in *S. oleracea* and the highest in *B. vulgaris*. As described before in other plant species, Fe deficiency caused an increase in the number of lateral roots in all species studied, and this was accompanied by root swelling in all species except in *N. officinale*. Large, swollen and yellow root distal parts were observed in *S. oleracea*, *P. crispum*, *C. melon*, *B. vulgaris* and *A. caudatus*, whereas *P. oleracea*, *C. officinalis* and *A. arvensis* roots were slightly yellow, but yellow root tips were absent.

On the other hand, *B. officinalis*, *E. californica*, *S. armeria*, *N. officinale*, *L. albus*, *A. cepa* and *Mentha x piperita* did not show any root yellowing. Leaf Chl concentrations were 0.8-3.7 and 0.2-1.8 μmol g^{-1} FW in Fe-sufficient and Fe-deficient leaves, respectively (Table 3). Chlorophyll decreased with Fe deficiency in all species, with decreases ranging from approximately 40% in *N. officinale*, *Mentha x piperita* and *A. cepa* to 90% in *B. officinalis*, *P. oleracea*, *S. oleracea* and *B. vulgaris*.

Flavin analysis by HPLC/UV-VIS/MS showed that Rbfl occurred in all root samples. In Fe-sufficient plants, root Rbfl concentrations conditions ranged from 0.2 to 3.9 nmol g^{-1} FW, with the lowest concentration found in *P. oleracea* and *Mentha x piperita* and the highest in *C. melon* (Table 3). In Fe-deficient plants, root Rbfl concentration ranged from 0.01 to 10.2 nmol g^{-1} FW, with *P. oleracea* and *Mentha x piperita* showing the lowest and *P. crispum* the highest concentrations. Root Rbfl concentrations increased with Fe deficiency in roots of *S. oleracea*, *P. crispum*, *C. melo*, *B. vulgaris*, *A. caudatus*, and *A. cepa*; increases ranged from 2- to 6-fold, with the lowest increase found in *C. melo* and the highest in *B. vulgaris*. Root Rbfl concentration did not change significantly with Fe shortage in the remaining nine species. Also, Rbfl derivatives were found in the roots of several species when Fe-deficient: Rbfl-sulphates were found in *S. oleracea*, *B. vulgaris* and *A. caudatus* and an unknown flavin compound was found in *C. melo* (not shown). 7-carboxy-Rbfl, 7-hydroxy-Rbfl, and 7α-hydroxy-Rbfl were not found in any of the species studied (only in *M. truncatula*).

Root FCR activities in plants grown in Fe-sufficient conditions ranged from 0.1 to 0.3 μmol Fe reduced g^{-1} FW h^{-1}, except in *P. crispum*, which had a FCR activity of 0.8 μmol Fe reduced g^{-1} FW h^{-1} (Table 3). In Fe-deficient plants, root FCR activity ranged from 0.1 to 3.0 μmol Fe reduced g^{-1} FW h^{-1}, with *B. officinalis* showing the lowest

activity and *A. cepa* the highest. In all species studied, FCR activities were increased by Fe deficiency, except in *B. officinalis* and *E. californica*, where changes were not statistically significant. Increases in root FCR activity with Fe deficiency ranged from approximately 2- to 14-fold, with *P. oleracea* showing the lowest and *S. armeria* the highest increases.

Root PEPC activity in Fe sufficient plants ranged from 0.02 to 0.51 μmol g^{-1} FW min^{-1}, with *B. officinalis* and *C. officinalis* showing the lowest and *A. caudatus* the highest activities (Table 3). In Fe-deficient roots, PEPC activity ranged from 0.01 to 3.18 μmol g^{-1} FW min^{-1}, with *B. officinalis* showing the lowest and *S. armeria* the highest values. In nine out of the 15 species PEPC activity was increased by Fe deficiency, with increases ranging from 40% (*L. albus*) to 12.4-fold (*S. armeria*). *A. arvensis* and *E. californica* also showed slight (although not significant) activity increases with Fe deficiency, whereas four species, *B. officinalis*, *P. oleracea*, *N. officinale* and *Mentha x piperita*, did not show changes in PEPC activity in response to Fe deficiency.

In summary, upon Fe shortage six species showed increases in root Rbfl concentration (four of them also having Rbfl derivatives) and FCR activity, although they were not among the highest FCR activities measured. Moreover, FCR activity increases in these six species were similar to those found in other species in which root Rbfl concentration did not change with Fe deficiency. Root FCR and PEPC activities and root Rbfl concentration were inversely correlated to leaf Chl concentration (Pearson correlation coefficients (r) of -0.456, -0.336 and -0.324, respectively, $p<0.05$). No significant correlation was found between Rbfl and either PEPC or FCR activities, whereas the later two showed a good correlation between them (r of -0.710, $p<0.05$). A

multivariate statistical analysis (PCA) considering root FW, leaf Chl, root FCR and PEPC activities and root Rbfl concentrations indicated that the 15 plant species can be distributed in three different groups (Fig. 6). All 15 species, when grown in Fe-sufficient, control conditions, are located in the same group in the PCA analysis. This group partially overlaps in the PCA analysis with a second group including eight species showing no increases in Rbfl and none or moderate increases in FCR and PEPC activities. A different group is constituted by only two species, *S. armeria* (a metal hyperaccumulator) and *A. cepa*, which showed the largest increases in FCR and PEPC activities when Fe-deficient. It is remarkable that *A. cepa*, the only monocotyledonous species studied, also showed increases in Rbfl with Fe deficiency. The other five species which show an increased concentration of Rbfl and/or the occurrence of Rbfl derivatives in the roots when grown in Fe-deficient conditions belonged to a separated group in the PCA analysis.

Discussion

In the present study, we found, using high resolution MS techniques, that three flavin derivatives, 7-hydroxy-Rbfl, 7α-hydroxy-Rbfl and 7-carboxy-Rbfl, were produced along with Rbfl in Fe-deficient *M. truncatula* roots. Flavins were preferentially accumulated in the roots of plants grown at pH 7.7 (in the presence of $CaCO_3$) and partially exported to the solution when plants were grown at pH 5.5 (in the absence of $CaCO_3$). None of these three flavins has been previously reported to occur in plants. The most abundant one was 7-hydroxy-Rbfl, accounting for 4-16% of the total flavins in the roots and for approximately 70% of the total flavins in the nutrient solution. This is the first time that a hydroxylated Rbfl derivative has been reported to be the major flavin compound released by roots upon Fe deficiency. The two other flavins annotated,

7α-hydroxy-Rbfl and 7-carboxy-Rbfl, were less abundant but also occurred in both Fe deficiency treatments. These two minor flavins are the main catabolic Rbfl derivatives in animal urine (Chastain and McCormick 1986; Ohkawa et al. 1983a, b). Up to now, only Rbfl and two other derivatives, 5' and 3'-Rbfl-sulphates, had been described to occur in roots in response to Fe deficiency in Strategy I plant species (Susín et al. 1993; Welkie and Miller 1993).

Two lines of evidence, i.e., the localization and time-course development of the different responses studied, suggest that flavin accumulation in *M. truncatula* roots is more closely related to FCR activity than to proton extrusion activity. First, the highest concentration of flavins occurred in the cortex and epidermal cells of the near the apex root region, the same zone where the FCR activity was located, whereas proton extrusion occurred along the whole root length. Another root region, the sub-apical zone, also contained some flavins in the cortex cells, but showed no FCR activity. Second, the time-course appearance of the responses upon Fe shortage showed that FCR and flavin accumulation were only marked after 3 d, whereas proton extrusion reached high values more rapidly, as early as 1 d after treatment onset. In a previous study with Fe-deficient *M. truncatula*, the increase in the expression of *MtHA1* was found to precede those of *MtFRO* and *MtDMRLs*, with proton extrusion also preceding FCR activity and flavin accumulation (Andaluz et al. 2009). A similar, near the root apex localization of flavins has previously been shown in other species, such as *Nicotiana tabacum* (Welkie and Miller 1960) and *B. vulgaris* (Susín et al. 1993). Flavin accumulation and root hair development seem to be regulated separately in *M. truncatula*, because root hairs were located in a region that only had low flavin contents and little FCR activity. However, in *B. vulgaris* the near the apex root region is the one

that develops root hairs, and also shows high flavin contents and FCR activity. Since the apical root region is involved in nutrient uptake and rizhosphere exploration, a role of flavins in Fe-uptake and/or Fe-sensing processes is likely. Flavin accumulation in the roots has been suggested to have a direct role in FCR activity, either as a cofactor for the enzyme or facilitating electron flow for its activity (González-Vallejo et al. 1998; Higa et al. 2010; López-Millán et al. 2000). Also, the accumulation of flavin compounds with a higher solubility than that of Rbfl may facilitate an electron bridge from cell sources (*e.g.*, mitochondria) to the FCR in the plasma membrane.

Although it may be possible that microbial degradation of Rbfl during the 6 d treatment period may result in the occurrence of 7-hydroxy-Rbfl and related compounds, it must be taken into account that these flavins already occur in the *M. truncatula* root itself, and also that none of them (not even traces) were found in roots and exudates of any of the other species studied. Furthermore, 7-hydroxy-Rbfl and related compounds were not found in *B. vulgaris* roots and nutrient solutions (Susín et al. 1993; 1994).

In the experiment involving 15 different plant species grown under Fe deficiency in the presence of $CaCO_3$, all species accumulating flavins showed increases in FCR activity. However, flavin accumulation was not closely correlated to the induction of FCR and PEPC root activities in the species studied, supporting that flavin accumulation is a relatively common component, but not a mandatory part, of the Strategy I response. The absence of a strict correlation is not surprising, since FCR is strictly localized in the root plasma membrane whereas flavin accumulation may be a much more complex phenomenon, involving production in the cytoplasm, as well as export to the vacuole and the rhizosphere. On the other hand, the existence of a strong

correlation between the root PEPC and FCR activities in the different species studied confirms that PEPC plays a key role in the Fe-deficiency Strategy I response (López-Millán et al. 2000; Zocchi 2006). Data from this and previous studies reporting the presence of flavin compounds in different Fe-deficient plant species are summarized in Fig. 7. Flavins have been shown so far to occur in plant roots or nutrient solutions in 29 species from 8 families, whereas they were absent in 37 species from 13 families. In four families, flavins occurred in certain species whereas in others they were absent, confirming previous reports (Welkie 2000): for instance, in the Fabaceae family flavins occur in *M. truncatula* but not in *L. albus*. The presence of some Rbfl derivatives appears to be restricted to certain families: Rbfl-sulphates have been found only several species of the Amaranthaceae family, hydroxylate Rbfl-derivatives have been found only in *M. truncatula* (Fabaceae family) and a different, still unidentified Rbfl-derivative occurs in two species (*C. melo* in this work and *C. sativus* -G. Zocchi, personal communication-) in the Curcubitaceae family. The fact that no flavins have been reported so far in Fe-deficient plants of the Brassicaceae family, including the common model species *A. thaliana*, may hinder the study of flavin accumulation and export mechanisms. *Medicago truncatula* can be used as a model species to elucidate the role of flavin accumulation and export in Strategy I Fe-deficiency studies.

It is not surprising that Rbfl-derivatives could have been undetected in earlier studies on accumulated and exported flavins. In most of the previous studies on Fe deficiency that have reported the presence of flavin-type compounds in the roots (Nagarajah and Ulrich 1966; Pound and Welkie 1958; Weinstein et al. 1954; Welkie and Miller 1993) or nutrient solutions (Higa et al. 2010; Welkie 2000), the identification of flavins was only made by comparison of the UV-VIS spectrum of the total root extract and/or

growth media with that of Rbfl, which are practically indistinguishable. In future studies on Fe deficiency, the real identity of the flavins present in plants and/or nutrient solution must be ascertained using technologies such as HPLC-MS or others.

The presence of $CaCO_3$ in the nutrient solution affects markedly the allocation of Rbfl (Rodríguez-Celma et al. 2011) and Rbfl-derivatives (this work) in Fe-deficient *M. truncatula*, as it also occurs in sugar beet (Susín et al. 1994; Susín et al. 1993). This treatment does not cause major change in the availability of other nutrients (López-Millán et al. 2001). In both plant species flavin root accumulation is highly favoured at pH 7.7 (when $CaCO_3$ is present), whereas flavins are preferentially exported to the nutrient solution at pH 5.5 (when $CaCO_3$ is absent; this is a non-buffered solution and pH changes from the initial value of 5.5 to 4 or lower). Also, at pH 5.5 flavin production was rapid, starting at 1 d after treatment onset. The presence of $CaCO_3$ seems to delay temporarily the synthesis of flavins in *M. truncatula*, but in the long term flavins are accumulated in the roots and partially exported. Although Fe deficiency is commonly associated with high pH soils, the H^+-ATPase-mediated proton extrusion to the rhizosphere may facilitate flavin export, allowing a possible role for flavins related to their presence in the rhizosphere near FCR activity zones. Taken overall, results found support the existence of a still unidentified, pH-dependent PM transporter mediating the export of flavins to the nutrient solution.

The presence of highly soluble Rbfl derivatives (hydroxy-Rbfl in *M. truncatula*, Rbfl-sulphates in the Amaranthaceae family, and an unknown derivative found in the Cucurbitaceae family) in the roots and nutrient solutions of Fe-deficient plants may also suggest an extracellular role of flavins in Fe deficiency. The solubility of these derivatives is one or two orders of magnitude higher than that of Rbfl. For instance,

Rbfl-sulphates can be in the mM range, whereas Rbfl has a maximum solubility of approximately 140 μM (Susín et al. 1994). Flavin concentrations near the *M. truncatula* roots could have reached the μM range or higher if nutrient solution movement had been restricted. It has been hypothesized that highly soluble flavin compounds could be present in the rhizosphere in concentrations high enough to play a direct role in extracellular Fe reduction (González-Vallejo et al. 1998), as recently shown in the microorganism *Shewanella* (von Canstein et al. 2008), and/or be involved in other indirect processes that increase soil Fe availability by, for instance, modifying the rhizosphere microbiome (Jordan et al. 1992; Susín et al. 1993; Yang et al. 2002). Flavins are also able to chelate Fe(II) and other metals (Albert 1953) by a mechanism possibly involving the isoalloxacine moiety of the molecule. However, there is no published evidence in plants for any of such mechanisms.

Materials and Methods

Plant material

Medicago truncatula cv. 'Jemalong' plants were grown in a controlled environment chamber with a photosynthetic photon flux density at leaf height of 350 μmol m^{-2} s^{-2} photosynthetically active radiation, 80% relative humidity (RH) and at a 16 h-23°C/8 h-19°C, day/night regime (Rodríguez-Celma et al. 2011). Seeds were scarified by nicking the seed coat, then imbibed overnight in distilled water and germinated on filter paper for three days in darkness and at 100% RH. Seedlings were grown for an additional two-week period in half-strength Hoagland nutrient solution (pH 5.5) with 45 μM Fe (III)-EDTA. Plants were then transplanted to 10 L plastic buckets (six plants per bucket) containing half-strength Hoagland nutrient solution and treatments were imposed. Control (Fe-sufficient, +Fe) plants were grown with 45 μM Fe(III)-EDTA (pH 5.5) and

Fe-deficient plants were grown with no added Fe (0 μM Fe) with (pH 7.7; -Fe + $CaCO_3$) or without (pH 5.5; -Fe) 1 g L^{-1} $CaCO_3$ for one, three and six days.

Other species of horticultural interest belonging to a wide spectrum of plant families were also grown in the growth chamber in the conditions described above. Species used included *Borago officinalis* L. (borage), *Eschscholzia californica* (california poppy), *Portulaca oleracea* (purslane), *Spinacia oleracea* L. (spinach), *Nasturtium officinale* (watercress), *Petroselinum crispum* (parsley), *Calendula officinalis* (marigold), *Cucumis melo* (melon), *Anthemis arvensis* (camomile), *Beta vulgaris* ssp. cicla 'Witerbi Mangold' (swiss chard), *Mentha x piperita* (mint), *Lupinus albus* (white lupin), *Amaranthus caudatus* (amaranth), *Allium cepa* (onion) and *Silene armeria* (catchfly). Commercial seeds were germinated in vermiculite for two to three weeks and then transferred to half strength Hoagland nutrient solution (10 plants of a given species per 10 L plastic buckets) for two more weeks. After this time, four plants of each species were transferred to 4 L plastic buckets containing nutrient solution with 0 (Fe-deficient; -Fe + $CaCO_3$) or 45 μM Fe(III)-EDTA (Fe-sufficient; +Fe). The pH of the Fe-free nutrient solution was buffered at approximately 7.7 by adding 1 mM NaOH and 1 g L^{-1} of $CaCO_3$. Plants were sampled or used in the different analyses 10 days after treatment onset.

Root sampling and flavin extraction

Roots of all species were excised with a razor blade approximately 15-20 mm from the root apex, frozen in liquid N_2 and stored at -80ºC until analysis. For extraction of flavin-type compounds, frozen roots (*ca.* 100 mg) were ground in liquid N_2 using a Retsch M301 mill (Retsch GmbH, Haan, Germany) with 250 μL of 1 mM ammonium acetate, pH 6.0, containing 5% methanol. Extracts were filtered through PVDF 0.45 μm

ultrafree-MC centrifugal filter devices (Millipore, Billerica, MA, USA) and stored at -80ºC until analysis.

To study the spatial localization of flavins along *M. truncatula* roots, root sections were excised with a razor blade at 1, 3 and 6 d after the onset of Fe-deficiency treatments (root pictures are shown in Supplementary Fig. S1). At 1 d only the apical zone (0-5 mm), containing root hairs, was sampled. At 3 d, two zones were sampled, a smooth apical one (0-5 mm from the apex) and a second sub-apical one containing root hairs (6-12 mm from the apex). Finally, at 6 d, two zones were sampled, a smooth apical one (0-10 mm from the apex) and a second sub-apical one containing root hairs (11-20 mm from the apex) (see Supplementary Fig. S1D). Root sections were immediately frozen in liquid N_2 and stored at -80ºC. Flavin extraction was carried out as indicated above.

Flavin extraction from nutrient solutions

Nutrient solutions of *M. truncatula* plants were collected 6 d after the onset of the Fe-deficiency treatments. Flavins were concentrated from the filtered nutrient solutions (500 mL, PVDF 0.45 µm membrane filters) using SepPack C_{18} cartridges (Waters, Milford, MA, USA), and then eluted with 2 mL of 100% methanol and stored at -80º until analysis.

Flavin analysis by HPLC/Vis/ESI-MS(TOF)

All eluents, buffers and standard solutions were prepared with type I water (Milli-Q Synthesis, Millipore, Bedford, MA, USA). Ammonium acetate (99.99%, Sigma), Li hydroxide monohydrate (99.995%, Aldrich), formic acid (50%, Fluka), and methanol

(LC-MS grade, Riedel-de-Haën) were purchased from Sigma-Aldrich (St. Louis, MO, USA).

High-performance liquid chromatography was carried out with a Waters Alliance 2795 HPLC system (Waters) equipped with on-line degasser, auto-sampler module and column oven. The column used was an analytical HPLC column (Symmetry® C18, 15 cm x 2.1 mm i.d., 3.5 µm spherical particle size, Waters) protected by a guard column (Symmetry® C18, 10 mm x 2.1 mm i.d., 3.5 µm spherical particle size, Waters). Autosampler and column temperatures were 6 and 30 ºC, respectively. Injection volume was 50 µL and flow rate was 100 µL min^{-1}. The mobile phase was built using three solvents: type I water (A), methanol (B) and 20 mM ammonium acetate in type I water, pH 6.0 (C). The pH was maintained at 6.0 by pumping 5% of solvent C during the chromatographic run. For separation of the flavins, a linear gradient from 5 to 50% B (0–35 min) was used. Then, to wash the column, the concentration of B was increased linearly from 50 to 95% from min 35 to 38, and this solvent composition was maintained until min 58. Finally, to regenerate the column, the solvent was changed linearly to 5% B until min 60 and then was maintained at 5% B until min 80, when a new sample could be injected.

Flavin compounds were detected by coupling the HPLC to a photodiode array detector (PDA 2996 from Waters). UV-VIS absorption spectra were recorded from 200 to 600 nm. Riboflavin was identified by comparison of the retention time and the UV-Vis spectra with those of a standard (purity ≥98%, SIGMA, Saint Louis, Missouri, USA). All flavins were quantified using a Rbfl calibration curve (peak areas at 445 nm). The exit flow from the PDA 2996 was connected to the ESI source (125 µm i.d. PEEK tubing; Upchurch Scientific, Oak Harbor, WA, USA) of a time-of-flight mass

spectrometer [MS(TOF); micrOTOF, Bruker Daltonics, Bremen, Germany]. The ESI-MS(TOF) operating conditions were optimized by direct injection of 10 μM solutions of Rbfl, FAD and FMN standards. Mass spectra were acquired in the *m/z* 50–1000 range in negative and positive ionization mode. In negative ion mode, settings were -500, 3000 and -135.6 V of endplate, spray tip and orifice voltages, respectively. In positive ion mode, settings were -500, 4500 and 167.8 V of endplate, spray tip and orifice voltages, respectively. The nebulizer gas (N_2) pressure, drying gas (N_2) flow rate and drying gas temperature were 1.6 bar, 8.0 L min^{-1} and 180 °C, respectively. The mass axis was calibrated externally and internally using Li-formate adducts [10 mM LiOH, 0.2% (v/v) formic acid and 50% (v/v) 2-propanol]. The internal mass axis calibration was carried out by introducing the Li-formate adducts solution with a divert valve at min 2 and 37 in each HPLC run. Bruker Daltonik software packages micrOTOF Control v.2.2, HyStar v.3.2 and Data Analysis v.4.0 were used to control the ESI-MS(TOF) apparatus, interface the HPLC with the MS system and process data, respectively. Molecular formulae were assigned based on (i) exact molecular mass, with errors < 2 ppm, and (ii) the SigmaFit™ algorithm (Ojanperä et al. 2006), with a threshold tolerance value of 0.04. SigmaFit™ provides a numerical comparison of theoretical and measured isotopic patterns, with smaller values indicating a closer match between them.

Flavin analysis by HPLC/ESI-CID-MS^2(QTOF)

HPLC/ESI-CID-MS^2(QTOF) analysis was carried out with an 1100 HPLC system (Agilent Technologies) coupled to a quadrupole time of flight (QTOF) equipped with an ESI source (microTOF-Q, Bruker Daltonik). The HPLC conditions were the same as those described in the previous section. The ESI-CID-MS^2(QTOF) operating conditions were optimized in order to maximize product ion signals using direct injections of a 10

μM solution of Rbfl. ESI-CID-MS^2(QTOF) analysis was carried out in positive and negative ion mode, with capillary and endplate offset voltages of 4500 and -500 V in positive mode, and 4000 and -500 V in negative mode, using Ar as collision gas. Optimal collision cell energies of 10 and -10 eV were used for positive and negative mode, respectively, with an isolation width for the precursor ion of 4 *m/z* units for FC1 and FC3 ions, and 2 *m/z* units for FC2 and Rbfl due to their close *m/z* values (379.12/377.11 and 377.15/375.13 in positive and negative mode, respectively). To allow coupling with the HPLC system, the nebulizer (N_2) gas pressure and the drying (N_2) gas flow rate were 1.6 bar and 8.0 L min^{-1}, respectively. Spectra were acquired in the *m/z* 50–1200 range. The mass axis was calibrated externally and internally using Li-formate adducts as described above. Bruker Daltonik software packages micrOTOF Control v.2.3, HyStar v.3.2 and Data Analysis v.4.0 were used to control the MS(QTOF) apparatus, interface the HPLC with the MS system and process data, respectively. Product ions were identified using the Smart Formula and Smart Formula 3D™ tools of the Data Analysis software, using mass accuracy and SigmaFit™ criteria.

Quantum chemistry calculations

Density-Functional Theory (DFT) calculations were carried out with the Gaussian 09 software (Gaussian 09 revision A.2, Gaussian Inc., Wallingford CT, 2009). Molecular geometries in aqueous solution were optimized using the hybrid B3LYP functional (Becke 1993) and the 6-31+G** basis set (Francl et al. 1982). Solvent effects were included using the SMD Model (Marenich et al. 2009). Vertical electronic excitation energies were computed by using the time-dependent DFT approach (TDDFT) (Casida 1995; Gross and Kohn 1990; Gross et al. 1995; Runge and Gross 1984) and the SMD-B3LYP/6-311+G** model chemistry on optimized geometries. The default Gaussian 09

parameters were used in every case. Molecular orbital contours for the highest occupied molecular orbital (HOMO) and lowest unoccupied molecular orbital (LUMO) were plotted with Molekel 5.4 (Varetto, U. Swiss National Supercomputing Centre, Manno, Switzerland).

Three-dimensional root fluorescence measurements

Roots of Fe-deficient *M. truncatula* plants, grown in the -Fe and -Fe+$CaCO_3$ treatments for 1, 3 and 6 d, were excised with a razor blade and embedded in 5% agar. The root sections sampled were from the root apex to approximately 5–6, 10–12 and 15–20 mm for Fe-deficient plants at 1, 3 and 6 d after treatment onset, respectively. Then, consecutive 70 µm-thick transversal root slices were obtained from the root sections using a vibrating blade microtome (VT1000 S, Leica Microsystems GmbH, Wetzlar, Germany). Flavins have a green fluorescence when excited with blue light both *in vitro* and also *in vivo* in plant roots (Susín et al. 1994; Susín et al. 1993). Fluorescence images of the root transversal slices (2592 x 1994 pixels; *x*- and *y*-axis resolution of 360 x 270 µm) were taken at 200x magnification with an inverted microscope (DM IL LED, Leica Microsystems GmbH) equipped with a fluorescence kit (340-380 excitation wavelength and 425 nm cut off filter; A1 filter cube, Leica Microsystems GmbH) and a CCD camera (DFC 240C, Leica Microsystems GmbH). Only one of every two 70 µm-slices was analysed, and therefore the effective resolution of the fluorescence analysis in the *z*-axis was 140 µm. Depending on the length of the root sections, 27-82 root slices were analysed per sample. Fluorescence signal quantification was carried out with imaging processing and analysis software (ImageJ, Wright Cell Imaging Facility; http://www.uhnresearch.ca/facilities/wcif).

Localization of acidification and Fe reducing activity in *M. truncatula* roots

M. truncatula root acidification and Fe reduction assays were carried out in agar in Petri dishes. Whole roots were excised, rinsed in type I water, blotted dry and then immersed in 0.6% pH 6.0 agar plates containing 500 μM $CaSO_4$, and either 200 μM Fe(III)-EDTA and 100 μM BPDS for the Fe reductase assay or 0.0025% bromocresol purple for the root acidification-assay. Roots were kept in the reaction media for two hours in the dark and at 4ºC.

Chlorophyll determination

For chlorophyll determination, disks were taken from fully expanded leaves from plants illuminated for 2-3 h and then frozen in liquid N_2. Chlorophylls were extracted with 100% acetone in the presence of Na ascorbate, and extracts were analysed spectrophotometrically (Abadía and Abadía 1993). Samples from 3 plants per treatment were taken for pigment quantifications.

FCR and phospho*enol*pyruvate carboxylase activities in horticultural species

In all species, except *M. truncatula*, Fe(III) reductase (FCR) activity was determined 2-3 h after light onset in whole root systems of intact plants by following the formation of the Fe(II)-$BPDS_3$ complex from Fe(III)-EDTA at 535 nm for 60 min, as described in Andaluz et al. (2009). The experiment was run with one batch of plants and 3 plants per treatment were taken for activity measurements.

Phospho*enol*pyruvate carboxylase (PEPC; EC 4.1.1.31) activity determination was carried out with approximately 50 mg FW of the root material was ground in liquid N_2 to powder in a Retsch M301 mill (Retsch GmbH, Haan, Germany), and then homogenized in 0.5 mL of extraction buffer containing 30 mM sorbitol, 1% BSA and

1% PVP in 100 mM HEPES-KOH, pH 8.0. The homogenate was centrifuged for 15 min at 10000 g and 4°C, and the supernatant was collected and analysed immediately. PEPC activity was determined in a coupled enzymatic assay with malate dehydrogenase in a final volume of 1 mL of the reaction buffer (López-Millán et al. 2000). The experiment was run in one batch of plants, and 3 plants per treatment were taken for activity measurements. Univariate and multivariate statistical analyses were carried out. Differences between treatments were defined using a Student t-test ($p < 0.10$). Principal Component Analysis (PCA) was applied to the whole dataset using SPSS v. 15 (SPSS Inc, Chicago, USA).

Funding

This work was supported by the Spanish Ministry of Science and Innovation (MICINN; projects AGL2009-09018, AGL2010-16515 and CTQ2008-02942 co-financed with FEDER), the trilateral Project Hot Iron (ERA- NET Plant Genome Research KKBE; MICINN EUI2008-03618), and the Aragón Government (groups A03 and E39). J.R-C was supported by an I3P-CSIC predoctoral fellowship and S V-R by a postdoctoral contract JAE-CSIC.

Acknowledgements

The authors thank Katie M. Zak and A. Calviño for assistance in growing and harvesting plants.

References

Abadía, J. and Abadía, A. (1993) Iron and plant pigments. In *Iron chelation in plants and soil microorganisms* Edited by Barton, L.L. and Hemming, B.C. pp. 327-343. Academic, San Diego.

Abadía, J., López-Millán, A.-F., Rombolà, A. and Abadía, A. (2002) Organic acids and Fe deficiency: a review. *Plant Soil* 241: 75-86.

Abadía, J., Vázquez, S., Rellán-Álvarez, R., El-Jendoubi, H., Abadía, A., Álvarez-Fernández, A. and López-Millán, A.F. (2011) Towards a knowledge-based correction of iron chlorosis. *Plant Physiol. Biochem.* 49: 471-482.

Albert, A. (1953) Quantitative studies of the avidity of naturally occurring substances for trace metals. III. Pteridines, riboflavin and purines. *Biochem. J.* 54: 646-654.

Andaluz, S., Rodriguez-Celma, J., Abadia, A., Abadia, J. and Lopez-Millan, A.F. (2009) Time course induction of several key enzymes in *Medicago truncatula* roots in response to Fe deficiency. *Plant Physiol. Biochem.* 47: 1082-1088.

Becke, A.D. (1993) Density-functional thermochemistry. III. The role of exact exchange. *J. Chem. Physics* 98: 5648-5652.

Benedito, V.A., Torres-Jerez, I., Murray, J.D., Andriankaja, A., Allen, S., et al. (2008) A gene expression atlas of the model legume *Medicago truncatula*. *Plant J.* 55: 504-513.

Casida, M.E. (1995) In *Recent Advances in Density Functional Methods, Part I*. Edited by Chong, D.P. World Scientific, Singapore.

Cesco, S., Neumann, G., Tomasi, N., Pinton, R. and Weisskopf, L. (2010) Release of plant-borne flavonoids into the rhizosphere and their role in plant nutrition. *Plant Soil* 329: 1-25.

Colditz, F. and Braun, H.P. (2010) *Medicago truncatula* proteomics. *J. Proteomics*.

Chastain, J.L. and McCormick, D.B. (1986) Quantitation of products from riboflavin in rat urine. *Fed. Am. Soc. Exp. Biol.* 45: 825-829.

Francl, M.M., Pietro, W.J., Hehre, W.J., Binkley, J.S., Gordon, M.S., DeFrees, D.J. and Pople, J.A. (1982) Self-consistent molecular orbital methods. XXIII. A polarization-type basis set for second-row elements. *J. Chem. Physics* 77: 3654-3665.

Frolich, E. and Wallace, A. (1966) Flavin excretion by roots of iron-deficient tobacco. In *Current topics in plant nutrition*. Edited by Wallace, A. pp. 10-11. Wallace Publ., Los Angeles.

González-Vallejo, E.B., Susín, S., Abadía, A. and Abadía, J. (1998) Changes in sugar beet leaf plasma membrane Fe(III)-chelate reductase activities mediated by Fe deficiency, assay buffer composition, anaerobiosis and the presence of flavins. *Protoplasma* 205: 163-168

Gross, E.K.U. and Kohn, W. (1990) Time-Dependent Density-Functional Theory. In *Advances in Quantum Chemistry*. Edited by Per-Olov, L. pp. 255-291. Academic Press.
Gross, E.K.U., Ullrich, C.A. and Gossman, U.J. (1995) *Density Functional Theory*. Plenum Press, New York.

Hall, B. and Guerinot, M. (2006) The role of ZIP family members in iron transport. In *Iron Nutrition in Plants and Rhizospheric Microorganisms*. Edited by Barton, L.L. and Abadia, J. pp. 311-326. Springer Netherlands.

Higa, A., Mori, Y. and Kitamura, Y. (2010) Iron deficiency induces changes in riboflavin secretion and the mitochondrial electron transport chain in hairy roots of *Hyoscyamus albus*. *J. Plant Physiol.* 167: 870-878.

Ishimaru, Y., Kakei, Y., Shimo, H., Bashir, K., Sato, Y., Sato, Y., Uozumi, N., Nakanishi, H. and Nishizawa, N.K. (2011) A rice phenolic efflux transporter is essential for solubilizing precipitated apoplasmic iron in the plant stele. *J. Biol. Chem*.

Jin, C.W., You, G.Y., He, Y.F., Tang, C., Wu, P. and Zheng, S.J. (2007) Iron deficiency-induced secretion of phenolics facilitates the reutilization of root apoplastic iron in red clover. *Plant Physiol.* 144: 278-285.

Jordan, C.M., Wakeman, R.J. and DeVay, J.E. (1992) Toxicity of free riboflavin and methionine–riboflavin solutions to *Phytophthora infestans* and the reduction of potato late blight disease. *Can. J. Microbiol.* 38: 1108-1111.

Lindsay, W.L. and Schwab, A.P. (1982) The chemistry of iron in soils and its availability to plants. *J. Plant Nutr.* 5: 821-840.

López-Millán, A.F., Morales, F., Andaluz, S., Gogorcena, Y., Abadía, A., De Las Rivas, J. and Abadía, J. (2000) Responses of sugar beet roots to iron deficiency. Changes in carbon assimilation and oxygen use. *Plant Physiol.* 124: 885-898.

López-Millán, A. F., Morales, F., Abadía, A. and Abadía, J. (2001) Changes induced by Fe deficiency and Fe resupply in the organic acid metabolism of sugar beet (*Beta vulgaris*) leaves. *Physiologia Plantarum* 112: 31-38.

López-Millán, A.F., Morales, F., Gogorcena, Y., Abadía, A. and Abadía, J. (2009) Metabolic responses in iron deficient tomato plants. *J. Plant Physiol.* 166: 375-384.

Marenich, A.V., Cramer, C.J. and Truhlar, D.G. (2009) Universal solvation model based on solute electron density and on a continuum model of the solvent defined by the bulk dielectric constant and atomic surface tensions. *J. Phys. Chem. B* 113: 6378-6396.

Massey, V. (2000) The chemical and biological versatility of riboflavin. *Biochem. Soc. Trans.* 28: 283-296.

Mukherjee, I., Campbell, N.H., Ash, J.S. and Connolly, E.L. (2006) Expression profiling of the Arabidopsis ferric chelate reductase (FRO) gene family reveals differential regulation by iron and copper. *Planta* 223: 1178-1190.

Nagarajah, S. and Ulrich, A. (1966) Iron nutrition of the sugar beet plant in relation to growth, mineral balance, and riboflavin formation. *Soil Science* 102: 399-407.

Ohkawa, H., Ohishi, N. and Yagi, K. (1983a) Hydroxylation of the 7- and 8-methyl groups of riboflavin by the microsomal electron transfer system of rat liver. *J. Biol. Chem.* 258: 5629-5633.

Ohkawa, H., Ohishi, N. and Yagi, K. (1983b) New metabolites of riboflavin appeared in rat urine. *Biochem. Int.* 6: 239-247.

Ohwaki, Y. and Sugahara, K. (1997) Active extrusion of protons and exudation of carboxylic acids in response to iron deficiency by roots of chickpea (Cicer arietinum L.). *Plant Soil* 189: 49-55.

Ojanperä, S., Pelander, A., Pelzing, M., Krebs, I., Vuori, E. and Ojanperä, I. (2006) Isotopic pattern and accurate mass determination in urine drug screening by liquid chromatography/time-of-flight mass spectrometry. *Rapid Commun. Mass Spectrom.* 20: 1161-1167.

Pound, G.S. and Welkie, G.W. (1958) Iron nutrition of *Nicotiana tabacum L.* in relation to multiplication of tobacco mosaic virus. *Virology* 5: 371-381.

Rodríguez-Celma, J., Lattanzio, G., Grusak, M.A., Abadía, A., Abadía, J. and López-Millán, A.F. (2011) Root responses of *Medicago truncatula* plants grown in two different Iron deficiency conditions: changes in root protein profile and riboflavin biosynthesis. *J. Proteome Res.* 10: 2590-2601.

Runge, E. and Gross, E.K.U. (1984) Density-Functional Theory for time-dependent systems. *Phys. Rev. Letters* 52: 997.

Santi, S. and Schmidt, W. (2009) Dissecting iron deficiency-induced proton extrusion in *Arabidopsis* roots. *New Phytol.* 183: 1072-1084.

Schmidt, W. (1999) Mechanisms and regulation of reduction-based iron uptake in plants. *New Phytol.* 141: 1-26.

Stenchuk, N.N., Kutsiaba, V.I., Kshanovskaia, B.V. and Fedorovich, D.V. (2001) Effect of *rib83* mutation on riboflavin biosynthesis and iron assimilation in *Pichia guilliermondii*. *Mikrobiologiia* 70: 753-758.

Susín, S., Abián, J., Peleato, M., Sánchez-Baeza, F., Abadía, A., Gelpi, E. and Abadía, J. (1994) Flavin excretion from roots of iron-deficient sugar beet (*Beta vulgaris L.*). *Planta* 193: 514-519.

Susín, S., Abián, J., Sánchez-Baeza, F., Peleato, M.L., Abadía, A., Gelpi, E. and Abadía, J. (1993) Riboflavin 3'- and 5'-sulfate, two novel flavins accumulating in the roots of iron-deficient sugar beet (*Beta vulgaris*). *J. Biol. Chem.* 268: 20958-20965.

von Canstein, H., Ogawa, J., Shimizu, S. and Lloyd, J.R. (2008) Secretion of flavins by Shewanella species and their role in extracellular electron transfer. *Appl. Environ. Microbiol.* 74: 615-623.

Wallace, A. (1971) Root excretion in tobacco plants and possible implications in the iron nutrition of higher plants. In *Regulation of the Micronutrient Status of Plants by Chelating Agents and Other Factors*. Edited by Wallace, A. pp. 136-139. Wallace Publ., Los Angeles.

Weinstein, L.H., Robbins, W.R. and Perkins, H.F. (1954) Chelating Agents and Plant Nutrition. *Science* 120: 41-43.

Welkie, G.W. (2000) Taxonomic distribution of dicotyledonous species capable of root excretion of riboflavin under iron deficiency. *J. Plant Nutr.* 23: 1819 - 1831.

Welkie, G.W. and Miller, G.W. (1960) Iron nutrition of *Nicotiana tabacum L.* in relation to riboflavin, riboflavin-5-phosphate, and flavin adenine dinucleotide content. *Plant Physiol.* 35: 516-520.

Welkie, G.W. and Miller, G.W. (1993) *Plant iron uptake physiology by nonsiderophore systems*. Academic PressSan Diego (USA).

Worst, D.J., Gerrits, M.M., Vandenbroucke-Grauls, C.M. and Kusters, J.G. (1998) *Helicobacter pylori* ribBA-mediated riboflavin production is involved in iron acquisition. *J. Bacteriol.* 180: 1473-1479.

Yang, G., Bhuvaneswari, T.V., Joseph, C.M., King, M.D. and Phillips, D.A. (2002) Roles for riboflavin in the Sinorhizobium-alfalfa association. *Mol. Plant Microbe Interact.* 15: 456-462.

Zocchi, G. (2006) Metabolic changes in iron-stressed dicotyledonous plants. In *Iron Nutrition in Plants and Rhizospheric Microorganisms*. Edited by Barton, L.L. and Abadía, J. pp. 359-370. Eds. Springer.

Table 1. Ions found (in positive and negative mode) in the ESI-MS(TOF) and ESI-MS(QTOF) spectra of flavins present in roots of Fe-deficient *Medicago truncatula*. Measured and calculated mass-to-charge ratios (*m/z*), mass errors, SigmaFit™ values and elemental formulae are given for both parent and product ions. SigmaFit™ is an algorithm that provides a numerical comparison of theoretical and measured isotopic patterns.

Compound	Ionization Mode	Parent ion formula	Measured *m/z*	Calculated *m/z*	Error mDa	SigmaFit™	Product ion formula	Neutral Loss	Measured *m/z*	Calculated *m/z*	Error mDa	SigmaFit™
Riboflavin	Negative	$C_{17}H_{19}N_4O_6$	375.1315	375.131	-0.5	0.007	$C_{13}H_{11}N_4O_2$	$C_4H_8O_4$	255.0888	255.0887	0	0.03
							$C_{12}H_9N_4O_2$	$C_5H_{10}O_4$	241.0735	241.0731	-0.4	0.017
							$C_{12}H_{10}N_3O$	$C_5H_9NO_5$	212.0831	212.0829	-0.2	0.018
	Positive	$C_{17}H_{21}N_4O_6$	377.1466	377.1456	-1	0.011	$C_{12}H_{11}N_4O_2$	$C_5H_{10}O_4$	243.0876	243.0877	0	0.012
							$C_{11}H_{10}N_3O_2$	$C_6H_{11}NO_4$	216.0774	216.0768	-0.7	0.024
							$C_{11}H_8N_3O$	$C_6H_{13}NO_5$	198.0678	198.0662	-1.6	0.126
							$C_{10}H_{10}N_3$	$C_7H_{11}NO_6$	172.0890	172.0869	-2.1	0.019
FC1	Negative	$C_{17}H_{17}N_4O_8$	405.0959	405.1052	0.5	0.035	$C_{13}H_9N_4O_4$	$C_4H_8O_4$	285.0651	285.0629	-2.2	0.09
							$C_{12}H_9N_4O_2$	$C_5H_8O_6$	241.0750	241.0731	-1.9	0.011
							$C_{11}H_8N_3O$	$C_6H_9NO_7$	198.0681	198.0673	-0.8	0.769
	Positive	$C_{17}H_{19}N_4O_8$	407.1216	407.1197	-1.9	0.031						
FC2	Negative	$C_{16}H_{17}N_4O_7$	377.111	377.1103	-0.7	0.007	$C_{16}H_{15}N_4O_6$	H_2O	359.1003	359.0997	-0.6	0.109
							$C_{12}H_9N_4O_3$	$C_4H_8O_4$	257.0685	257.068	-0.5	0.066
							$C_{11}H_7N_4O_3$	$C_5H_{10}O_4$	243.0536	243.0524	-1.2	0.077
							$C_{11}H_8N_3O_2$	$C_5H_9NO_5$	214.0628	214.0622	-0.6	0.76
	Positive	$C_{16}H_{19}N_4O_7$	379.1243	379.1248	0.5	0.007	$C_{11}H_9N_4O_3$	$C_5H_{10}O_4$	245.0671	245.0669	-0.2	0.077
							$C_{10}H_8N_3O_3$	$C_6H_{11}NO_4$	218.0561	218.056	-0.1	0.069
							$C_{10}H_6N_3O_2$	$C_6H_{13}NO_5$	200.0408	200.0455	4.7	n.a.
							$C_9H_8N_3O$	$C_7H_{11}NO_6$	174.0678	174.0662	-1.6	0.771
FC3	Negative	$C_{17}H_{19}N_4O_7$	391.1274	391.1259	-1.5	0.015	$C_{13}H_{11}N_4O_3$	$C_4H_8O_4$	271.0863	271.0837	-2.6	0.09
	Positive	$C_{17}H_{21}N_4O_7$	393.1398	393.1404	0.6	0.002	$C_{12}H_{11}N_4O_3$	$C_5H_{10}O_4$	259.0838	259.0826	-1.3	0.009
							$C_{11}H_{10}N_3O_3$	$C_6H_{11}NO_4$	232.0731	232.0717	-1.5	0.026

$C_{11}H_8N_3O_2$	$C_6H_{13}NO_5$	214.0635	214.0611	-2.4	0.18
$C_{10}H_{10}N_3O$	$C_7H_{11}NO_6$	188.0841	188.0818	-2.2	0.013
$C_{10}H_8N_3$	$C_7H_{13}NO_7$	170.0742	170.0713	-2.9	0.01

Table 2. Concentration (in nmol g^{-1} FW) of flavins accumulated in the root and exported to the nutrient solution by *Medicago truncatula* plants in response to two different Fe-deficiency conditions, with and without $CaCO_3$. Data are means ± standard deviation (n=5). Numbers in parenthesis indicates the percentage of total flavins. FC1, FC2 and FC3 stand for 7-carboxy-Rbfl, 7-hydroxy-Rbfl, and 7α-hydroxy-Rbfl, respectively.

Treatment	Total Balance		Accumulated in the root				Exported to the nutrient solution			
	Accumulated	Exported	Rbfl	FC1	FC2	FC3	Rbfl	FC1	FC2	FC3
+Fe	-	-	2±2	-	-	-	-	-	-	-
-Fe	298 (65%)	158 (35%)	194±28 (65%)	5±1 (2%)	48±11 (16%)	51±8 (17%)	40±10 (25%)	1±0 (<1%)	109±13 (69%)	9±2 (6%)
-Fe+$CaCO_3$	1014 (94%)	65 (6%)	863±45 (85%)	4±1 (<1%)	43±5 (4%)	103±9 (10%)	16±4 (25%)	0±0 (0%)	46±18 (71%)	3±1 (4%)

Table 3. Effects of Fe deficiency on the root fresh weight (in g), leaf chlorophyll concentrations (Chl, in µmol g^{-1} FW), root riboflavin concentration (Rbfl , nmol g^{-1} FW), root ferric chelate reductase (FCR, µmol Fe reduced g^{-1} FW h^{-1}) and root phospho*enol*pyruvate carboxylase (PEPC, in µmol g^{-1} FW min^{-1}) activities of plant species of horticultural interest. Plants were grown in nutrient solution in the presence of $CaCO_3$. Data are means ± standard deviation (n=3) and significant changes ($p < 0.1$) marked with *.

Species	T	FW (g)	% decrease	Chl	% decrease	Rbfl	Fold -Fe/+Fe	FCR	Fold -Fe/+Fe	PEPC	Fold -Fe/+Fe
B. officinalis	+Fe	5.28±0.00	49	2.71±0.16	94*	2.62±0.90	1.2	0.13±0.01	0.5	0.02±0.01	0.5
	-Fe	2.70±1.08		0.17±0.03		3.16±1.05		0.07±0.05		0.01±0.01	
E. californica	+Fe	0.26±0.00	17	3.74±0.45	80*	2.16±0.78	1.2	0.28±0.01	1.1	0.25±0.07	1.6
	-Fe	0.22±0.00		0.76±0.05		2.52±0.98		0.31±0.01		0.39±0.11	
P. oleracea	+Fe	0.27±0.00	11	2.35±0.35	89*	0.20±0.20	1	0.31±0.01	1.5*	0.44±0.01	0.8
	-Fe	0.24±0.00		0.28±0.11		0.20±0.11		0.47±0.01		0.36±0.01	
S. oleracea	+Fe	2.81±0.00	6	3.14±0.19	86*	1.16±0.81	4.7*	0.11±0.01	1.6*	0.12±0.05	1.5*
	-Fe	2.64±0.00		0.43±0.02		5.41±2.76		0.18±0.01		0.19±0.01	
N. officinale	+Fe	4.41±0.00	27	3.07±0.08	41*	1.61±0.59	0.7	0.16±0.01	1.7*	0.34±0.09	1.1
	-Fe	3.23±0.00		1.82±0.17		1.19±0.22		0.28±0.02		0.39±0.06	
P. crispum	+Fe	1.23±0.00	60	1.50±0.18	81*	1.80±0.41	5.7*	0.77±0.02	2.0*	0.23±0.18	5.3*
	-Fe	0.49±0.00		0.28±0.11		10.2±1.98		1.52±0.01		1.22±0.04	
C. officinalis	+Fe	3.78±0.00	55	1.72±0.32	77*	0.79±0.16	1	0.15±0.01	2.3*	0.02±0.01	4.5*
	-Fe	1.70±0.00		0.40±0.03		0.83±0.25		0.33±0.05		0.09±0.01	
C. melo	+Fe	5.84±0.00	51	2.36±0.12	52*	3.88±0.80	1.7*	0.15±0.01	2.3*	0.24±0.11	7.9*
	-Fe	2.83±0.00		1.13±0.15		6.75±1.65		0.36±0.01		1.90±0.33	
A. arvensis	+Fe	0.86±0.00	35	1.60±0.40	81*	0.70±0.17	1	0.24±0.02	2.4*	0.09±0.05	2

	-Fe	0.56±0.05		0.30±0.10		0.66±0.19		0.59±0.01		0.19±0.07	
B. vulgaris	+Fe	10.69±0.00	89	1.99±0.34	88*	1.19±0.63	6.4*	0.20±0.01	3.3*	0.07±0.03	3.6*
	-Fe	1.14±0.01		0.24±0.03		7.58±2.88		0.66±0.14		0.24±0.01	
Mentha x piperita	+Fe	2.34±0.07	19	1.83±0.15	40*	0.19±0.10	0.1	0.25±0.07	3.8*	0.06±0.03	0.7
	-Fe	1.89±0.45		1.09±0.11		0.01±0.04		0.93±0.01		0.04±0.01	
L. albus	+Fe	4.96±0.21	13	2.98±0.28	53*	1.81±0.32	1.1	0.10±0.01	4.3*	0.27±0.02	1.4*
	-Fe	4.33±0.58		1.39±0.16		2.08±0.45		0.44±0.06		0.38±0.01	
A. caudatus	+Fe	0.67±0.00	77	1.64±0.30	68*	0.89±0.15	6.2*	0.21±0.01	7.0*	0.51±0.25	4.5*
	-Fe	0.16±0.00		0.53±0.23		5.50±3.65		1.44±0.02		2.52±1.21	
A. cepa	+Fe	0.42±0.02	22	0.80±0.10	38*	0.42±0.19	1.9*	0.27±0.04	11.1*	0.35±0.07	8.5*
	-Fe	0.33±0.00		0.50±0.10		0.78±0.03		3.04±0.01		2.99±0.60	
S. armeria	+Fe	2.46±0.03	65	2.33±0.50	48*	0.56±0.18	1	0.07±0.01	14.2*	0.26±0.19	12.4*
	-Fe	0.86±0.38		1.21±0.40		0.59±0.25		0.97±0.03		3.18±0.40	

Figure legends

Fig. 1. Flavin compounds present in: (A) standard solutions (FAD, FMN and Rbfl), (B) root extracts of Fe-deficient *M. truncatula* plants and (C) nutrient solution where Fe-deficient *M. truncatula* plants had been grown (in the absence of $CaCO_3$). Flavins were separated with a C_{18} column and detected at 445 nm. The UV-VIS spectrum of each flavin compound is also presented in insets.

Fig. 2. High-resolution MS and MS^2 spectra of Rbfl, FC1, FC2 and FC3 in positive and negative ionization mode. The parent ion is labelled in bold in each MS spectrum, and the corresponding MS^2 fragmentation spectrum is shown in insets. The structure of Rbfl, as well as the putatively assigned structures for FC1, FC2 and FC3, are shown next to MS spectra, highlighting the chemical modifications found with respect to Rbfl.

Fig. 3. Longitudinal distribution of the flavin fluorescence along the roots of *M. truncatula* plants grown under Fe deficiency for 1, 3 and 6 days, without or with $CaCO_3$. Length measurements in the Y-axis begin at the the root apex.

Fig. 4. Distribution of the flavin fluorescence in root transversal sections from Fe-deficient *M. truncatula* plants. Sections with high concentrations of flavins were studied: the yellow zone near the apex (B, D, F, H) and yellow sub-apical zone (A, C, E, G). Roots were sampled from plants treated without (A, B, E, F) and with $CaCO_3$ (C, D, G, H), for 3 (A-D) and 6 d (E-H).

Fig. 5. Concentrations of flavin compounds in the sub-apical and near the apex yellow zones from Fe-deficient *M. truncatula* plants, treated without (open bars) and with $CaCO_3$ (bold bars) for 1, 3 and 6 d. FC1, FC2 and FC3 stand for 7-carboxy-Rbfl, 7-hydroxy-Rbfl, and 7α-hydroxy-Rbfl, respectively.

Fig. 6. Score scatter plot of species studied. Principal component analysis (PCA), showing the score scatter plot of PCA component 1 (PCA1) vs. PCA component 2 (PCA2), shows the association between 15 plant species, using as independent variables root FW, leaf Chl content, root Rbfl content and root FCR and PEPC activities for control plants (+Fe, green circles) and Fe-deficient plants grown in the presence of $CaCO_3$ (-Fe + $CaCO_3$, yellow circles).

Fig.7. Taxonomic distribution of plant species studied for flavin accumulation and/or excretion from roots upon Fe shortage. Species in bold are the ones included in this study for flavin accumulation. Species included in a yellow box are those found to accumulate flavin compounds in roots or exudate flavins to the nutrient solution.

Fig. 1.

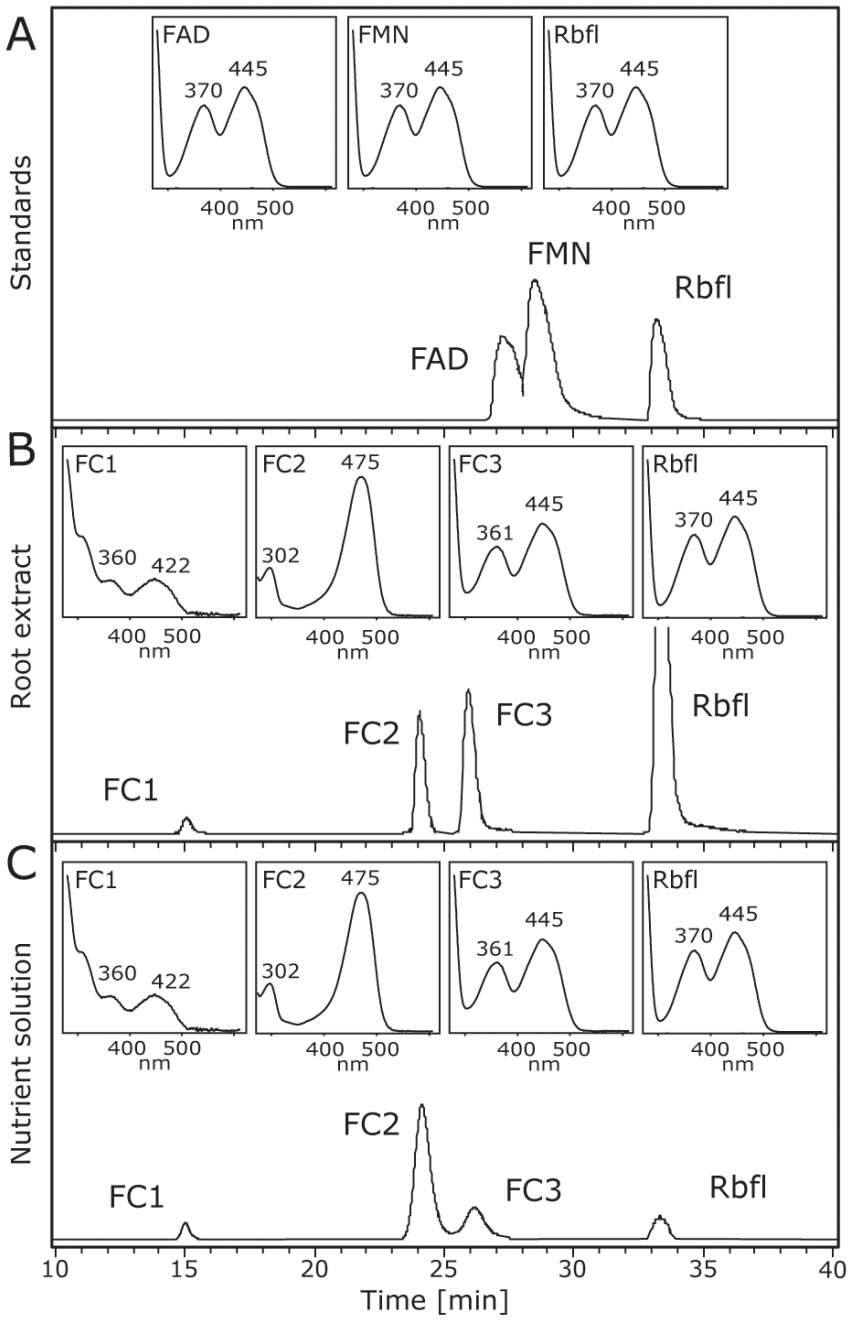
A
Standards
FAD
FMN
Rbfl
370
445
400 500
nm
FMN
Rbfl
FAD
B
Root extract
FC1
FC2
FC3
Rbfl
360
422
302
475
361
445
370
FC1
FC2
FC3
Rbfl
C
Nutrient solution
FC1
FC2
FC3
Rbfl
10
15
20
25
30
35
40
Time [min]

Fig. 2.

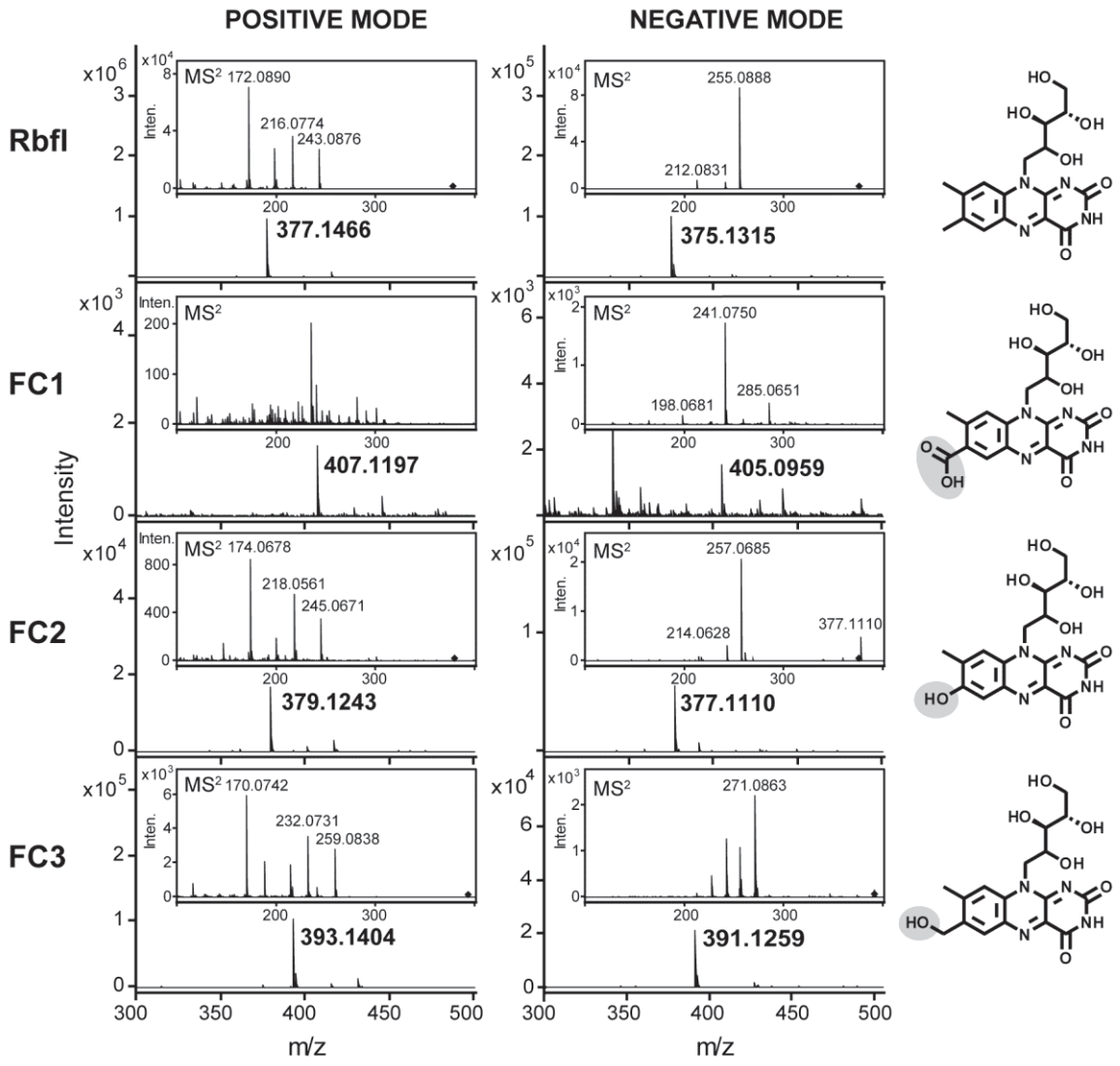
POSITIVE MODE
NEGATIVE MODE
Rbfl
FC1
FC2
FC3
Intensity
m/z
MS² 172.0890
216.0774
243.0876
377.1466
MS² 255.0888
212.0831
375.1315
MS² 241.0750
198.0681
285.0651
407.1197
405.0959
MS² 174.0678
218.0561
245.0671
379.1243
MS² 257.0685
214.0628
377.1110
377.1110
MS² 170.0742
232.0731
259.0838
393.1404
MS² 271.0863
391.1259

Fig. 3.

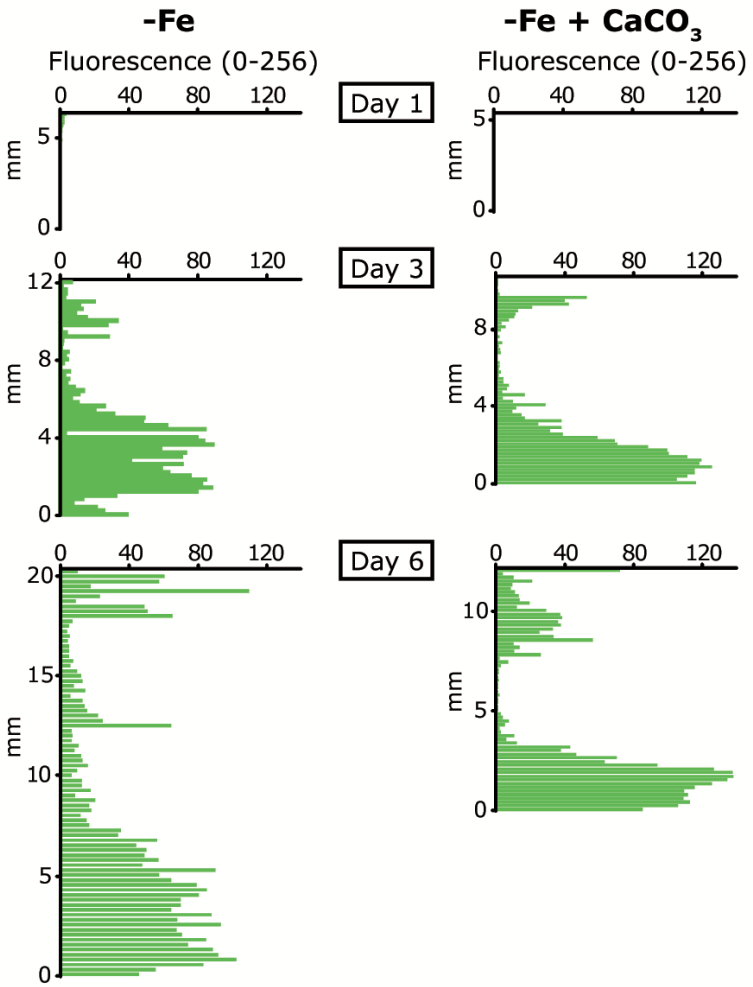
-Fe
Fluorescence (0-256)
-Fe + CaCO3
Fluorescence (0-256)
Day 1
Day 3
Day 6
mm
0
40
80
120

Fig. 4.

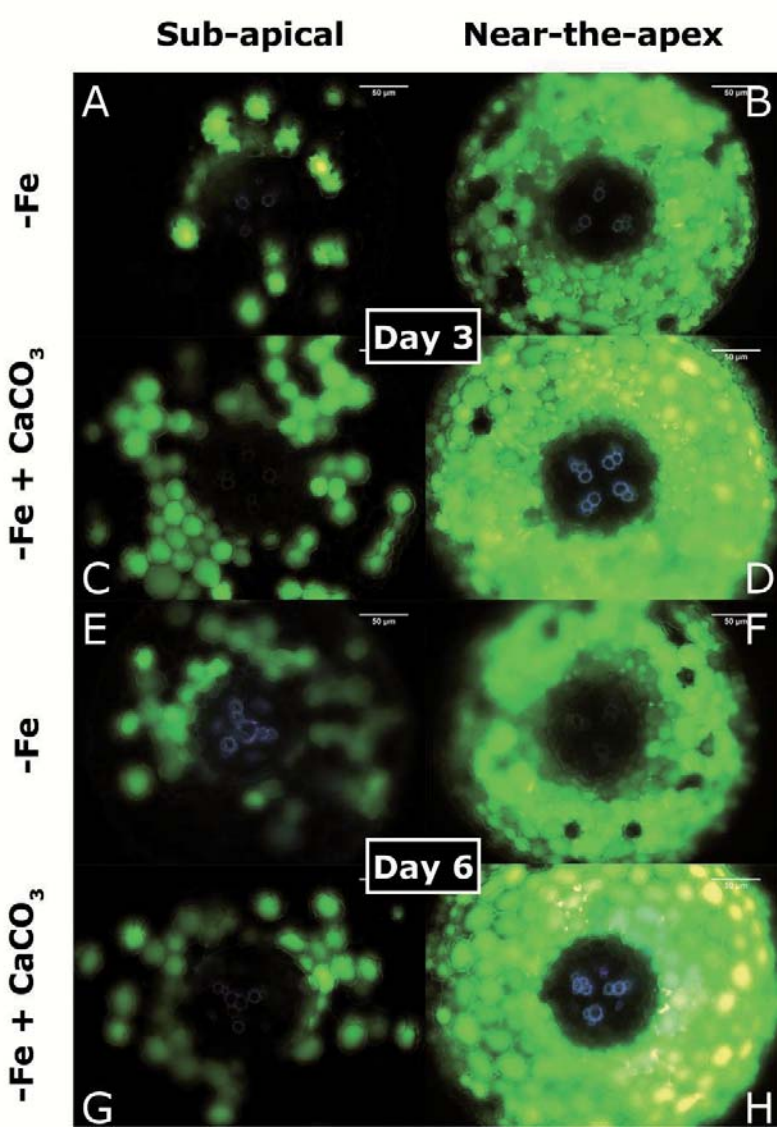
Sub-apical
Near-the-apex
-Fe
-Fe + CaCO3
Day 3
-Fe
-Fe + CaCO3
Day 6
A
B
C
D
E
F
G
H

Fig. 5.

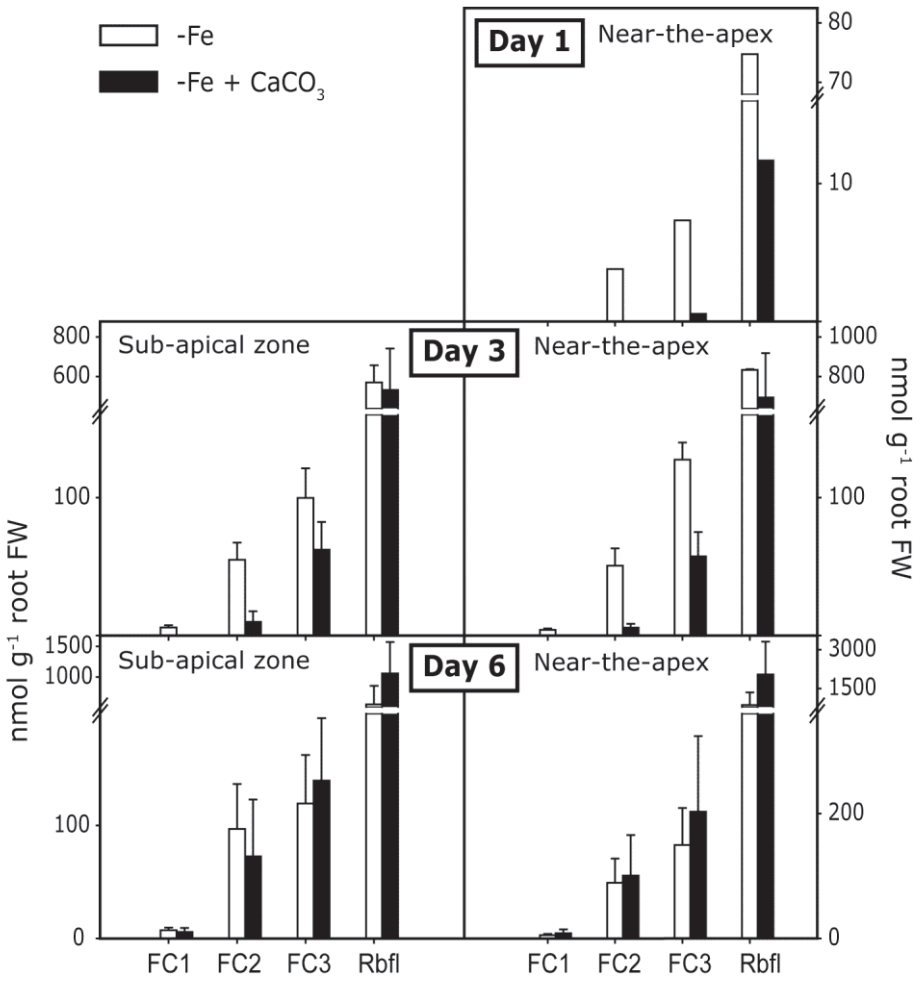
-Fe
-Fe + CaCO3
Day 1
Near-the-apex
Sub-apical zone
Day 3
Near-the-apex
Sub-apical zone
Day 6
Near-the-apex
nmol g-1 root FW
nmol g-1 root FW
FC1
FC2
FC3
Rbfl
FC1
FC2
FC3
Rbfl

Fig. 6.

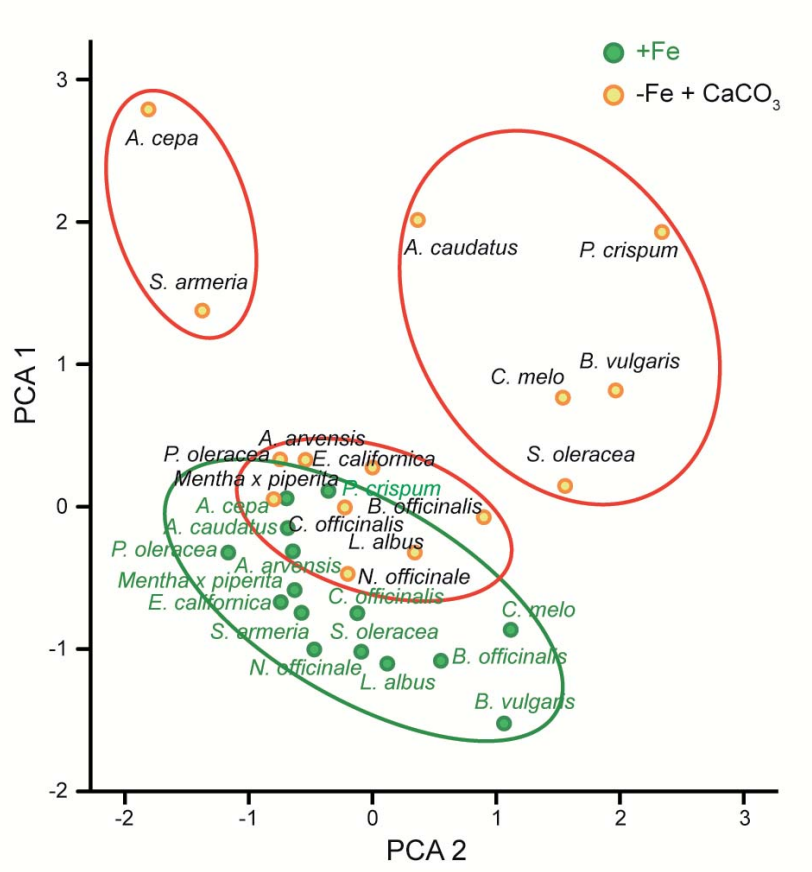
+Fe
-Fe + CaCO3
A. cepa
S. armeria
A. caudatus
P. crispum
C. melo
B. vulgaris
S. oleracea
A. arvensis
P. oleracea
E. californica
Mentha x piperita
P. crispum
A. cepa
B. officinalis
A. caudatus
C. officinalis
L. albus
P. oleracea
A. arvensis
N. officinale
Mentha x piperita
C. officinalis
E. californica
C. melo
S. armeria
S. oleracea
B. officinalis
N. officinale
L. albus
B. vulgaris
PCA 1
PCA 2
3
2
1
0
-1
-2
-2
-1
0
1
2
3

Fig.7

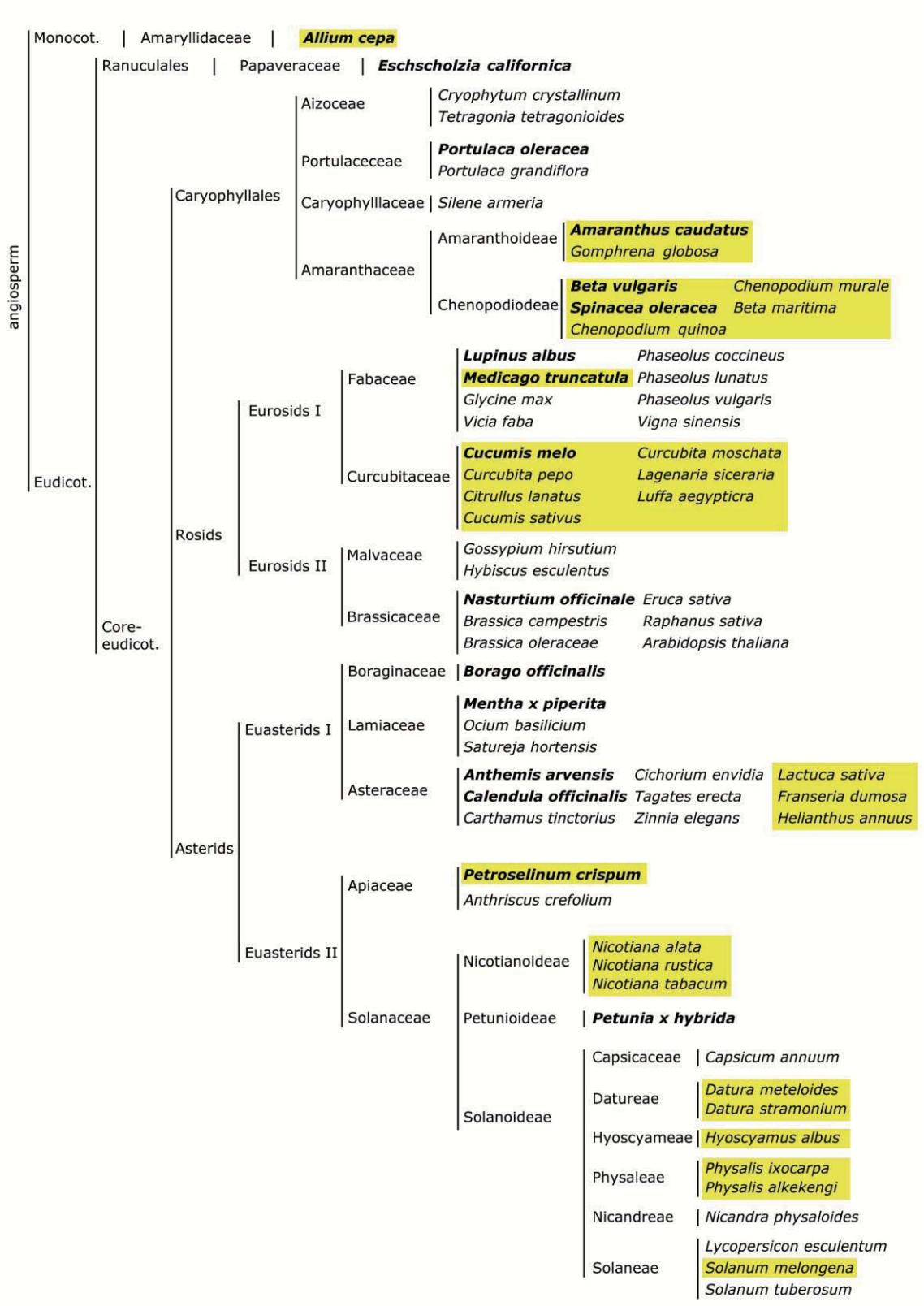
angiosperm
Monocot.
Amaryllidaceae
Allium cepa
Eudicot.
Ranuculales
Papaveraceae
Eschscholzia californica
Core-eudicot.
Caryophyllales
Aizoceae
Cryophytum crystallinum
Tetragonia tetragonioides
Portulaceceae
Portulaca oleracea
Portulaca grandiflora
Caryophylllaceae
Silene armeria
Amaranthaceae
Amaranthoideae
Amaranthus caudatus
Gomphrena globosa
Chenopodiodeae
Beta vulgaris
Chenopodium murale
Spinacea oleracea
Beta maritima
Chenopodium quinoa
Rosids
Eurosids I
Fabaceae
Lupinus albus
Phaseolus coccineus
Medicago truncatula
Phaseolus lunatus
Glycine max
Phaseolus vulgaris
Vicia faba
Vigna sinensis
Curcubitaceae
Cucumis melo
Curcubita moschata
Curcubita pepo
Lagenaria siceraria
Citrullus lanatus
Luffa aegypticra
Cucumis sativus
Eurosids II
Malvaceae
Gossypium hirsutium
Hybiscus esculentus
Brassicaceae
Nasturtium officinale
Eruca sativa
Brassica campestris
Raphanus sativa
Brassica oleraceae
Arabidopsis thaliana
Asterids
Euasterids I
Boraginaceae
Borago officinalis
Lamiaceae
Mentha x piperita
Ocium basilicium
Satureja hortensis
Asteraceae
Anthemis arvensis
Cichorium envidia
Lactuca sativa
Calendula officinalis
Tagates erecta
Franseria dumosa
Carthamus tinctorius
Zinnia elegans
Helianthus annuus
Euasterids II
Apiaceae
Petroselinum crispum
Anthriscus crefolium
Solanaceae
Nicotianoideae
Nicotiana alata
Nicotiana rustica
Nicotiana tabacum
Petunioideae
Petunia x hybrida
Solanoideae
Capsicaceae
Capsicum annuum
Datureae
Datura meteloides
Datura stramonium
Hyoscyameae
Hyoscyamus albus
Physaleae
Physalis ixocarpa
Physalis alkekengi
Nicandreae
Nicandra physaloides
Solaneae
Lycopersicon esculentum
Solanum melongena
Solanum tuberosum

RESUMEN

OBJETIVOS

El objetivo general de la tesis doctoral consiste en estudiar los efectos de la deficiencia de Fe y de la toxicidad por Cd en las raíces de dos plantas modelo, *Solanum lycopersicum* y *Medicago truncatula*, desde el punto de vista de la proteómica. Con este enfoque se pretende en primer lugar dibujar un mapa general de las alteraciones metabólicas producidas por ambos estreses nutricionales, y en segundo lugar utilizar esta plataforma para identificar posibles alteraciones desconocidas hasta la fecha que requieran un estudio en mayor profundidad. El estudio de estos estreses nutricionales tiene importancia desde el punto de vista agronómico, para evitar pérdidas de productividad, mejorar la calidad del cultivo y también para elaborar posibles estrategias de fitoremediación en suelos contaminados. Este proyecto también es interesante desde el punto de vista de seguridad alimentaria, con el fin último de establecer bases científicas para mejorar el contenido de Fe en cultivos comestibles o forrajeros y evitar el paso de Cd a la cadena trófica.

Se plantean los siguientes objetivos específicos:

1- Caracterización de los cambios producidos por la toxicidad leve y severa por Cd en el perfil proteico de la raíz de tomate.

2- Caracterización de las respuestas fisiológicas de la raíz de *Medicago truncatula* a la deficiencia de Fe.

3- Caracterización de los cambios producidos por deficiencia de Fe directa e inducida por la presencia de carbonato cálcico en el medio de cultivo en el perfil proteico de la raíz de *Medicago truncatula*.

4- Identificación de los compuestos de naturaleza flavínica producidos en las raíces de *Medicago truncatula* deficientes en Fe y caracterización del patrón de acumulación y excreción de los mismos.

5- Estudio de la posible relación entre la inducción de la producción y excreción de compuestos de naturaleza flavínica y las respuestas principales de la Estrategia I en especies de interés hortícola.

METODOLOGÍA

Material Vegetal

Para realizar la mayor parte de los experimentos, se han utilizado dos especies modelo: tomate (*Solanum lycopersicum* Mill. cv Tres cantos) y *Medicago truncatula* cv Jemalong. Para el estudio de la toxicidad de Cd se han muestreado raíces completas de tomate, mientras que en el estudio de la deficiencia de Fe en *M. truncatula* se han utilizado tanto raíces enteras como distintas secciones de las raíces laterales, características de esta deficiencia nutricional en esta especie. Las raíces se congelaron inmediatamente en N_2 líquido tras su muestreo y se mantuvieron a -80ºC hasta su análisis.

Las plantas se cultivaron en cámaras de crecimiento con condiciones de luz, humedad relativa y fotoperiodo controladas. Las semillas de tomate se germinaron en vermiculita y las de *M. truncatula* en placas Petri con papel de filtro y humedad del 100%, ambas especies en oscuridad y durante 1 semana. Posteriormente, las plántulas se pre-cultivaron en hidroponía en una solución nutritiva completa ½ Hoagland, donde se mantuvieron durante dos semanas hasta que las plantas adquirieron un tamaño adecuado. Transcurrido ese periodo, se iniciaron los tratamientos.

La toxicidad por Cd se estudió en tomate añadiendo 10 o 100 µM $CdCl_2$ a la solución nutritiva control. Las raíces se muestrearon a los 10 días de tratamiento.

La deficiencia de Fe se estudió en *M. truncatula* en dos escenarios: i) deficiencia de Fe (0 µM Fe, pH 5,5) y ii) deficiencia de Fe en presencia de carbonato cálcico (0 µM Fe + 1 g L^{-1} $CaCO_3$, pH 7,7, simulando las condiciones normalmente encontradas en suelos calizos típicos del área Mediterránea).

Para la caracterización de las respuestas típicas de *M. truncatula* (perteneciente a la Estrategia I) a la deficiencia de Fe, se midieron la actividad de la reductasa férrica, la exportación de protones, la actividad de la enzima fosfo*enol*piruvato carboxilasa y la acumulación de riboflavina utilizando los protocolos descritos previamente para *M. truncatula* y remolacha (López-Millán et al., 2000). Se realizaron medidas en los días 1, 3, 5, 7, 9, y 11 después del inicio del tratamiento. El estudio de proteómica diferencial en raíz se hizo con raíces muestreadas 6 días después del inicio del tratamiento. Por último, la caracterización de la inducción de la síntesis de compuestos flavínicos se llevó a cabo en los días 1, 3 y 6 después del inicio del tratamiento.

Otras especies de interés hortícola de un amplio espectro de familias vegetales se cultivaron en las condiciones control y de deficiencia de Fe a alto pH descritas anteriormente, para el estudio de la relación entre las respuestas radiculares características de la Estrategia I y la producción de compuestos flavínicos. Se cultivaron *Borago officinalis* L. (borraja), *Eschscholzia californica* (amapola), *Portulaca oleracea* (verdolaga), *Spinacia oleracea* L. (espinaca), *Nasturtium officinale* (berro de agua), *Petroselinum crispum* (perejil), *Calendula officinalis* (caléndula), *Cucumis melo* (melón), *Anthemis arvensis* (manzanilla), *Beta vulgaris* ssp. cicla 'Witerbi Mangold' (acelga),

Mentha x piperita (menta), *Lupinus albus* (altramuz), *Amaranthus caudatus* (amaranto), *Allium cepa* (cebolla) y *Silene armeria* (silene).

Medidas bioquímicas

Actividades enzimáticas

La actividad de la fosfo*enol*piruvato carboxilasa (PEPC) se midió en las raíces de *M. truncatula* y de las especies de interés hortícola según (López-Millán et al., 2000). El extracto se realizó partiendo de 100 mg de peso fresco de raíz utilizando 1 mL de solución de extracción (30 mM sorbitol, 1% BSA y 1% PVP en 100 mM HEPES-KOH, pH 8,0). El extracto se clarificó por centrifugación y la actividad PEPC se midió espectrofotométricamente en un ensayo acoplado con la actividad de la malato deshidrogenasa (L-malato:NAD-oxidoreductasa; EC 1.1.1.37).

La actividad reductasa férrica (FCR) se midió en raíces intactas de *M. truncatula*. Para ello, las plantas fueron colocadas en el medio de reacción (100 mM Fe(III)-EDTA, 100 mM batofenantrolina disulfonato (BPDS) y 1 mM MES pH 5,5) en recipientes opacos. La actividad enzimática se determinó midiendo espectrofotométricamente la concentración del complejo Fe(II)-BPDS a 535 nm, tras una hora de incubación en la cámara de cultivo.

Para la determinación de la extrusión de protones (H^+-ATPasa), cada planta se colocó en un recipiente opaco conteniendo 100 ml de solución nutritiva fresca sin tamponar en la cámara de cultivo. El descenso de pH se determinó midiendo la diferencia de pH transcurridas 24 h.

El estudio de la localización de las actividades enzimáticas FCR y extrusión de protones en las raíces de *M. truncatula* se realizó en placas Petri conteniendo un 0,6% agar a pH 6,0. La acidificación se estudió añadiendo 0,0025% de azul de bromocresol como indicador, mientras que la actividad FCR se determinó por la aparición de color rojo en el agar suplementado con 200 µM de Fe(III)-EDTA y 100 µM BPDS.

Determinación de clorofila

Para la determinación de la clorofila en hojas de especies de interés hortícola se tomaron discos de hojas totalmente desarrolladas muestreados a las 4 h de luz. Las clorofilas fueron extraídas con acetona en presencia de ascorbato y se analizaron espectrofotométricamente (Abadía y Abadía, 1993).

Análisis de la expresión génica en *M. truncatula*

En un primer estudio se analizó por RT-PCR semi-cuantitativa la expresión temporal de los genes de *M. truncatula* que codifican para la reductasa férrica de raíz (FCR), PEPC, H^+-ATPasa y 6,7-dimetil-8-ribitil-lumacina sintasa (DMRLs, implicada en la biosíntesis de riboflavina).

Para la FCR y H^+-ATPasa se utilizaron las secuencias anotadas del cDNA de *M. truncatula* (MtFRO1: AY439088, MtHA1: AJ132892) como referencia para el diseño de "primers" específicos. Para la PEPC y la DMRLs se usó la herramienta TBLASTX para buscar en *M. truncatula* secuencias homólogas a las descritas en las bases de datos para *A. thaliana*, *S. lycopersicum*, *M. sativa*, *G.max*, *N. tabacum* y *S. oleracea*. Se encontraron dos secuencias TC de *M. truncatula* que podían ser ortólogos para PEPC y DMRLs. Se realizó el alineamiento con la herramienta ClustalW y se comprobó que dichos TC contenían el cDNA completo. Se diseñaron "primers" específicos para amplificar por PCR la secuencia completa de ambos genes y posteriormente se procedió a su secuenciación. En base a las secuencias obtenidas se diseñaron los "primers" específicos para realizar la RT PCR.

El RNA total fue aislado de las raíces usando el RNeasy PLant Mini kit (Quiagen GmbH, Hilden, Alemania) de acuerdo a las instrucciones del fabricante, y la concentración e integridad del RNA se aseguró por espectroscopía UV y utilizando electroforesis en gel de agarosa no desnaturalizante. Tres µg de RNA total fueron usados para la reacción de retro-transcripción, obteniendo los cDNA correspondientes. Los cDNA fueron amplificados por PCR y los productos de amplificación se visualizaron en geles TBE agarosa con bromuro de etidio. Se usó la actina como gen de referencia y la cuantificación se hizo usando el software Quantity One 4.5.1 Chemidoc EQ software (Bio-Rad, CA, Estados Unidos).

Para un estudio más concreto de la ruta de biosíntesis de la riboflavina se estudió por RT-PCR cuantitativa la expresión de los genes de la ruta: 6,7-dimetil-8-ribitil-lumazina sintasa (DMRLs), GTP ciclohidrolasa II (GTPcII), riboflavina desaminasa-reductasa (ribD), y riboflavina sintasa (ribE). El RNA total fue aislado de las raíces laterales usando el RNeasy PLant Mini kit (Quiagen GmbH, Hilden, Alemania) de acuerdo a las instrucciones del fabricante, y la concentración e integridad del RNA se aseguró por espectroscopía UV (ND-1000 Nano Drop, Wilmington, DE, Estados Unidos) y utilizando electroforesis en gel de agarosa no desnaturalizante. Para la eliminación del DNA genómico el RNA se trató con TURBO DNA-free kit de Ambion Inc. (Austin, TX, Estados Unidos). Alrededor de 1 µg de RNA fue retro-transcrito y el cDNA obtenido se amplificó y cuantificó en un 7900 HT Fast Real Time PCR (Applied Biosystems) con SYBR green (Applied Biosystems, Warrington, Reino Unido). Se usó la actina como gen de referencia.

Análisis de flavinas

Extracción, separación y detección

Se ha desarrollado un método cromatográfico para la detección y cuantificación de rioboflavina, así como de otros compuestos flavínicos que pudieran estar presentes en muestras de raíz de distintas especies. Se analizó el contenido en flavinas en raíces de *M. truncatula* así como en las soluciones nutritivas en las que se estableció la deficiencia de Fe.

El tejido radicular (aproximadamente 100 mg) se molió en nitrógeno líquido y se homogeneizó con fase de extracción (1 mM acetato de amonio, pH 6,0, 5% metanol). El extracto así obtenido se filtró (PVDF 0,45 μm) antes de su análisis por HPLC-UV/VIS-MS. Para el análisis de solución nutritiva aproximadamente 500 ml fueron filtrados (PVDF 0,45 μm) y concentrados utilizando columnas C18 (SepPack C18 cartridges; Waters Corp., Milford, MA, Estados Unidos).

La separación cromatográfica se llevó a cabo en un Waters Alliance 2795 (Waters) con una columna C18 de 3,5 μm de tamaño de partícula (Symmetry® C18, 15 cm x 2,1 mm d.i., Waters). El volumen inyectado fueron 50 μl y el flujo 0,1 ml min^{-1}. El programa cromatográfico constó de tres partes, una primera fase de separación cromatográfica donde se incrementó linealmente la concentración de metanol de 5 a 50% en 35 minutos, seguida de una fase de lavado al 95% de metanol durante 20 minutos, y por último, una fase de re-equilibrado con el 5% de metanol durante 20 minutos más. Se utilizó un 5% de acetato amónico 20 mM pH 6,0 a lo largo de todo el proceso.

Las flavinas presentes en las muestras se detectaron y cuantificaron por espectroscopía UV-VIS (PDA 2996 de Waters), usando cantidades conocidas de riboflavina como patrón y una longitud de onda de 445 nm.

Determinación estructural

La determinación de las estructuras de los compuestos flavínicos se realizó por espectrometría de masas con dos detectores distintos, y ayudada por cálculos teóricos de los espectros UV-VIS.

Por un lado la cromatografía se acopló a un detector micrOTOF de Bruker (Bruker Daltonik, Bremen, Germany), que nos permitió obtener la masa exacta de los compuestos flavínicos, y por otro lado la cromatografía se acopló a un detector miroQTOF de Bruker (Bruker Daltonik), que nos permitió obtener los espectros de fragmentación con las masas exactas de los iones hijos.

Para los cálculos de los espectros UV-VIS teóricos se utilizó la Density-Functional Theory (DFT). Los cálculos se realizaron mediante el software Gaussian 09 (Gaussian 09 revision A.2, Gaussian Inc., Wallingford CT, 2009). Para la determinación estructural se compararon los cambios del espectro UV-VIS de los compuestos desconocidos respecto al espectro de la riboflavina en datos experimentales y teóricos.

Localización de las flavinas en raíz

La localización transversal de las flavinas en la raíz y el estudio de su distribución longitudinal se realizó en las zonas amarillas de las raíces de plantas de *M. truncatula* deficientes en Fe, que fueron cortadas con bisturí y embebidas en agar al 5%. A continuación se realizaron cortes de 70 µm de grosor con un vibratomo (VT1000 S, Leica Microsystems GmbH, Wetzlar, Germany), y las secciones se analizaron con un microscopio de fluorescencia invertido (DM IL LED, Leica Microsystems GmbH), ya que las flavinas presentan fluorescencia verde al ser excitadas con luz azul (340-380 de longitud de onda de excitación y 425 nm como longitud de onda de corte de emisión; A1 filter cube, Leica Microsystems GmbH). Las imágenes transversales de la raíz fueron tomadas a una magnificación de 200x y se analizó una de cada dos secciones (2592 x 1994 pixels; resolución ejes x-y: 360 x 270 µm; resolución del eje-z: 140 µm). Dependiendo de la longitud de la raíz amarilla estudiada se analizaron entre 27 y 82 secciones transversales para el estudio longitudinal. Para la cuantificación de la señal fluorescente se usó el programa ImageJ (ImageJ, Wright Cell Imaging Facility; http://www.uhnresearch.ca/facilities/wcif).

Proteómica

Extracción de proteínas

Las proteínas solubles de raíz de tomate y *M. truncatula* se obtuvieron utilizando un protocolo de extracción fenólica.

Para la extracción se recogió material de dos raíces hasta aproximadamente 1 g de materia fresca. El tejido se pulverizó en N_2 líquido en un mortero y se homogeneizó con fenol saturado en Tris-HCl 0,1 M (pH 8,0) en presencia de 5mM β-mercaptoetanol para evitar peroxidaciones. Después de 30 min en agitación a 4ºC, el extracto crudo se filtró (PVDF, 0,45 µm) y centrifugó a 5000g durante 15 min a 4ºC, separándose en dos fases. La fase fenólica (inferior) contiene las proteínas del extracto, y la acuosa (superior) los compuestos solubles en agua. A continuación, la fase fenólica se lavó con un volumen de Tris-HCl 0,1 M (pH 8,0) saturado con fenol conteniendo 5 mM β-mercaptoetanol. La incubación para el lavado y la separación de las fases se realizó como se ha descrito anteriormente. La nueva fase fenólica limpia se recogió y las proteínas presentes se precipitaron en frío con una solución 0,1 M de acetato amónico en metanol, y se incubaron al menos 4 h a -20ºC para asegurarse la precipitación completa de las proteínas. El precipitado proteico se recuperó por centrifugación y se lavó tres veces con metanol hasta la desaparición del olor a fenol. Finalmente, el precipitado se secó bajo corriente de nitrógeno y se rehidrató con buffer de rehidratación para 2-DE (8 M urea, 2% (p/v) CHAPS, 50 mM DTT, 2 mM PMSF y 0,2% (v/v) IPG buffer pH 3-10) durante 2,5 h a 38ºC. Para evitar la presencia de agregados no solubilizados la muestra se centrifugó durante 10 min a 15000 g y se filtró (PVDF, 0,45 µm). La concentración de proteínas se midió mediante el kit RC DC Protein Assay BioRad (BioRad, Hercules, CA, USA), basado en el método de Lowry.

Electroforesis Bidimensional

Se realizaron experimentos preliminares para decidir el rango de pH de la primera dimensión o isoelectroenfoque (IEF), fijándose un rango entre 5-8 como el más apropiado para los estudios en cuestión. Para la primera dimensión se utilizaron tiras de 7 cm ReadyStrip IPG (BioRad) con un rango de pH de 5-8. El isoelectroenfoque se realizó en un aparato Protean IEF Cell (BioRad). Las tiras se rehidrataron con 125 μL de buffer conteniendo 150 μg de proteínas del extracto de raíz y trazas de azul de bromofenol. Después de la primera dimensión las tiras se equilibraron y se sometieron a un proceso de reducción y alquilación con DTT y iodoacetamida antes de llevar a cabo la separación en una segunda dimensión. Para la segunda dimensión (SDS-PAGE), las tiras de isoelectroenfoque se colocaron sobre geles verticales del 12% de acrilamida (8x10x0,1 cm), se selló la unión con agarosa al 0,5% con trazas de azul de bromofenol y la separación electroforética se llevó a cabo a 20 mA por gel durante aproximadamente 1h y 30 min. Una vez terminada la electroforesis los geles se tiñeron con Coomassie-blue R-250 (Sigma, Barcelona, España). Los geles fueron escaneados y el análisis de imagen se hizo con el PDQuest 8.0 (BioRad).

Para el tratamiento estadístico solo se tuvieron en cuenta aquellas manchas consistentes entre los geles, es decir, aquellas que estaban presentes en al menos el 80% de los geles de un tratamiento. Los valores perdidos fueron estimados con el algoritmo seqKNN con el programa R 2.7.0. Para la comparación entre tratamientos se utilizó la prueba-t con una confianza de 0,1 y un cambio de intensidad por encima de 2. El análisis multivariante se realizó usando el SPSS v.15 (SPSS Inc., Chicago, USA). Los geles se realizaron con raíces de plantas de 5 tandas diferentes crecidas por separado (5 réplicas biológicas) para cada tratamiento.

Digestión tríptica e identificación

Solo se analizaron aquellas manchas proteicas que cumplieron los criterios definidos para que las diferencias entre tratamientos fueran consideradas como significativas (prueba-t 0,1 y cambio de intensidad de más de dos veces). Las manchas se cortaron y digirieron en equipos automatizados (ProPic de Genomic Solutions oEXQuest de BioRad para el cortado de los geles y Progest para las digestiones). El protocolo de digestión incluyó los pasos habituales de lavado de la tinción con acetonitrilo, equilibrado con bicarbonato sódico y secado de las piezas de gel, que luego fueron rehidratadas con la solución de tripsina para su digestión. Los péptidos obtenidos se concentraron y purificaron con microcolumnas C18 (ZipTip, Millipore, MA, USA), y se eluyeron directamente en la placa del analizador MALDI-TOF. Las masas obtenidas para cada digestión se contrastaron con las bases de datos NCBInr y Plant EST disponibles usando el motor de búsqueda MASCOT (Matrix Science, London, U.K.). Para asignar la función a las proteínas identificadas utilizamos a anotación GO (http://www.geneontology.org) o el programa KOBAS (http://kobas.cbi.pku.edu.cn), basado en las rutas metabólicas descritas en la base de datos KEGG (http://www.genome.jp/kegg/pathway.html).

APORTACIONES DEL DOCTORANDO

Objetivo 1: Toxicidad por Cd en la raíz de tomate

Se realizó un estudio de proteómica diferencial por técnicas de electroforesis bidimensional, utilizando raíces de plantas de tomate cultivadas en tres concentraciones de Cd en la solución nutritiva, 0 (control), 10 (toxicidad leve) y 100 µM (toxicidad severa). Los resultados obtenidos han permitido identificar las diferentes respuestas que ocurren en la raíz de tomate cuando se somete a toxicidad de Cd, dependiendo de la concentración de este elemento en el medio de cultivo (Rodríguez-Celma et al., 2010).

En el tratamiento de toxicidad leve por Cd (10 µM) se observa un aumento generalizado de proteínas relacionadas con la glicólisis, el ciclo del ácido cítrico y la cadena respiratoria (Rodríguez-Celma et al., 2010). Este tipo de respuesta ya se había observado en otros estudios realizados con especies no tolerantes en condiciones de toxicidad similares (Sarry et al., 2006; Roth et al., 2006). El aumento de actividad de la ruta de glicólisis y de la producción de energía en raíz podría servir para compensar la baja eficiencia fotosintética observada en estas plantas (López-Millán et al., 2009). Los cambios metabólicos encontrados son similares a los descritos, utilizando un enfoque fisiológico, en plantas sometidas a deficiencia de Fe, otro estrés que también conduce a una disminución de la eficiencia fotosintética (López-Millán et al., 2009). Hay que destacar que las plantas de tomate cultivadas en toxicidad leve de Cd presentan clorosis en las hojas jóvenes, un síntoma característico de la deficiencia de Fe, así como una disminución de la concentración de Fe en hoja (López-Millán et al., 2009). Es más, en consonancia con estas observaciones, un estudio proteómico realizado en raíz de tomate cultivado en deficiencia de Fe describe cambios en algunas proteínas también detectadas en nuestro trabajo (Li et al., 2008). A la vista de los resultados, y teniendo en cuenta la baja concentración de Fe en hoja observada en plantas cultivadas en toxicidad leve de Cd (López-Millán et al., 2009), podemos concluir que los cambios en la ruta de glicólisis y de producción de energía observados son más bien debidos a una deficiencia de Fe inducida por el Cd que a sus efectos tóxicos directos. Se ha llegado a conclusiones similares en estudios fisiológicos sobre los efectos de la toxicidad por Cd (Larbi et al., 2002; López-Millán et al., 2009; Li et al., 2008; Fodor et al., 2005).

Los resultados obtenidos en el tratamiento de toxicidad leve por Cd contrastan con los obtenidos en el caso de una toxicidad severa. En este último caso, lo que se observa es un descenso generalizado de las proteínas de la ruta de glicólisis y de producción de energía (Rodríguez-Celma et al., 2010), sin que haya cambios consistentes en el ciclo del ácido cítrico. Además de estos cambios, se observó un aumento de proteínas de desintoxicación y relacionadas con el estrés oxidativo, así como un aumento en proteínas de función chaperona. Estos aumentos son marcadores comunes de estrés en plantas (Kieffer et al., 2009), sugiriendo que son debidos a un efecto tóxico directo del Cd. Este tipo de respuesta es común a la observada en especies más tolerantes a Cd, como el álamo, donde se observan cambios similares incluso a concentraciones bajas del metal pesado (Kieffer et al., 2008).

Algunas respuestas son comunes en los dos tratamientos de toxicidad por Cd. Por un lado, existe un aumento generalizado de proteínas relacionadas con estrés, tanto oxidativo como biótico y un aumento de proteínas chaperonas. Por otro, también observamos grandes cambios en la biosíntesis de pared celular (Rodríguez-Celma et al., 2010). Ambos aumentos podrían responder a una adaptación a los efectos tóxicos del Cd.

El Cd en el citoplasma puede generar especies reactivas de oxígeno debido a una interacción con la función de otros metales pesados, lo que explicaría el aumento observado en proteínas relacionadas con la defensa ante el estrés oxidativo. Estos procesos pueden afectar a funciones claves como el plegamiento de proteínas. El aumento observado en algunas chaperonas ayudaría a mitigar la desnaturalización de proteínas incluso en presencia de Cd en el citoplasma, mientras que los aumentos en proteasas llevarían a la degradación de aquellas proteínas demasiado afectadas. Los cambios observados en proteínas de la ruta de síntesis de la pared celular pueden estar relacionados con un mecanismo de desintoxicación ante el Cd utilizado por las plantas de tomate. Como se ha comentado en la introducción, una de las estrategias de desintoxicación más común en plantas no tolerantes consiste en la retención del metal pesado en la pared celular de las raíces, evitando su entrada en la planta y posterior traslocación a la parte aérea. En consonancia con esta hipótesis, se ha descrito que en tomate la mayoría del Cd absorbido por el tomate se encuentra en la raíz (López-Millán et al., 2009).

En la Figura 7 se puede observar un resumen de las distintas respuestas a nivel metabólico obtenidas para los dos tratamientos, quedando de manifiesto los aumentos comunes a ambos tratamientos para proteínas relacionadas con el estrés y la síntesis de pared celular, y el comportamiento opuesto en las rutas de producción de energía.

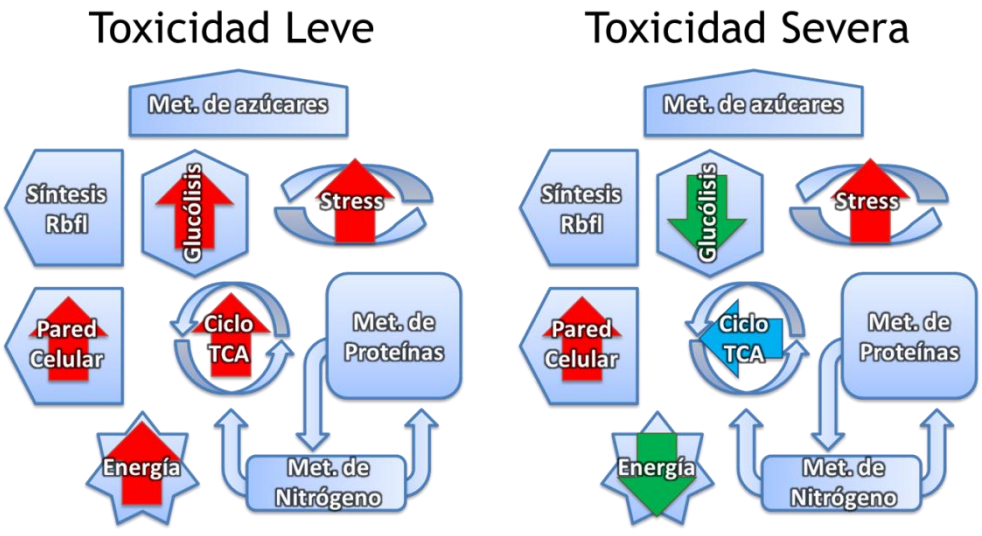

Fig. 7 Esquema general del metabolismo poniendo de manifiesto los cambios observados en los tratamientos de toxicidad por Cd

Objetivo 2: Deficiencia de Fe en raíz de *M. truncatula*: Respuestas fisiológicas

Se realizó una caracterización de las respuestas de las raíces de *Medicago truncatula* a la deficiencia de Fe, con el fin de utilizar esta planta como nuevo modelo para el estudio de este estrés nutricional en plantas. Para ello se cultivaron plantas de *M. truncatula* en condiciones de suficiencia y deficiencia de Fe, midiendo la evolución de algunas de las respuestas de la Estrategia I a lo largo del tratamiento. La caracterización consistió en el estudio de la aparición en el tiempo y del comportamiento de las respuestas características de las raíces de plantas de Estrategia I a la deficiencia de Fe desde un punto de vista fisiológico y de expresión génica (Andaluz et al., 2009). *Medicago truncatula* es una planta para la cual se dispone de un gran número de herramientas moleculares que facilitarán posteriores estudios tanto proteómicos como transcriptómicos. Además, la planta es de tamaño adecuado para la realización de estudios fisiológicos, tiene un periodo corto de crecimiento y se autopoliniza.

Se estudiaron la actividad de la reductasa férrica mediada por MtFRO, la acidificación del medio de cultivo mediada por MtHA1, la actividad de la fosfo*enol*piruvato carboxilasa mediada por MtPEPC y por último la acumulación de flavinas, una respuesta que no siempre está presente en especies de Estrategia I. Una vez comprobado que *M. truncatula* induce todas las respuestas anteriormente mencionadas, se procedió a la determinación de la inducción de la expresión de los genes responsables de estas actividades. En el caso de la acumulación de riboflavina se estudió la acumulación de los transcritos de la DMRLs, enzima implicada en la biosíntesis de este compuesto. La actividad reductasa férrica de raíz y fosfo*enol*piruvato carboxilasa, así como la acidificación del medio y producción de riboflavina fueron mayores en las plantas deficientes que en las controles, y los genes correspondientes, MtFRO, MtHA1, MtPEPC y MtDMRL también aumentaron sus niveles de expresión. En la Figura 8 podemos observar la evolución temporal de las respuestas estudiadas, tanto a nivel de actividad como de transcritos (en el último caso se representa la intensidad una vez normalizada).

La primera respuesta en manifestarse fue un aumento en el nivel de transcrito de MtHA1, que ocurrió tan solo un día después del establecimiento de la deficiencia. Estos altos niveles de expresión de MtHA1 se mantuvieron a lo largo de todo el experimento. Sin embargo, no se observó un incremento en la acidificación del medio hasta el día 5. El segundo evento que apareció fue un aumento en los niveles de expresión de MtDMRL, acompañado de un aumento de la actividad PEPC en raíz, al tercer día tras el inicio de la deficiencia. Sin embargo, los niveles de expresión de MtPEPC no tuvieron un cambio significativo hasta el día 5, sugiriendo que esta inducción de la actividad podría ser independiente de la regulación transcripcional. También en este quinto día de deficiencia ocurrió el aumento en el nivel de expresión de MtFRO1, con lo que los cuatro genes estudiados estaban ya regulados positivamente. En el séptimo día de deficiencia los niveles de riboflavina y actividad reductasa férrica en las raíces deficientes aumentaron, aunque el máximo para actividad reductasa no ocurrió hasta el noveno día (Andaluz et al., 2009). Estos resultados indican que los cuatro genes estudiados (MtDMRL, MtFRO1,

MtPEPC1 y MtHA1) están involucrados y regulados, directa o indirectamente, en la respuesta a la deficiencia de Fe en *M. truncatula*. Sin embargo, tanto la expresión como la actividad fisiológica correspondiente de los distintos genes siguieron patrones temporales diferentes, sugiriendo la existencia de regulación tanto a nivel transcripcional como post-transcripcional.

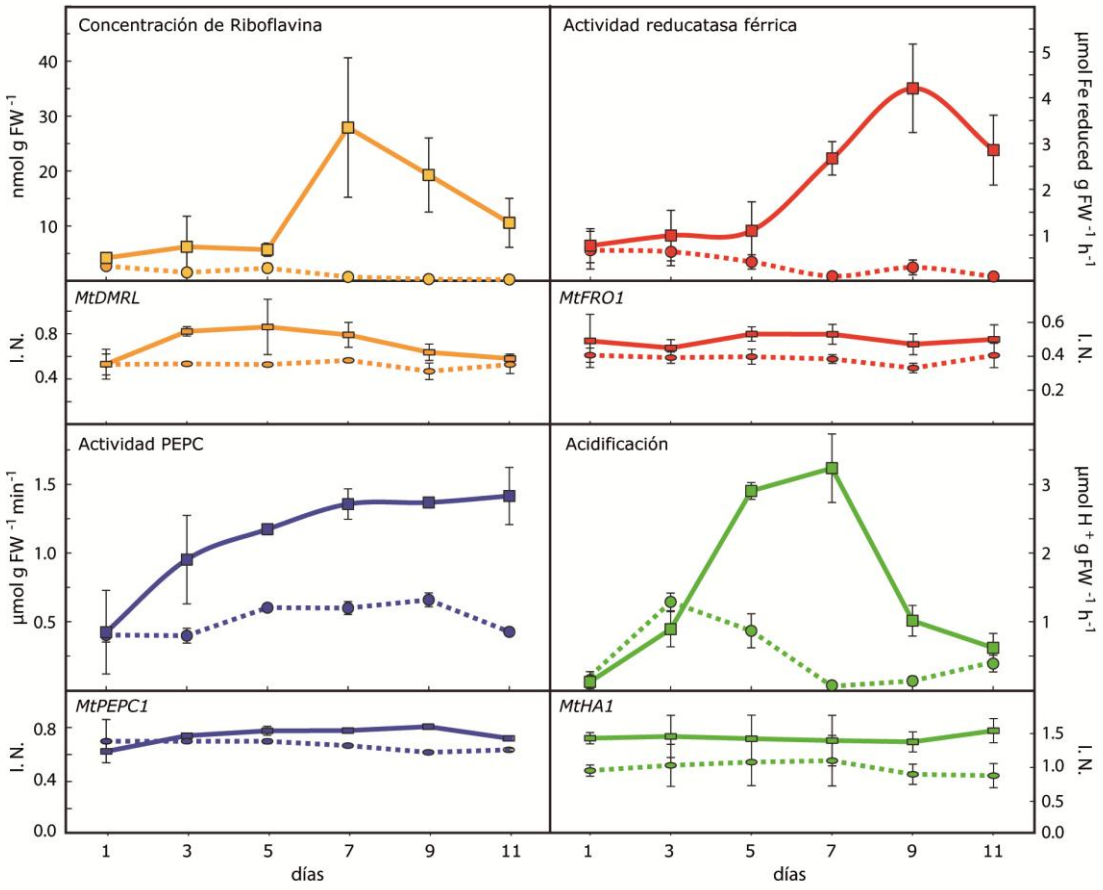

Fig. 8 Evolución temporal de las respuestas típicas de Estrategia I en *M. truncatula*

A pesar de que la producción de riboflavina o derivados ha sido descrita para muchas especies en deficiencia de Fe (Susín et al., 1993; Welkie, 2000), ésta ha sido la primera vez que se observó una regulación positiva a nivel de expresión génica de la enzima DMRLs implicada en la síntesis de riboflavina. A nivel de producción de metabolito se observó que la curva de concentración de riboflavina en deficiencia de Fe coincidía con la mostrada para la actividad reductasa férrica de raíz. La función que pueden jugar las flavinas en la deficiencia de Fe es aún desconocida, aunque nuestros resultados sugieren que podría guardar relación con la actividad reductasa férrica, ya que siguen la misma tendencia temporal.

El incremento en la actividad de la PEPCasa ocurrió de forma temprana en la deficiencia de Fe, y su actividad se mantuvo alta a lo largo de todo el experimento, lo que indica la importancia de este enzima dentro de la respuesta de adaptación a la deficiencia de Fe. A pesar de ello, el aumento en la expresión génica llegó más tarde. Un aumento de

la actividad PEPCasa se había descrito en varias especies en respuesta a la deficiencia de Fe tanto a nivel de actividad como de concentraciones de proteína y de transcrito (Abadía et al., 2002; Zocchi, 2006). Los aumentos en la actividad PEPCasa están localizados en las capas más externas del córtex radicular, que son las más activas en cuanto a extrusión de protones. Por esa razón se había propuesto que este aumento de la actividad PEPCasa venía causado por el aumento del pH citoplasmático como consecuencia de la extrusión de protones. Sin embargo nuestros datos no apoyan esa teoría, ya que la inducción de la actividad PEPCasa y la acidificación no siguieron el mismo patrón temporal, ni a nivel de transcritos ni de respuesta. La actividad PEPCasa se indujo antes y se mantuvo tras el fin de la inducción de la acidificación. Por tanto, en *M. truncatula*, la extrusión de protones no parece ser causa directa de la inducción de la actividad PEPCasa en deficiencia de Fe.

Objetivo 3: Deficiencia de Fe en raíz de *M. truncatula*: Proteómica

Se realizó un estudio de proteómica diferencial por técnicas de electroforesis bidimensional, utilizando raíces de plantas de *M. truncatula* cultivadas en condiciones de suficiencia de Fe (45 µM, control) y en condiciones de deficiencia de Fe (0 µM) a dos pH distintos, a pH 5,5 y a pH 7,7 (en el último caso tamponando con carbonato de calcio). Los resultados se completaron utilizando pruebas complementarias, incluyendo RT-PCR cuantitativa y cuantificación de riboflavina (Rodríguez-Celma et al., 2011a).

Los resultados obtenidos nos han permitido identificar las diferentes respuestas que se dan en la raíz de *M. truncatula* frente a la deficiencia de Fe en dos condiciones de pH distintas, 5,5 y 7,7. Las respuestas observadas fueron similares en su conjunto, aunque con una mayor intensidad en el caso de la deficiencia de Fe a alto pH (condiciones normalmente encontradas en los suelos agronómicos que presentan deficiencia de Fe). Las respuestas se resumen en la figura 9.

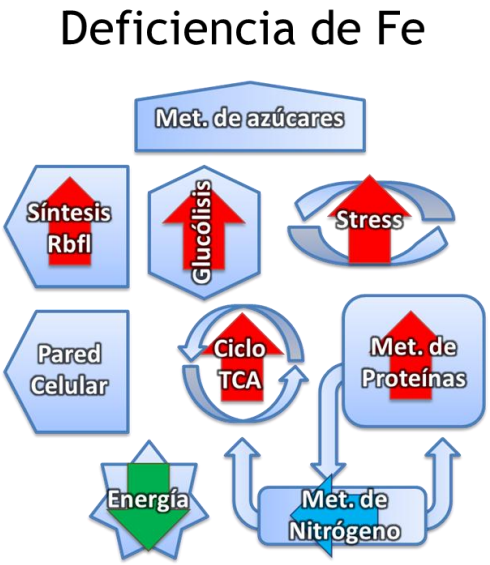

Fig. 9 Esquema general del metabolismo poniendo de manifiesto los cambios observados en los tratamientos de deficiencia de Fe

En los perfiles proteicos de raíces de plantas deficientes se observa la aparición *de novo* de las enzimas GTP-ciclohidrolasa II y DMRLs. Ambas enzimas forman parte de la ruta de biosíntesis de riboflavina. Se realizó un estudio complementario por medio de RT-PCR cuantitativa de todos los genes de la ruta de biosíntesis de riboflavina en *M. truncatula*, resultando todos ellos sobre-expresados en las muestras de deficiencia de Fe. Esto indica que la biosíntesis radicular de riboflavina está regulada por Fe, como también ocurre en cepas flavinogénicas de levadura. Se realizó también una cuantificación de la riboflavina en raíz y solución nutritiva de estas plantas, la cual reveló un comportamiento diferencial en función del pH del medio de cultivo. En *M. truncatula*, cuando el pH externo era alto (tamponado a 7,7 con carbonato cálcico) la cantidad de riboflavina exportada al medio fue mínima, solo un 2% del total producido. Sin embargo, cuando el pH externo no se encontraba tamponado (con un descenso de 5,5 a 4,0 a lo largo del

tratamiento por la extrusión de protones) la cantidad de riboflavina exportada fue mayor, llegando a ser un 17% de la riboflavina producida. Esta dependencia del pH es consistente con estudios previos en otras especies vegetales (Susín et al., 1994). Se puede plantear la hipótesis, por tanto, de que la exudación de la riboflavina al medio de cultivo podría estar mediada por un gradiente de protones, o por un transportador antiporte con protones.

En los dos tratamientos de deficiencia de Fe también se encontró una acumulación de proteínas relacionadas con el reciclado del nitrógeno y el catabolismo de proteínas. Se observó un aumento en proteínas relacionadas con la proteolisis y el reciclado de grupos amino, así como un aumento en proteínas transaminasas. Estos resultados están en concordancia con unos recientemente publicados para pepino (Donnini et al., 2010) y sugieren un reciclado del nitrógeno de las proteínas, ya que la absorción normal de nitrógeno del suelo en casos de deficiencia de Fe disminuye, al desaparecer la nitrito reductasa, una enzima que contiene Fe. Este fenómeno de reciclado podría servir como fuente anaplerótica de N y C para la síntesis de carboxilatos y metabolitos secundarios.

Junto a estas dos nuevas respuestas descritas, también se encontraron otros cambios ya descritos en la bibliografía de proteínas relacionadas con la glicólisis y el ciclo del ácido cítrico, así como cambios en la cadena de transporte electrónico. Se observó también un aumento y reorganización de proteínas relacionadas con el estrés oxidativo.

Objetivo 4: Flavinas en raíz de *M. truncatula* con la deficiencia de Fe

Una vez comprobado el aumento en la producción de riboflavina en raíces de *M. truncatula* con la deficiencia de Fe a nivel proteómico y genómico, se realizó un estudio más detallado, cualitativo y cuantitativo, sobre la producción y tipo de otros derivados de riboflavina en los tratamientos de deficiencia de Fe descritos anteriormente, procediéndose a su identificación, localización y al estudio del patrón de acumulación o excreción al medio de cultivo (Rodríguez-Celma et al., 2011b).

Se han identificado tres nuevos derivados de riboflavina no descritos previamente en plantas, asignados putativamente a 7-hidroxi-riboflavina, 7α-hidroxi-riboflavina y 7-carboxi-riboflavina, cuyas estructuras se presentan en la Figura 10. La identificación se realizó por métodos de separación basados en HPLC y de determinación estructural por técnicas de espectrometría de masas de alta resolución y estimación teórica de espectros UV-VIS. El derivado de riboflavina más abundante fue la 7-hidroxi-riboflavina, que fue el compuesto mayoritario encontrado en solución nutritiva (un 70% de las flavinas de solución nutritiva). Es la primera vez que se describe en la literatura que un derivado hidroxilado de riboflavina sea la flavina exportada mayoritariamente por la raíz de plantas cultivadas con deficiencia de Fe. Los otros dos derivados encontrados, 7α-hidroxi-riboflavina y 7-carboxi-riboflavina, se habían descrito en la ruta de degradación de riboflavina en el hígado (Chastain y McCormick, 1986; Ohkawa et al., 1983).

Los estudios de localización indicaron que las flavinas se acumulan en la porción apical de la raíz. La localización de la actividad reductasa férrica también ocurrió en esas zonas, no así la acidificación, que ocurrió a lo largo de toda la raíz. Estos datos, junto a los datos descritos anteriormente en el Objetivo 2 (Andaluz et al., 2009) y a los de desarrollo temporal de estas respuestas en el presente objetivo, sugieren que la producción de flavinas está más relacionada con la actividad reductasa que con la acidificación del medio.

La presencia de carbonato de calcio en la solución nutritiva afectó al patrón de acumulación/excreción de las flavinas. En el caso de deficiencia de Fe a pH 5,5 los derivados de riboflavina fueron preferentemente exportados al medio (un 35% de las flavinas totales), mientras que en la deficiencia de Fe a pH alto (7,7 por la presencia de carbonato en el medio de cultivo) solo el 6% se exportó durante los 6 días de tratamiento (Fig. 10). La síntesis de riboflavina y derivados también pareció verse afectada por la presencia de carbonato, ya que se retrasó el inicio de la síntesis, si bien alcanzando mayores valores al final del tratamiento que los observados a pH 5,5. La presencia de transportadores pH-dependientes de membrana aún no identificados podría explicar las diferencias de comportamiento entre los dos tratamientos.

La función de estás flavinas en la deficiencia de Fe todavía es un tema controvertido. Se ha especulado con que podrían funcionar como un puente de electrones intracelular que comunique el poder reductor generado en la mitocondria con el necesario para la actividad de la reductasa férrica en la membrana plasmática. Asimismo, se ha propuesto que una vez excretadas a la rizosfera las flavinas puedan interaccionar con los

microorganismos de una forma que resulte beneficiosa para la planta (Jordan et al., 1992; Susín et al., 1993; Yang et al., 2002). Los datos aportados en el presente estudio sugieren una posible función extracelular de estos compuestos, quizá facilitando la solubilización, y por tanto la adquisición, de Fe. Los derivados de riboflavina producidos por plantas descritos hasta ahora (los presentados aquí para *M. truncatula* y los sulfatos de riboflavina descritos en Susín et al., 1993 para remolacha) presentan una característica común, ya que son altamente solubles en agua. Recientemente, se ha descrito en el microorganismo *Shewanella* que flavinas (quizá FMN) altamente solubles pueden jugar un papel importante en la reducción extracelular del Fe que necesitan estas bacterias para su supervivencia (von Canstein et al., 2008). Se conoce también que las flavinas son capaces de quelar Fe, así como otros metales, por medio de la estructura de anillo de isoaloxacina (Albert, 1953). Por tanto, las flavinas altamente solubles podrían jugar un papel tanto en la reducción del Fe(III) de la rizosfera, debido a sus características redox, como en su quelación, influyendo en dos factores que aumentarían la solubilidad, y por tanto la disponibilidad del Fe para la planta. Sin embargo, todavía no se ha probado la existencia de ninguno de estos mecanismos en plantas.

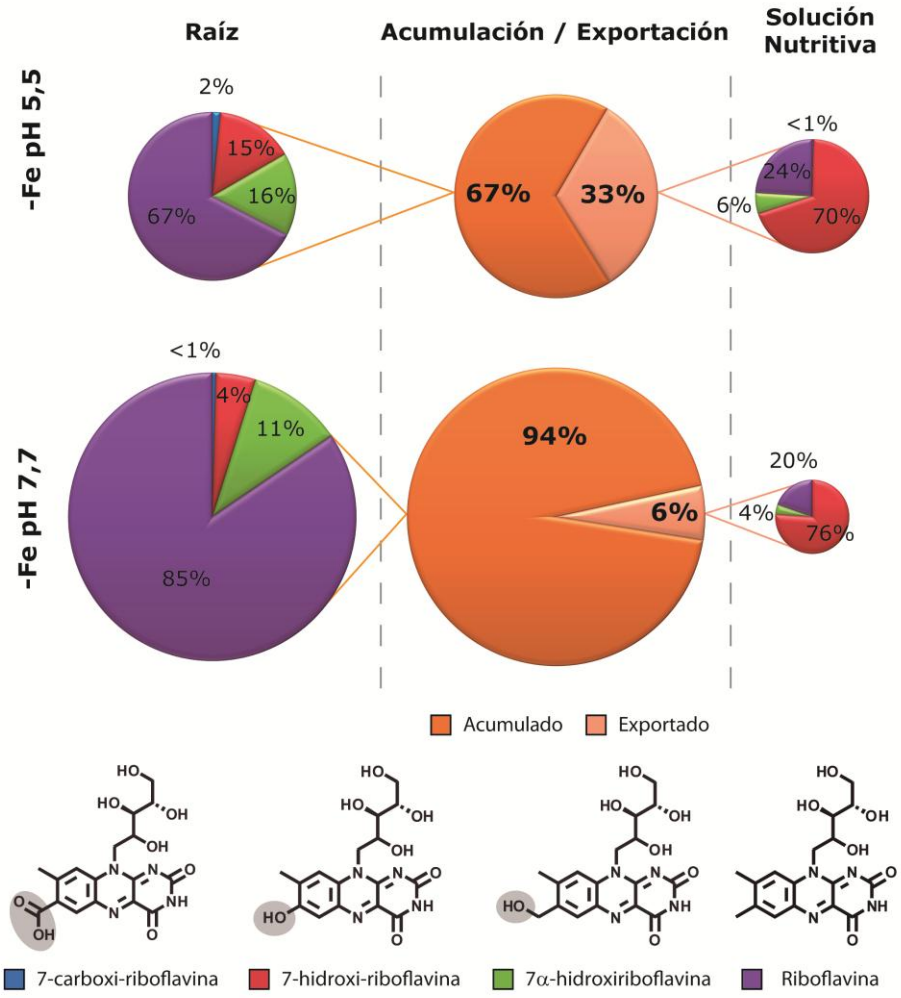

Fig. 10 Estructura de los compuestos derivados de riboflavina encontrados y patrones de acumulación/exportación según el tratamiento. El tamaño de los círculos es proporcional a la cantidad total de compuesto.

Objetivo 5: Respuestas a la deficiencia de Fe en diversas especies de Estrategia I

Se realizó un estudio con 15 especies de distintas familias sometidas a deficiencia de Fe a pH 7,7 utilizando como tampón carbonato cálcico. Se midieron peso fresco, concentración de clorofila en hoja, actividades reductasa férrica y PEPC en raíz y cantidad de riboflavina en raíz, para poder establecer posibles relaciones entre los parámetros (Rodríguez-Celma et al., 2011b). En función de los resultados de los objetivos anteriores, la hipótesis inicial consistió en que aquellas especies que acumulan flavinas en deficiencia de Fe presentarían una mayor actividad reductasa férrica, lo cual podría explicar la similar distribución espacial y temporal de estas respuestas en raíces. La confirmación de esta hipótesis podría abrir la posibilidad de que las flavinas tuvieran una función en el transporte intracelular de electrones desde las mitocondrias a la reductasa férrica de membrana plasmática.

En efecto, todas las especies que acumularon flavinas en condiciones de deficiencia de Fe mostraron aumentos en actividad reductasa. Sin embargo, no hubo una correlación significativa entre los dos parámetros, por lo que la acumulación de flavinas puede ser considerado un componente, pero no una respuesta obligatoria de la Estrategia I. Esta falta de correlación puede deberse a la complejidad de las dos respuestas, ya que mientras la actividad reductasa está estrictamente localizada en la membrana plásmática, las flavinas pueden estar localizadas intracelularmente en el citoplasma (en contacto con la reductasa férrica), almacenadas en vacuolas (no disponibles) o incluso en el exterior celular.

Uno de los resultados más interesantes de este estudio es la buena correlación entre las actividades reductasa férrica y PEPC ($r = -0{,}710$; $p<0{,}05$), confirmando que el aumento en la actividad de la PEPC es una respuesta común a la deficiencia de Fe en todas las plantas de Estrategia I. La enzima juega un papel importante en la unión entre procesos de adaptación metabólica al estrés y los procesos de adquisición de Fe por la raíz (López-Millán et al., 2000; Zocchi, 2006).

Teniendo en cuenta las especies estudiadas en este trabajo y las descritas en la bibliografía se pueden obtener varias conclusiones (Rodríguez-Celma et al., 2011b; Susín et al., 1993; Welkie, 2000). Hasta ahora se ha descrito acumulación y/o excreción de flavinas en respuesta a la deficiencia de Fe en 29 especies pertenecientes a 8 familias, mientras que no se han encontrado flavinas en 37 especies de 13 familias (Fig. 11). Existen 4 familias con especies que producen y que no producen flavinas en deficiencia de Fe (por ejemplo la familia Fabaceae, donde *M. truncatula* produce flavinas mientras *L. albus* no), por lo que la producción de flavinas no sigue un patrón taxonómico claro. Sí que parece existir, sin embargo, una relación entre la familia taxonómica y el tipo de derivado de riboflavina producido, ya que la acumulación/exportación de sulfatos de riboflavina está restringida a especies de la familia Amaranthaceae, mientras que los compuestos hidroxilados solo se han encontrado en *M. truncatula* (familia Fabaceae). Un derivado de la riboflavina distinto de los anteriores, aún sin identificar, se ha encontrado

en *C. melo* (en este trabajo) y *C. sativus* (comunicación personal de G. Zocchi) de la familia Cucurbitaceae.

El hecho de las flavinas se hayan estudiado poco en relación con la deficiencia de Fe puede deberse a su ausencia en la familia Brassicaceae, a la que pertenece la especie modelo *Arabidopsis thaliana*. La especie *M. truncatula* podría por tanto servir como un buen modelo para el estudio de la función que tienen las flavinas en la respuesta a la deficiencia de Fe de Estrategia I y la dilucidación de sus mecanismos de acumulación y exportación.

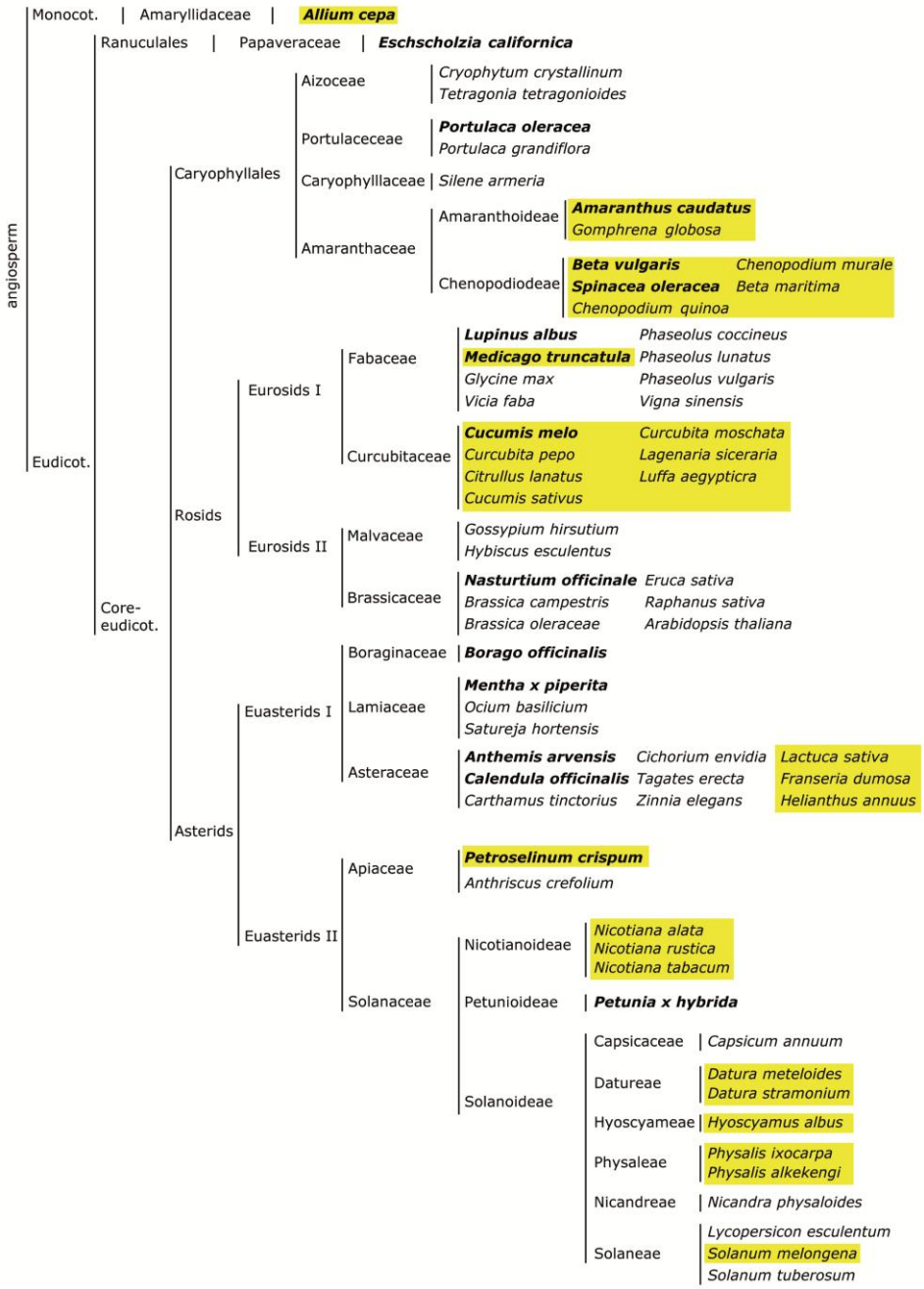

Fig. 11 Árbol taxonómico de especies en las que se ha estudiado la producción de flavinas en deficiencia de Fe. Están resaltadas en amarillo aquellas especies para las que se ha descrito un aumento de producción de flavinas en deficiencia de Fe

CONCLUSIONES

1. La proteómica diferencial es una buena herramienta para describir de una forma global los cambios que se producen a consecuencia de estreses nutricionales, al mismo tiempo que es una herramienta exploratoria capaz de descubrir nuevos puntos de interés para ser estudiados con mayor profundidad.

2. La intoxicación leve por Cd en raíz de tomate produce cambios metabólicos similares a los descritos en deficiencia de Fe que no se observan en el caso de intoxicación severa. Ambos niveles de intoxicación comparten sin embargo cambios en la respuesta de estrés y reorganización de la pared celular debidos a la acción intrínseca del Cd.

3. La especie modelo *Medicago truncatula* induce todas las respuestas ante la deficiencia de Fe descritas en raíces de plantas de Estrategia I tanto a nivel génico como de actividad enzimática. El distinto desarrollo temporal de las respuestas estudiadas indica la existencia de una regulación post-transcripcional.

4. La deficiencia de Fe en raíces de *Medicago truncatula* produce un aumento en el reciclado del nitrógeno presente en las proteínas, cuyos aminoácidos sirven como fuente anaplerótica de N y C para la producción de carboxilatos y metabolitos secundarios.

5. El aumento en la síntesis de riboflavina en deficiencia de Fe en *Medicago truncatula* está asociado a un aumento en la expresión de cuatro de los genes implicados en su ruta biosintética (GTPcII, DMRLs, rib D y ribE), así como en la cantidad de proteína de GTPcII y DMRLs, y es más acusado en condiciones de alto pH externo en el entorno radicular.

6. En deficiencia de Fe las raíces de *Medicago truncatula* acumulan y/o exportan al medio de cultivo no solo riboflavina, sino tres nuevos derivados no descritos hasta la fecha en plantas: 7-hidroxi-riboflavina, 7α-hidroxi-riboflavina y 7-carboxi-riboflavina, siendo el compuesto 7-hidroxi-riboflavina el mayoritariamente exportado al medio de cultivo.

7. La correlación entre la aparición en el tiempo de la actividad reductasa férrica y la síntesis de flavinas en raíz, así como su co-localización espacial indican que ambas respuestas a la deficiencia de Fe están relacionadas.

8. La producción de flavinas en raíces de plantas deficientes en Fe es un fenómeno extendido en el reino vegetal, aunque no sigue una distribución taxonómica clara, mientras que la producción de un determinado tipo de derivado de riboflavina sí parece estar restringida cada familia.

9. Existe una alta correlación entre las actividades reductasa férrica y fosfo*enol*piruvato carboxilasa de raíz en las especies vegetales estudiadas, confirmando que la fosfo*enol*piruvato carboxilasa juega un papel importante en la respuesta a la deficiencia de Fe en plantas de Estrategia I.

10. *Medicago truncatula* es un buen modelo para el estudio de la función que tienen las flavinas en la respuesta a la deficiencia de Fe en plantas de Estrategia I, así como para dilucidar los mecanismos de acumulación y excreción de estos compuestos. Ningún miembro de la familia Brassicaceae, a la que pertenece *Arabidopsis thaliana*, presenta esta respuesta.

REFERENCIAS

Abadía, J., y Abadía, A. (1993). Iron and plant pigments. In Iron chelation in plants and soil microorganisms L.L. Barton, y B.C. Hemming, eds. (San Diego: Academic), pp. 327-343.

Abadía, J., López-Millán, A.-F., Rombolà, A., y Abadía, A. (2002). Organic acids and Fe deficiency: a review. Plant and Soil *241*, 75-86.

Abadía, J., Vázquez, S., Rellán-Álvarez, R., El-Jendoubi, H., Abadía, A., Álvarez-Fernández, A., y López-Millán, A.F. (2011). Towards a knowledge-based correction of iron chlorosis. Plant Physiol Biochem *49*, 471-482.

Adriano, D.C., y Weber, J.T. (2001). Influence of fly ash on soil physical properties and turfgrass establishment. J Environ Qual *30*, 596-601.

Albert, A. (1953). Quantitative studies of the avidity of naturally occurring substances for trace metals. III. Pteridines, riboflavin and purines. Biochem J *54*, 646-654.

Alcántara E, de la Guardia M D and Romera F J 1991 Plasmmalemma redox activity and H^+ extrusion in roots of Fe-deficient cucumber plants. Plant Physiol. 96, 1034-1037.

Alhendawi R A, Römheld V, Kirby E A and Marschner H 1997 Influence of increasing bicarbonate concentrations on plant growth, organic acid accumulation in roots and iron uptake by barley, sorghum and maize. J. Plant Nutr. 20, 1731-1753.

Ali, G., Srivastava, P.S., y Iqbal, M. (2000). Influence of cadmium and zinc on growth and photosynthesis of *Bacopa monniera* cultivated *in vitro*. Biologia Plantarum *43*, 599-601.

Alloway, B.J., Jackson, A.P., y Morgan, H. (1990). The accumulation of cadmium by vegetables grown on soils contaminated from a variety of sources. Sci Total Environ *91*, 223-236.

Andaluz, S., Lopez-Millan, A.F., De las Rivas, J., Aro, E.M., Abadia, J., y Abadia, A. (2006). Proteomic profiles of thylakoid membranes and changes in response to iron deficiency. Photosynth Res *89*, 141-155.

Andaluz, S., Rodríguez-Celma, J., Abadía, A., Abadía, J., y López-Millán, A.F. (2009). Time course induction of several key enzymes in Medicago truncatula roots in response to Fe deficiency. Plant Physiol Biochem *47*, 1082-1088.

Astolfi, S., Zuchi, S., y Passera, C. (2005). Effect of cadmium on H^+ATPase activity of plasma membrane vesicles isolated from roots of different S-supplied maize (*Zea mays* L.) plants. Plant Science *169*, 361-368.

Award F, Römheld V and Marschner H 1988 Mobilization of ferric iron chlorosis in calcareous soil by plant-borne chelators (phytosiderophores). J. Plant Nutr. 11, 701-713.

Balestrasse, K.B., Gallego, S.M., y Tomaro, M.L. (2004). Cadmium-induced senescence in nodules of soybean (*Glycine max* L.) plants. Plant and Soil *262*, 373-381.

Barceló, J., y Poschenrieder, C. (1990). Plant water relations as affected by heavy metal stress: A review. Journal of Plant Nutrition *13*, 1-37.

Barret-Lennard E G, Marschner H and Römheld V 1983 Mechanism of short term Fe(III) reduction by roots. Evidence against the role of secreted reductants. Plant Physiol 73, 893-898.

Benavides, M.P., Gallego, S.M., y Tomaro, M. (2005). Cadmium toxicity in plants. Brazilian Journal of Plant Physiology *17*, 21-34.

Bell P F, Chaney R L and Angle J S 1988 Staining localization of ferric reduction on roots. J. Plant Nutr. 11, 1237-1252.

Bienfait H F, Bino R J, van der Bliek A M, Duivenvoorden J F and Fontaine J M 1983 Characterization of ferric reducing activity in roots of Fe-deficient *Phaseolus vulgaris*. Physiol. Plant. 59, 196-202.

Bjellqvist B, Ek K, Righetti PG, Gianazza E, Gorg A, Westermeier R, Postel W: Isoelectric focusing in immobilized pH gradients: principle, methodology and some applications. J Biochem Biophys Methods 1982, 6:317-339.

Blonder J, Terunuma A, Conrads TP, Chan KC, Yee C, Lucas DA, Schaefer CF, Yu LR, Issaq HJ, Veenstra TD, Vogel JC: A proteomic characterization of the plasma membrane of human epidermis by high-throughput mass spectrometry. J Invest Dermatol 2004, 123:691-699.

Bovet, L., Eggmann, T., Meylan-Bettex, M., Polier, J., Krammer, P., Marin, E., Feller, U., y Martinoia, E. (2003). Transcript levels of AtMRPs: cadmium treatments induce AtMRP3. Plant Cell and Environment *26*, 371-381.

Brancadoro L, Rabotti G, Scienza A and Zocchi G 1995 Mechanisms of Fe efficiency in roots of vitis ssp in response to iron deficiency stress. Plant and Soil 171, 229-234.

Briat J F and Lobréaux S 1997 Iron transport and storage in plants. Trends in Plant Science 2, 187-193.

Brown J C 1966 Fe and Ca uptake as related to root-sap and stem-exudate citrate in soybeans. Physiologia Plantarum 19, 968-976.

Brown J C and Ambler J E 1974 Iron-stress response in tomato.I. Sites of Fe reduction, absorption and transport. Physiol. Plant. 31, 221-224.

Brüggemann W, Moog P R, Nakagawa H, Janiesh P and Kuiper P J C 1990 Plasma membrane-bound NADH: Fe^{3+}-EDTA reductase and iron deficiency in tomato (*Lycopersicum esculentum*). Is there a Turbo reductase? Physiol. Plant. 79, 339-346.

Brumbarova, T., Matros, A., Mock, H.P., y Bauer, P. (2008). A proteomic study showing differential regulation of stress, redox regulation and peroxidase proteins by iron supply and the transcription factor FER. Plant J *54*, 321-334.

Candiano G, Bruschi M, Musante L, Santucci L, Ghiggeri GM, Carnemolla B, Orecchia P, Zardi L, Righetti PG: Blue silver: a very sensitive coloidal Coomassie G-250 staining for proteome analysis. Electrophoresis 2004, 25:1327-1333.

Chamrad DC, Korting G, Stuhler K, Meyer HE, Klose J, Bluggel M: Evaluation of algorithms for protein identification from sequence databases using mass spectrometry data. Proteomics 2004, 4:619-628.

Chaney R L, Brown J C and Tiffin L O 1972 Obligatory reduction of ferric chelates in iron uptake by soybeans. Plant Physiol. 50, 208-213.

Chaney R L 1984 Diagnostic practices to identify iron deficiency in higher plants. J. Plant Nutr. 7, 47-67.

Chen Y and Barak P 1982 Iron nutrition of plants in calcareous soils. Adv. Agron. 35, 217-240.

Chevallet M, Luche S, Diemer H, Strub JM, Van Dorsselaer A, Rabilloud T: Sweet silver: a formaldehyde-free silver staining using aldoses as developing agents, with enhanced compatibility with mass spectrometry. Proteomics 2008, 8:4853-4861.

Clark R B 1983 Plant genotype differences in the uptake, translocation, acumulation and use of mineral elements required for plant growth. Plant and Soil 72, 175-196.

Clauser KR, Baker P, Burlingame AL: Role of accurate mass measurement (+/-10 ppm) in protein identification strategies employing MS or MS/MS and database searching. Anal Chem 1999, 71:2871-2882.

Clemens, S., Antosiewicz, D.M., Ward, J.M., Schachtman, D.P., y Schroeder, J.I. (1998). The plant cDNA LCT1 mediates the uptake of calcium and cadmium in yeast. Proc Natl Acad Sci U S A *95*, 12043-12048.

Clemens, S., Naumann, B., y Hippler, M. (2009). Proteomics of metal mediated protein dynamics in plants - iron and cadmium in the focus. Front Biosci *14*, 1955-1969.

Cobbett, C., y Goldsbrough, P. (2002). Phytochelatins and metallothioneins: roles in heavy metal detoxification and homeostasis. Annu Rev Plant Biol *53*, 159-182.

Cohen C K, Fox T C, Garvin D F and Kochian L V 1998 The role of iron-deficiency stress responses in stimulating heavy-metal transport in plants. Plant Physiol 116, 1063-1072.

Colinge J, Masselot A, Giron M, Dessingy T, Magnin J: OLAV: towards highthroughput tandem mass spectrometry data identification. Proteomics 2003, 3:1454-1463.

Connolly E L, Fett J P and Guerinot M L 2002 Expression of the IRT1 metal transporter is controlled by metals at the levels of transcript and protein accumulation. Plant Cell 14, 1347-1357.

Corthals GL, Rose K: Quantitation in proteomics. Proteome research: New frontiers in functional genomics. Wilkins. Springer-Verlag; 2007.

Craig R, Beavis RC: TANDEM: matching proteins with tandem mass spectra. Bioinformatics 2004, 20:1466-1467.

Curie C and Briat J F 2003 Iron transport and signaling in plants. Annu Rev Plant Biol 54, 183-206.

Curie, C., Panaviene, Z., Loulergue, C., Dellaporta, S.L., Briat, J.F., y Walker, E.L. (2001). Maize yellow stripe1 encodes a membrane protein directly involved in Fe(III) uptake. Nature *409*, 346-349.

Chastain, J.L., y McCormick, D.B. (1986). Quantitation of products from riboflavin in rat urine. Journal Name: Fed Proc, Fed Am Soc Exp Biol; (United States); Journal Volume: 45:4; Conference: 70 annual meeting of the Federation of American Society for Experimental Biology, St Louis, MO, USA, 13 Apr 1986, Medium: X; Size: Pages: 825.

Chen, W., Chang, A.C., y Wu, L. (2007). Assessing long-term environmental risks of trace elements in phosphate fertilizers. Ecotoxicol Environ Saf *67*, 48-58.

Cornett J D and Johnson G V 1991 Ferric chelate reduction by suspension culture cells and roots of soybean: a kinetic comparison. Plant Soil 130, 75-80.

De Nisi P and Zocchi G 2002 Immunodetection of H^+-ATPase and PEPC in roots of cucumber grown under Fe-deficiency. *In* 11th International Symposium on Iron Nutrition and Interactions in Plants, Udine, Italy, 2002. pp 70.

De Vos C R, Lubberding H J and Bienfait H F 1986 Rhizosphere acidification as a response to iron deficiency in bean plants. Plant Physiology 81, 842-846.

De Vos, C.H.R., Bookum, W.M.T., Vooijs, R., Schat, H., y De Kok, L.J. (1993). Effect of copper on fatty acid composition and peroxidation of lipids in the roots of copper-tolerant and -sensitive *Silene cucubalus*. Plant Physiology and Biochemistry *31*, 151–158.

Dell'Orto M, Santi S, De Nisi P, Cesco S, Varanini Z, Zocchi G and Pinton R 2000 Development of Fe-deficiency responses in cucumber (Cucumis sativus L.) roots: involvement of plasma membrane H(+)-ATPase activity. J Exp Bot 51, 695-701.

Diezel W, Kopperschlager G, Hofmann E: An improved procedure for protein staining in polyacrylamide gels with a new type of Coomassie Brilliant Blue. Anal Biochem 1972, 48:617-620.

Dinkelaker B, Hengeler C and Marschner H 1995 Distribution and function of proteoid rootsand other root clusters. Bot. Acta 108, 183-200.

Dixon, R.A., Gang, D.R., Charlton, A.J., Fiehn, O., Kuiper, H.A., Reynolds, T.L., Tjeerdema, R.S., Jeffery, E.H., German, J.B., Ridley, W.P., *et al.* (2006). Applications of metabolomics in agriculture. J Agric Food Chem *54*, 8984-8994.

Dong, J., Wu, F., y Zhang, G. (2006). Influence of cadmium on antioxidant capacity and four microelement concentrations in tomato seedlings (*Lycopersicon esculentum*). Chemosphere *64*, 1659-1666.

Donnini, S., Prinsi, B., Negri, A., Vigani, G., Espen, L., y Zocchi, G. (2010). Proteomic characterization of iron deficiency responses in *Cucumis sativus L.* roots. BMC Plant Biology *10*, 268.

Eckhardt U, Mas Marques A and Buckhout T J 2001 Two iron-regulated cation transporters from tomato complement metal uptake-deficient yeast mutants. Plant Mol Biol 45, 437-448.

Edmond, C., Shigaki, T., Ewert, S., Nelson, M.D., Connorton, J.M., Chalova, V., Noordally, Z., y Pittman, J.K. (2009). Comparative analysis of CAX2-like cation transporters indicates functional and regulatory diversity. Biochem J *418*, 145-154.

Eide, D., Broderius, M., Fett, J., y Guerinot, M.L. (1996). A novel iron-regulated metal transporter from plants identified by functional expression in yeast. Proc Natl Acad Sci U S A *93*, 5624-5628.

Eng J, McCormack A, Yates JR: An approach to correlate tandem mass spectral data of peptides with amino acid sequences in a protein database. J Am Soc Mass Spectrom 1994, 5:976-989.

Fazekas de St Groth S, Webster RG, Datyner A: Two new staining procedures for quantitative estimation of proteins on electrophoretic strips. Biochim Biophys Acta 1963, 71:377-391.

Fenyo D, Qin J, Chait BT: Protein identification using mass spectrometric information. Electrophoresis 1998, 19:998-1005.

Fiehn, O. (2002). Metabolomics--the link between genotypes and phenotypes. Plant Mol Biol *48*, 155-171.

Field HI, Fenyo D, Beavis RC: RADARS, a bioinformatics solution that automates proteome mass spectral analysis, optimises protein identification, and archives data in a relational database. Proteomics 2002, 2:36-47.

Fodor, A., Szabó-Nagy, A., y Erdei, L. (1995). The effects of cadmium on the fluidity and H^+-ATPase activity of plasma membrane from sunflower and wheat roots. Journal of Plant Physiology *14*, 787-792.

Fox, T.C., y Guerinot, M.L. (1998). Molecular Biology of Cation Transport in Plants. Annu Rev Plant Physiol Plant Mol Biol *49*, 669-696.

Fox T C, Schaff J E, Grusak M A, Norvell W A, Chen Y, Chaney R L and Kochian L V 1996 Direct measurement of Fe ^{59}-labeled Fe^{2+} influx in roots of pea using a chelator buffer system to control free Fe^{2+} in solution. Plant Physiol 111, 93-100.

Garnier, L., Simon-Plas, F., Thuleau, P., Agnel, J.P., Blein, J.P., Ranjeva, R., y Montillet, J.L. (2006). Cadmium affects tobacco cells by a series of three waves of reactive oxygen species that contribute to cytotoxicity. Plant Cell Environ *29*, 1956-1969.

Gerke J 1997 Aluminum and iron (III) species in the soil solution including organic complexes with citrate and humic substances. Zeitschrift für Pflanzenernährung und Bodenkunde 160, 427-432.

Gong, J.M., Lee, D.A., y Schroeder, J.I. (2003). Long-distance root-to-shoot transport of phytochelatins and cadmium in Arabidopsis. Proc Natl Acad Sci U S A *100*, 10118-10123.

Gorg A, Weiss W, Dunn MJ: Current two-dimensional electrophoresis technology for proteomics. Proteomics 2004, 4:3665-3685.

Goshe MB, Smith RD: Stable isotope-coded proteomic mass spectrometry. Curr Opin Biotechnol 2003, 14:101-109.

Guerinot, M.L. (2000). The ZIP family of metal transporters. Biochim Biophys Acta *1465*, 190-198.

Guerinot M L and Yi Y 1994 Iron: nutritious, noxious, and not readily available. Plant Physiol. 104, 815-820.

Hall, J.L. (2002). Cellular mechanisms for heavy metal detoxification and tolerance. J Exp Bot *53*, 1-11.

Han DK, Eng J, Zhou H, Aebersold R: Quantitative profiling of differentiationinduced microsomal proteins using isotope-coded affinity tags and mass spectrometry. Nat Biotechnol 2001, 19:946-951.

Hanikenne, M., Kramer, U., Demoulin, V., y Baurain, D. (2005). A comparative inventory of metal transporters in the green alga Chlamydomonas reinhardtii and the red alga Cyanidioschizon merolae. Plant Physiol *137*, 428-446.

Hanikenne, M., Talke, I.N., Haydon, M.J., Lanz, C., Nolte, A., Motte, P., Kroymann, J., Weigel, D., y Kramer, U. (2008). Evolution of metal hyperaccumulation required cis-regulatory changes and triplication of HMA4. Nature *453*, 391-395.

Hardiman, R.T., y Jacoby, B. (1984). Absorption and translocation of Cd in bush beans *Phaseolus vulgaris*. Physiol Plant *61*, 670-674.

He, Z.L., Yang, X.E., y Stoffella, P.J. (2005). Trace elements in agroecosystems and impacts on the environment. Journal of Trace Elements in Medicine and Biology *19*, 125-140.

Hernandez P, Muller M, Appel RD: Automated protein identification by tandem mass spectrometry: issues and strategies. Mass Spectrom Rev 2006, 25:235-254.

Hether N H, Olsen R A and Jackson L L 1984 Chemical identification of iron reductants exuded by plant roots. J. Plant Nutr. 7, 667-676.

Heukeshoven J, Dernick R: Improved silver staining procedure for fast staining in PhastSystem Development Unit. I. Staining of sodium dodecyl sulfate gels. Electrophoresis 1988, 9:28-32.

Higuchi K, Suzuki K, Nakanishi H, Yamaguchi H, Nishizawa N K and Mori S 1999 Cloning of nicotianamine synthase genes, novel genes involved in the biosynthesis of photosiderophores. Plant Physiol. 119, 471-479.

Huff, J., Lunn, R.M., Waalkes, M.P., Tomatis, L., y Infante, P.F. (2007). Cadmium-induced cancers in animals and in humans. Int J Occup Environ Health *13*, 202-212.

Hutchinson T C 1967 Coralloid root systems in plants showing lime-induced chlorosis. Nature 214, 943-945.

James P, Quadroni M, Carafoli E, Gonnet G: Protein identification by mass profile fingerprinting. Biochem Biophys Res Commun 1993, 195:58-64.

Jones D L 1998 Organic acids in the rizosphere-a critical review. Plant Soil 205, 25-44.

Jones D L and Darrah P R 1995 Influx and efflux of organics acids accross the soil-root interface of Zea mays L. and its implications in rizosphere C flow. Plant and Soil 173, 103-109.

Jones D L, Darrah P R and Kochian L V 1996 Critical-evaluation of organic-acid mediated iron dissolution in the rizosphere and its potential role in root iron uptake. Plant Soil 180, 57-66.

Jordan, C.M., Wakeman, R.J., y DeVay, J.E. (1992). Toxicity of free riboflavin and methionine–riboflavin solutions to Phytophthora infestans and the reduction of potato late blight disease. Canadian Journal of Microbiology *38*, 1108-1111.

Kapp EA, Schutz F, Connolly LM, Chakel JA, Meza JE, Miller CA, Fenyo D, Eng JK, Adkins JN, Omenn GS, Simpson RJ: An evaluation, comparison, and accurate benchmarking of several publicly available MS/MS search algorithms: sensitivity and specificity analysis. Proteomics 2005, 5:3475-3490.

Kirkham, M.B. (2006). Cadmium in plants on polluted soils: Effects of soil factors, hyperaccumulation, and amendments. Geoderma *137*, 19-32.

Korenkov, V., Hirschi, K., Crutchfield, J.D., y Wagner, G.J. (2007). Enhancing tonoplast Cd/H antiport activity increases Cd, Zn, and Mn tolerance, and impacts root/shoot Cd partitioning in Nicotiana tabacum L. Planta *226*, 1379-1387.

Korshunova, Y.O., Eide, D., Clark, W.G., Guerinot, M.L., y Pakrasi, H.B. (1999). The IRT1 protein from Arabidopsis thaliana is a metal transporter with a broad substrate range. Plant Mol Biol *40*, 37-44.

Kupper, H., Lombi, E., Zhao, F.J., y McGrath, S.P. (2000). Cellular compartmentation of cadmium and zinc in relation to other elements in the hyperaccumulator Arabidopsis halleri. Planta *212*, 75-84.

Küpper, H., Šetlík, I., Spiller, M., Küpper, F.C., y Prášil, O. (2002). Heavy metal-induced inhibition of photosynthesis: targets of in vivo heavy metal chlorophyll formation. Journal of Phycology *38*, 429-441.

Landsberg, E.-C. (1982). Transfer cell formation in the root epidermis: A prerequisite for fe-efficiency? Journal of Plant Nutrition *5*, 415 - 432.

Larbi, A., Morales, F., Abadía, A., Gogorcena, Y., Lucena, J.J., y Abadía, J. (2002). Effects of Cd and Pb in sugar beet plants grown in nutrient solution: induced Fe deficiency and growth inhibition. Funct Plant Biol *29*, 1453-1464.

Li L, Cheng X and Ling H Q 2004 Isolation and characterization of Fe(III)-chelate reductase gene LeFRO1 in tomato. Plant Mol Biol 54, 125-136.

Lin, R., Wang, X., Luo, Y., Du, W., Guo, H., y Yin, D. (2007). Effects of soil cadmium on growth, oxidative stress and antioxidant system in wheat seedlings (*Triticum aestivum L.*). Chemosphere *69*, 89-98.

Lindsay, W.L., y Schwab, A.P. (1982). The chemistry of iron in soils and its availability to plants. Journal of Plant Nutrition *5*, 821-840.

Link AJ, Eng J, Schieltz DM, Carmack E, Mize GJ, Morris DR, Garvik BM, Yates JR, 3rd: Direct analysis of protein complexes using mass spectrometry. Nat Biotechnol 1999, 17:676-682.

Loeppert R H 1986 Reactions of iron and carbonates in calcareous soils. J. Plant Nutr. 9, 195-215.

Loeppert R H and Hallmark C T 1985 Indigenous soil properties influencing the availability of iron in calcareous soils. Soil Sci. Soc. Am. J. 49, 597-603.

López MF, Berggren K, Chernokalskaya E, Lazarev A, Robinson M, Patton WF: A comparison of silver stain and SYPRO Ruby Protein Gel Stain with respect to protein detection in two-dimensional gels and identification by peptide mass profiling. Electrophoresis 2000, 21:3673-3683.

López-Millán A F, Musetti V and Grusak M A 2005 Identification and characterization of a Fe (III)-reductase, MtFRO-1, in *Medicago truncatula*.

López-Millán, A.-F., Sagardoy, R., Solanas, M., Abadía, A., y Abadía, J. (2009). Cadmium toxicity in tomato (*Lycopersicon esculentum*) plants grown in hydroponics. Environ Exp Bot *65*, 376-385.

López-Millán, A.F., Morales, F., Andaluz, S., Gogorcena, Y., Abadía, A., De Las Rivas, J., y Abadía, J. (2000). Responses of sugar beet roots to iron deficiency. Changes in carbon assimilation and oxygen use. Plant Physiol *124*, 885-898.

Lozano-Rodríguez, E., Hernández, L.E., Bonay, P., y Carpena-Ruíz, R.O. (1997). Distribution of cadmium in shoot and root tissues of maize and pea plants: physiological disturbances. Journal of Experimental Botany *48*, 123-128.

Maestri, E., Marmiroli, M., Visioli, G., y Marmiroli, N. (2010). Metal tolerance and hyperaccumulation: Costs and trade-offs between traits and environment. Environmental and Experimental Botany *68*, 1-13.

Maksymiec, W., Wojcik, M., y Krupa, Z. (2007). Variation in oxidative stress and photochemical activity in Arabidopsis thaliana leaves subjected to cadmium and excess copper in the presence or absence of jasmonate and ascorbate. Chemosphere *66*, 421-427.

Mann M, Wilm M: Error-tolerant identification of peptides in sequence databases by peptide sequence tags. Anal Chem 1994, 66:4390-4399.

Marschner, H. (1995). Mineral nutrition of higher plants (London: Academic Pres).

Mengel K and Geurtzen G 1986 Iron chlorosis on calcareous soils. Alkaline nutritional condition as the cause for the chlorosis. J. Plant Nutr. 9, 161-173.

Miller I, Crawford J, Gianazza E: Protein stains for proteomic applications: which, when, why? Proteomics 2006, 6:5385-5408.

Mocquot, B., Vangronsveld, J., Clijsters, H., y Mench, M. (1996). Copper toxicity in young maize (*Zea mays* L.) plants: effects on growth, mineral and chlorophyll contents, and enzyme activities. Plant and Soil *182*, 287-300.

Molloy MP: Two-dimensional electrophoresis of membrane proteins using immobilized pH gradients. Anal Biochem 2000, 280:1-10.

Moog, P., y Brüggemann, W. (1994). Iron reductase systems on the plant plasma membrane-A review. Plant and Soil *165*, 241-260.

Moog P R, van der Kooij T A W, Brüggemann W, Schiefelbein J W and Kuiper P J C 1995 Responses to iron deficiency in *Arabidopsis thaliana*: The turbo iron reductase does not depend on the formation of root hairs and transfer cells. Planta 195, 505-513.

Morales F, Abadía A and Abadía J 1990 Characterization of the xanthophyll cycle and other photosynthetic pigment changes induced by iron deficiency in sugar beet (*Beta vulgaris* L.). Plant Physiol. 94, 607-613.

Morales F, Cerovic Z G and Moya I 1994 Characteristics of blue-green fluorescence in the mesophyll of sugar beet (*Beta vulgaris* L.) leaves affected by iron deficiency. Plant Physiol. 106, 127-133.

Morales F, Grasa R, Abadía A and Abadía J 1998 Iron chlorosis paradox in fruit trees. Journal of Plant Nutrition 21, 815-825.

Morel, M., Crouzet, J., Gravot, A., Auroy, P., Leonhardt, N., Vavasseur, A., y Richaud, P. (2009). AtHMA3, a P1B-ATPase allowing Cd/Zn/Co/Pb vacuolar storage in Arabidopsis. Plant Physiol *149*, 894-904.

Mori S 1999 Iron acquisition by plants. Curr Opin Plant Biol 2, 250-253.

Moulder R, Filen JJ, Salmi J, Katajamaa M, Nevalainen OS, Oresic M, Aittokallio T, Lahesmaa R, Nyman TA: A comparative evaluation of software for the analysis of liquid chromatography-tandem mass spectrometry data from isotope coded affinity tag experiments. Proteomics 2005, 5:2748-2760.

Nakanishi, H., Ogawa, I., Ishimaru, Y., Mori, S., y Nishizawa, N.K. (2006). Iron deficiency enhances cadmium uptake and translocation mediated by the Fe^{2+} transporters OsIRT1 and OsIRT2 in rice. Soil Science and Plant Nutrition *52*, 464-469.

Neuhoff V, Arold N, Taube D, Ehrhardt W: Improved staining of proteins in polyacrylamide gels including isoelectric focusing gels with clear background at nanogram sensitivity using Coomassie Brilliant Blue G-250 and R-250. Electrophoresis 1988, 9:255-262.

Neuhoff V, Stamm R, Eibl H: Clear background and highly sensitive protein staining with Coomassie Blue dyes in polyacrylamide gels: A systematic analysis. Electrophoresis 2005, 6:427-448.

Ohkawa, H., Ohishi, N., y Yagi, K. (1983). Hydroxylation of the 7- and 8-methyl groups of riboflavin by the microsomal electron transfer system of rat liver. J Biol Chem *258*, 5629-5633.

Okumura N, Nishizawa N K, Umehara Y, Ohata T, Nakanishi H, Yamaguchi T, Chino M and Mori S 1994 A dioxygenase gene (Ids2) expressed under iron deficiency conditions in the roots of Hordeum vulgare. Plant Mol Biol 25, 705-719.

Olmos, E., Martinez-Solano, J.R., Piqueras, A., y Hellin, E. (2003). Early steps in the oxidative burst induced by cadmium in cultured tobacco cells (BY-2 line). J Exp Bot *54*, 291-301.

Olsen R A, Bennett J H, Blume D and Brown J C 1981 Chemical aspects of the Fe stress response mechanism in tomatoes. J. Plant Nutr. 3, 905-921.

Opiteck GJ, Lewis KC, Jorgenson JW, Anderegg RJ: Comprehensive on-line LC/LC/MS of proteins. Anal Chem 1997, 69:1518-1524.

Ong SE, Mann M: Mass spectrometry-based proteomics turns quantitative. Nat Chem Biol 2005, 1:252-262.

Palagi PM, Hernandez P, Walther D, Appel RD: Proteome informatics I: bioinformatics tools for processing experimental data. Proteomics 2006, 6:5435-5444.

Papoyan, A., y Kochian, L.V. (2004). Identification of Thlaspi caerulescens genes that may be involved in heavy metal hyperaccumulation and tolerance. Characterization of a novel heavy metal transporting ATPase. Plant Physiol *136*, 3814-3823.

Pappin DJ, Hojrup P, Bleasby AJ: Rapid identification of proteins by peptidemass fingerprinting. Curr Biol 1993, 3:327-332.

Park, S., Cheng, N.H., Pittman, J.K., Yoo, K.S., Park, J., Smith, R.H., y Hirschi, K.D. (2005). Increased calcium levels and prolonged shelf life in tomatoes expressing Arabidopsis H+/Ca2+ transporters. Plant Physiol *139*, 1194-1206.

Patton WF: Detection technologies in proteome analysis. J Chromatogr B Analyt Technol Biomed Life Sci 2002, 771:3-31.

Patton WF, Beechem JM: Rainbow's end: the quest for multiplexed fluorescence quantitative analysis in proteomics. Curr Opin Chem Biol 2002, 6:63-69.

Pence, N.S., Larsen, P.B., Ebbs, S.D., Letham, D.L., Lasat, M.M., Garvin, D.F., Eide, D., y Kochian, L.V. (2000). The molecular physiology of heavy metal transport in the Zn/Cd hyperaccumulator Thlaspi caerulescens. Proc Natl Acad Sci USA *97*, 4956-4960.

Peng J, Gygi SP: Proteomics: the move to mixtures. J Mass Spectrom 2001, 36:1083-1091.

Perfus-Barbeoch, L., Leonhardt, N., Vavasseur, A., y Forestier, C. (2002). Heavy metal toxicity: cadmium permeates through calcium channels and disturbs the plant water status. Plant J *32*, 539-548.

Perkins DN, Pappin DJ, Creasy DM, Cottrell JS: Probability-based protein identification by searching sequence databases using mass spectrometry data. Electrophoresis 1999, 20:3551-3567.

Pich A, Manteuffel R, Hillmer S, Scholz G and Schmidt W 2001 Fe homeostasis in plant cells: does nicotianamine play multiple roles in the regulation of cytoplasmic Fe concentration? Planta 213, 967-976.

Pierce A, Unwin RD, Evans CA, Griffiths S, Carney L, Zhang L, Jaworska E, Lee CF, Blinco D, Okoniewski MJ, et al: Eight-channel iTRAQ enables comparison of the activity of six leukemogenic tyrosine kinases. Mol Cell Proteomics 2008, 7:853-863.

Pinot, F., Kreps, S.E., Bachelet, M., Hainaut, P., Bakonyi, M., y Polla, B.S. (2000). Cadmium in the environment: sources, mechanisms of biotoxicity, and biomarkers. Rev Environ Health *15*, 299-323.

Pinton R, Cesco S, de Nobili M, Santi S and Varanini Z 1998 Water and pyrophosphate extractable humic substances fractions as a source of iron for Fe-deficient cucumber plants. Biol .Fert .Soils 26, 23-27.

Pomponi, M., Censi, V., Di Girolamo, V., De Paolis, A., di Toppi, L.S., Aromolo, R., Costantino, P., y Cardarelli, M. (2006). Overexpression of Arabidopsis phytochelatin synthase in tobacco plants enhances Cd(2+) tolerance and accumulation but not translocation to the shoot. Planta *223*, 180-190.

Poschenrieder, C., Gunse, B., y Barcelo, J. (1989). Influence of cadmium on water relations, stomatal resistance, and abscisic Acid content in expanding bean leaves. Plant Physiol *90*, 1365-1371.

Rabilloud T: Mechanisms of protein silver staining in polyacrylamide gels: a 10-year synthesis. Electrophoresis 1990, 11:785-794.

Rabilloud T, Vuillard L, Gilly C, Lawrence JJ: Silver-staining of proteins in polyacrylamide gels: a general overview. Cell Mol Biol (Noisy-le-grand) 1994, 40:57-75.

Rabotti G, de Nisi P and Zocchi G 1995 Metabolic implications in the Biochemical responses to iron Deficiency in Cucumber (*Cucumis sativus* L.) roots. Plant Physiol. 107, 1195-1199.

Richardson, M.D., Hoveland, C.S., y Bacon, C.W. (1993). Photosynthesis and stomatal conductance of symbiotic and nonsymbiotic tall fescue. In (Madison, WI, ETATS-UNIS: Crop Science Society of America).

Righetti PG, Castagna A, Antonioli P, Boschetti E: Prefractionation techniques in proteome analysis: the mining tools of the third millennium. Electrophoresis 2005, 26:297-319.

Robinson, N.J., Procter, C.M., Connolly, E.L., y Guerinot, M.L. (1999). A ferric-chelate reductase for iron uptake from soils. Nature *397*, 694-697.

Rodríguez-Celma, J., Lattanzio, G., Grusak, M.A., Abadía, A., Abadía, J., y López-Millán, A.F. (2011a). Root responses of *Medicago truncatula* plants grown in two different iron deficiency conditions: changes in root protein profile and riboflavin biosynthesis. J Proteome Res *10*, 2590-2601.

Rodríguez-Celma, J., Rellán-Álvarez, R., Abadía, A., Abadía, J., y López-Millán, A.F. (2010). Changes induced by two levels of cadmium toxicity in the 2-DE protein profile of tomato roots. J Proteomics *73*, 1694-1706.

Rodríguez-Celma, J., Vázquez-Reina, S., Orduna, J., Abadía, A., Abadía, J., Álvarez-Fernández, A., y López-Millán, A.F. (2011b). Characterization of flavins in roots of Fe-deficient Strategy I plants, with *Medicago truncatula* on the focus. Plant Cell Physiology, In press.

Rogers E E, Eide D J and Guerinot M L 2000 Altered selectivity in an Arabidopsis metal transporter. Proc Natl Acad Sci U S A 97, 12356-12360.

Romera F J, Alcántara E and de la Guardia M D 1992 Role of roots and shoots in the regulation of the Fe efficiency responses in sunflower and cucumber. Physiol. Plant. 85, 141-146.

Romero-Puertas, M.C., Palma, J.M., Gómez, M., del Río, L.A., y Sandalio, L.M. (2002). Cadmium causes the oxidative modification of proteins in pea plants. Plant Cell and Environment *25*, 677-686.

Romero-Puertas, M.C., Rodríguez-Serrano, M., Corpas, F.J., Gómez, M., del Río, L.A., y Sandalio, L.M. (2004). Cadmium induced subcellular accumulation of $O^{2-\cdot}$ and H_2O_2 in pea leaves. Plant Cell and Environment *27*, 1122-1134.

Römheld V and Marschner H 1981 Iron deficiency stress induced morphological and physiological changes in root tips of sunflower. Physiol. Plant. 53, 354-360.

Römheld V and Marschner H 1983 Mechanism of iron uptake by peanuts plants. I. Fe(III) reduction, chelate splitting, and release of phenolics. Plant Physiol. 71, 949-954.

Römheld V, Müller C and Marschner H 1984 Localization and capacity of proton pumps in roots of intact sunflower plants. Plant Physiol. 76, 603-606.

Rosenfield C L, Reed D W and Kent M W 1991 Dependency of iron reduction on developement of a unique root morphology in *Ficus benjamina* L. Plant Physiol. 95, 1120-1124.

Ross PL, Huang YN, Marchese JN, Williamson B, Parker K, Hattan S, Khainovski N, Pillai S, Dey S, Daniels S, et al: Multiplexed protein quantitation in Saccharomyces cerevisiae using amine-reactive isobaric tagging reagents. Mol Cell Proteomics 2004, 3:1154-1169.

Ryan, J.A., Pahren, H.R., y Lucas, J.B. (1982). Controlling cadmium in the human food chain: a review and rationale based on health effects. Environ Res *28*, 251-302.

Sakaguchi T, Nishizawa N K, Nakanishi H, Yoshimura E and Mori S 1999 The role of potassium in the secretion of mugineic acids family phytosiderophores from iron-deficient barley roots. Plant Soil 215, 221-227.

Salt, D.E., Blaylock, M., Kumar, N.P., Dushenkov, V., Ensley, B.D., Chet, I., y Raskin, I. (1995). Phytoremediation: a novel strategy for the removal of toxic metals from the environment using plants. Biotechnology (N Y) *13*, 468-474.

Sandalio, L.M., Dalurzo, H.C., Gomez, M., Romero-Puertas, M.C., y del Rio, L.A. (2001). Cadmium-induced changes in the growth and oxidative metabolism of pea plants. J Exp Bot *52*, 2115-2126.

Sanitá di Toppi, L., y Gabbrielli, R. (1999). Response to cadmium in higher plants. Environmental and Experimental Botany *41*, 105-130.

Santi, S., y Schmidt, W. (2009). Dissecting iron deficiency-induced proton extrusion in *Arabidopsis* roots. New Phytol *183*, 1072-1084.

Sanz M, Cavero J and Abadía J 1992 Iron chlorosis in the Ebro river basin, Spain. Journal of Plant Nutrition 15, 1971-1981.

Schmidt, W. (1999). Mechanisms and regulation of reduction-based iron uptake in plants. New Phytologist *141*, 1-26.

Schmidt W 2003 Iron solutions: acquisition strategies and signaling pathways in plants. TRENDS Plant Sci 8, 188-193.

Schmidt W and Janiesch P 1991 Ferric reduction by *Geum urbanum*: a kinetic study. J. Plant Nutr. 14, 1023-1034.

Schmidt W and Schuck C 1996 Pyridine nucleotide pool size changes in iron-deficient *Plantago lanceolata* roots during reduction of external oxidants. Physiol. Plant. 98, 215-221.

Schneider, T., Schellenberg, M., Meyer, S., Keller, F., Gehrig, P., Riedel, K., Lee, Y., Eberl, L., y Martinoia, E. (2009). Quantitative detection of changes in the leaf-mesophyll tonoplast proteome in dependency of a cadmium exposure of barley (*Hordeum vulgare L.*) plants. Proteomics *9*, 2668-2677.

Senden, M.H.M.N., Van der Meer, A.J.G.M., Verburg, T.G., y Wolterbeek, H.T. (1994). Effects of cadmium on the behaviour of citric acid in isolated tomato xylem cell walls. Journal of Experimental Botany *45*, 597-606.

Shinmachi F, Hasegawa I and Yazaki J 1995 Difference in riboflavin secretion phenomenon as a result of iron-deficiency among plant species. Japanese J. Soil Sci. Plant Nutr. 66, 337-341.

Sijmons P C and Bienfait H F 1984 Mechanism of iron reduction by roots of *Phaseolus vulgaris* L. J. Plant Nutr. 7, 687-693.

Sijmons P C and Bienfait H F 1983 Source of electrons for extracellular Fe(III) reduction in iron-deficient bean roots. Physiol. Plant. 59, 409-415.

Sijmons P C, Lanfermeijer F C, De Boer A H, Prins H B A and Bienfait H F 1984a Depolarization of cell membrane potential during trans-plasma membrane electron transfer to extracellular electron acceptors in iron-deficient roots of *Phaseolus vulgaris* L. Plant Physiol. 76, 943-946.

Singh, P.K., y Tewari, R.K. (2003). Cadmium toxicity induced changes in plant water relations and oxidative metabolism of Brassica juncea L. plants. J Environ Biol *24*, 107-112.

Standing KG: Peptide and protein de novo sequencing by mass spectrometry. Curr Opin Struct Biol 2003, 13:595-601.

Stephan U W, Schmidke I and Pich A 1994 Phloem translocation of Fe, Cu, Mn and Zn in Ricinus seedlings in relation to the concentrations of nicotianamine, an endogenous chelator of divalen metal-ions, in different seedling parts. Plant Soil 165, 181-188.

Stockwin LH, Blonder J, Bumke MA, Lucas DA, Chan KC, Conrads TP, Issaq HJ, Veenstra TD, Newton DL, Rybak SM: Proteomic analysis of plasma membrane from hypoxia-adapted malignant melanoma. J Proteome Res 2006, 5:2996-3007.

Susín, S., Abadía, A., González-Reyes, J.A., Lucena, J.J., y Abadía, J. (1996). The pH requirement for in vivo activity of the iron-deficiency-induced "turbo" ferric chelate reductase: a comparison of the iron-deficiency-induced iron reductase activities of intact plants and isolated plasma membrane fractions in Sugar beet. Plant Physiol *110*, 111-123.

Susín, S., Abián, J., Peleato, M., Sánchez-Baeza, F., Abadía, A., Gelpi, E., y Abadía, J. (1994). Flavin excretion from roots of iron-deficient sugar beet (*Beta vulgaris L.*). Planta *193*, 514-519.

Susín, S., Abián, J., Sánchez-Baeza, F., Peleato, M.L., Abadía, A., Gelpi, E., y Abadía, J. (1993). Riboflavin 3'- and 5'-sulfate, two novel flavins accumulating in the roots of iron-deficient sugar beet (*Beta vulgaris*). J Biol Chem *268*, 20958-20965.

Switzer RC, 3rd, Merril CR, Shifrin S: A highly sensitive silver stain for detecting proteins and peptides in polyacrylamide gels. Anal Biochem 1979, 98:231-237.

Tabb DL, Saraf A, Yates JR, 3rd: GutenTag: high-throughput sequence tagging via an empirically derived fragmentation model. Anal Chem 2003, 75:6415-6421.

Tagliavini M, Abadía J, Rombolá A D, Abadía A, Tsipouridis C and Marangoni B 2000 Agronomic means for the control of iron chlorosis in deciduous fruit plats. J. Plant Nutr. 23, 2007-2023.

Takagi S 1976 Naturally occurring iron-chelating compounds in oat- and rice-root washings. Soil Sci. Plant Nutr. 22, 423-433.

Takahashi M, Yamaguchi H, Nakanishi H, Shioiri T, Nishizawa N K and Mori S 1999 Cloning two genes for nicotianamine aminotransferase, a critical enzyme in iron acquisition (Strategy II) in graminaceous plants. Plant Physiol. 121, 947-956.

Terry N 1980 Limiting factors in photosynthesis. I. Use of iron stress to control photochemical capacity *in vivo*. Plant Physiology 65, 114-120.

Terry N and Abadía J 1986 Function of iron in chloroplast. Journal of Plant Nutrition 9, 609-646.

Thimm O, Essigmann B, Kloska S, Altmann T and Buckhout T J 2001 Response of Arabidopsis to iron deficiency stress as revealed by microarray analysis. Plant Physiol 127, 1030-1043.

Tonge R, Shaw J, Middleton B, Rowlinson R, Rayner S, Young J, Pognan F, Hawkins E, Currie I, Davison M: Validation and development of fluorescence two-dimensional differential gel electrophoresis proteomics technology. Proteomics 2001, 1:377-396.

Tuloup M HC, Coro I, Hoogland C, Binz P-A, Appel RD: Aldente and BioGraph: An improved peptide mass fingerprinting protein identification environment. In Swiss

Proteomics Society 2003 Congress: Understanding Biological Systems through Proteomics; Basel, Switzerland. FontisMedia; 2003: 174-176.

Ueno, D., Iwashita, T., Zhao, F.J., y Ma, J.F. (2008). Characterization of Cd translocation and identification of the Cd form in xylem sap of the Cd-hyperaccumulator Arabidopsis halleri. Plant Cell Physiol *49*, 540-548.

Unlu M, Morgan ME, Minden JS: Difference gel electrophoresis: a single gel method for detecting changes in protein extracts. Electrophoresis 1997, 18:2071-2077.

Vázquez, M.D., Barceló, J., Poschenrieder, C., Madico, J., Hatton, P., A.J.M., B., y G.H., C. (1992). Localization of zinc and cadmium in Thlaspi caerulescens (Brassicaceae), a metallophyte that can hyperaccumulate both metals. J Plant Physiol *140*, 350–355.

Verret, F., Gravot, A., Auroy, P., Leonhardt, N., David, P., Nussaume, L., Vavasseur, A., y Richaud, P. (2004). Overexpression of AtHMA4 enhances root-to-shoot translocation of zinc and cadmium and plant metal tolerance. FEBS Lett *576*, 306-312.

Vert G, Grotz N, Dedaldechamp F, Gaymard F, Guerinot M L, Briat J F and Curie C 2002 IRT1, an Arabidopsis transporter essential for iron uptake from the soil and for plant growth. Plant Cell 14, 1223-1233.

von Canstein, H., Ogawa, J., Shimizu, S., y Lloyd, J.R. (2008). Secretion of flavins by Shewanella species and their role in extracellular electron transfer. Applied and environmental microbiology *74*, 615-623.

Von Wiren, N., Mori, S., Marschner, H., y Romheld, V. (1994). Iron inefficiency in maize mutant *ys1* (*Zea mays* L. cv Yellow-Stripe) is caused by a defect in uptake of iron phytosiderophores. Plant Physiol *106*, 71-77.

Washburn MP, Wolters D, Yates JR, 3rd: Large-scale analysis of the yeast proteome by multidimensional protein identification technology. Nat Biotechnol 2001, 19:242-247.

Waters B M, Blevins D G and Eide D J 2002 Characterization of FRO1, a pea ferric-chelate reductase involved in root iron acquisition. Plant Physiol 129, 85-94.

Wei L, Loeppert R and Ocumpaugh W 1997 Fe-Deficiency Stress Response In Fe-Deficiency Resistant and Susceptible Subterranean Clover - Importance Of Induced H+ Release. J. Exp. Bot. 48, 239-246.

Welkie, G.W. (2000). Taxonomic distribution of dicotyledonous species capable of root excretion of riboflavin under iron deficiency. Journal of Plant Nutrition *23*, 1819 - 1831.

Welkie, G.W., y Miller, G.W. (1993). Plant iron uptake physiology by nonsiderophore systems (Academic PressSan Diego (USA)).

Wilkins MR, Sanchez JC, Gooley AA, Appel RD, Humphery-Smith I, Hochstrasser DF, Williams KL: Progress with proteome projects: why all proteins expressed by a genome should be identified and how to do it. Biotechnol Genet Eng Rev 1996, 13:19-50.

Wilkins MR, Williams KL: Cross-species protein identification using amino acid composition, peptide mass fingerprinting, isoelectric point and molecular mass: a theoretical evaluation. J Theor Biol 1997, 186:7-15.

Wittmann-Liebold B, Graack HR, Pohl T: Two-dimensional gel electrophoresis as tool for proteomics studies in combination with protein identification by mass spectrometry. Proteomics 2006, 6:4688-4703.

Wu CC, MacCoss MJ, Howell KE, Yates JR, 3rd: A method for the comprehensive proteomic analysis of membrane proteins. Nat Biotechnol 2003, 21:532-538.

Wua, F., Zhang, G., y Dominy, P. (2003). Four barley genotypes respond differently to cadmium: lipid peroxidation and activities of antioxidant capacity. Environmenatl and Experimental Botany *50*, 63-78.

Yang, G., Bhuvaneswari, T.V., Joseph, C.M., King, M.D., y Phillips, D.A. (2002). Roles for riboflavin in the Sinorhizobium-alfalfa association. Mol Plant Microbe Interact *15*, 456-462.

Yen M R, Tseng Y H and Saier M H 2001 Maize *Yellow Stripe1*, an iron-phytosiderophore uptake transporter, ia a member of the oligopeptide transporter (OPT) family. Microbiology 147, 2881-2883.

Yi EC, Li XJ, Cooke K, Lee H, Raught B, Page A, Aneliunas V, Hieter P, Goodlett DR, Aebersold R: Increased quantitative proteome coverage with (13)C/(12)C-based, acid-cleavable isotope-coded affinity tag reagent and modified data acquisition scheme. Proteomics 2005, 5:380-387.

Young T F and Terry N 1982 Transport of iron into leaves following iron resupply to iron stressed sugar beet plants. J. Plant Nutr. 5, 1273-1283.

Yruela, I., Pueyo, J.J., Alonso, P.J., y Picorel, R. (1996). Photoinhibition of photosystem II from higher plants. Effect of copper inhibition. J Biol Chem *271*, 27408-27415.

Zhang N, Aebersold R, Schwikowski B: ProbID: a probabilistic algorithm to identify peptides through sequence database searching using tandem mass spectral data. Proteomics 2002, 2:1406-1412.

Zhang X, Jin QK, Carr SA, Annan RS: N-Terminal peptide labeling strategy for incorporation of isotopic tags: a method for the determination of sitespecific absolute phosphorylation stoichiometry. Rapid Commun Mass Spectrom 2002, 16:2325-2332.

Zocchi, G. (2006). Metabolic changes in iron-stressed dicotyledonous plants. In Iron Nutrition in Plants and Rhizospheric Microorganisms, L.L. Barton, y J. Abadía, eds. (Eds. Springer), pp. 359-370.

APÉNDICE

REVISTAS SCI, ÍNDICE DE IMPACTO Y CUARTIL

- *Plant physiology and biochemistry*
  Factor de Impacto: **2,402**
  Área: Plant Sciences (**Q1**, 43/187)

- *Jounal of proteomics*
  Factor de Impacto: **5,075**
  Área: Biochemical research methods (**Q1**, 10/71)

- *Jounal of proteome research*
  Factor de Impacto: **5,460**
  Área: Biochemical research methods (**Q1**, 9/71)

- *Plant & cell physiology*
  Factor de Impacto: **4,257**
  Área: Plant Sciences (**Q1**, 15/187)

CARTA DE ACEPTACIÓN

Fecha: Fri, 21 Oct 2011 07:54:40 -0400 (EDT)
De: myhirai@psc.riken.jp
Para: anaflor@eead.csic.es
Asunto: PCP-2011-E-00313.R2 **Accept without revision** (mail74)

Dear Dr.López-Millán,

I am very pleased to notify you that your manuscript entitled "Characterization of Flavins In Roots of Fe-deficient Strategy I Plants, With Medicago truncatula On The Focus" PCP-2011-E-00313.R2, has been accepted for publication in Plant and Cell Physiology on 21-Oct-2011.

IN ORDER TO PROCEED WITH THE PRODUCTION PROCESS, WE WILL NEED TO RECEIVE YOUR COPYRIGHT FORM. PLEASE NOTE WE HAVE NOW STARTED ONLINE LICENCE FORM.

Licence to Publish – Oxford University Press will need your permission to publish your accepted article in the journal. The PCP Production Editor will be contacting you with the instructions on how to complete the licence to publish form online.

OPTIONAL OPEN ACCESS – Plant and Cell Physiology authors can opt, at an additional charge, to make their paper freely available online to all immediately upon publication, as part of the Oxford Open initiative. On the Licence to Publish form you will be asked whether you wish to publish your article under an Open Access model and agree to pay the relevant additional charge. Applicable Open Access charges can be found at http://www.oxfordjournals.org/our_journals/pcp/for_authors/general.html. If you do not select the Open Access option, your paper will be published in the journal with standard subscription-based access and you will not be charged.

Materials required for production will automatically be exported from ScholarOne Manuscripts. Should any revision is required for submitted files (i.e. resolution issue, file format etc.) you will be contacted by our typesetter directly.

If you have any queries regarding production, please contact:

Ms. Sarah Beattie, Oxford Journals, oxford University Press, Great Clarendon Street, Oxford OX2 6DP; UK Tel: +44 (0)1865 353 784 Fax: +44 (0)1865 355970;
email: pcp@oup.com

AUTHOR CHARGES

- Page charge. No page charge is sought for articles up to 8 printed pages. For articles of 9 or more printed pages, the author will be billed a page charge of 20,000 yen per printed page in excess of 8 printed pages.

- Handling charge. Members of the Society are charged a handling fee of 20,000 yen and non-member authors are charged 30,000 yen per accepted manuscript .

****

PCP welcomes suitable photographs or illustrations for our cover illustration. Please contact the editorial office at pcp.editorialoffice@oup.com for information within 1 week after acceptance.

These photos should have some connection with the topic of the manuscript.

If your photos are used, you will receive 50 free reprints of your article bound with the colour cover, along with a high-resolution JPEG image of the cover.

****

Thank you very much for submitting such a fine work to the journal.

Sincerely,

Masami Yokota Hirai
Editor Plant and Cell Physiology

CONTRIBUCIÓN EN CO-AUTORÍA

ANA FLOR LÓPEZ MILLÁN, Científico Titular del CSIC

CERTIFICA

La contribución del doctorando Jorge Rodríguez Celma en la obtención de los datos experimentales referentes al contenido de flavinas, así como en su interpretación, redacción y posterior presentación, en el artículo realizado en co-autoría:

Andaluz S, Rodríguez-Celma J, Abadia A, Abadía J, López-Millán AF. Time course induction of several key enzymes in *Medicago truncatula* roots in response to Fe deficiency. *Plant physiology and biochemistry* **2009**, 47: 1082-1088.

Incluído en la tesis doctoral "Respuesta radicular a la deficiencia de Fe y toxicidad de Cd" presentada en la modalidad de compendio de publicaciones.

Zaragoza, Octubre de 2011

Fdo. Ana Flor López Millán